Sheffield Hallam University

A Sheffield Hallam University thesis

THE PLASTIC DEFORMATION OF NON-METALLIC

INCLUSIONS IN STEEL

A thesis submitted to the Council for National Academic
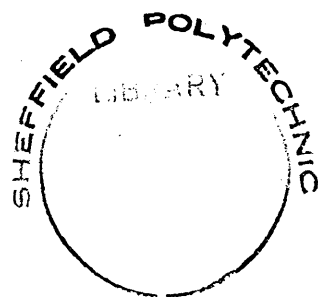Awards for the degree of

DOCTOR OF PHILOSOPHY

in

THE SHEFFIELD CITY POLYTECHNIC

by

STEWART WILLIAM ROBINSON, B.Sc.

March 1977

THE PLASTIC DEFORMATION OF NON-METALLIC INCLUSIONS IN STEEL

This thesis is based on an investigation sponsored by the British Steel Corporation and carried out during the period December 1973 to December 1976 at Sheffield City Polytechnic and the British Steel Corporation Special Steels Division Research and Development Department at Swinden Laboratories. During this period regular meetings were held to discuss the progress of the work and the following Conferences/Seminars were attended.

(i) "Non-Metallic Inclusions in Steel - Their Occurrence and Effects". Series of seminars held at Sheffield City Polytechnic 1973/74.

(ii) "Inclusions and Their Effects on Steel Properties". B.S.C. Conference held at Bodington Hall, the University of Leeds, 17 - 19th September, 1974.

(iii) "Controlled Processing of High Strength Low Alloy Steels". B.S.C. Conference held at the University of York, 28 - 30th September, 1976.

In addition the following lecture modules, from the part-time M.Sc. in Industrial Metallurgy at Sheffield City Polytechnic, were attended.

(i) Mechanical Metallurgy
(ii) High Strength Alloys
(iii) Arc Furnace Steelmaking
(iv) Numerical Methods and Programming
(v) Process Metallurgy - Transport Phenomena

The results obtained in this investigation and the theories developed are, to be best of my knowledge, original except where reference is made to other authors. No part of this thesis has been submitted for degrees at any other College or University.

March 1977

ACKNOWLEDGEMENTS

TO KIRSTY AND NICOLA, TWO SMALL PARTICLES OF
INDIGENOUS ORIGIN, WHO OFTEN INSISTED ON BEING
INCLUDED IN THIS INVESTIGATION

"Whatever effects inclusions have, they are an inseperable
part of the composite product called steel - not only must
they be lived with, they must be exploited".

Kiessling 1968

CONTENTS

SUMMARY

A comprehensive review of the literature concerning the various types of inclusions commonly encountered in commercial steels, has been carried out. The conditions of formation of both sulphide and oxide inclusions have been discussed, and in particular the effects of the various oxo- and sulpho-phillic elements which can be employed to modify the more usual inclusion populations. The effect of working on the inclusion morphology has also been reviewed with particular emphasis being given to the various factors which affect inclusion behaviour. The behaviour of the more common types of inclusions, during hot working, has also been reviewed.

The experimental work has investigated the effects of deformation temperature and the degree of matrix strain on the morphology of various types of silicate inclusions, during hot rolling. The 'Relative Plasticities' of plastic inclusions were determined and the mechanisms of fracture and dissemination of brittle non-plastic inclusions was investigated.

It was shown that crystalline and glassy silicate inclusions behaved in a 'brittle' or 'rigid' manner at lower rolling temperatures, depending on the size of the inclusions and the reduction attempted, but that at some critical temperature the behaviour suddenly became 'plastic' or 'fluid'. This transition temperature was shown to be related to the solidus temperature, in the case of crystalline silicate inclusions, but was dependent on the temperature at which the viscosity of glassy silicate inclusions fell below some critical value. This latter temperature was often considerably less than the corresponding solidus temperature.

The stability of the various types of glassy inclusions has also been investigated and it has been shown that in those cases where the glassy phases are unstable, complex non-equilibrium structures may develop on extended soaking at the working temperatures.

The mechanisms of formation of aluminous inclusions, produced on deoxidation with aluminium, have been investigated and theories have been proposed to explain the various inclusion morphologies observed. The effect of hot rolling on the morphology of these inclusion clusters has been investigated and an explanation for the strings of small angular alumina particles, often observed in commercial products, has been outlined.

Modern commercial steelmaking practices invariably produce a liquid product which contains a fine suspension of non-metallic particles. By the use of advanced post smelting techniques, such as vacuum degassing, vacuum arc remelting and electroslag refining, it is possible to eliminate the major fractions of these suspensions. However, such techniques are costly and only become economically viable in the case of high strength and special alloy steel production. For the manufacture of the major part of commercial tonnage grade steels, the steelmaker is left with the alternative of ensuring that his steelmaking practice gives rise to the types of inclusions the least injurious, or the most beneficial, to the particular property requirements of the steel user.

Non-metallic inclusions can be classified into two major groups, sulphides and oxides, although several other minor types, such as nitrides and selenides, also occur but far less frequently.

Sulphide inclusions are usually produced within the steel ingot or casting during solidification, and control of this type of inclusion depends largely on the steelmakers control of the sulphur content of the melt prior to casting. Manganese sulphide is the usual form of sulphide found in steels, although other forms may be produced in specially treated steels. The morphology of this sulphide is largely dependent on the state of deoxidation at the time of solidification, the inclusions having a globular, or TYPE I, morphology at low degrees of deoxidation. In heavily deoxidized steels the inclusions have an idiomorphic morphology, usually termed TYPE III, whilst at intermediate degrees of deoxidation they have a vermiform character, being precipitated in fan like colonies along the grain boundaries; this morphology being known as TYPE II. There is currently some dispute about the mechanism by which the latter two inclusion types are formed, but whatever this mechanism is, the

vermiform morphology remains one of the most deleterous with respect to the mechanical properties.

Oxide inclusions can arise from various sources during the steelmaking process, but of these it is the products of reoxidation during teeming and the erosion products of the ladle nozzle and refractories that have been found to be of primary importance. In addition to these, secondary products of deoxidation are formed during solidification and cooling and it is these types of inclusions which are most frequently found in the final product, particularly when the casting temperature is low and the inclusions have little time to float out of the ingot.

Oxidic inclusions are classified into three groups depending on their mode of occurrence- these are the PRIMARY, SECONDARY and EXOGENOUS types of inclusion. PRIMARY inclusions are those produced in the liquid steel by precipitation reactions brought about by the various steelmaking additions made to the melt, and are typified by the primary products of deoxidation. SECONDARY types are those formed within the ingot or casting during solidification and arise from the changing solubilities of oxygen and sulphur. These are typified by the fine interdendritic manganowustite precipitates found in rimming steel ingots. Manganese sulphide inclusions also belong to this group. The EXOGENOUS inclusions are those produced by erosion or corrosion of the various refractory materials with which the steel comes into contact during the steel-making process. Although this system provides a good general basis for the classification of inclusions, there are areas of broad overlap between the various classes. For example, primary inclusions are often precipitated onto exogenous nuclei, and exogenous particles may become so altered by reaction with the dissolved deoxidants that they bear little resemblance to the refractory material from which they originated. It can be appreciated that the

choice of deoxidant usually has a pronounced effect on the composition and constitution of the oxidic inclusions present in the final product.

During hot working the inclusions present may behave in a rigid, brittle or plastic manner, depending on the conditions of working and on the relative strengths of the inclusion and matrix materials. When they behave in a plastic or fluid manner they tend to deform in sympathy with the steel matrix, becoming elongated in the working direction to form long, thin, internal discontinuities which act as long co-planar cracks lying in the rolling plane. Similarly brittle inclusions tend to break up and become disseminated along the metal flow lines, forming long, thin fragmented stringers. These can also act as internal cracks, particularly if matrix welding between the disseminated inclusion fragments is incomplete. Rigid inclusions do not elongate or fracture and hence do not produce such platelike discontinuities. They can, however, promote the formation of conical voids in association with the matrix-inclusion interface. In such cases the matrix and inclusion become decohesed due to the inability of the deforming matrix to maintain complete peripheral contact with the inclusion as it flows around it. The voids thus produced also lie in the working plane and may act as sites for preferred crack initiation, particularly in fatigue situations. In some cases these rigid inclusions are associated with a peripheral shell of a more plastic material, for example manganese sulphide sometimes found associated with the more aluminous calcium aluminates. In such cases the plastic phase is stripped from the more rigid phase forming long tail-like discontinuities extending into the surrounding matrix.

In general, non-metallic inclusions are found to be detrimental to the mechanical properties of the steel. They are known to lower the tensile strength, can drastically reduce the fatigue life, are the chief cause of mechanical anisotropy in flat rolled products and are the main reason for the scatter band width in the toughness

properties. However, certain sulphide and low melting point silicate dispersions do enhance the machining properties of the steel and are used to advantage in free machining grades.

The recognition of the harmful effects of inclusions on the mechanical properties has resulted in a concentrated research effort, over the last two decades, into understanding the origins of non-metallic inclusions and their mechanisms of formation; the effects of processing on their morphology and distribution, and the effects they ultimately have on the properties of the steels containing them.

1.2   THE REASONS FOR AND THE AIMS OF THE INVESTIGATION

Although there have been numerous investigations into the origins of non-metallic inclusions, and the effects they ultimately have on the mechanical properties, investigations into the effects of deformation on the morphologies of the inclusions have been less numerous. Those investigations which have been reported have mainly been concerned with the behaviour of sulphidic inclusions, the behaviour of oxidic types being less well defined.

The purpose of the present study was to investigate some of the factors influencing the behaviour of the inclusions during hot working and to obtain fundamental information on the behaviour of the more common types of oxidic inclusions.

The aims of the study were to provide information on :

1.   The transition between rigid and fluid behaviour of silicate inclusions on increasing the temperature of deformation.

2.   The mechanisms of fracture and dissemination of brittle types of silicate inclusions.

3.   The effects of prolonged soaking treatments at high temperatures on the constitution of glassy silicate inclusions and the effects this has on their behaviour during subsequent working treatments.

4. The mechanisms of fracture and dissemination of aluminous agglomerates produced on deoxidation by aluminium.

5. The behaviour of aluminous types modified by calcium to produce calcium aluminate type inclusions.

Although it was originally intended to investigate the effects of hot working on several different types of calcium aluminate inclusions, this objective was not achieved. This was due in part to difficulties experienced in obtaining the requisite degree of calcium reaction in the experimental melts and also to the additional time spent investigating the mechanisms of formation of the different particle morphologies in the inclusion clusters produced on deoxidation by Aluminium; a study which was not envisaged in the original research program.

SECTION 2

LITERATURE REVIEW

2. LITERATURE REVIEW

Although this investigation was concerned primarily with the behaviour of oxidic inclusions on hot working, it was felt that the work would be incomplete if it did not include a review of current views concerning the types of inclusions commonly found in steels and their modes of occurrence. A review of the literature concerning sulphide inclusions is also included for the sake of completeness.

2.1 INCLUSION TYPES COMMONLY FOUND IN STEELS

2.1.1. Sulphide Inclusions

Although the greatest variety of morphologies, compositions and constitutions are exhibited by the oxidic types of inclusions, they do not constitute the major fraction of the non-metallic inclusions present in steels. Widdowson (1) states that a moderately clean bulk processed steel typically contains 0.10 Wt % of non-metallic inclusions. Of these, assuming a sulphur content of 0.015%, 0.09% are present in the form of sulphides. Because of their greater numbers the sulphide inclusions can have a significantly greater effect on the mechanical properties than do the oxides. Consequently much work has been, and is being, conducted into finding methods of eliminating the sulphide inclusions, or of rendering them less harmful.

At 1600°C. sulphur has unlimited solubility in liquid steel but it is insoluble in the solid state, and must be precipitated from the metal as it solidifies. In the absence of other more stable sulphide forming elements FeS is the precipitated phase and forms as a low melting point eutectic in the interdendritic spaces FIG. I. The presence of this low melting point constituent gives rise to the familiar problem of hot shortness, and for this reason the steel

usually contains manganese, in the ratio of at least 4:1, Mn:S,
which forms a more stable sulphide than that of iron FIG. 14a,
and gives rise to the familiar dove grey inclusions frequently
observed in steel microstructures.

(i)   Manganese Sulphides

The morphology of the manganese sulphides depend on the
steelmaking practice. Simms & Dahle (2) have classified these
morphologies as types I, II and III, the actual types produced
depending largely on the state of deoxidation of the melt at the time
of casting, and its alloy content.

In steels containing more than 0.02 Wt % of dissolved
oxygen, the steel undergoes a monotectic reaction during solidifi-
cation, producing sulphur and oxygen rich liquid globules at the
solidification front, FIG. 2. According to Baker and Charles (3)
those globules formed early in the solidification sequence, contain
more dissolved oxygen than those globules produced later, and can
produce duplex oxide-sulphide structures upon their subsequent
solidification. Below a limiting oxygen content of 0.01% Dahl (4)
states that only the vermiform type II sulphides are formed, there
being a gradual transition between types I and II at oxygen contents
between 0.02 and 0.01%. Traditionally type II sulphides have been
regarded as a eutectic structure being produced by a eutectic
reaction in the last remaining liquid to solidify, (2) FIG. 2. However,
it has recently been suggested that this sulphide morphology is, in
fact, a co-operative monotectic form, the globular type I morphology
being the degenerate form, (5). The effect of aluminium, (2), in
changing the morphology from type I to type II is generally accepted
to be the action of the aluminium removing oxygen from solution.
However, Friedriksson (5) has obtained both types I and II at low
oxygen to sulphur ratios, in experimental melts, and has suggested
that the absence of type II from the silicon treated steels was due to
the silicate droplets being efficient nuclei for the liquid type I
sulphides. Deoxidation by aluminium alone produces a solid oxide

which is presumably not an efficient nucleant for liquid MnS. In fact Buzek (19) has observed small alumina particles within type III sulphides, on which nucleation may have occurred. Similar particles have been reported by Duckworth and Inneson (6) and it is possible that alumina may promote the formation of type III sulphides, which are probably solid at steelmaking temperatures, by providing sites of nucleation. Type II sulphides are found in steels deoxidized by silicon, silicon and manganese, and aluminium where the aluminium cover is low. In steels with very low oxygen contents, as for example in correctly treated aluminium killed melts, an idiomorphic form of manganese sulphide is formed. These sulphides are precipitated in crystalline form directly from the melt, although the exact nature of their formation is still a matter of some dispute. Some workers believe that other elements are required before the type III morphology will appear, (5), their action being to depress the freezing point of the melt and to move the MnS-Fe eutectic closer to the iron rich corner of the phase diagram, FIG. 3. The MnS is then precipitated on cooling as a proeutectic constituent. Baker and Charles (3) have argued that if this were the case then type III sulphides would exhibit flotation effects and become segregated within the ingot. They also argue that by increasing the sulphur content of the melt the type II morphology should be replaced by the type III morphology. Since neither of these phenomenon are observed, these workers assert that type III manganese sulphides are unlikely to be formed by proeutectic precipitation, and support the view that this morphology results from a eutectic reaction, the sulphide forming as a divorced constituent. More recently Pickering (7) has observed that the skeletal or anchor shaped form of manganese sulphide, found in cast irons and alloy steels, is typical of the initial stages of a primary crystallisation and that in these cases the sulphide may have been produced as a primary precipitate. However, Friedriksson and Hillert (5) include this morphology in an additional group they have called type IV. This type has a fishbone

or chinese script morphology which they believe results from a normal eutectic solidification. This morphology has only been observed unambiguously in experimental melts containing high levels of sulphur and solidified under carefully controlled conditions. The morphology is very similar to the type II morphology and it would be difficult to distinguish the two types in commercial steels containing small volume fractions of sulphide. However, this hypothesis can be used to explain an anomalous observation reported earlier by Simms (8) who found that on deoxidizing a medium manganese steel with aluminium, type II sulphides could be converted to type III by a moderate excess of aluminium, but that with a high Al excess the morphology reverted to one resembling type II. In terms of Friedriksson & Hillerts hypothesis, this reversion is simply the appearance of the co-operative eutectic type IV morphology replacing they type III divorced eutectic morphology.

There is now sufficient evidence to make a generalised conclusion on the probable mechanisms of formation of the different sulphide morphologies. The type I morphology results from a normal monotectic type reaction during the solidification sequence. The type II morphology appears at intermediate degrees of deoxidation and may result from a co-operative monotectic type reaction. At high degrees of deoxidation the type III morphology is formed as the divorced constituent of a eutectic reaction whilst the more usual co-operative eutectic produces the type IV morphology which may often be confused with the type II morphology.

The FeS content of the manganese sulphides initially precipitated can be substantial, FIG. 4; Salmon - Cox and Charles (9) reporting as much as 20% FeS in freshly precipitated manganese sulphides, the equilibrium Fe:Mn ratio only being approached during subsequent cooling or heat treatment. The substitution of manganese by other sulphophilic elements is well known and the elements chromium, calcium, zirconium and the rare earth elements are all known to behave in this way, (10, 11) FIG. 14a. Chromium substituted

manganese sulphides are often found in stainless steels, and usually appear in the idiomorphic type III morphology (7, 11, 16) and the complete mutual solubility of chromium and manganese sulphides has been reported (17). Substitution of manganese by calcium and magnesium have also been reported (7, 16) but although calcium and manganese sulphides are isomorphous, their mutual solubility is incomplete, manganese sulphide being able to dissolve a maximum of 12% CaS (27).

(ii)   Sulphide Modification

During hot working, manganese sulphides behave plastically, forming elongated thin stringers which are very deleterious to the mechanical properties. Sulphide modification treatments are designed to replace the highly plastic manganese sulphide with a less plastic form and to ensure that the highly deleterious type II morphology does not occur. Kiessling (11) states that chromium has the most effective solid solution strengthening effect on manganese sulphide, FIG. 35b, and Pickering (12) has pointed out that the sulphide inclusions present in low manganese, high chromium stainless steels are much less prone to form elongated stringers on hot working. However, solid solution strengthening of MnS by chromium is not a practical proposition due to the large amounts of the element required to obtain sufficient partitioning between the sulphide and matrix. The alternative is to promote the formation of a harder, less plastic and more stable type of sulphide and it is in this direction that significant progress has been made in recent years.

According to Pickering (12) those elements used to modify the sulphide population should satisfy as many of the following conditions as possible.

(i)   The element must form a sulphide more stable than manganese sulphide.

(ii)   The element should have a greater affinity for sulphur than for oxygen, nitrogen or carbon.

(iii)   The element should have a low vapour pressure at steelmaking temperatures and should be soluble in liquid steel.

(iv)   The sulphides produced should not form low melting point eutectics with the steel or other phases present and although volatile sulphides would be useful for desulphurizing treatments, they would be of little use for preventing the formation of thin stringers on working.

(v)   The addition of the element to the liquid steel should be capable of a controlled non-violent reaction and give a predictable recovery.

(vi)   The sulphide formed should have a high melting point and consequently a low plasticity at working temperatures.

Arrowsmith (15) states that the objective of sulphide modification is to produce inclusions which are resistant to rolling deformation and, since they must not crack, they must also be small. A final requirement is that they must be distributed homogeneously, since clusters of refractory globular inclusions would also produce deleterous fragmentary stringers on working.

These considerations limit the choice of sulphide modifiers to the elements of groups II, III and IV of the periodic table, the elements of the other groups forming sulphides which are either volatile, unstable, or less stable than manganese sulphide. The rare earth elements of group III have been shown to have a strong modifying potential, as have the elements titanium and zirconium from group IV and calcium from group II (11 - 15) FIG. 14a. The elements hafnium, tantalum and even uranium have been suggested as possible sulphide modifiers, but their expense and/or problems of hygiene limit them to areas of academic interest (19).

(iii)   <u>Modification by Calcium Additions</u>

Simms and Dahle (2) first investigated the possibility of employing calcium as a deoxidizer for steel, but concluded that the presence of calcium had no apparent effect on the inclusion morphology in calcium-silicon treated steels compared with conventional silicon-manganese killed steels. In discussion of Simms & Dahle's paper however, Grotts (2) presented evidence to show that calcium-silicon treatments used to supplement deoxidation by aluminium could produce considerable improvements in ductility. Subsequent investigations (18 - 24) provided metallographic evidence to show that calcium additions to aluminium killed steels, minimised the tendency to form type II sulphides and limited the formation of the very deleterious alumina clusters, by replacing them with the less refractory calcium aluminates.

Calcium is often used in modern steelmaking for the modification of both oxide and sulphide inclusions, being most frequently used to eliminate alumina galaxies and type II sulphides from aluminium killed grain refined steels.

Calcium is only sparingly soluble in liquid steel, a solubility of 0.032 Wt % Ca being reported by Sponseller and Flinn (25) for calcium in pure iron. Miyashita and Nishikawa report a minimum solubility of 0.0103 Wt % Ca for calcium in pure iron at $1600^{\circ}C$. Additionally, calcium vapourizes when immersed in liquid steel, a vapour pressure of 1.6 atmospheres at $1600^{\circ}C$ being reported (25). This combination of high vapour pressure and sparing solubility make the control of calcium additions very difficult and undoubtedly accounts for the disagreement between early investigators into the effects of calcium. The use of the more usual calcium bearing deoxidant alloys such as calcium silicide, in sulphide modification treatments, has given, and still gives, very erratic results. In order to make calcium treatment more controllable it is necessary to lower its vapour pressure at steelmaking temperatures, and to

increase its solubility in the molten steel. Third element interactions have been reported to increase the solubility, steels containing 0.74% C having a calcium solubility of 0.052% (25). Aluminium is also reported to increase the solubility. Hilty, Crafts and Soloman (21) have shown that barium can have a significant influence in lowering the vapour pressure of the calcium. In addition barium is very dense and barium-calcium alloys have the virtue that they sink rapidly to the bottom of the melt, giving a reduced bubble size and hence increased residence time of the calcium vapour. Barium itself has an even lower solubility in steel than calcium and is only rarely observed in inclusions produced by the addition of calcium barium alloys (23). The advent of the calcium-barium alloys, for the treatment of aluminum deoxidized steels, has given a marked improvement in the control and predictability of calcium treatments in recent years.

The CaS-MnS system shows a marked solubility gap (27), manganese sulphide only being able to dissolve 12% CaS in solid solution. This results in the formation of isolated particles of very stable calcium sulphide in melts given sufficiently heavy calcium treatments. CaS is also frequently observed as a peripheral layer around calcium aluminate inclusions, produced by reaction of the calcium with the less stable oxide inclusions present in the melt at the time of the addition. Salter and Pickering (16) have postulated that such peripheral calcium sulphide can be formed by the reaction of basic admixed slag particles with aluminium added as a deoxidant. Whilst the calcium silicate slag particles can dissolve sulphur, its solubility in calcium aluminate is limited (28) and on reaction is precipitated as CaS around the periphery of the inclusion. Hilty and Farrel (13) state that the chief advantage of calcium treatment is the elimination of type II sulphides from low carbon, aluminium killed, grain refined steels. These workers found that a calcium level of only 12.5 ppm was sufficient to begin the conversion of type II sulphides to type III. At higher calcium levels the sulphides contained a greater proportion of CaS and formed predominantly in association

with the calcium aluminate oxide phases. Although Salter and Pickering's explanation for this association might account for a few instances of association it will not account for the preferential association found by these workers. No really satisfactory explanation for this phenomenon has yet been proposed. It does, however, present an interesting possibility, since it eliminates the sulphide as an individual particle from the microstructure. For the same volume fraction of sulphide, the larger less numerous type I inclusions are less detrimental to the fracture toughness than the finer more numerous type III sulphides. Hence the association of sulphide and oxide inclusions could provide a method for obtaining the ductility and toughness properties usually associated with high quality low sulphur steels, in the cheaper grades of steel containing the more usual levels of sulphur. Additionally, the reduction in the levels of the tesselated stresses in the matrix around the inclusions, arising from this association, can give a marked improvement in the fatigue properties.

(iv)   Modification by Rare Earth Additions

The rare earth elements (R. E.) have very high affinities for both oxygen and sulphur, FIG. 14, and also for carbon and nitrogen, their affinity for oxygen being even greater than that of aluminium. For this reason steel melts to be treated with R. E. alloys must be fully deoxidized before the addition is made, the usual choice of deoxidant being aluminium.

The types of oxide, sulphide and oxysulphide phases formed by the R. E. elements is large and the phases precipitated in treated steels depends largely on the oxygen and sulphur contents of the melt at the time of the addition (29, 30) and on the RE:S ratio; complete elimination of all MnS types only being achieved at RE:S ratios greater than 3. 0 (14, 32). Wilson (14) and Wilson and Wells (31) have recently summarised the types of phases most frequently found in R. E. treated steels. Small additions of between 0. 008 and 0. 020%

are reported to produce further deoxidation and to modify the remaining alumina inclusions, forming $(R.E.) Al_{11}O_{18}$ and $(R.E.)$ AlO_3 types. Manganese sulphides containing one or two per cent of R.E. are also produced, often being associated with the aluminous phases. At R.E. levels of 0.02% the $(R.E.) AlO_3$ oxide becomes predominant, there being very few purely aluminous types present after treatment. The R.E. substituted manganese sulphides produced at this level of addition contain typically 3-5% R.E. With additions of between 0.02 and 0.07% the R.E. oxysulphide phase $(R.E.)_2O_2S$ appears, and is often found associated with a peripheral R.E. sulphide phase of the $(R.E.)_xS_y$ type. Several forms of R.E. sulphide are known to occur although $(R.E.)S$ itself is but infrequently observed, only appearing at high R.E. contents (14). Schindlerova & Buzek (33) report the complete modification of the sulphides at RE concentrations between 0.01 and 0.02%, which is in fair agreement with Wilson's observations. These workers (33) also found that at the higher RE levels large clusters of refractory RE sulphide and oxysulphide phases occur, producing serious defects akin to those produced by alumina. It is now generally accepted that it is the formation of such clusters that impair the mechanical properties of heavily modified R.E. treated steels. These clusters can produce severe lamination in wrought products (12) and Davies (34) has reported that severe bottom cone formation can occur in R.E. treated steels, which can also result in rather large local concentrations of R.E. sulphide and oxysulphide clusters.

The R.E. alloys used in modification treatments may be either MISCHMETAL, containing

     50% Ce, 25% La, 10% Nd and 5% Pr and others

or RARE EARTH SILICIDE, containing

     35% Fe, 30% Si, 18% Ce and 9% La.

In general mischmetal is preferred to the silicide since recovery of the silicon from the latter is almost 100%. However, mischmetal is more expensive and the final choice rests on an economic and compositional balance.

It is interesting to note that the sulphides and oxysulphides produced from these alloys often contain R.E. ratios quite different to the ratios in the alloys used (31), and Wilson (30) has predicted on thermodynamic grounds the partitioning of the various elements between the sulphide and oxysulphide phases.

The recovery of the R.E. in the melt largely depends on the method of its addition. Initially these alloys were added directly to the mould during teeming, to minimise losses due to refractory reactions and stream reoxidation. Bingel and Scott (36) reported recoveries of 60-80% using this method but found that the treatments required to give complete modification of the sulphides gave very unclean ingots containing a large number of the deleterous sulphide-oxysulphide clusters. Similar results were reported by Bennett and Sandell (37) who also reported recoveries of 12 - 41% for additions made during vacuum degassing. Because of the inferior cleanliness sometimes encountered with mould additions, several attempts involving ladle additions have been reported (14, 36, 37). Results indicate that this practice, despite the lower recoveries ($\sim$ 30%), results in a cleaner product and provides the most convenient method of addition. Wilson (14) has also reported trials involving the plunging of the R.E. alloy into the melt in order to minimise losses due to oxidation at the surface. Lu and McLean have derived equations to predict the minimum R.E. requirements for the successful modification of steel melts of differing oxygen and sulphur contents (29). However, these equations do not allow for losses due to reoxidation and reaction with the refractories and must be viewed with caution.

With the correct levels of addition, manganese sulphides are completely replaced by R.E. sulphides or oxysulphides. Modification may, however, be quite inhomogeneous and frequently regions of the ingot may still contain manganese sulphides.

Although the R.E. elements are capable of forming carbides and nitrides these phases have never been reported to occur in steels

treated with the R.E's. Furthermore, Wilson (30) has predicted from a thermodynamic viewpoint that they should not be formed. This fact is of great advantage in the area of HSLA steels which depend on the precipitation of various nitrides for their strength properties. In these steels sulphide modifiers which also form carbides and nitrides cannot be used.

(v)   Modification by Zirconium Additions

The addition of zirconium to fully killed steel melts results in the formation of zirconium substituted manganese sulphides, which Pickering reports to be able to dissolve up to 12% by weight (7). At this level of substitution the sulphide corresponds to $MnZrS_2$. These sulphides show less tendency to elongate during hot rolling, presumably due to their increased melting point. With additions in excess of that required to give saturation of the sulphides, carbide and carbo-sulphide phases are produced which are known to reduce the toughness properties. Buzek et al (19) investigated the effects of zirconium on the mechanical properties of steels over the range 0.02 - 0.26% Zr. These workers found that as little as 0.02% Zr was sufficient to prevent the formation of type II sulphide morphology, whilst at 0.07% Zr the morphology was completely type III, at which stage a minimum was reached in the anisotropy ratio of the toughness properties. Increasing the zirconium level to 0.1% led to the formation of Zr_3S_4 as yellow, angular particles, all the sulphide being in this form with zirconium contents greater than 0.15%. Henderson and Little (38) found that zirconium levels above those required for the saturation of the MnS led to the formation of the carbosulphide phase $Zr_4C_2S_2$ which had a lamellar as cast morphology. Pollard (39) has also observed this phase in zirconium treated steels and Henderson & Little (38) suggested that the phase may form grain boundary films and hence drastically reduce the toughness properties. The appearance of this phase limits the amount of zirconium which

can safely be added to the steel and consequently the complete elimination of mechanical anisotropy is not possible.

The strong affinity of zirconium for nitrogen, which even surpasses that of aluminium, results in the formation of zirconium nitride particles which Mihelich (40) states act as nuclei on which the sulphide is precipitated. In contrast to this, Buzek (19) observed ZrO_2 particles at the centres of the sulphide phases, suggesting nucleation on the oxide phases. This author also found that the degree of substitution of manganese by zirconium is affected by the carbon content of the steel; possibly due to the partitioning of the zirconium between the sulphide and carbide phases. Pollard (39) found that the efficiency of the modification was also affected by the manganese content, the degree of substitution being less, the higher the manganese content. The increased level of zirconium required to give full modification at these higher manganese contents led to the appearance of the deleterious carbo-sulphide phase before full modification could be reached. In these cases it is suggested that a reduction in the manganese content can be beneficial in allowing a greater degree of modification at the same zirconium level, without the appearance of the carbo-sulphide phase. Any loss of hardenability, due to the reduction in manganese, could then be safely offset by a small increase in the chromium content.

Zirconium treated steels, in addition to having increased ductility and toughness in the transverse directions, are completely free from strain ageing, strain age embrittlement and blue brittle behaviour, due to the denitriding potential of the zirconium (40). The additions are made to fully killed steels, as with the Rare Earth treatments, the zirconium being added in the form of zirconium silicide, ferro-silicon-zirconium or even zirconium metal scrap.

(vi)   Modification by Titanium Additions

It has been known for some time that the presence of titanium in stainless steels can prevent the formation of manganese

sulphides. However it is only in the space of the last few years that interest has been shown in the possible use of this element as a sulphide modifier.

Titanium can form a number of sulphide, carbide, carbo-sulphide and carbo-sulphonitride phases in steels. Like the other sulphide modifiers, titanium has a high affinity for oxygen and can only be added to fully deoxidized melts. All the common phases are hexagonal in structure and have been summarized as (18)
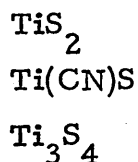
$$TiS_2$$
$$Ti(CN)S$$
$$Ti_3S_4$$

Jellinek (41) gives a general form $(Ti)_{1-x}S$ with either metal or sulphur vacancies to form the various types of sulphide; in fact Ti_3S_4 may be regarded as TiS_2 with sulphur atoms removed from alternate basal planes, (18). Because of its greater affinity for nitrogen than for sulphur, enough titanium must be added to precipitate all the nitrogen before the sulphides can be formed. Although Banks and Gladman obtained sulphide modification with titanium levels in excess of 0.15% (18), Buzek reports (19) that at levels greater than 0.13% type II manganese sulphides are replaced by needles of Ti_2S, which precipitate eutectically at the grain boundaries and have the same deleterous effect on the mechanical properties as type II sulphides. With titanium contents below 0.13% the sulphides are of type II MnS, and according to Buzek, contain no dissolved titanium, although a surface enrichment of up to 15% is reported. In contrast Banks and Gladman obtained analysis of type II MnS containing up to 3% Ti. It is reported that the oxide inclusions in aluminium killed melts were also modified and contained up to 22% TiO_2 after the titanium additions, whereas additions made to non- aluminium treated melts produced Ti_2O_3 inclusions. The high affinity of titanium for nitrogen precludes its use from steels which depend on nitride precipitation for their strength properties.

(vii)   <u>Modification by Other Additions</u>

Buzek (19) has investigated the effects of Tantalum and Uranium on sulphide morphology.

Tantalum additions were investigated within the range 0.005 - 0.58%. It was found that the mechanical properties deteriorated as the tantalum content increased and this was found to be due to the formation of large numbers of yellow needles along the grain boundaries, which were identified as tantalum carbide.

The effects of uranium were investigated within the range zero to 0.28%, the type II sulphide morphology being eliminated at uranium contents as low as 0.02%. At levels above 0.04% spherical uranium sulphides were produced and gave a corresponding increase in the mechanical properties. Although such promising initial results have been obtained, it is unlikely that uranium can be of use in commercial practice due to the problems of hygiene that would be encountered and to the high cost of the uranium alloys required.

Hafnium is believed to have effects similar to those of zirconium (7, 19) but because of its prohibitive cost it is unlikely to be of commercial application.

2.1.2.   <u>Oxide Inclusions</u>

The multiplicity of oxidic inclusion types found in commercial steels makes their classification, in anything but the broadest sense, very difficult. It is generally accepted that these inclusions are formed as a result of deoxidation reactions, or by the reaction of a deoxidant with pre-existing inclusions, whether these latter types are exogenous oxides arising from the refractory surfaces or from the slag, or the uneliminated products of previous deoxidation reactions. The types of inclusions formed as a result of such reactions have compositions belonging to the system -

$$CaO - Al_2O_3 - SiO_2 - MnO - FeO$$
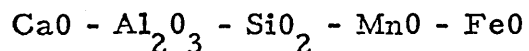
although the oxides MgO, TiO and ZrO may also be introduced as a result of reactions involving inclusions originating from the refractories. In addition, the oxides of chromium may be present

in the oxide inclusions found in stainless steels, and the oxides of
titanium, zirconium and the rare earths may be introduced in
steels treated with these elements (SECTION 2.1.1).

The choice of a suitable deoxidant is determined by the
need for a high efficiency of deoxidation and by economic considerations.
The choice for a particular steel is further limited by the need to
choose a deoxidant whose products will be the least injurious or the
most beneficial to the specific property requirements of the steel.
These factors usually limit the choice to either aluminium or silicon
based deoxidants, although combinations of one or both of these with
other elements such as manganese and calcium are also frequently
used. Ferrosilicon, ferromanganese, silicomanganese, ferro-
aluminium, aluminium, calcium silicide and various combinations,
with or without more exotic components, are frequently used as
deoxidants.

(i)   Aluminous Inclusions

Of all the deoxidation practices used, deoxidation by
aluminium is the most common. This is because of the ease with
which the additions can be made, the speed with which deoxidation
occurs, the speed with which the aluminous inclusions produced
can be removed, but chiefly because of the low residual oxygen
concentration in the melt and the low cost and availability of aluminium
itself.

There have been a number of investigations into the
deoxidation of iron-oxygen melts by aluminium, most notably those
of Plockinger and co-workers (42 - 45). Sloman and Evans (46)
conducted the first extensive investigation into the effects of
deoxidation by aluminium on iron-oxygen melts. These workers
concluded that aluminium additions in stoichiometric excess of the
oxygen content produced alumina inclusions whilst additions of less
that stoichiometric proportion gave rise to mixed oxide phases
containing the spinel phase hercynite, their constitution depending

on the aluminium to oxygen ratio, FIG. 5. Around the same time Hilty and Crafts (47) presented evidence suggesting that iron oxygen melts containing aluminium may not equilibriate with pure alumina but with $FeO-Al_2O_3$ phases. However, further evidence to support this view has not appeared in the literature.

Plockinger and his co-workers (42) investigated the effects of aluminium deoxidation by taking suction samples directly from the melt at various intervals after making the aluminium addition. These w orkers found that the primary deoxidation products underwent a marked change in composition during the course of their formation. Initially the inclusions had a very low aluminium content, the inclusions consisting mainly of wustite, whose composition changed rapidly during the first few seconds after the aluminium addition, the alumina content increasing until the spinel phase was precipitated, FIG. 5. At normal steelmaking temperatures, the spinel phase is solid, although in the presence of manganese the phase has a lower melting point, that of Galaxite being $1560^{o}C$. FIG. 6; in fact Waudby (48) found that solid spinel type inclusions are not produced on deoxidizing steel melts containing more than 1% Mn. With further increase in time Plockinger found that the spinel inclusions developed a two phase structure, the outer layers of the inclusion being rich in alumina, the core retaining its spinel composition.

According to Plockinger et al (42) alumina can only be nucleated at high degrees of supersaturation, because of the high activation energy of formation of the alumina molecule. Consequently liquid mixed oxide phases are nucleated which have good coagulating properties but which are rapidly reacted by the aluminium in solution. Whilst ever the inclusions remain liquid their composition remains homogeneous, but on reaching the spinel composition the inclusions become solid and further reaction develops a rim-core structure. Small clusters of almost pure alumina are purportedly formed in the same way, the rim-core structure being eliminated by the complete reaction of the inclusions facilitated by their small

size. In fact Koch (49) observed the reduction of the surface layers of hercynite particles deliberately inserted into a suitable iron-aluminium melt, to a depth of $15 \mu m$, indicating that complete reaction of small hercynite particles can occur.

According to Plockinger's theory the aluminium deoxidant takes a short but finite time to dissolve in the liquid metal, the aluminium content increasing in the vicinity of the deoxidant until liquid mixed iron-aluminium oxides are precipitated. Plockinger states that these mixed oxides are precipitated homogeneously. However, Frohberg and Potschke (50) and Forster (49) consider that nucleation will occur heterogeneously on solid alumina particles formed at the surface of the aluminium deoxidant, upon its addition to the melt. Waudby (48) also holds this opinion and points out that the deoxidants already have an oxide layer on their surface before their addition to melt.

Plockinger (42) also reported the formation of alumina inclusions having a spherical glassy morphology. These inclusions are almost perfectly spherical in habit, resembling small glassy silicates rather than crystalline alumina inclusions. Although analysis of this type of inclusion reveals them to be almost pure alumina, it has been assumed by most workers (42, 48, 52) that they must have been liquid when formed in order to develop their spherical morphology. Plockinger (42) suggests that they may be precipitated initially as liquid mixed oxides, their small size facilitating their rapid reduction to form almost pure alumina inclusions whilst retaining their globular habit. However, as pointed out by Waudby and Salter (52) any such reaction should rapidly produce a solid reaction rim and further reaction would then precipitate iron globules internally. Since these inclusions are characterized by their glassy appearance and complete absence of enclosed metal, it is difficult to accept Plockinger's postulate. Choudhury and Wahlster (53) have suggested an alternative explanation. These workers propose that the heat liberated on the formation of the alumina molecules could locally raise the temperature sufficiently for the alumina to be momentarily liquified. Again, a simple heat balance (52) shows that the maximum possible temperature rise is

of the order of 50°C. At present there is no satisfactory explanation for the formation of this particular morphology.

Although the technique of taking suction samples directly from the melt has been widely employed to follow the course of deoxidation reactions, the technique must be viewed with some caution. The method of making the deoxidant additions usually results in a very heterogeneous distribution of the deoxidant elements within the melt, and consequently the deoxidation reactions are very heterogeneous. Suction samples taken at an early stage during the deoxidation are, therefore, likely to give unrepresentative results, the sample having been taken from a small volume in an undefined region of the melt. The products of deoxidation obtained within the suction samples are thus not necessarily representative of the complete distribution.

Bogdandy (51) has investigated the deoxidation of iron oxygen melts using a system whereby unidirectional diffusion of the deoxidant into the oxygen rich melt occurred. The deoxidant was floated on the surface of the melt contained within an alumina tube held vertically within a H.F. furnace melt. Deoxidation by pure aluminium and various iron aluminium alloys were investigated. In each case the zone of the melt immediately below the melt-deoxidant interface developed a distribution of alumina dendrites. As the holding time increased, the thickness of this dendritic zone increased, though slowly, and the size of the individual dendrites increased markedly. Immediately beneath this dendritic zone was a region of low oxygen activity, as indicated by the absence of oxide inclusions on solidification. The remainder of the melt was substantially unaffected by the aluminium and produced the usual distribution of secondary wustite globules on solidification. These results conflict with Plockinger's theory, which predicts the formation of liquid mixed oxides, nucleated homogeneously, before the $[Al]^2 [O]^3$ supersaturation, is sufficient to nucleate pure alumina. It would appear from this latter investigation that the homogeneous nucleation of oxide deoxidation products, in oxygen

rich melts deoxidized by aluminium, results in the precipitation of pure alumina without the formation of intermediate liquid mixed oxides. The alumina grows dendritically by the diffusion of oxygen, from the oxygen rich liquid into the dendritic zone, the corresponding forward diffusion of aluminium being at a slower rate. The non-equilibrium liquid mixed oxide phases observed by Plockinger and his co-workers, and by subsequent investigators (48 - 50, 52) are possibly only precipitated heterogeneously at degrees of supersaturation too low to nucleate alumina itself.

It is well known that alumina in contact with pure iron of low oxygen activity has a very high surface energy, TABLE 1. Waudby (48) has suggested that liquid mixed oxides may be nucleated in preference to alumina because of their lower interfacial energy. However Bogdandy (51) states that the critical nucleus size for the nucleation of alumina, at the levels of supersaturation required, is of the order of atomic dimensions. This would suggest that it is not interfacial energy but activation energy which controls the nucleation. In addition, the formation of pure alumina precipitates in melts of normal oxygen activity would not be inhibited in this way, the interfacial energy of alumina with iron melts containing $0.07\%O_2$ being even lower than that of liquid silicates (54).

The advent of scanning electron microscopy (S.E.M.) has allowed the morphologies of aluminous inclusions to be studied in detail, (55 - 58). Rege et al (55) showed that small clusters of alumina inclusions were often of a dendritic form when seen in three dimensions. Okohira et al (57) used this technique (S.E.M.) to determine the shapes of aluminous inclusions present in the ladle and tundish during a continuous casting process. These workers classified the inclusions they observed according to their morphologies. Three basic forms were observed, dendritic, globular and idiomorphic, although these types were further subdivided into other groups. These workers concluded that the dendritic forms had been produced by comparatively 'long term' diffusional growth. The clusters of spherical particles were thought to have formed by

'short term' diffusional growth and by the reduction of reoxidation products or admixed slag particles. The idiomorphic types were thought to be of exogenous origin. A 'dumpling' like form was though to be composed of sintered globular types. Ooi (58) studied the morphologies of alumina inclusions produced in both stirred and unstirred melts. In the unstirred melts the inclusions were found to be mainly of the dendritic type, whereas in the stirred melt few dendritic types were observed, the inclusions having mostly a globular morphology, in many cases the small globules being sintered together into a spherical mass containing sinter porosity. These are presumably the 'dumpling' types observed by Okohira (57). The few dendritic types that were observed often appeared to have their dendrite arms amputated, and according to these workers are the s ource of the small globular inclusions. However, the mechanism by which the arms are amputated is suggested to be by gradual melting off, which is difficult to accept in view of the high melting point of alumina. These workers conclude that most of the inclusions produced by the deoxidation reactions on first adding the aluminium, are eliminated before teeming takes place. The aluminous inclusions found in the ingot stage, it is suggested, are produced by stream reoxidation during teeming.

Aluminous inclusions can arise from sources other than the primary products of deoxidation. In order to protect the metal from reoxidation on its contact with the atmosphere it is usual to add excess aluminium. This excess is also available to react with the less stable oxides present in the refractory linings, admixed slag particles and oxide inclusions produced by earlier deoxidation treatments.

Waudby et al (59) have reported on an extensive investigation into the effects of aluminium additions on silicate inclusions present in steel melts. These workers showed that in the case of large highly siliceous inclusions, reaction with the dissolved aluminium produces an aluminous reaction rim which greatly reduces the rate

of further reaction. This inhibition was found to result in the retention of non-equilibrium products into the solidified samples. On re-heating, the reaction was observed to continue by diffusion of the aluminium from the surrounding metal matrix to the inclusion-metal interface. Reaction between the dissolved aluminium and the less highly siliceous inclusions was found to occur much more rapidly, resulting in the formation of equilibrium reaction products in very short times. It is also reported that after the initial sharp decrease in the total oxygen content of the melt, on first adding the aluminium, the oxygen content was quickly refurbished in those cases where the aluminium addition was small.

Pickering (60) has reported on the use of aluminium in the production of balanced and rimming steel ingots and has shown that the addition of aluminium, to control the extent of the rimming action, has a dramatic effect on the types of inclusions present in the solid ingot. The inclusions present in the liquid metal during the rimming period are typically iron manganese silicates, some of which become entrapped in the solidified rim of the ingot. Upon the addition of aluminium to stop the rimming action, Galaxite ($MnO.Al_2O_3$), Hercynite ($FeO.Al_2O_3$) and Alumina inclusions can be produced, the type depending on the level of the aluminium addition. Any aluminium excess has the effect of reducing the less stable oxide phases in the siliceous inclusions already present in the melt. The extent of the reaction depends on the amount of excess aluminium available for reaction and the length of time before the inclusion becomes trapped in the solidifying metal. Initially the spinel phases are produced by reaction with the less stable iron and manganese oxides and with sufficient amounts of aluminium the inclusion may be fully reacted to form purely aluminous types. Ring like clusters of alumina particles have often been observed in the cores of rimming steel ingots and it is now thought that these rings constitute the undispersed products of reactions of the type just outlined.

Aluminous inclusions can also arise from the reaction of

the excess aluminium with the refractories of the vessels containing the steel, (61). In general, the refractory erosion products produced early in the steelmaking process have sufficient time to be eliminated from the melt, and it is the erosion and corrosion products from the ladle refractories and runner assemblies that constitute the major sources of exogenous inclusions. During teeming, erosion of the ladle nozzle is particularly severe and modern practices use high grade nozzle inserts, such as zirconium silicate or magnesite, in order to minimise the effect. The build up of large alumina aggregates in the bore of the ladle nozzle, during the teeming of aluminium killed grain refined steels, has been frequently observed (1) and is a characteristic of all deoxidizers precipitating solid deoxidation products, (13). Apart from the constrictive effects of such deposits, they are intermittently dislodged and can give rise to gross internal defects in wrought product. Similar local accumulations have been observed in uphill teeming holloware and the problem is so acute during the continuous casting operation that various preventative techniques have been developed.

(ii)   Calcium Aluminates

Thermodynamically calcium is one of the strongest oxide and sulphide forming elements available to the steelmaker, and its use in sulphide modification has already been reviewed, SECTION 2.1.1. (iii). Because of its strong oxide forming potential, modification of the refractory oxide inclusions, formed on deoxidation by aluminium, is also a practical reality. FIG.14b. The difficulties of making calcium additions, and the measures taken to minimise these have already been reviewed.

According to Pickering (12) small additions of the modern calcium bearing aluminium alloys can produce purely aluminous inclusions due to losses of calcium by surface oxidation, but moderate additions can produce calcium aluminates containing up to 30% CaO. As can be seen from the $CaO-Al_2O_3$ phase diagram, FIG. 7 these

inclusions are liquid at steelmaking temperatures and coalesce easily
to form larger more easily eliminated inclusions. Because they
are liquid they do not form the very large aggregates formed by
alumina and the substitution of alumina clusters by softer and less
r efractory calcium rich calcium aluminates provides a method of
preventing the formation of the injurious fragmentary alumina
stringers usually associated with aluminium killed steel. Several
workers have also reported improved steel cleanliness by the use of
the modern calcium-aluminium deoxidants as opposed to deoxidation by
Al alone (62 - 64).

Because of the difficulties associated with adding calcium to
steel melts, Engh and others (64) have attempted to modify the
existing aluminous inclusions by injecting lime bearing slag powder
directly into the melt. Preliminary work indicates that very low
residual oxygen levels of 5 - 10 ppm can be obtained using this
technique and that the normal inclusion population is replaced by mixed
oxysulphides with high calcium contents. The removal of sulphur by
this technique is of obvious benefit, and the association of calcium
sulphide with the calcium aluminates produced can have a significant
effect in improving the fatigue properties.

Calcium aluminates have been observed in non-calcium
treated steels resulting from the reaction of admixed slag particles
with dissolved aluminium (16). All five types of calcium aluminate have
been observed during the steelmaking process and it has been reported
that the more aluminous types are eliminated from the melt more
rapidly than the calcium rich types (16). Pickering (7) states that
the most aluminous form, $CaO.6Al_2O_3$, has the δ alumina structure
and because of its high melting point forms as clusters of irregular
particles akin to those formed by alumina. The less aluminous forms
are most frequently observed as components of multiphase inclusions
in which calcium sulphide is frequently observed as a peripheral
phase.

(iii) Mangano-Wustite Inclusions

Wustite and manganosite form a continuous series of solid solutions which are precipitated from oxygen rich melts by monotectic reaction, FIG. 8. The globules can occur as either large primary deoxidation products or more usually as a fine dispersion of liquid globules formed interdendritically during the solidification of the ingot. They are frequently encountered in such a form in rimming steel ingots where their composition may vary widely, depending on the manganese content of the melt. Because of its relatively high melting point, $1850^{\circ}C$. (65), pure manganosite and the more manganiferous oxides form as translucent idiomorphic or dendritic crystals (66). Although they form a continuous series of solid solutions, FeO-MnO globules are sometimes encountered which contain a second phase. Pickering (7) states that in many cases these second phases are rich in manganese, the inclusion initially being precipitated as a solid manganese rich oxide in the molten steel. During subsequent solidification wustite precipitates on the solid nucleus, the cooling rate being such that equilibrium is not attained. The resulting inclusions are apparently two phased, but are in fact non-equilibrium products. Fischer and Fleischer (67) found that the initially precipitated globules were rich in iron, but provided that cooling was sufficiently slow diffusional equilibrium could be approached. Yavoiskii and Haase (68) have shown that significant changes in the composition of mangano-wustite inclusions can take place on reheating, equilibrium often taking several hours at temperatures between 1000 and 1300 $^{\circ}C$. FIG. 9. This process is analagous to that reported by Salmon - Cox and Charles (9) in the case of manganese sulphides. Sloman and Evans (69) have reported that some duplex manganowustite inclusions contain manganese sulphide as the second phase.

The other oxides of iron, Haematite (Fe_2O_3) and Magnetite (Fe_3O_4) are seldom, if ever, found as the constituents of inclusions, and although wustite should decompose below $560^{\circ}C$. FIG. 8, this reaction has not been observed in the case of non-metallic inclusions, although precipitation may occur at sub-microscopic levels.

(iv)   Silicate Inclusions

Crystalline iron-manganese silicates are often observed in rimming steel ingots and are produced when small fragments of entrained scum become trapped at the advancing dendritic interface during the rimming period (60). These silicates are iron and manganese rich, the small proportion of silica arising from the low silicon content normally present in these steels. Silicon in the form of ferrosilicon and silicomanganese, is often employed to deoxidize melts which are to be used in the production of steels requiring good surface finishes, manganese and silicon being employed in combination because of their synergistic effect on the deoxidation process (22).

The $FeO-MnO-SiO_2$ system is shown in FIG.10 and contains three binary compounds in addition to the three component oxides. This system contains no ternary compounds. The olivine phases Fayalite, $2FeO.SiO_2$, and Tephroite $2MnO.SiO_2$, are isostructural, belong to the orthorhombic system, and exhibit complete mutual solubility (7). When present as a primary precipitate they have a characteristic lath like morphology (65) but are more frequently observed as one of the constituents of a eutectic matrix associated with primary manganowustite dendrites. The mono-silicate phase Rhodonite, $MnO.SiO_2$ is only partially substituted by FeO, the corresponding iron monosilicate, Grunerite $FeO.SiO_2$, being reported to be unstable when pure (70) although Kiessling (65) states that the phase may be stabilized by CaO and MgO. Inclusions containing Rhodonite have seldom been reported.

There have been a number of investigations on the deoxidation of iron with silicon, (71 - 78). At low silicon levels duplex crystalline inclusions consisting of primary manganowustite dendrites in a eutectic matrix are produced. At higher silicon levels these pass into the olivine region of the phase system, FIG.10, and occasional single phased inclusions of either Fayalite - Tephroite or Rhodonite have been observed (60, 65). At higher silicon levels the products of deoxidation are usually glassy and are often duplex, having compositions lying within the liquid miscibility gap which extends

right across the ternary system.

Under certain circumstances during silicon deoxidation the inclusions can develop a 'raspberry' morphology (71, 76, 78 - 80). These are usually observed in rapidly chilled specimens (79) and reduced agitation is reported to favour their formation (78). They are reported to be a form of vitreous silica (79) and are composed of a central inclusion surrounded by smaller satellite inclusions which are often joined to the main body. Zapffe and Simms (76) explain their morphology as a coalescence phenomenon, whereas Turpin and Elliott (79) and Torsell (78) postulate a growth theory. Hillert and Hillert (80) accept the view that these inclusions are a form of vitreous silica and argue that the rosette precipitates frequently observed in siliceous slags and siliceous inclusions are of the same type. However, these precipitates have been traditionally regarded as Cristobalite rosettes, produced by the crystallization of silica from the slag or inclusion, (60, 65, 81). More recently Shiraiwa (81) has observed the precipitation of these rosettes from glassy siliceous synthetic slags, on reheating to temperatures in the range 900 - 1400°C. At temperatures below 1470°C Cristobalite is unstable with respect to the Tridymite modification and although FeO and MnO are known to stabilize the cristobalite form (82), it is difficult to under-stand how this form can precipitate in preference to Tridymite at such low temperatures.

Silica can also occur in two other crystalline forms, Quartz and Tridymite. The tridymite modification has been reported to occur as a lath or needle-like phase in synthetic slags and complex inclusions of exogenous origin, whilst Quartz is usually reported as a blocky or angular phase in similar inclusions. It is, however, unusual to find crystalline silica as a constituent of non-metallic inclusions, it more usually occurring in the vitreous form.

The ferrosilicon, ferromanganese and silicomanganese deoxidants used are rarely pure and often contain one or two percent of stronger deoxidants which can play a disproportionate role in the deoxidation reactions (1, 11, 16, 83). Morgan et al (56) found that the siliceous inclusions produced on deoxidizing a conventionally

produced carbon-manganese steel with commercial ferrosilicon and calcium silicide could contain as much as 40% of alumina, due to the presence of $1\frac{1}{2}$ Wt % of aluminium in the deoxidants used. The appearance of manganese alumino-silicates in nominally silicon-manganese deoxidized steels is well understood in these terms.

The $MnO-Al_2O_3-SiO_2$ and $FeO-Al_2O_3-SiO_2$ systems are shown in FIGS. 11 and 12. The similarity of the systems is obvious, and is to be expected from the chemical similarity of the manganosite and wustite phases. The systems differ in the additional binary compound Rhodonite ($MnO-SiO_2$) present in the $MnO-SiO_2$ systems and the ternary compound Spessartite ($3MnO.Al_2O_3.3SiO_2$) whose iron counterpart Alamandine is reported not to occur in slags cooled from the liquid phase (84). Because of the inevitable presence of manganese in commercial steels the $MnO-Al_2O_3-SiO_2$ system is the more relevant when considering inclusion phase equilibria. The phases present are summarised in TABLE 2. The binary phases Tephroite and Rhodonite and the phases Wustite, Manganosite and Silica have been discussed previously. The binary alumino-silicate phase Mullite ($3Al_2O_3.2SiO_2$) has been observed in the inclusions in steels where reactions have occurred between iron-manganese silicates and the dissolved Aluminium (59) but is more usually observed as one of the constituents of complex erosion silicates of exogenous origin. The spinel phase Galaxite ($MnO.Al_2O_3$) is a common constituent in aluminium treated steels and Pickering (60) reports that this phase can occur as a dendritic precipitate in the silicate inclusions present in rimming steels. The iron form Hercynite ($FeO.Al_2O_3$) is not a common constituent due to the usual presence of manganese. The ternary garnet phase Spessartite ($3MnO.Al_2O_3.3SiO_2$) is only infrequently observed although Kiessling (11) states that it may be precipitated from glassy manganese-alumino silicates on heat treatment below 1195°C. The ternary cordierite phase ($2MnO.2Al_2O_3.5SiO_2$) is not reported to occur as a constituent in non-metallic inclusions.

Many steels are deoxidized by manganese and silicon, where the formation of refractory oxide clusters must be avoided or where nitrogen must not be removed from solution. In many cases however, the deoxidizing power of these elements is insufficient to prevent the formation of secondary inclusions upon solidification. In order to reach lower oxygen levels and prevent the formation of secondary inclusions, deoxidants containing calcium are used to supplement preliminary deoxidation by silicon and manganese. However, because these alloys usually contain one or two percent of other strong deoxidizers, such as aluminium, it is unusual to find simple manganese calcium silicates, calcium alumino silicates being the more usual form. These inclusions are usually single phased glassy silicates, only infrequently containing crystalline phases in spite of the great number of compounds in the $CaO-Al_2O_3-SiO_2$ system FIG. 13. However, crystalline phases may be precipitated on extended heat treatments.

(v) <u>Other Silicates</u>

Chromium and stainless steels often contain inclusions which contain chromium oxides, the spinel Chromite ($FeO.Cr_2O_3$) being frequently observed as isolated angular idiomorphs or as skeletal networks (7). Pickering has reported that chromite dendrites can precipitate from silicates formed at high temperatures (85). Spinel itself ($MgO.Al_2O_3$) is often observed as a constituent in slag or refractory inclusions, when they react with dissolved aluminium. It is also frequently observed in association with calcium aluminates when originating from a slag source, due to reaction of admixed slag particles with the dissolved aluminium, (11,16). Titanium and Zirconium oxides are also found, usually in small quantities, in eroded or corroded exogenous types. The oxides produced by the rare earths have been discussed in SECTION 2.1.1.

During hot working, zones of shear flow are set up within the bulk of the material being deformed. Any non-metallic inclusions contained within these zones are subjected to combinations of compressive and shear stresses and tend to deform in sympathy with the surrounding matrix. Whether these inclusions actually deform, or whether they maintain their as cast morphology, is dependant on a number of factors, not least of which is the strength of the inclusion relative to that of the surrounding matrix. Inclusions which behave plastically at the working temperature become elongated in the direction of working, non-plastic inclusions may maintain their original morphology or, if the shear stresses are of sufficient magnitude, may become fractured and disseminated along the lines of metal flow, forming long thin fragmentary stringers.

2.2.1   The Assessment of Inclusion Deformation

There have now been a number of investigations into the behaviour of non-metallic inclusions during working (86 - 114) and a method of assessing the overall inclusion deformation has been evolved. Since it is not possible to determine the absolute plasticity of the inclusions in situ, at the temperature of deformation, it has been customary to assess their deformation by comparison with the deformation of the steel, the ratio of inclusion to matrix deformation being termed the 'Relative plasticity', 'Relative Deformability' or 'Plasticity Index' and is given the symbol V .

The first extensive investigation into the effects of deformation on the morphology of second phase particles was reported by Unkle (86) as early as 1936, although several earlier papers had made reference to the behaviour of second phase particles during deformation (87 - 90). Unkle reported the effects of cold rolling on the morphologies of the second phase in duplex alloys belonging to the systems Cu-Zn, Pb-Cu-Zn, Fe-Cu, Cu-Sn and Al-Si. The

parameter used to assess the deformation of the second phase was
the ratio of the fractional reduction of the second phase to that
of the matrix, the initial and final diameters of the matrix and
second phase grains being determined on a statistical basis by lineal
analysis, in the short transverse direction

$$\frac{\frac{\Delta h}{h}}{\frac{\Delta H}{H}} = V$$

where

h = initial diameter of the second phase grains

Δh = change in diameter of the second phase grains

H = initial matrix grain size

ΔH = change in matrix grain diameter

Schiel and Schnell (91) further developed this concept of
comparing the deformation of the inclusions with that of the steel
sample. Cylindrical steel samples containing oxide and sulphide
inclusions were compressed, at various temperatures, and the
aspect ratios of the elliptically deformed inclusions were determined.
The ratio of this parameter with the diameter to thickness ratio of
the deformed steel sample was used as the deformability index of
the inclusions.

$$V = \frac{(a/b)_i}{(a/b)_m}$$

where

a_i = Major semi-axis of the deformed inclusion

b_i = Minor semi-axis of the deformed inclusion

a_m = Diameter of the compressed sample

b_m = Thickness of the compressed sample

Pickering (93) used a similar method for assessing the
deformability of the inclusions in hot rolled steel bar. However in

this case the aspect ratios of the deformed samples were calculated from the cross sectional areas of the specimens before and after deformation. In this case the inclusions were deformed into rotary ellipsoids and the results obtained are not directly comparable with those obtained by Schiel and Schnell which were obtained for the case of prolate ellipsoids.

The concept of using the ratio of inclusion to matrix deformation as the index of plasticity was further developed by Malkiewicz and Rudnik (93) who showed that the true strain of the deformed inclusions, assuming an initial spherical morphology, could be obtained from their aspect ratio after deformation. It can be shown APPENDIX 1 that the true strain of the deformed inclusion is equal to the natural logarithm of the aspect ratio, multiplied by 2/3 for the case of cylindrical strain or by 1/2 for plane strain.

$$\varepsilon_i = \log_e(\lambda)^{\beta}$$

the relative plasticity of the deformed inclusion is then simply

$$V = \frac{\varepsilon_i}{\varepsilon_m} = \frac{\beta \log_e \lambda}{\log_e H}$$

where

   ε_i = Inclusion true strain

   ε_m = Matrix true strain

   β = Factor of 1/2 for plane strain

      or 2/3 for cylindrical strain

   λ = Inclusion aspect ratio after deformation

   H = Matrix reduction ratio

This method of determining the relative plasticity has been used successfully in a number of subsequent investigations and Pickering's results (93) can be converted into this form by taking

their logarithms. Even though the method is mathematically correct it does have one or two inherent weaknesses. Firstly the inclusions are assumed to deform into a prolate spheroid morphology whose aspect ratio is constant in any plane perpendicular to the plane of the elliptic. Although this is approximately true in the initial stages of deformation, it does not adequately describe the situation at high strains, where the inclusions become irregular in form and of variable thickness. Secondly, the method is of a highly subjective nature, the choice of inclusions whose aspect ratio will be measured usually being entirely arbitary, and will normally lead to a bias towards the larger more easily measured inclusions. Finally it has been found that the relative plasticity varies with inclusion size and may be further complicated by a variation in inclusion composition with size (94). However, provided these limitations are borne in mind, the method provides one of the more useful tools for investigating the effects of deformation on inclusion morphology.

Malkiwicz and Rudnik (93) tried to minimize the effects of size variation by the use of a statistical approach to their measurements, but in order to eliminate the subjective influence of microscopical assessment, Baker and Charles (95) utilized the advantages of Quantitative Television Microscopy (Q.T.M.) in determining the plasticity indices of sulphide inclusions. These workers showed that the true strain of the inclusion was related to its projected length, in the longitudinal plane, by the equation, APPENDIX 2

$$\mathcal{E}_i = \log_e {}^{Pl}/_{Po}$$

where

     Po = The projected length per unit area before deformation

     Pl = The projected length per unit area after deformation

The derivation assumes a constant volume fraction of inclusions and is a condition not usually met in practice. These workers suggested that such errors could be corrected for by

multiplying the Projected Length (P. L.) by the ratio of the average to observed area fractions. This is equivalent to dividing each (P. L.) measurement by the measured area fraction.

$$\varepsilon_i = \log_e \frac{P_1/A_1}{P_o/A_o}$$

where

A_o = The area fraction in the underformed sample

A_1 = The area fraction in the deformed sample

However, this correction is only applicable to those cases where the difference in area fraction is due entirely to differences in the number of inclusions. Where the difference is due to a difference in the size distribution the suggested correction is likely to introduce errors rather than to eliminate them. This arises because the area of the inclusions is a function of the square of the radius whilst the projected length is in simple proportion to the radius.

In spite of this limitation, the concept of using the projected length has proved very reliable in predicting the effects of inclusions on the mechanical properties, particularly in the short, transverse direction, and assessments of steel cleanliness based on projected length measurements are found to be more useful than the older more empirical methods (96).

In a recent review by Gladman (97) a method is outlined for the determination of projected length which does not involve the use of advanced electronic instruments. It is shown that the projected inclusion length per unit area is numerically equal to the number of inclusions per unit length, intersected by a line perpendicular to the plane of projection. However, the method is based on the assumption of a random distribution of uniformly sized spheres, prior to deformation, and whether this model is a reliable approximation to the true situation is questionable. Even so, the method may prove useful as a laboratory check for the cleanliness of steel products, possibly to supplement, or even replace, the older more subjective assessments.

2.2.2. Factors Affecting Inclusion Behaviour

(i)   The Effects of Inclusion and Matrix Strength

One of the more predominant factors governing the behaviour of an inclusion, inside a deforming matrix, is its strength relative to that of the matrix. The relationship between this parameter, β , and the relative plasticity exhibited by the inclusions has been the subject of much investigation, both experimentally and theoretically, but its precise influence on inclusion behaviour is only now beginning to be understood. Results reported by various workers show different relationships between these parameters, although the expected trend towards decreasing relative plasticity with increasing relative strength is generally agreed.

Unkle (86) presented his results in graphical form relating the relative plasticity of the second phases to the yield strength ratio (INCLUSION:MATRIX) FIG. 15. These results indicate an upper limiting relative plasticity of the order of 1.6 for inclusions of zero-relative strength. Second phases of the same strength as the matrix were assumed to deform as the matrix deforms ($V = 1$) whilst phases harder than the matrix were found to deform less, phases with relative strengths of the order of 6 exhibiting almost zero relative plasticity.

Zeisloft and Hosford (98) deformed samples containing cylindrical synthetic inclusions of known flow stress, by both plane strain and uniaxial compression. The materials used in the investigation were soft white metal alloys of lead, tin and antimony, their relative plasticity being determined from their aspect ratios, after deformation, in accordance with the equations defined by Malkiewicz and Rudnik, (93). By plotting inclusion strain vs matrix strain values of the relative plasticity ($\mathcal{E}_i / \mathcal{E}_m$) were obtained for low matrix strains, which were then plotted against the flow stress ratio β , FIGS. 16 and 17. These workers found that as the flow stress ratio tended towards zero, the relative plasticity tended towards 3.0, a value of 2.9 being obtained for the case of water

inclusions in a Woods metal matrix. As the relative strengths increased, the relative plasticity decreased, being unity when the relative strength was unity. As the relative strength approached 2.0 the relative plasticity fell towards zero.

These results are very different from those obtained by Unkle, which were almost of a parabolic form and showed measurable plasticities at much greater relative strengths. The significance of this difference is discussed later.

Sundstrom (99) has extended a mathematical analysis by McClintock (100) on the deformation of holes, to the case of a plastic inclusion inside a plastic plate. The analysis takes the case for the plastic deformation of an ellipsoidal inclusion in an infinite plate deforming by plane strain, and is based on a strain hardening model in which both the inclusion and the matrix behave in accordance with an equation of the form,;

$$\sigma = \sigma_o \, \varepsilon^n$$

where

σ = The flow stress

σ_o = The initial flow stress

ε = The true strain

n = The work hardening exponent

The analysis assumes that the work hardening exponent is the same for both the inclusion and matrix materials, and consequently only approximates to the real situation. The solution obtained by Sundstrom is

$$\nu = \frac{\varepsilon_i}{\varepsilon_m} = \frac{2\,\frac{\text{Sinh}\,(1-n)}{(1-n)}}{2 + (\beta^{1/n} - 1)}$$

where

ν = The relative plasticity at zero strain

ε_i = The inclusion true strain

$\mathcal{E}_m$ = The matrix true strain

n = The work hardening exponent of both the inclusion and the matrix

β = The relative strength (flow stress ratio) of the inclusion

This result is plotted in FIG. 18 for various values of n; the results of Zeisloft and Hosford are included for comparison. This solution predicts, for materials having a low work hardening exponent (< 0.3), that inclusions having a flow stress greater than twice that of the matrix will show little tendency to deform, whilst inclusions which are fluid will deform little more than twice as much as the matrix. The agreement between Sundstrom's model at low 'n' values, and Zeisloft and Hosford's experimental results is quite marked, Sundstrom pointing out that the experimental results obtained at low values of β , where agreement is poorest, may in fact be too high due to inclusion volume changes occurring during the deformation. However, during normal hot working treatments there is little, if any, evidence to suppose that the inclusions work harden to any extent, let alone at the same rate as the matrix, and Sundstroms model would be expected to fit more closely those results obtained at lower temperatures where work hardening effects are more significant. Unkle's results, which were obtained at temperatures where a high degree of work hardening did occur, do in fact fit Sundstroms result quite closely, for values of n greater than 0.6, Compare FIGS. 15 and 18. Although there seems to be good agreement between the experimental data and Sundstrom's model, under conditions where work hardening is significant, the applicability of this model to conditions where work hardening is less significant is open to doubt.

Klevebring (101) has obtained theoretical values for the relative plasticities of manganese sulphides, directly from Sundstrom's equation, by substitution of a hot hardness ratio in place

of the flow stress ratio β . The hot hardness of the sulphide was obtained from the published data of Mann and Van Vlack (102). The variation of the theoretical relative plasticity with temperature obtained by this method is shown in FIG. 19 which also shows the experimentally determined values of Gove and Charles (103) for comparison. The agreement between the two curves is remarkable, although some scatter in the theoretical values should be noted. The same author also shows a similar agreement for the variation of the relative plasticity of manganese selenide with temperature.

It should be pointed out that the values of relative plasticity derived from a theoretical standpoint are those values that would be exhibited by an inclusion as it begins to deform from the spheroidal state. Since the relative plasticity decreases as the strain increases, (SECTION 2.2.2. (iii)), care must be taken when comparing experimentally determined values and those values predicted theoretically. The values already quoted from Zeisloft and Hosford (98) and Gove and Charles (103) do, in fact, relate to zero state of deformation and can be legitimately compared to those values predicted from Sundstrom's model. Those results quoted from Unkle (86) were calculated on a different basis and should be compared qualitatively.

Warrick and Van Vlack (104) have studied the effects of sample and deformation parameters on the fracture and deformation of included non-metallic phases. The model system used, employed the F.C.C. metals Pb, Al, Ag, Cu and brass as the matrix phase in which NaCl type ionic solids were dispersed as the inclusion materials. Samples were prepared by powder metallurgical techniques, and deformation performed by extrusion at both sub-zero and elevated temperatures. The amount of deformation of the inclusions was assessed in rather a complex manner, necessitated by the change in the type of deformation occurring between the surface and centre of the extruded bar, the surface deformation approximating

to conditions of plane strain, the centre deforming under conditions of cylindrical strain. The matrix and inclusion hardness were determined at the temperature of deformation using a modified micro-hardness testing machine. The deformation of the inclusions lying along the centre lines of the extruded samples was assessed by measurement of their aspect ratios, FIG. 20, and replotting these results in terms of the inclusion true strain, a plot of inclusion relative plasticity vs. relative hardness is obtained which can be compared with the results of Zeisloft and Hosford (98) and Sundstrom (99) FIG. 21. However, it must be remembered that these results were obtained at a matrix true strain of 1.4 (75% R.A.) whilst the other plots relate to a zero state of strain and are thus of higher plasticities. The general shape of the graph thus obtained conforms to the general form of Zeisloft and Hosfords results and Sundstrom's model (n < 0.4) and would probably lie even nearer to them if it were possible to correct the results for zero state of deformation. The only area showing significant deviation lies at high values of relative hardness where a small but measurable plasticity is present at values of β greater than 3.0. As with previous results, the graph passes close to the 1:1 co-ordinates.

More recently Gove and Charles (103) have reported a method of determining the relative plasticity of inclusions based on in situ micro-hardness determinations, of the inclusion and matrix, at the temperature of deformation. Various model systems were also employed to simulate the behaviour of inclusions of relative strengths, which were not easily obtained in real inclusion systems. By plotting the relative plasticities of these systems, at zero matrix strain, versus the measured inclusion relative hardness, they obtained an empirical relationship between the relative plasticity and relative hardness of the inclusions of the form,

$$\nu = 2 - \frac{H_i}{H_m} \qquad 0 \leqslant \nu \leqslant 2$$

where

V = Relative plasticity at zero strain

H_i = Inclusion hardness

H_m = Matrix hardness

As can be seen from FIG. 22 these results show a linear relationship between the relative plasticity and relative hardness, for a wide variety of inclusion systems. It has been suggested that the difference between these results and Sundstrom's model may be due to some deviation of the real system from Sundstroms assumption of the equality of inclusion and matrix work hardening rates (105). However, many of the plasticity values used in this work were obtained at relatively low deformation temperatures where work hardening effects can be expected to be more significant, and the use of a higher work hardening exponent in Sundstrom's equation does, in fact, predict a more linear relationship, curves for n = 0. 25 and 0. 8 being included in Fig. 22 for comparison.

Gay (106) has analysed the behaviour of spherical and eliptical particles, deformed by pure and simple shear, inside a Newtonian fluid matrix. The particles so treated were also viscous bodies, but their relative viscosities (Particle:matrix) were allowed to vary between wide limits. The analysis derives the relationship

$$\log_e (^a/b) = \log_e \left(\frac{a_i}{b_i} \right) + \left(\frac{5}{2R + 3} \right) \log_3 \left(\frac{\lambda_1}{\lambda_2} \right)^{\frac{1}{2}}$$

where

$^a/b$ = The axial ratio of the deformed particle

a_i/b_i = The axial ratio of the undeformed particle

R = The relative viscosity of the particle

$\left(\frac{\lambda_1}{\lambda_2} \right)^{\frac{1}{2}}$ = The axial ratio of the strain ellipse

Converting these parameters to the form used previously one obtains

$$2\,\varepsilon_i = 2(\varepsilon_i)_0 + \left(\frac{5}{2\beta + 3}\right) 2\,\varepsilon_m$$

where

ε_i = Inclusion true strain

$(\varepsilon_i)_0$ = Initial inclusion strain (usually zero)

β = Viscosity ratio

ε_m = Matrix true strain

Rearranging

$$V = \frac{\varepsilon_i}{\varepsilon_m} = \frac{5}{2\beta + 3}$$

where

V = The inclusion relative plasticity

The result is plotted in FIG. 23 where it is compared with Sundstrom's equation for the case of n = 0.8. Because Gay's model was based on a non-hardening Newtonian fluid matrix the result is unlikely to be completely valid in the case of non-metallic inclusions in steel, particularly at lower temperatures, but the result will serve as a useful comparison. This result indicates that inclusions having a very low relative viscosity should exhibit relative plasticities in the region of 1.7, which is rather low when compared with measured values. As with previous analyses a relative plasticity of unity is obtained at unit relative viscosity. At high values of relative viscosity the result differs significantly from Zeisloft and Hosford, and Warrick and Van Vlack's results, relative plasticities in the region of 0.5 being obtained as a relative viscosity of 3.0. The similarity of Gay's result and Sundstrom's equation (for n = 1) is quite marked.

$$V = \frac{5}{2\beta + 3} \qquad \text{Gay}$$

$$V = \frac{2}{\beta + 1} \qquad \text{Sundstrom} \quad (n = 1)$$

In the discussion of Unkle's paper (86) Rohn suggested that
the nature of the matrix flow around a second phase particle was
likely to be affected by the adhesion of the particle to the matrix, and
would obviously affect the behaviour of the inclusion. In those cases
where the adhesion of the inclusion to the surrounding matrix is less
than the cohesion of the matrix phase itself, then the shearing stresses
operating in the matrix will be able to break the interfacial bonds and
some degree of interface sliding will occur. At low relative strengths,
the inclusion is already trying to deform in excess of the matrix and
the interface bonding should have little effect. In fact in reply to
Rohn's observations Unkle presented evidence to suggest that this was
indeed the case. However, at higher strength ratios the interfacial
bonding can become of primary importance since a lack of bonding will
lead to a reduced relative plasticity.

A recent investigation by Ashok (107),into the effects of interface
adhesion,has shown that this parameter can assume as great a
significance as the relative strength in controlling the behaviour of
relatively hard second phases. This worker found that unbonded
inclusions of the same phase as the matrix (for example copper rods
inserted into holes drilled in a copper block), could in fact exhibit
relative plasticities significantly less than unity. Only when the
inclusion was strongly bonded to the matrix was a relative plasticity
of unity obtained for a relative strength of unity. In fact, Maunder
and Charles (114) had previously commented on the observation of
sulphide inclusion relative plasticities of less than unity when Chao
(133)had shown their relative hardness also to be less than unity. At
even greater relative strengths significant relative plasticities were
obtained in the case of strongly bonded second phases whilst unbonded
types exhibited rigid behaviour. Ashok's results are summarized
in FIG. 24 which indicates the marked difference in behaviour of
unbonded and bonded types.

If Unkle's results are replotted in terms of inclusion and matrix
true strains FIG. 25, the gradient at $\mathcal{E}_m = 0$ can be used to obtain

a more conventional form of the relative plasticity vs. relative strength relationship FIG. 26. If the form of this plot is compared to that obtained by Ashok for the strongly bonded inclusions it will be seen that the two curves are almost identical FIG. 24. This is not entirely unexpected since Unkle's results were also obtained for the case of strongly bonded second phase particles. The form of these graphs closely resemble those obtained by Gay and Sundstrom ($n >$ 0.6) and it is likely that these mathematical relationships do not apply to the case of unbonded or weakly bonded second phases where the shear stresses are not fully transferred across the inclusion-matrix interface.

In summary - the investigations reported to date indicate that an upper limiting relative plasticity is exhibited by inclusions of zero relative strength. Estimates of this limit vary from Zeisloft and Hosford's experimental value of 2.9 (98) down to Gay's theoretical limit of 1.7 (106), a value in the region of 2.0 - 2.3 being favoured by most investigators. It is interesting to note that in Unkle's original work (86) a semi-quantitative expression is derived which predicts an upper limiting relative plasticity of e, (2.7) for the case of inclusions of zero relative strength.

At higher relative strengths, the effects of interface adhesion become increasingly important, the difference in behaviour of bonded and unbonded inclusions becoming very significant. This undoubtedly accounts for the difference between Unkle's results and Gay (106) and Sundstrom's (99) mathematical models on the one hand and Zeisloft and Hosford (98), Warrick and Van Vlack (104), and Gove and Charles' (103) results on the other. In the case of strongly bonded inclusions significant deformation can occur with relative strengths as high as 6.0, whilst in the case of unbonded types little or no deformation is observed with relative strengths in excess of 2.0. The discrepancy between Zeisloft and Hosford's results and those of Gove and Charles lies mainly in the region of relative strengths 0 - 1.0. This may be due to void closure causing volume

changes, in the case of Zeisloft and Hosford's results, resulting in anomalously high relative plasticities in this region of relative strengths.

Since most non-metallic inclusions in steel are either unbonded or only weakly bonded to the matrix the results obtained by Unkle and the mathematical models developed by Gay and Sundstrom are possibly not representative of the situation regarding inclusions in steel, and behaviour more in accordance with Gove and Charles, and Ashok's results is more likely.

(ii)   The Effect of the Degree of Deformation

Although the initial plasticity exhibited by an inclusion might be quite different from that of the matrix, as it deforms the interfacial area, over which the matrix shear stresses can act, increases and the inclusion should become increasingly constrained to deform to the same extent as the matrix.   Logically, it would be expected that inclusions which are initially more plastic than the matrix should exhibit a decreasing rate of deformation with increasing matrix strain, whilst inclusions initially less plastic should show an increasing rate of strain, ultimately both types exhibiting the same rate of strain as the matrix.   This situation is shown schematically in FIG. 27 which is taken from the work of Smith (108) who states that very elongate inclusion forms will be constrained to deform at the same rate as their surroundings irrespective of their viscosity relative to that of the matrix.

In the real system, however, it has been found that the relative plasticity of the inclusions invariably decreases with increasing strain, irrespective of its initial value, and that the final relative plasticity, at high strains, is usually much lower than unity. (91, 92, 93, 95, 103).   The reason for the difference in behaviour between the ideal and real situations lies once more in the low work of adhesion of the inclusion-matrix interface.   In order to constrain

the inclusion to deform as the matrix deforms the matrix has to transfer a shear force, via the interface, onto the inclusion. Where a strong interface exists this can be done quite easily and the inclusion will deform as dictated by the matrix flow. In the case of a weakly bonded interface, interface sliding is able to occur and the inclusions deform with a decreasing rate as the matrix strain increases. In fact Zeisloft and Hosfords results exhibit the effect of increasing matrix constraint in the case of inclusions initially more plastic than the matrix, although those inclusions initially less plastic exhibit more linear behaviour FIG. 16.

A number of theories have been proposed to explain the observed decrease in relative plasticity with increasing matrix strain. Pickering (92) postulated that crystalline mangano-wustite inclusions may work harden appreciably more than the matrix, and thus increase their relative strength, as the deformation progressed. If it is valid then this proposal will also explain the observed reduction in the relative plasticity of manganese sulphides with increasing strain (95), since these are also crystalline at hot working temperatures. Although dislocation structures have been observed in manganese sulphide inclusions (109, 110) there is no evidence to suggest that these materials work harden appreciably at normal hot working temperatures. In fact Moore (111) found no difference in the hardness of sulphide inclusions before and after deformation, although it must be noted that this worker did experience some difficulty in obtaining accurate hardness measurements on the highly deformed sulphides. Uchiyama and Sumita (112) have however reported that the room temperature hardness of mangano-wustite inclusions is increased after hot working. Pickering (92) also suggested that as the inclusions become elongated t hey offer less impedence to the flow of the matrix around them so that the interfacial forces causing their deformation decrease, resulting in a reduced relative plasticity. This may, in fact, be a very important feature since the elongated inclusions will certainly offer less disturbance to the flow of the matrix during working. However, it must be remembered that this can only apply to those cases where

the inclusions are weakly bonded so that interface sliding can take place. In the case of strongly bonded phases the frictional constraint at the interface will actually increase and the inclusions will behave as dictated by the matrix.

Baker and Charles (95) suggested that the extra energy expended in creating new interface could be responsible for the observed reduction in plasticity. These workers showed that in the case of manganese sulphide inclusions, initially $7\mu m$ in diameter, the work expended in creating new interface, on rolling, amounted to less than 1% of the energy of deformation for a x2 reduction but almost 10% for a x32 reduction. These same workers also proposed that in the case of inclusions initially less deformable than the matrix, regions of frictional constraint are produced in the matrix above and below an elongated inclusion. The size of these 'dead' zones, by analogy with upset forging, increases as the area of interface increases and it is proposed that this accounts for the observed reduction in plasticity. The model system used to demonstrate this effect consisted of 'hard' inclusions of different aspect ratios embedded in layers of plasticine w hich were subsequently deformed. Although regions of constraint were produced in the case of the more elongate form, this was probably due to the adherence of the plasticine to the surface of the synthetic inclusion, thus simulating a strongly bonded inclusion. This shows that the mechanism proposed actually increases the shearing forces acting on a strongly bonded inclusion and is the mechanism by which the plasticity would approach that of the matrix. In the case of weakly bonded inclusions it is unlikely that such regions of constraint would be formed and in fact if a plasticine model is constructed in which the interface between the inclusion and matrix is well lubricated, such zones are not produced FIG. 28.

Gove and Charles have proposed a model whereby the steel matrix in the vicinity of the inclusion-metal interface becomes work

hardened to a greater extent than the bulk matrix. The inclusion thus becomes surrounded by a shell of harder matrix material which deforms less than the bulk and reduces the inclusions relative plasticity. Evidence in support of this mechanism consists of a series of microhardness measurements made around the interface of an aritificial copper inclusion deformed in an iron matrix at 600°C. Although increased hardness in the vicinity of the 'inclusion' is shown, the increase is slight and would probably be minimal at higher rolling temperatures. Again the effects of inclusion-matrix adhesion in this model were not known, and greater local work hardening would be expected to occur around inclusions strongly bonded to the matrix.

Overall it would appear that the effect of inclusion work hardening is not likely to be a significant feature of the deformation behaviour and localised matrix work hardening around the inclusions is probably minimal at normal hot working temperatures. The effects of frictional constraint at the inclusion-matrix interface would be to make the inclusions behave more in sympathy with the matrix, but this would depend on adequate bonding between the inclusion and the matrix. More usually inclusions are unbonded or only weakly bonded and the effects of frictional constraint are eliminated by interface sliding. The reduction in plasticity with increasing strain is most probably due to the decreasing disturbance, caused by the inclusion, to the metal flow as the inclusion becomes thinner, although the effect of energy absorption, due to interface creation, is likely to have an increasing effect at higher strains.

(iii)   Other Factors

Temperature

The temperature of deformation is probably the single most important parameter controlling the behaviour of included phases. The flow stress of both the matrix and the inclusion materials are very dependent on the working temperature and depending on how

these values change with respect to each other with changing temperature, the relative plasticity will be affected accordingly. The effect of working temperature on the behaviour of the various inclusion phases is discussed in SECTION 2.4.

Inclusion Size

Pickering (92), Malkiewics and Rudnik (93), and Uchiyama and Sumita (112) have all reported that larger inclusions tend to display greater plasticities than do smaller inclusions. Although little systematic work on the effect of inclusion size has been reported, there is a consensus of opinion that small inclusions exhibit lower relative plasticities (103, 105, 113). More recent evidence (94) indicates that the relationship between inclusion size and relative plasticity may not be so simple, and may be further complicated by a systematic variation in inclusion composition with the size.

Baker and Charles have suggested that the greater surface to volume ratio of the smaller inclusions may be the cause of their reduced plasticities.

Inclusion Constitution

Inclusion constitution can often be of paramount importance in determining the behaviour of an inclusion during hot working. Multi-phase crystalline silicates often become fragmented on working at low temperatures (92, 113, 114) becoming disseminated into long fragmentary stringers. In such cases fracture often occurs by the decohesion of the interfaces of the component phases, although trans-granular fracture also frequently occurs, (92). In some glassy silicate inclusions, hard internal precipitates may be formed and at high working temperatures the plastic silicate may be completely stripped from the precipitate, producing long tail-like discontinuities extending into the surrounding matrix (92, 95, 114). Alternatively, where finer more numerous precipitates are formed, they may act as mechanical supports and lead to a reduced plasticity, (92, 114). In some cases a highly siliceous glassy phase may be formed, due to

the composition lying within a liquid miscibility gap in the phase system; where the siliceous phase is precipitated as an envelope around the inclusion-matrix interface, the inclusion will be rendered non-plastic to much higher temperatures, unless the rim should become fractured, (141, 142). A similar situation arises when a silicate rim surrounds a sulphide inclusion (95). At low temperatures, where the sulphide has its greatest relative plasticity SECTION 2.4.1, the silicate rim acts as a mechanical support and prevents the inclusion deforming. At high temperatures however, the silicate softens, SECTION 2.4.2, and is stripped from the more rigid sulphide, forming the long tail-like discontinuities previously mentioned.

Strain Rate

Although the flow stress of steel is known to be very sensitive to the strain rate, at hot working temperatures (115) the effects of this parameter on the behaviour of non-metallic inclusions during hot working, has largely been ignored. It is to be expected that increasing the strain rate, which increases the flow stress of the matrix, will give increased values of relative plasticity, due to a reduction in the value of the flow stress ratio . However, should the inclusion have a greater strain rate sensitivity than the matrix, the relative plasticity may in fact be reduced at the higher strain rates, although this would depend on the rate of strain of the inclusion itself rather than that of the bulk sample. Overall the effects of strain rate are likely to be complex and are at present unresearched.

Hydrostatic Pressure

The importance of hydrostatic pressure in rendering apparently brittle substances plastic has been known for many years. Schiel and Schnell (91) referred to the unexpected plasticity of manganese sulphide inclusions, a substance which is usually quite brittle when isolated from its plastic matrix. The reason for this plasticity is undoubtedly the hydrostatic compression to which the sulphide is subjected during rolling. Although the effects of hydrostatic pressure on the behaviour

of inclusionshas not been extensively discussed in the literature, it can be expected to have an effect on inclusion plasticity, and factors such as specimen thickness, rate of deformation, rolling load and roll diameter, all of which affect the magnitude of the hydrostatic pressure, can also be expected to affect the relative plasticity exhibited by the inclusions.

Matrix Composition

Since the flow stress of a steel is a function of its composition, inclusions of the same composition and size can be expected to behave differently when present in steels of different compositions. Although this fact is quite obvious, it is frequently overlooked when the results of different workers are being compared.

2.2.3 Rigid Inclusions and the Formation of Interface Discontinuities

During the hot working of steel it is now well established that matrix discontinuities, in the form of small conical voids, are often produced in association with the interface of the more rigid types of non-metallic inclusions.

Rudnik (116) has investigated the formation of these discontinuities and concludes that they are a feature of the deformation of inclusions having relative plasticities of less than 0.5. Although this worker reports the presence of other defects, such as hot tears and cracks, in association with the voids, these are not unambiguously identified and may well have been a feature of the polishing technique used in preparing the microsections. A possible mechanism for the formation of these voids is also presented. It is suggested that the magnitude of the shearing forces generated at the inclusion-metal interface are sufficient to break the inclusion -metal bonds, causing surface flow of the inclusion and giving rise to a fishtailing effect with an associated conical void, FIG. 29.

Because of its significance to the process of ductile rupture, the formation of voids at second phase particles has received much attention. The stress at which voids are initiated has been shown by

Brown and Embury (117) to be very dependent on the strength of the particle-matrix bond, and Fishmeister, Easterling and Navara (118, 119, 120) have shown that minor quantities of alloying elements can affect the initiation of voids by affecting the work of adhesion of the second phase particles. Sundstrom (121) has shown that the critical stress for void nucleation, at constant work of adhesion, decreases as the particle size increases thus favouring void initiation at the larger less well bonded inclusions. This worker's results indicate that in the case of very weakly bonded particles, such as non-metallic inclusions, small changes in the work of adhesion, such as might be obtained by small changes in alloy content, can significantly affect the void forming potential. For the case of the more strongly bonded phases, significantly greater changes in bond strength are required to cause a similar change in the void forming potential, FIG. 30.

Klevebring (122) has reported the existence of a critical defect size below which voids are not nucleated, although it must be remembered that this size is not constant and is lowered by an increased stress or by decreasing the work of adhesion of the interface. The observation of a decreasing critical size with increasing matrix strain may well be a consequence of the increased stress level produced in the thinner specimen, although this theory does in fact predict a dependency, of the critical inclusion size, on the matrix strain. More recently Klevebring (123) has reported that the critical inclusion size reaches a minimum value at matrix strains in the region of 0.5 - 0.8, above which the critical size again increases. It is also reported that the critical size for manganowustite inclusions ($\sim 4 \mu m$) is about twice that of glassy silicate inclusions ($\sim 2 \mu m$), the difference being reported to be due to the difference in the work of adhesion of the two types of inclusion. On the basis of his results Klevebring states that the ratio of the works of adhesion of Silicate-Fe and (FeMn)0-Fe is 2 to 3. The temperature of deformation is reported to have only a small effect on the critical inclusion size (122), although a significant difference between the behaviour in the austenite and

ferrite regions is exhibited, the critical inclusion size in the austenite region being somewhat larger than in the ferrite region. This may well be an effect due to a small change in the work of adhesion of the inclusions as predicted by Sundstrom (121).

The formation of conical voids during working leads to a decrease in the density of the steel, and provides an indirect method of observing void formation. Gove and Charles (103) have reported on such a method used to follow the course of void formation during the hot rolling process. These workers showed that during the early stages of deformation the density of the steel decreased quite markedly FIG. 31 but eventually reached a minimum value after which the density began to increase. The initial decrease in density was shown to be due to the formation of conical voids which, according to these workers, grew to approximately one sixth of the volume of their associated inclusions. No explanation for the increase in density at the higher strains is given but is presumably due to the closing up of voids produced in the early stages of deformation. At these higher reductions a greater hydrostatic pressure is produced within the strip and Austen and Avitzur (124) and Thomason (125) have shown that this can inhibit the formation of conical voids, and will thus tend to close up those voids produced at an earlier stage in the deformation. The inflection in the plot of density vs matrix strain, at low strains FIG. 31, is stated to indicate the closing of pre-existing voids. However, since Klevebring has already shown that the critical inclusion size for void formation is large, at these low matrix strains (123), the inflection may more simply be explained by the absence of void initiation due to the absence of inclusions of the appropriate size. Void initiation only occurs when a strain is reached where the critical size approaches that of the mean inclusion diameter present in the steel. At higher strains the critical size again increases, voids are no longer produced, and the increased hydrostatic pressure begins to close up the voids already formed. It is interesting to note that the matrix strain at which the minimum density is reached is also the strain at which Klevebring predicts the minimum critical inclusion diameter.

A number of investigations have produced dislocation theories which predict the formation of voids at second phase particles (126 - 132) but the majority of these are concerned with the behaviour of dispersion strengthened alloys, deformed at room temperature, and are not really applicable to the high temperature deformation of materials in which cross slip is a significant feature.

2.2.4 The Deformation Behaviour of the More Common Inclusion Types

(i) The Behaviour of Manganese Sulphides

Manganese sulphide, in common with MgO and other NaCl-type structures can exhibit considerable plastic deformation when embedded within a ductile metal matrix. The hardness of the sulphide with respect to the matrix is the most significant feature controlling this behaviour, and Chao et al (133) have reported the effect of temperature on the hardness of polycrystalline and single crystal manganese sulphides. These forms are reported to exhibit no significant difference in behaviour FIG. 32, although both exhibit a slower rate of decrease in hardness, with respect to temperature, than do various types of plain carbon steel FIG. 33. The manganese sulphides present in steels are rarely pure, SECTION 1.1.1, and these workers also investigated the effect of temperature on the hot hardness of various FeS-MnS compositions. The FeS-MnS system is shown in FIG. 4 from which it can be seen that manganese sulphide can contain up to 72% FeS in solid solution at 1181 ^{o}C. This solubility is however, much reduced on cooling and precipitation of FeS occurs. The hardness of the FeS-MnS solid solutions were found to be slightly greater than for MnS itself, and is not entirely unexpected since the difference in ionic size between Fe^{++} and Mn^{++} is in the region of 9%. However, the hardness of those sulphides which contained precipitated FeS were found to be considerably greater than that of pure MnS. FeS has the NiAs hexagonal lattice type and it is possible that the precipitates produced are initially coherent and produce coherency hardening of

the sulphides. Recent evidence would seem to support this view, coherency fringes having been observed on H.V.E.M. examination of extracted type I manganese sulphides (109). Although precipitation hardening may be a reality at lower temperatures it is unlikely to be effective at normal hot working temperatures where strengthening is more probably due to solid solution effects. The effect of MnO on the sulphide hardness was found to be minimal at temperatures below $800^{\circ}C$, although its effect may be more significant at higher temperatures. The lack of strengthening by MnO was thought to be due to its low solubility in MnS, resulting in it forming grain boundary precipitates within the sulphide, which were reported to render the sulphide brittle. The same authors have also studied the effects of working on the deformation and fracture of oriented single crystal manganese sulphides (134, 135). It was found that the manganese sulphides deformed plastically at normal hot working temperatures, but on cold working exhibited considerable fracturing which was influenced markedly by the orientation of the sulphide.

Schiel and Schnell (91) referred to the deformation of manganese sulphides in their investigation of the deformation of slag inclusions. They reported that the deformability of the sulphides (probably type I) was practically independent of the forging temperature over the range -80 to $1250^{\circ}C$. Dahl (4) however, found that the relative plasticity of the sulphides decreased as the rolling temperature increased, and also showed that the behaviour of the sulphides differed from one type to another. He reports that type I sulphides are deformed to a lesser degree than type III sulphides, although both types were reported to exhibit decreasing deformation with increasing rolling temperature. The behaviour of the type II sulphides was not so well defined due to the formation of long inclusion stringers, by the joining of neighbouring particles, as a result of their vermiform morphology.

Dahl's findings are quite consistant with Chao's hardness data (133), and subsequent investigations (95, 114) have confirmed these findings. One possible explanation for Schiel & Schnell's

erroneous conclusion may have been the limited deformation to which their specimens were subjected.

Maunder and Charles (114) found that the relative plasticity of the sulphides in a commercial $3\frac{1}{2}$ ton, 0.2% C killed steel ingot, decreased with increasing rolling temperature, although these results may be complicated by the presence of more than one type of sulphide in the ingot (9). Baker and Charles (95) have reported an extensive investigation into the effects of deformation on types I and III manganese sulphides. It is shown that type I deform to a lesser extent than the matrix during hot rolling, the relative plasticity decreasing as the rolling temperature increased. The deformability of the type III sulphides was found to be somewhat greater, and was equal to that of the steel matrix at 800°C, although this again decreased with increasing rolling temperature. Gove and Charles (103) have also reported on the behaviour of type I sulphides on rolling, although in this case their relative plasticities at lower working temperatures were reported.

The results reported by these workers are summarised in FIG. 34. The results of Maunder and Charles, and of Baker and Charles, in the case of type I sulphides, show the same overall general trend, although the latter's results lie at somewhat lower values. This is surprising in view of the fact that Maunder's results were taken at a matrix strain of 2.1 (88% reduction) and would be expected to have lower values than measurements extrapolated to the case of zero matrix strain, as in the case of Baker's results. This may, however, be due to the use of Quantitative television microscopy in determining the relative plasticity, in the case of Baker's results, which will include the behaviour of very small inclusions exhibiting much lower plasticities than the larger types. It must be noted, however, that Maunder and Charles reported that the overall reduction of the specimens did not significantly affect the relative plasticity and that the effect of inclusion size was negligible. Gove and Charles' results lie well above those of Baker and Charles, and exhibit values more in line with those that would be expected, at zero strain, on the

basis of Maunder's findings. Baker's results, for the case of the type III sulphides have not been corroborated, but it is likely that these too are lower than would be obtained by optical determination, for the same reasons, although the smaller size of the type III sulphides may reduce the difference.

The effects of deformation on type II sulphides has also been reported by Baker and Charles (136). Because of its morphology, it is not possible to determine the relative plasticity of this sulphide type, in the manner used for globular forms, and the assessment is largely qualitative. These workers found that the as cast sulphide rods were flattened during deformation, but more importantly that the whole of the sulphide colony became rotated into the rolling plane, and markedly reduced the through thickness properties of the rolled material. It was found, however, that a short reheating to a temperature in the region of 1200°C would begin to spherodise the deformed sulphide rods and could refurbish the as cast mechanical properties. Subsequent investigations (137 - 139) have shown that such heat treatments not only spherodise the elongated sulphides, but also produce particle coarsening effects, both of which serve to increase the strength and toughness properties and reduce the anisotropy ratio.

There is now sufficient evidence in the literature to conclude that the relative plasticity of manganese sulphides increase from type I to type III, that of type II being less well defined but possibly either intermediate to types I and III or similar to type III. The reason for the decrease in plasticity is thought to be due to the higher oxygen content of the type I sulphides giving increased high temperature hardness. However, since it is not possible to determine the oxygen content of the manganese sulphides directly by Electron probe microanalysis, due to the masking of OKα lines by MnLα , this postulate is circumstantial, being based on the higher oxygen content of the steels in which type I sulphides are formed. Unfortunately, the FeS content of the sulphides on which the relative plasticity is assessed, is only rarely quoted in the literature, even though, in view of Chao's results (133), this also will have an effect on their plasticity. The FeS content of type I sulphides is likely to be higher than that of types II or III, due to

the effect of the oxygen content, although extended heat treatments may reduce the FeS level and may subsequently affect the relative plasticity. The effect of FeS on the solubility of MnO in MnS is not well known, but if it should increase the solubility, the combined solid solution hardening effects of FeS and MnO may explain the decreased plasticity of type I. The effects of FeS and MnO on sulphide plasticity are currently unknown and these effects are now under separate investigation (140).

(ii)   The Behaviour of Other Sulphides

The solid solution strengthening effects of elements other than iron in manganese sulphide, at high temperatures, have not been investigated. Although Kiessling (11) FIG. 35 gives data for the hardness of MnS containing various amounts of the transition elements from the first long period, these results were obtained at room temperature on quenched specimens and may have little significance to their high temperature effects. Chao did report hot hardness results for manganese sulphide containing 1% CaS in solid solution (133) FIG. 32 which showed that the hot hardness up to 800°C was greater than that of pure MnS. However, at higher temperatures the hardness appeared to decrease rapidly and the hardening effect became unclear. It is likely that greater strengthening, leading to much reduced plasticity, can be achieved by larger amounts of CaS in solution, the solid solution limit being around 12%. Calcium sulphide itself, having a melting point in excess of 2500°C (11) is likely to be non-plastic at working temperatures, as evidenced by the lack of mechanical anisotropy in calcium modified steels.

There has been no systematic investigation of the effects of rare earth treatments on the deformability of the sulphides, reported in the literature. The occurrence of both undeformed and elongated inclusions, often in the same microstructure, in rare earth treated steels is thought to be due to variable or incomplete modification of the sulphide population, but it has also been suggested that this may be due to the presence of sulphide and oxysulphide phases of different relative plasticities (35). There is, however, evidence to show that in

such cases the more elongated types are richer in manganese, and that in general the sulphides are more plastic than the oxysulphides (31). More recently Banks and Gladman (18) have obtained evidence indicating that complete modification by R.E. treatment produces sulphides and oxysulphides which exhibit little or no deformation on working.

The effects of titanium and zirconium on sulphide plasticity are also ill defined, although Banks and Gladman (18) did report that the behaviour of manganese sulphide itself is relatively unaffected by the small amount of titanium able to dissolve and that sufficient titanium must be added to ensure that the MnS is completely replaced by the non-plastic Y phase (Ti(CN)S) in order to obtain the benefits of Titanium modification. The effects of zirconium on the plasticity of MnS has not been quantified, although its effect in reducing the mechanical anisotropy in wrought products is well known (19). The appearance of the carbo-sulphide phase $Zr_4C_2S_2$ at higher zirconium levels, as a eutectic or grain boundary precipitate, results in a marked increase in the anisotropy ratio of the wrought steel. Pollard (39) observed that although the carbo-sulphide phase itself was non-plastic, the eutectic or grain boundary precipitate colonies rotate during deformation and become aligned in the rolling plane, in much the same way that type II sulphide colonies rotate (136) and give similarly deleterious effects on the mechanical properties.

(iii)   The Behaviour of Silicate Inclusions

In steels silicate inclusions may occur as either spherical glassy particles, which frequently contain precipitated crystalline phases or second glassy phases, or they may be complex crystalline inclusions containing a number of different phases. Whatever their form all silicate inclusions exhibit similar behaviour with respect to working temperature. Pickering (92) found that siliceous inclusions behave either rigidly, in the case of spherical glassy silicates, or in a brittle manner in the case of crystalline duplex silicates, on working

at lower hot working temperatures, but that both types exhibited a rapid transition from rigid to plastic (fluid) behaviour, over a narrow temperature range, at higher working temperatures. Subsequent investigations (114, 141, 142) have confirmed these findings, although it is now recognised that the temperature of transition from rigid to fluid behaviour is a characteristic of the inclusion composition (141). Kiessling (113) has attempted to relate the transition temperature to the variation in oxide content FIG. 36. Such a simple relationship is, however, unlikely in view of the variation in the effects of composition on solidus and liquidus temperatures, although the relation-ship may be more straightforward in the case of glassy inclusions. It has been established, however, that the transition temperature does increase with increasing silica content, its value being in excess of $1300^{\circ}C$, (113, 142), in the case of highly siliceous types, ($>$ 95% SiO_2).

The principal factors on which the transition temperature depend are not well established although Ekerot, (141), has developed a theory to explain this transition in terms of the inclusion viscosity, in the case of glassy siliceous inclusions. In such cases the inclusion stress-strain relationship is postulated to obey Newtonian flow, and is described by the equation :-

$$\sigma = \mu \, \dot{\varepsilon}$$

where

σ = The apparent flow stress

μ = The viscosity

$\dot{\varepsilon}$ = The strain rate

Assuming that the transition from rigid or brittle behaviour occurs when the matrix and inclusion flow stresses are equal, then according to this author, for a typical strain rate of $200 \, s^{-1}$ and a matrix flow stress of $15 \, Kp.cm^{-2}$ ($1.5 \, MN.m^{-2}$), the inclusion and matrix flow strengths are equal when the viscosity of the inclusion is $10^{7.5}$ poise, ($3.16 \, MN.s.m^{-2}$). Although the glass softening

temperature is defined in the literature as the temperature at which the viscosity falls to $10^{7.6}$ poise, (5.75 MN.s.m^{-2}), and would seem to correspond to the concept of a transition in behaviour, the derivation of the critical viscosity is incorrect. Substituting the values given for the strain rate and steel flow stress in the above equation, yields a value of 0.75×10^4 N.s.m^{-2} ($\sim 10^{4.9}$ poise), for the critical viscosity, and not the value claimed by the author. Additionally the form of the equation used is not mathematically correct. In the case of Newtonian flow, the relationship between the apparent flow stress and the viscosity, is of the form:-

$$\tau = \mu \frac{dv}{dx}$$

where

τ = The shear yield strength

$\frac{dv}{dx}$ = The velocity gradient acting across the inclusion

The equation used in the calculation above uses the strain rate ($\dot{\varepsilon}$) in place of the velocity gradient and the yield strength (σ) in place of the shear yield strength. The equation is thus not mathematically correct: it can be shown for the case of simple shear, that the strain rate, ($\dot{\varepsilon}$) is related to the velocity gradient by the equation:-

$$\frac{dv}{dx} = 2 \dot{\varepsilon} \, \text{Cosh} \, \varepsilon$$

where

$\dot{\varepsilon}$ = The strain rate

ε = The true strain

and this gives the stress-strain relationship of the form :

$$\tau = 2\mu \dot{\varepsilon} \, \text{Cosh} \, \varepsilon$$

However, for zero strain, i.e. the initial deformation, Cosh ε = 1 and the equation becomes :

$$\tau = 2\mu \dot{\varepsilon}$$

The yield strength is related to the shear strength by the equation :

$$\sigma = 2\tau$$

and the stress-strain relationship becomes

$$\sigma = 4\mu\dot{\varepsilon}$$

Even using this corrected form of the equation, substitution of Ekerot's values for (σ) and ($\dot{\varepsilon}$) gives a value for the critical viscosity of only $\sim 0.2 \times 10^4$ N.s.m^{-2}, ($10^{4.3}$ poise). The value of 15 Kp.cm^{-2}, (1.5 MN.m^{-2}), quoted as the flow stress of steel during hot working is obviously incorrect, a value of 10^3 Kp.cm^{-2}, (100 MN.m^{-2}), being more realistic, (115). Substitution of this value, at a strain rate of 200 s^{-1}, into the corrected equation gives a value of 0.5 MN.s.m^{-2} ($10^{6.7}$ poise), for the critical viscosity, and corresponds to a temperature somewhat above the glass softening point. It will be seen in SECTION 4.4.1 that a more rigorous derivation of this relationship in fact leads to values of critical viscosity in the region of the glass softening point.

Ekerot (141, 142) has reported the rigid-plastic transition behaviour of silicate inclusions over a wide composition range, and Shiraiwa (81) has reported the softening temperatures of both crystalline and glassy silicates of similar compositions, as measured by high temperature hardness tests on synthetic slags. If the observed transition temperatures are compared with the measured glass softening temperatures, TABLE 3, it will be seen that the inclusions apparently transform from rigid to plastic behaviour at temperatures 100 - 300°C above the measured softening temperature.

In the case of crystalline silicates, Shiraiwa shows that their softening temperatures lie some 100 - 200°C above the corresponding glass softening temperature FIG. 37 and it is to be expected that the rigid-plastic transition for crystalline silicate inclusions will occur at a correspondingly increased temperature. From these findings it would appear that in the case of crystalline silicate inclusions the critical temperature for the rigid-plastic transition will correspond to the solidus temperature of the silicate concerned, whilst the critical temperature for the corresponding glassy silicate may be some 100 - 300°C lower.

At higher temperatures the behaviour of the inclusions is less

well defined. Pickering (92) found the relative plasticity to be unchanged at temperatures above the transition, whilst Ekerot (141) reports that the relative plasticity may increase, decrease or even remain unchanged as the deformation temperature is increased further. In view of the fact that the inclusion viscosity and steel flow strength are unlikely to alter in such a way that their relative strength remains unaltered, some change in relative plasticity is to be expected.

Because of the relationship between the apparent flow stress and the strain rate, for these fluid inclusions, their behaviour is likely to be very sensitive to the effects of the strain rate, SECTION 2.2.3. This parameter will not only affect the value of the relative plasticity exhibited, but will also affect the transition temperature. It must also be remembered that Ekerot's results (141, 142) were obtained from samples reduced 50% by plane strain and that values of relative plasticity at this reduction will necessarily be different from values obtained at other reductions. Unfortunately it is not -possible to extrapolate these results to the case of zero strain, in order to obtain a value of maximum relative plasticity, but since values as high as 2.2 are reported at this reduction, it is not unlikely that values in the region of 2.5 - 3.0 would be obtained for the relative plasticity at zero strain. These values are greater than those obtained by Gove and Charles (103) and those predicted by Gay (106) and Sundstrom (99) and are more in line with those predicted by Unkle (86).

(iv)   The Behaviour of Other Phases

Manganowustite Inclusions

The behaviour of iron manganese oxides on hot working is not well defined, reports by Pickering (92) and Uchiyama and Sumita (112) being the only references in the literature containing results specific to manganowustite types.

Pickering reports that the relative plasticity of wustite inclusions decreases with increase in rolling temperature, FIG.38

indicating that the hardness of the oxide is less temperature sensitive than that of the steel. This condition is similar to that exhibited by manganese sulphide and may be a feature of crystalline phases having the NaCl type lattice. Uchiyama and Sumita found that the relative plasticity of these inclusions increased as the manganese content increased FIG. 39, although the effect was small. Kiessling (113) states that although the PLASTICITY of (FeMn)0 inclusions decreases as the MnO content increases, the strengthening effect of Mn on the matrix at higher manganese levels, is even greater and the relative plasticity exhibited by the inclusions may actually increase. This is certainly in agreement with Uchiyama and Sumita's results FIG. 39 which show an initial slight decrease in relative plasticity, corresponding to a high degree of partitioning of the Mn into the inclusions giving an increased hardness of the (FeMn)0. At higher Mn levels, less Mn is partitioned into the inclusions and solid solution strengthening of the matrix causes the relative plasticity to increase. A minimum relative plasticity is reached in steels containing $\sim$ 0.2% Mn, corresponding to a 50% MnO content in the inclusion.

Both these workers found a difference in the behaviour of the smaller and larger inclusion species, the smaller inclusions being more resistant to deformation, and the larger ones being prone to fracture at high strains. The relative plasticities reported were in the region of 0.1 to 0.2 and were obtained at matrix strains of the order of 2.0. These values indicated a low value for the initial relative plasticity, at ε = 0, and a value in the region of 1.0 - 1.5 would seem likely.

On the basis of these results it appears that the relative plasticity of these phases is small, when compared to those exhibited by the glassy silicates and type III sulphides, and although the effects of decreasing plasticity with increasing working temperature seem proven, the effects of composition, particularly MnO content, are less well established. It

is possible that these inclusions may exhibit some bonding to the

matrix, which would markedly affect their behaviour (SECTION 2.2) and it would be interesting to compare the relative plasticities to their relative hardness should the latter become available.

Alumina and Related Types

Although the literature does not contain specific reference to the behaviour of alumina inclusions during hot working, the effects of fragmentary alumina stringers on the mechanical and physical (surface finish) properties has been well reported. At normal hot working temperatures alumina is non-deformable and although individual small particles may in themselves behave rigidly, the more usual alumina aggregates behave in a brittle manner and become fragmented and disseminated in the rolling direction. The mechanisms of fracture and possible associated void formation are, however, unknown.

The more aluminous forms of calcium aluminate are comparatively hard and have high melting points FIG. 7, TABLE 4, the hardness increasing with the alumina content (113). Although non-deformable themselves, Kiessling (113) states that these phases are often associated with phases of the spinel type which may be crushed and appear as fragmented stringers in heavily deformed samples. The more calcareous forms, although not commonly found in steels, may be more plastic, the melting points of $C_{12}A_7$ and C_3A being lower than that of steel TABLE 4.

Spinel types are usually non-plastic and behave rigidly, although Kiessling (113) reports that fracture may occur at heavy reductions. Although plastic deformation of certain spinels has been observed at temperatures as low as $1300^\circ C$ (143) such deformation has not been observed in steels.

3.1 EXPERIMENTAL DETAILS

3.1.1. Selection of a Base Material and the Inclusion Types Investigated

Because the deformability of non-metallic inclusions, at hot rolling temperatures, is primarily a function of the flow stress ratio of the inclusion and matrix materials, it was important to ensure that the steel matrix was of a constant and homogeneous composition, so that different ingots would exhibit constant matrix properties. It was also necessary to use a material which had a high oxygen solubility at the steelmaking temperature, in order to obtain an adequate volume fraction of oxide inclusions. For these reasons Swedish (low metalloid) iron was chosen for the base material.

The types of inclusion to be investigated were selected on the basis of their frequency of occurrence in commercial steels, and a number of melts were produced which were deoxidized to give inclusions occurring in the systems

(i) $Fe-Mn-0$

(ii) $FeO-MnO-SiO_2$

(iii) $FeO-CaO-SiO_2$

(iv) $FeO-Al_2O_3-SiO_2$

(v) $CaO-Al_2O_3$

(vi) Al_2O_3

3.1.2 Manufacture of Steels and Ingot Preparation

The Swedish iron was air melted, in 50 kg heats, in an induction furnace, and after deoxidation was teemed into 25 kg ingots. All the melts were teemed at $1600^{o}C$ at which temperature the solubility of oxygen was known to be in the region of 0.16 Wt % (113). The amounts of deoxidant required were calculated on this basis. The melts were chill cast into iron moulds, in order to retain as many inclusions as possible and to try to ensure their uniform distribution.

Thirteen ingots were made, in most cases two separate ingots, containing different types of inclusions, being produced from a single 50 kg melt.

The furnace had a magnesite lining but serious contamination of the inclusions by this material was not expected.

Details of the melts manufactured were :-

(a)   Melt 1

50 kg of iron were air melted and on reaching 1600°C half was cast into a sand mould (Cast 1B). A previous trial had shown that a chill cast of undeoxidized iron produced very small wustite inclusions which were unsuitable for plasticity measurements. It was hoped that the slower cooling and solidification rates afforded by sand casting would allow the formation of larger wustite inclusions.

To the remaining 25 kg of metal, 1% Mn and 0.075% Si were added, in the form of the pure metals. After holding for $\frac{1}{2}$ - 1 minute this was tapped into an iron mould. (Cast 6). Further melts were produced in the same way, but with the following modifications, in order to produce the different types of inclusions required.

(b)   Melt 2

After melting, 0.06% Si metal was added and 25 kg was tapped (Cast 4). A further 0.1% Si was added to the melt and the remaining 25 kg was tapped (Cast 5).

(c)   Melt 3

0.36% Al metal was added and 25 kg was tapped immediately (Cast 7). After reoxidizing the remaining melt, by induction stirring, additions of 0.13% Al and 0.13%Si were made simultaneously, and the melt was tapped (Cast 8).

(d)   Melt 4

1% Si metal was added and 25 kg was tapped (Cast 4B).

0.2% Al was immediately added to the remaining melt and then tapped (Cast 8B).

(e)   Melt 5

1% Mn and 0.3% Si were added and 25 Kg was tapped (Cast 6B).

(f)   Melt 6

        0.8% Si metal was used to predeoxidize this melt before a
        complex calcium bearing deoxidant was added. After holding
        for 5 minutes under an argon blanket, to eliminate the silicates
        produced, a 1% addition of Hypercal was made and the melt
        was tapped immediately (Cast 10).

(g)   Melt 7

        This melt was made exactly as melt 6 but employing a 1%
        Calsibar addition instead of Hypercal (Cast 11).

(h)   Melt 8

        This melt was made as for the previous two, but using a 1%
        addition of Superseed (Cast 12).

(i)   Melt 9

        1.3% Al metal used for deoxidation (Cast 7B).

        The composition of the three commercial deoxidants employed
are given in TABLE 5.

        In order to prevent excessive loss of the deoxidants by premature
oxidation at the melt surface, all the deoxidant additions were made
under an argon blanket. This was accomplised by flooding the top of
the steelmaking crucible with argon, immediately before making the
deoxidant additions. The amounts of the deoxidants used were based
primarily on stoichiometric calculations with allowances being made
for losses by vapourization and preoxidation into the slag. The casts
produced, and the types of inclusions expected, are summarised in
TABLE 6.

        The cast ingots were of a taper section approximately 4" square
at the top and $3\frac{1}{4}$" square at the base, their overall length being 16".
The top and bottom of each ingot were cut off and used for chemical
analysis. Further thin slices were taken from the top, middle and
bottom of the ingot for optical examination. The top half of each ingot
was sectioned into eight parallel sided bars $1\frac{1}{2}$" wide, $7\frac{1}{2}$" long and
5/8" thick. The thickness was machined to a tolerance of $\pm$ 0.010".
These bars were used for hot rolling, and the thickness tolerance was
designed to ensure that constant reductions were obtained throughout
the investigation.

The sectioning of the ingot is shown in FIG.40. The thickness and length dimensions of the test bars were calculated so that a reasonable size of specimen could be cut from the bar after each pass during hot rolling, without the bar becoming unmanageably small.

3.1.3. Hot Rolling Programme

This programme consisted of six reductions at temperatures of $925^\circ C$, $1000^\circ C$, $1150^\circ C$ and $1275^\circ C$. This range of temperatures effectively covered the usual deformation temperature ranges employed in commercial practices. The reductions used were calculated on a true strain basis, a strain of 0.3 being performed at each pass. The hot rolling schedule is shown in TABLE 7. Samples were cut from the entry end of the test bar after each pass, care being taken to ensure that this was the same for each pass. This was done in order to eliminate any chilling effects that the cold tongs produced when the bars were removed from the furnace. The test bars were heated to the rolling temperature in a muffle furnace, using a nitrogen atmosphere to prevent excessive oxidation. The temperature of the furnace was monitored constantly with a Pt-Pt.Rh thermocouple. It had been determined previously that a 15 minutes soak at the rolling temperature would be sufficient to equilibriate the temperature of the test bars, at the required temperature. This was done by inserting a small thermocouple into a 1/16" hole drilled into the centre of one of the test bars and monitoring the temperature rise when the bar was placed with three others, in a furnace set at the highest working temperature. The bars were heated four at a time to the required working temperature. After checking the furnace temperature one bar was removed and rolled, a $1\frac{1}{2}$ - 2" sample being cut from the entry end before the bar was returned to the furnace. A second bar was then removed and subjected to the same treatment. This process was continued until all four bars had been subjected to six reductions, six samples having been obtained from each bar. The

continuous removal and replacement of bars caused some temperature
fluctuations within the furnace, particularly during the first and
second series of passes where the bars were still quite massive.
Because of this, short soaking periods were allowed between successive
passes; the maximum drop in furnace temperature recorded during any
one pass sequence being $40^{\circ}C$ at the two lower rolling temperatures and
$50^{\circ}C$ at the two higher temperatures. The maximum temperature loss
occurred during the first pass sequence, this loss being smaller on
the second and negligible by the third sequence.

3.1.4 Heat Treatment Programme

Preliminary examination of the cast samples showed that
several casts contained glassy types of inclusions, and in order to
determine the effects that soaking at various temperatures would have
on them, a programme of extended soaking treatments was devised.
This consisted of sealing small samples of the as cast materials
inside silica tubes in an argon atmosphere, and heating the tubes
for various times at the four rolling temperatures. Samples from
seven of the casts were treated in this way, treatment times of 5, 50
and 100 hours being employed. Twelve tubes were prepared each
containing seven samples, one from each of the casts required. The
individual samples were separated from each other by asbestos wool,
in order to prevent welding. The pressure of the argon atmosphere
in each tube was calculated so that it would equal atmospheric pressure
at the treatment temperature.

Since the silica tubes would tend to flux with the furnace
linings at the higher treatment temperatures, these tubes were
supported on carbon base plates during heat treatment.

3.1.5 Optical Microscopy

Samples from the as cast, heat treated and hot rolled specimens
were mounted and prepared for optical examination by the usual
metallographic methods. Wet grinding through emery paper grades 80,

120, 220, 320, 400 and 600 was followed by diamond lapping on $6\mu m$, $1\mu m$ and $\frac{1}{4}\mu m$ wheels. All the samples were then given a light final polish on a Selvyt cloth covered with an aqueous paste of $1/20\mu m$ γ alumina. Optical examination was performed in the unetched condition, although a repeat polish-etch technique was employed with some of the hot rolled samples in order to delineate matrix discontinuities. The hot rolled samples were mounted in the longitudinal section so that the inclusion elongation could be assessed. No reference to orientation was made with the as cast and heat treated samples.

3.1.6 Electron Probe Microanalysis

The as cast, heat treated and some of the hot rolled samples were examined on an Electron Probe Microanalyser in order to determine the compositions of the phases present in the inclusions.

This instrument is based on a comparative principle, the content of any particular element in the excited area, being determined by direct proportion of the intensity of characteristic X-rays generated from that area to the intensity generated from a standard of known composition. The apparent concentration (K_A) obtained from this ratio is not the true concentration, due to the effects of scattering, absorption and fluorescence, and certain corrections must be applied.

The instruments used in this investigation were Cambridge Microscan Mk. II and V instruments and although binary correction data were available for the Mk. V instrument, they were not available for the relevant oxide systems in the case of the Mk. II instrument. The correction data required were obtained by substitution of the appropriate absorption, fluorescence and scattering factors into the ICL 1905 Computer Program, details of which are given in reference 144. Correction data for the binary oxide systems shown in TABLE 8 were obtained in this way. The comparison standards for Ca, Sr and Ba were in the form of fused fluorides, and fluoride-oxide correction factors were obtained for these elements. Similar correction factors were obtained for Fe-FeO and Mn-MnO for use with these metal standards. A typical binary correction chart is shown in FIG. 41.

3.1.7. Electron Microscopy

(i) High Voltage Electron Microscopy (H.V.E.M.)

In one cast the glassy as cast inclusions appeared to have crystallised either during deformation or interpass reheating. In order to confirm the crystallinity, the inclusion fragments were extracted from the most heavily deformed sample and were examined by H.V.E.M. Two methods of extraction were employed, Electrolytic extraction and Carbon Replica extraction.

In the first case a 50 grm sample of the hot rolled strip was pickled in hot 50% hydrochloric acid to remove the scale, and then coiled into a small cylinder. This was then made the anode of a Klinger-Koch electrolysis cell and the matrix iron dissolved. The cell contained an aqueous electrolyte containing 5% sodium citrate, 1.2% potassium bromide, 0.6% potassium iodide and concentrated hydrochloric acid, 5 mls of acid being added to the electrolyte in the anode chamber for every ampere hour of the electrolysis. The basic features of the cell are shown in FIG. 42. After extraction the inclusion fragments were separated by centrifuge, washed several times in distilled water and finally in alcohol. The fragments were then dispersed in a small volume of water free methanol.

Carbon coated microscope grids were prepared using the standard technique and a drop of the inclusion dispersion was pipeted onto each grid. These were then examined in a 1 MV electron microscope.

In the second method the hot rolled strip was polished in the rolling plane to a $\frac{1}{4}\mu m$ finish and then deeply etched for 6 - 7 minutes in a 5% solution of bromine in water free methanol. After washing in methanol the sample was immediately vapour coated with carbon in a vacuum of better than 10^{-6} torr. After coating, the carbon film was scribed into small squares which were detached electrolytically using a 6% Nital solution and an applied voltage of $\sim$ 30v, followed by floating off onto the surface of distilled water. The detached films were captured on 100 mesh grids, dried on filter paper and then examined in the 1 MV electron microscope.

In an attempt to index the diffraction patterns obtained, a computer program was written which would list all the possible interplanar spacings, together with their corresponding crystallographic indices, for the complex mineral crystal structures encountered. The programme devised was capable of calculating the interplanar spacings for any type of crystal lattice, except hexagonal, for all planes between ($\bar{7}$ $\bar{7}$ $\bar{7}$) and (7 7 7) inclusive. All spacings greater than a selected minimum value were then listed, together with their corresponding (hkl) values, in both increasing order of (hkl) value and increasing 'd' value. The programme together with the input instructions and final print-out for the Rhodonite (Triclinic) lattice are shown in APPENDIX 3.

(ii)   Scanning Electron Microscopy (S.E.M)

Selected samples were examined by scanning electron microscopy in order to determine the three dimensional geometry of the inclusions. This was performed after deeply etching the polished samples in water free -5% Bromine-Methanol and immediately coating the specimens with either gold or gold-palladium alloy, in order to render the surface of the inclusions conducting. The gold coatings were applied by sputtering whilst the gold-palladium coatings were vacuum deposited and were only used when sputtering facilities were not available. The coated samples were examined immediately using a Phillips P.S.E.M. 500 Scanning Electron Microscope. A low accelerating voltage of 6 - 12 KV was normally employed in order to minimise fluorescence effects.

3.1.8   Relative Plasticity Measurements

When the strain imposed upon a deformable inclusion contained within a deforming matrix is compared with the strain suffered by the matrix, the resulting ratio is referred to as the RELATIVE PLASTICITY of the inclusion :-

$$\nu = \mathcal{E}_i / \mathcal{E}_m$$

where

$$\mathcal{V} = \text{Relative plasticity}$$

$$\mathcal{E}_i = \text{Inclusion true strain}$$

$$\mathcal{E}_m = \text{Matrix true strain}$$

Although the true strain of the matrix material is easily assessed, measurements of the true strain suffered by the inclusion are more difficult to make, and often only average or approximate values can be obtained.

It has been shown, APPENDIX I, that the true strain of an originally spherical element is given by the natural logarithm of its aspect ratio, multiplied by some constant, which is a function of the type of deformation. Extending this relationship to spherical inclusions yields the equations first defined by Malkiewics and Rudnik (93)

$$\mathcal{E}_i = \tfrac{1}{2} \log_e \lambda \qquad \text{for plane strain}$$

$$\mathcal{E}_i = 2/3 \log_e \lambda \qquad \text{for cylindrical strain}$$

where

$$\lambda = \text{Inclusion aspect ratio}$$

$$\mathcal{E}_i = \text{Inclusion true strain}$$

It is found that when measured values of inclusion true strain are plotted against the matrix true strain, the values do not conform to a linear relationship, FIG. 43. As defined above, the relative plasticity of the inclusion is the gradient of the chord of $\mathcal{E}_i$ vs $\mathcal{E}_m$ from the origin through ($\mathcal{E}_m{}^j$, $\mathcal{E}_i{}^j$). It can be appreciated that even if the inclusion should cease to deform at some stage, having a "TRUE" relative plasticity of zero, the gradient of the chord would continue to have a finite value and the inclusion would still exhibit an "APPARENT" relative plasticity. Accordingly it is the gradient of the curve $\mathcal{E}_i$ vs $\mathcal{E}_m$ at the point ($\mathcal{E}_m{}^j$, $\mathcal{E}_i{}^j$) which defines the inclusion "TRUE" relative plasticity and in this work the symbols $\mathcal{V}_T$

and V_A will be used to denote the "TRUE" and "APPARENT RELATIVE PLASTICITY" respectively, so that

$$V_T = \left| \frac{d\,\mathcal{E}_i}{d\,\mathcal{E}_m} \right|\, \mathcal{E}_m \quad = \text{TRUE RELATIVE PLASTICITY}$$

$$V_A = \left| \frac{\mathcal{E}_i}{\mathcal{E}_m} \right|_{\mathcal{E}_m} \quad = \text{APPARENT RELATIVE PLASTICITY}$$

It can be seen that unless values of relative plasticity, as quoted in the literature, are qualified by statements concerning both the type of deformation and the matrix strain at which the values were measured, the values of relative plasticity will be of little significance.

V_T, the inclusion True Relative Plasticity, will always decrease more rapidly with increasing matrix strain than V_A, the Apparent Relative Plasticity. The True and Apparent Relative Plasticities have equal values at zero matrix strain, their values also being a maximum at this point. Since this maximum value of relative plasticity can be employed to compare the relative plasticities of various types of inclusions, it is useful to define this value as the "INITIAL" relative plasticity, V_i where :-

$$V_i = \left| \frac{\mathcal{E}_i}{\mathcal{E}_m} \right|_{\mathcal{E}_m = 0} = \left| \frac{d\,\mathcal{E}_i}{d\,\mathcal{E}_m} \right|_{\mathcal{E}_m = 0} = \begin{array}{l}\text{INITIAL}\\ \text{RELATIVE}\\ \text{PLASTICITY}\end{array}$$

This value appears to be a property of the inclusion concerned, at the deformation temperature, and depends only on the relative strength of the inclusion and on the work of adhesion between the inclusion and matrix; although the inclusion size may also have an effect in the case of the smaller inclusions.

In this work the true strains of the deformed inclusions were determined from their aspect ratios, in accordance with the equations defined above. An average value for the logarithm of the aspect ratio was determined from the measurement of a minimum

of 25 individual inclusions in each hot rolled sample. After plotting the results thus obtained as a function of matrix strain, at each of the deformation temperatures, values of the True (V_T^2), and Apparent, (V_A), relative plasticities were obtained from these graphs and replotted as functions of both matrix strain and temperature of deformation, in three dimensional form.

An attempt was made to obtain relative plasticity measurements by the use of Quantitative Television Microscopy using a Quantimet 720B. Using the equations defined in APPENDIX 2, it was hoped to obtain an alternative assessment of inclusion deformation from projected length measurement, for comparison with the assessments made by more conventional means.

Quantitative assessments of the behaviour of the more refractory types of inclusions, (Alumina and the aluminous Calcium Aluminates), was not feasible and qualitative assessments, using optical and scanning electron microscopy were made.

3.2   EXPERIMENTAL RESULTS

3.2.1.   The Effects of Deoxidation on the Inclusions Present in the As-Cast Materials

(i)   Undeoxidised Melts

Cast 1B contained an interdendritic distribution of wustite globules which had been formed during ingot solidification and cooling, FIG. 8, PLATE I.   These inclusions were up to $10 \mu m$ in diameter and were marginally larger than those obtained by chill casting a similar material, which contained inclusions up to $8 \mu m$ in diameter.   Electron Probe Microanalysis (E.P.M.A.) confirmed the inclusions to be pure iron oxide, the manganese content being less than 0.1%.

(ii)   Silicon Deoxidised Melts

Cast 4 contained a dispersion of large duplex silicates, PLATE 2, and a fine background dispersion of wustite globules. E.P.M.A. showed the primary phase of the duplex silicates to be pure wustite and the matrix to be an iron silicate containing 73% FeO and 27% SiO_2.   The secondary inclusions were found to be 100% FeO.   The primary duplex silicates were hypoeutectic binary iron silicates, FIG. 44, whose sizes varied up to $40 \mu m$, although a few isolated particles of up to $100 \mu m$ were observed.

Cast 5 also contained a dispersion of duplex silicates but these contained less primary phase than similar inclusions from Cast 4, FIG. 44.   The larger inclusions generally contained less primary phase, which was also in a finer form, PLATE 3a, than in the smaller inclusions which contained large primary phase dendrites, PLATE 3b.   This primary phase was again found to be 100% FeO and the matrix composition near to the eutectic composition at 74% FeO, 26% SiO_2.   These inclusions had sizes ranging from $10 \mu m$ to $100 \mu m$ diameter although isolated particles of up to $\sim 150 \mu m$ were again observed.   The general size range was slightly larger than that found in Cast 4.   A fine interdendritic dispersion of secondary inclusions had once more formed on solidification and were found

to be composed of 100% FeO.

Cast 4B contained a dispersion of spherical glassy silicates which in a number of cases had become solidified whilst in the process of coalescing, PLATE 4. E.P.M.A. showed the inclusions to be highly siliceous binary iron silicates containing 12% FeO and 88% SiO_2, FIG. 44. The inclusions exhibited a size range from 5-50μm diameter. In this case the level of deoxidation had been sufficient to prevent the formation of secondary interdendritic inclusions.

(iii)   Silicon-Manganese Deoxidised Melts

Cast 6 was found to contain several different types of inclusion. The most abundant were large duplex silicates similar to those observed in casts 4 and 5. However in this case the primary phase appeared to be somewhat translucent, PLATE 5a, in some cases the matrix having a lath like or feathery appearance. E.P.M.A. revealed the primary phase to be manganowustite containing 72% FeO and 19% MnO, the matrix being an iron manganese silicate containing 9% FeO, 58% MnO and 32% SiO_2, FIG. 45.

The second type of inclusion appeared to have a eutectic structure, Plate 5b, exhibiting a mixed lamellar-granular morphology. These inclusions were not as abundant as the former type but were of similar size, both being in the range 60 - 110μm diameter. Analysis showed the overall composition to lie in the region of the manganowustite - (fayalite-tephroite) eutectic valley or possibly even slightly to the silica rich side. The overall composition obtained was 14% FeO, 58% MnO, 27% SiO_2 the individual phases being too small for analysis.

A third type of inclusion was observed only infrequently and was of a smaller size than the previous two forms, the maximum observed diameter being ~ 50μm. These inclusions contained lath like internal structures and were occasionally observed in the coalescing form, PLATE 5c. Analysis revealed the composition to be near to the tephroite composition, 10% FeO, 56% MnO, 34% SiO_2.

Two forms of background, secondary, inclusions were observed, one having a spherical glassy morphology, which can be seen in the background of PLATE 5c. Analysis revealed its composition to be very similar to the matrix composition of the first type, 11% FeO, 56% MnO, 36% SiO_2. The second form had a dendritic morphology and were found to be manganowustite containing 30% FeO and 66% MnO, PLATE 5d.

Cast 6B contained only transparent spherical glassy silicates, PLATE 6, sometimes observed in the coalescing form. E.P.M.A. showed all the inclusions to be of similar compositions falling within the range 11 - 15% FeO, 32 - 37% MnO and 50 - 56% SiO_2, FIG. 45. The size of the inclusions varied up to $60\,\mu m$ diameter.

(iv)   Aluminium-Silicon Deoxidised Melts

Cast 8 contained numerous spherical glassy silicates, PLATE 7a, most of which were single phased. A few inclusions exhibited lath like or dendritic internal precipitates, PLATE 7b. Examination by S.E.M. revealed still further types containing precipitates with both rosette and cuboid morphologies, PLATE 7c, but again these were in the minority. S.E.M. also revealed numerous fine dendrites of alumina interspersed between the larger glassy inclusions, PLATE 7d. The dendritic internal phases were identified in some cases as alumina, and in other cases as alumina rich hercynite containing 74% Al_2O_3 and 25% FeO. An analysis of the rosette precipitates was not obtained, none of the inclusions examined optically containing precipitates of this form. However, the few inclusions observed which contained blocky precipitates gave their compositions near to hercynite at 60% Al_2O_3, 41% FeO. The analyses of the glassy inclusions were found to be rather variable, silica levels as low as 40% and as high as 60% being obtained, FIG. 46. However, most of the single phase inclusions had compositions lying in the region of 14 - 27% FeO, 45 - 61% SiO_2, $\sim$ 20% Al_2O_3. The inclusions generally had sizes in the range 10 - $100\,\mu m$ diameter but an occasional particle of up to $160\,\mu m$ diameter was observed.

Cast 8B contained very few inclusions and was not investigated further.

<u>Melts Deoxidised with Complex Commercial Deoxidants</u>

Cast 10 was deoxidised with Hypercal, a commercial deoxidant based on calcium, aluminium and silicon but which also contains barium in order to improve the calcium recovery, TABLE 5. The as cast samples were found to contain small clusters of irregular particles, closely resembling alumina clusters, PLATE 8a. Many of the particles within these clusters were found on analysis to be pure alumina, but other particles gave compositions close to that of calcium hexaluminate (CA_6) 92% Al_2O_3, 7% CaO, FIG. 7. A few isolated particles contained more than one phase and were found to consist of corundum blocks and laths, together with blocks of calcium hexaluminate in a silicate matrix, PLATE 8b, TABLE 8. The sizes of the individual particles varied up to 40μm diameter, whilst the clusters were up to 120μm in diameter.

Cast 11 was deoxidised with Calsibar, which is also a commercial deoxidant containing calcium. However, this alloy contains very little aluminium, the chief component being silicon. Like the Hypercal alloy, Calsibar also contains barium in order to improve the calcium recovery. The inclusions produced by this deoxidant were spherical glassy silicates, PLATE 9a, which tended to have a violet colouration. E.P.M.A. showed the inclusions to be iron-calcium silicates of rather variable iron and calcium contents, FIG. 47; the compositions lying in the range 10 - 20 FeO, 10 - 20% CaO and 70 - 80% SiO_2. It was interesting to find that the periphery of these inclusions was often richer in CaO than the interior, though this was by no means true in every case, PLATES 9b and c. The diameters of the inclusions varied up to 40μm although one isolated multiphase silicate had a diameter of 80μm.

Cast 12 was deoxidised with Superseed which is another commercial deoxidant, but which is based on strontium and silicon. The inclusions produced were again spherical glassy silicates, PLATE 10a, which were found to be binary iron silicates containing 25% FeO

and 75% SiO_2, FIG. 44. Coalescing clusters of inclusions were frequently observed, PLATE 10b, but the size of the inclusions were generally smaller than in the previous casts, the maximum observed diameter being ~ 30 μm. Strontium was not detected in the analysis of any of the inclusions.

(vi)   General Observations

Some variation in the size and number of inclusions was found between the top, middle and bottom samples from most of the ingots, there generally being a greater number of inclusions, and of a larger size, in the top half of the ingots. This segregation had occurred in spite of the rapid freezing which had taken place during the chill casting. The difference in volume fraction and size distribution of the inclusions was greater between the bottom and middle of the ingot than it was between the middle and the top, and the top halves of the ingot were generally found to have very homogeneous and uniform distributions.

The compositions of the inclusions contained in the cast materials, obtained by electron probe microanalysis, are summarised in TABLE 8, and the chemical analyses obtained from the machined test bars are shown in TABLE 9.

3.2.2   Deoxidation with Aluminium

Cast 7 (0.36% Al addition) was found to contain very few oxide inclusions and a replacement cast (7B) was made employing a much heavier aluminium addition (1.3%). This cast contained numerous large agglomerates of alumina in the top of the ingot, their size decreasing towards the middle. The bottom sample contained very few clusters, those which were observed being very small. However, this sample did contain large numbers of isolated alumina particles and appeared to contain almost as much inclusion material as the middle and top samples, but not in the form of clusters. The size of the clusters varied widely, the largest observed being over 800 μm in

diameter, containing many thousands of individual alumina particles, PLATE 11a.

Closer inspection of these clusters revealed them to be composed of several different particle morphologies. The larger clusters contained a number of large globular particles containing enclosed metal and varying in size up to $40 \mu m$ or $50 \mu m$, PLATES 11b and c. These were often surrounded by a mixture of small spherical and rod like particles, PLATE 11c, and smaller irregular particles containing enclosed metal, PLATE 11d; in a few cases these exhibited more than one phase, PLATE 11e. Examination of these clusters by scanning electron microscopy, in the sample deformed by 0.3 true strain at $925^{\circ}C$, revealed them to be an intricate weave of alumina dendrites, small globular forms of alumina and larger globules having a 'honeycomb' or grain structure on their surface, PLATES 11f and g. Where the plane of polish intersected one of these larger globules, the polished surface was often revealed to contain porosity of the type observed in sintered structures, PLATE 11h.

Because of the complexity of these deoxidation products, as revealed by S.E.M., it was decided to investigate further the mechanism of formation of alumina inclusions on deoxidation by aluminium. To this end a 10 kg melt of Swedish iron was prepared by H.F. induction melting in air. On reaching $1650^{\circ}C$ a small 750 g ingot was teemed using a cast iron mould having thick (2.5 cm) walls. This mould contained a small (7.5 g) slug of aluminium, (1% by mass), onto which the melt was poured. The aluminium deoxidised the ingot in the mould, but since solidification was very rapid, the deoxidation was very inhomogenious and different regions within the ingot solidified in various stages of deoxidation. The remainder of the metal was then deoxidised by adding 114 g (1.2%) of pure (99.99) aluminium, and suction samples were taken after 5, 30 and 90 seconds, by evacuating a $\frac{1}{2}$" diameter silica tube with its end held well below the surface of the melt. The samples obtained in this way

were $\frac{1}{2}$" diameter rods of approximately 350 g in weight. However, the first sample (5 sec.) of this series was lost due to the failure of the vacuum system, resulting in the metal running back into the melt. In order to determine whether $\propto$ alumina would sinter readily in the presence of molten iron, a quantity (200 g) of $\propto$ alumina powder was poured into the melt in the furnace whilst being stirred. This was teemed immediately (10 - 15 secs.) into a 7 kg cast iron mould. Surprisingly this ingot contained very little alumina, most of this being left in the furnace as a glaze on the refractory lining.

Examination of the mould deoxidised ingot revealed as many particle morphologies as the as cast specimens from cast 7B. The ingot also contained a number of clearly defined interfaces of the type shown in PLATE 12a. These consisted of an undeoxidised region, containing FeO type inclusions, separated from a fully deoxidised region, containing aluminous inclusions, by a band of material containing alumina dendrites. Adjacent to this was a narrow region containing very few inclusions. Scanning electron microscopy showed clearly the dendritic nature of the inclusions within this band, PLATE 12b, and revealed a number of different dendrite morphologies, PLATE 12c. Examination of the apparently undeoxidised region showed it to contain a number of hercynite + wustite primary inclusions, PLATE 12d, in the region closest to the inclusion free zone, and also revealed many small alumina dendrites apparently nucleating on the small wustite inclusions; these also exhibited some evidence of reaction at their surfaces, PLATES 12e and f. Behind the band of dendrites, in the fully deoxidised region, the inclusions were well dispersed and exhibited morphologies ranging from a truly dendritic morphology, PLATE 12g, through a partially spherodized dendritic morphology, PLATE 12h, to a fully spheroidal morphology, PLATE 12i. The regions at the extremities of the dendritic bands usually contained a mixture of hercynite/wustite inclusions and partially reacted forms in which the outer layers of the inclusions were more highly aluminous than the interior, which frequently retained a composition close to

that of hercynite, 74% Al_2O_3, 26% FeO, PLATES 12j, k and 1. A large number of these partially reacted inclusions were observed distributed throughout the ingot, PLATES 12m and n, and small spherical inclusions having a 'glassy' appearance were frequently observed, PLATE 12p. The large sintered globular type of inclusion, so prominent in the clusters observed in cast 7B, were rarely observed in this mould deoxidised ingot, in fact solidification had been so rapid as to suppress the formation of all but the smallest of clusters.

In contrast, the second suction sample taken after furnace deoxidation, (30 seconds), was found to contain a number of very large alumina clusters distributed throughout the suction sample. These clusters contained particles having a number of different morphologies, no one morphology being predominant. In fact the dominant morphology varied from region to region within any one cluster, some regions having a predominantly dendritic character, PLATE 13a, others being more globular or sintered, PLATE 13b. The dendritic structures often showed marked evidence of spherodization, PLATE 13a. Other regions showed an even greater degree of globularization and PLATES 13c, d and e show how the spherodization and collapse of these dendritic structures lead to the formation of the sintered globular structures seen in PLATE 13b. Optical examination of the specimens revealed a number of the large globular structures containing enclosed metal, PLATE 13f, of the type first observed in cast 7B. On examination by S.E.M. these globules were again revealed to be sintered structures. A curious feature of these globules, which ranged in size from a few microns in diameter to well over $50 \mu m$, was that they nearly all showed evidence of a cavity extending from the surface of the globule into its interior, PLATE 13g. A few of these particles had been sectioned diametrically revealing the depth of the cavity, which in most cases became larger in the interior giving the globule the appearance of a hollow sphere.

The third suction sample, taken after 90 seconds, was found to contain a few, well dispersed, small alumina clusters exhibiting particle morphologies of the type observed in the previous sample.

The 7 kg ingot to which alumina powder had been added, contained a few isolated well sintered clusters, but these were too few to exclude the possibility that they had been retained from the aluminium deoxidation treatment.

3.2.3 The Effects of Heat Treatment on the Inclusions

Preliminary examination showed that casts 4B (Si), 6B (Si, Mn), 8(Al, Si)*, 11(Ca, Si) and 12(Sr, Si) contained glassy inclusions, and samples from these casts were heat treated as outlined in SECTION 3.4.1. In addition samples from casts 6(Si, Mn) and 10(Ca, Al) which contained crystalline inclusions, were given the same treatments, in order to determine the effects, if any, on this type of inclusion.

Optical examination of the heat treated samples showed that only inclusions from casts 6, 6B and 8 had been affected by the heat treatment, those from casts 4B, 10, 11 and 12 being optically unchanged even after the longest periods at temperature.

(i) Cast 6 (Si, Mn Deoxidised)

Treatments at $925^{\circ}C$ served only to spherodize the eutectic matrix of the duplex silicates, PLATE 14a. In a few inclusions metallic iron globules were precipitated in the granular matrix, their numbers increasing with increasing treatment time, PLATE 14b.

At $1000^{\circ}C$ the matrix began to loose its granular character, becoming translucent in appearance. The metallic globules were again produced, but after even the shortest treatment time, (5h), they were much larger than in any of the samples treated at $925^{\circ}C$, PLATE 14c.

On treatment at $1150^{\circ}C$ the inclusions had tended to lose their spherical outline, possibly indicating some degree of softening of the eutectic matrix, PLATE 14d, although this temperature was still well below the eutectic temperature, FIG. 45.

Similar structures were obtained at $1275^{\circ}C$, and a third light phase present in a few of the inclusions was identified as manganese sulphide, PLATE 14d.

* Symbols in brackets after the cast number denote the deoxidant(s) used.

(ii)   Cast 6B (Si, Mn Deoxidised)

Treatment for 5 hours at both 925 and 1000°C induced the precipitation of a dark phase having a globular or rosette like morphology, PLATE 15a; the precipitates produced at 925°C being smaller but more numerous than those produced at 1000°C. Analysis of this phase was difficult due to its size, but more than 90% SiO_2 was obtained in most cases and the phase was probably vitreous silica. Treatments for longer periods at these temperatures produced complete devitrification of the glassy matrix, giving a granular type of structure containing at least two phases, PLATE 15b. The fineness of the structure prevented analysis of the individual phases present but an average analysis of 52-56% SiO_2, 29-32% MnO, and 12-15% FeO was obtained which came close to the rhodonite composition, FIG. 45. These longer treatment times had once more produced the metallic globules first observed in cast 6. These were again found to be pure iron.

The 5 hours treatment at 1150°C produced some apparently complex structures. A few inclusions still retained their glassy structure, in which globular silica had precipitated, PLATE 15c. However, the majority of the inclusions exhibited a granular matrix in which both globular silica and a third light phase had precipitated, PLATE 15d. The proportion of the lighter phase varied, some inclusions containing very little, PLATE 15d, others containing substantial amounts, PLATE 15e. This phase was found to have a composition of 61% MnO, 4% FeO, 38% SiO_2, which is also the composition of the rhodonite-tephroite eutectic, FIG. 45. The granular matrix had a composition of 47% MnO, 4% FeO, 51% SiO_2. Treatment at 1150°C for longer periods, (50 and 100 hours), produced inclusions containing one or two large silica globules in a coarse granular matrix which had a composition lying within the rhodonite + (rhodonite-tephroite) eutectic phase field, PLATE 15f, FIG. 45.

Treatment at 1275°C for 50 hours produced crystalline inclusions in which the silica had a pronounced rosette morphology and the matrix had a lath like appearance. The matrix again had a composition in the rhodonite + (rhodonite-tephroite) eutectic region

of the phase diagram, PLATES 15g and h.

(iii)   <u>Cast 8 (Al-Si Deoxidised)</u>

Due to the wide composition range of the inclusions in this cast, heat treatment produced a number of different structures.

Treatments at 925°C resulted in the formation of three predominant types of structure:-

(a)   Inclusions containing an internal lath like structure, PLATE 16a.

(b)   Inclusions containing a light grey phase in the core which often contained crescent shaped regions of a darker phase, PLATE 16b.

(c)   Inclusions having a pronounced rim-core structure, PLATE 16c.

Inclusions having this latter structure (c) had an apparently crystalline rim which gave an analysis close to that of iron-cordierite; 20 - 22% FeO, $\sim$ 53% SiO_2, 24 - 27% Al_2O_3, (c.f. cordierite 22% FeO, 46% SiO_2, 32% Al_2O_3). The rim and core regions were separated by a dark phase having a glassy appearance and an analysis close to that of the peritectic at 1210°C; 28% FeO, 54% SiO_2, 16% Al_2O_3 (c.f. Peritectic 34% FeO, 48% SiO_2, 20% Al_2O_3, FIG. 46). However, in view of the small dimensions of these regions, this analysis should not be regarded as accurate. The core region of these inclusions consisted of a light grey phase, often containing many small metallic globules, PLATE 16c. The core analyses were usually found to be in the region of the fayalite - cordierite - silica eutectic trough; 45 - 50% FeO, 35 - 45% SiO_2, 9 - 12% Al_2O_3), (c.f. eutectic $\sim$ 48% FeO, 41% SiO_2, 12% Al_2O_3) and the metal globules were found to be iron, although their small size often caused matrix fluorescence, preventing accurate analysis.

The second type of inclusion, (b), PLATE 16b, also had a rim-core appearance, although this was far less pronounced than in the previous case, (c) PLATE 16c. Analyses obtained from the rim and core regions of these inclusions (b) were very similar to those obtained in the previous case, (compare the analyses given in PLATES

16b and 16c), but although analyses were obtained for the various constituent phases, these were usually found to be non-stoichiometric and did little to explain the complex structures observed.

The lath like structures contained in the first type of inclusion, (a) PLATES 16a and d, gave analyses close to the eutectic valley between the peritectic at $1205^{\circ}C$ and the eutectic at $1083^{\circ}C$; 35 - 40% FeO, 45 - 50% SiO_2, 15 - 20% Al_2O_3 (c.f. FIG. 46). The granular phase occurring between the laths in PLATE 16d was found to have a composition very close to that of the peritectic at $1205^{\circ}C$; 20 - 27% FeO; 48 - 55% SiO_2, 19 - 25% Al_2O_3. (c.f. peritectic 34% FeO, 48% SiO_2, 20% Al_2O_3).

The rim-core, (c), types of inclusion were observed to be the predominant form in the sample heat treated for 5 hours, whilst the other forms, (b and a), were predominant in the samples heat treated for 50 to 100 hours.

After 5 hours at $1000^{\circ}C$ the inclusions exhibited complex structures which contained a number of precipitated phases in a eutectic type of matrix, PLATES 16e and f. Analysis of the component phases revealed the structure to be non-equilibrium containing phases outside their normal stoichiometry ranges, and sometimes containing a greater number of phases than can equilibriate in a three component system. Nearly all of the inclusions contained large blocky precipitates, identified as hercynite of almost stoichiometric composition; 41% FeO, 59% Al_2O_3. A number of inclusions contained a light grey phase having a composition intermediate to that of fayalite and iron cordierite, in the region of the non-equilibrium garnet phase alamadine: 50% FeO, 36% SiO_2, 11% Al_2O_3. (c.f. alamandine, 43% FeO, 37% SiO_2, 20% Al_2O_3). Some inclusions also contained regions with compositions close to that of fayalite. A lath like or blocky dark grey phase, present in small amounts, PLATE 16e, was found to be a non-stoichiometric phase with a composition closest to that of mullite; 15% FeO, 15% SiO_2, 70% Al_2O_3, (c.f. mullite 30% SiO_2, 70% Al_2O_3). The eutectic areas analysed were of various compositions

but were always in the region of one of the eutectic troughs in the phase diagram.

After 50 and 100 hours at temperature, the inclusions had the appearance of coarse three phase structures, PLATE 16g, the component phases being analysed as fayalite, hercynite, and silica of almost stoichiometric compositions. Although all the inclusions analysed contained only these three phases it is possible that other inclusions contained a mullite-hercynite-silica phase assemblage. Two phase inclusions of the silica-hercynite type were also observed, PLATE 16h. The form of the inclusions after 50 and 100 hours indicates the non-equilibrium nature of the inclusions after 5 hours at temperature.

Treatment at 1150°C resulted in the precipitation of hercynite, some inclusions precipitating very little, others precipitating large amounts, PLATE 16i. No fayalite or mullite were observed even after the longest periods at temperature, and it is probable that the inclusion matrix was liquid at this temperature, as indicated by the formation of equilibrium dihedral angles with the metal matrix grain boundaries. Blocky or angular dark precipitates were sometimes observed in association with the hercynite, in the 100 hour sample, PLATE 16j; these were analysed as pure silica. The cracks apparently associated with this phase are an interesting feature and may indicate dimensional changes occurring during crystallisation.

Blocky hercynite precipitates were again produced on treatment at 1275°C, but not in the quantities produced at 1150°C. The glassy inclusion matrix was retained on quenching back to room temperature and was in all probability liquid at the treatment temperature.

3.2.4. <u>The Effects of Hot Rolling on the Inclusions</u>

(i) <u>Cast 1B (Undeoxidised)</u>

In each of the hot rolled samples examined, the wustite inclusions exhibited a wide variability in deformation, some inclusions remaining undeformed whilst others, of apparently identical size and composition, exhibited marked deformation, PLATES 17a and b. This variability in

deformation did not follow any logical sequence, samples deformed at both high and low temperatures (1275 and 925°C), and to both large and small reductions (1.8 and 0.3), containing both undeformed and elongated inclusions. Inclusion size also appeared to have had little effect on the deformation exhibited, except that the very smallest inclusions(< 3μm diameter) always remained undeformed, PLATE 17b. Closer inspection of some of the larger inclusions by S.E.M. revealed a second phase present on their surface, PLATE 17c. However, this feature was not peculiar to either the highly deformed or the undeformed types, PLATES 17c and d. This phase was identified by Energy Dispersive X-Ray Analysis (E.D.A.X.) as iron sulphide, FeS (Triolite).

(ii)   Casts 4, 5 and 6 (Silicon and Silicon-Manganese Deoxidised)

Both casts 4 and 5 were silicon deoxidised and contained very similar duplex silicate inclusions, those in cast 5 containing slightly less primary phase, FeO, than those in cast 4; (compare PLATES 2 and 3). Consequently both types of inclusions behaved similarly during hot rolling.

Deformation at the lower temperatures of 925 and 1000°C, resulted in the formation of conical voids at the inclusion-matrix interface, into which small fragments of the inclusion were often eroded, PLATE 18a. Erosion and fragmentation of the smaller duplex inclusions had apparently occurred by decohesion of the interface between the primary phase and the silicate matrix, PLATE 18a, although in some cases fragmentation also occurred by cracking through the silicate matrix, PLATE 18b. In contrast, the larger d uplex inclusions, with the finer substructure, often became fragmented through a more generalised crushing, PLATES 18c and d. It is apparent from PLATE 18c that a large hydrostatic pressure must have been generated during rolling in order to cause the metallic matrix intrusions observed.

At 1150°C the matrix of these duplex inclusions was apparently liquid, and the inclusions deformed plastically. With increasing reduction the inclusions became progressively thinner until the thickness

approached the diameter of the primary FeO particles. Subsequent reductions tended to strip the fluid matrix from the primary particles which ultimately became isolated in the metal matrix. This sequence of events can be seen from PLATES 19a to e. S.E.M. revealed the eutectic nature of the silicate matrix and the extent of its stripping from the primary phase, PLATE 19f. Also revealed were large numbers of small ($< 3\mu m$) secondary FeO inclusions, which had apparently remained completely undeformed under these conditions, ($\mathcal{E} = 1.2$, T = 1150°C), PLATE 19g.

Deformation at 1275°C resulted in a similar sequence of events except that the primary FeO had largely dissolved in the silicate matrix, at this temperature, FIG. 44. Consequently very little stripping of the silicate from the remaining primary phase was observed. The FeO taken into solution was subsequently reprecipitated on cooling, PLATES 20a to e.

The inclusions from cast 6 (Si-Mn) had a similar crystalline as cast structure as those from cast 4 and 5 except that the primary phase was manganowustite containing 72% MnO, as compared with pure wustite. On hot rolling the inclusions all behaved in a brittle manner analogous to the low temperature behaviour of the inclusions from casts 4 and 5. However, in this case such behaviour was observed at even the highest rolling temperatures.

(iii)   Cast 6B (Silicon-Manganese Deoxidised)

Inclusions present in the samples hot rolled at 925, 1000 and 1150°C exhibited no deformation even at the highest reductions, although at the higher temperature, (1150°C), the inclusions had begun to lose their glassy nature, becoming slightly opaline in appearance, PLATE 21a. This plate also shows a conical void at the inclusion matrix interface, which was a characteristic feature of the deformation of the plastic matrix around the more rigid inclusions, at low strains.

At 1275°C the inclusions exhibited both plastic and brittle behaviour, the behaviour becoming more brittle as the deformation

progressed. After the first pass, ($\mathcal{E}$ = 0.3), all the inclusions had
an oblate morphology, were opaline in appearance, and contained
rosette like precipitates, PLATE 21b. After the second pass, ($\mathcal{E}$ = 0.6),
the inclusions had a similar but more elongated appearance, PLATE 21c,
and a few of the inclusions had become fragmented, PLATE 21d, in
some cases exhibiting a duplex crystalline structure, PLATE 21e.
At higher reductions, the elongated, (plastic), types of inclusions
became progressively fewer, and the numbers of fragmented inclusions
increased. The fragmented types were observed in different stages of
dissemination, some obviously having only just become fragmented,
PLATES 21f to i, others having fragmented at some previous pass and
were in the process of becoming disseminated, PLATES 21j to l. At
high reductions, ($\mathcal{E}$ = 1.5 or 1.8) those inclusions fragmented at an
early stage had become widely disseminated and the individual isolated
fragments appeared to have become rotated into the direction of metal
flow, often apparently exhibiting some degree of deformation by
surface flow, PLATES 21m and n.

Examination by (S. E. M.) revealed the morphologies of these
inclusions to be more complex than had been discerned from optical
examination. Those inclusions fragmented at low strains were found
to be composed of small crystallites in a eutectic matrix, PLATES
22a and b. The structure of this matrix was found to be complex,
PLATE 22c. Unfortunately analysis facilities were not available
and a more complete description of this structure was not obtained.
At higher strains this type of inclusion became disseminated through
a process of hot tearing, the plastic inclusion matrix being torn and
stretched out between the separating primary crystallites, PLATE
22d. At high strains these crystallites were completely disseminated,
but retained a surface film of the eutectic which gave the inclusion
fragments the appearance of deforming by surface flow, PLATE 22e,
a phenomenon already observed on optical examination. Those
inclusions which did not fragment until a later stage in the deformation
programme, contained substantially less plastic matrix material,

whilst those inclusions which did not fragment until the highest deformations were reached, contained almost no plastic matrix material. Consequently they became fragmented into a large number of crystallites, PLATE 22f.

Although optical examination of the as cast structure revealed no evidence of a secondary inclusion population, examination of the hot rolled samples showed a number of smaller inclusions having a lath like or eutectic type of structure, PLATE 22h.

H. V. E. M. examination of the inclusion fragments extracted from the sample hot rolled to a strain of 1.8 at $1275^{\circ}C$, confirmed the crystalline nature of the inclusions. However, even at this high voltage the penetration of the beam was only able to reveal the structure of the smallest fragments, the majority being too thick to penetrate. Most of the fragments examined had a lath like or feathery structure, PLATE 23a and b. Selected area diffraction revealed many of the laths to be tephroite, PLATE 23c, and some patterns contained evidence of a second precipitate, having a larger lattice spacing. Not all of the fragments examined had a crystalline structure, a few being apparently glassy, in some cases containing a second phase which may also have been glassy, PLATE 23d. Other fragments exhibited mixed types of structure, some regions having the lath or feathery appearance described above, other regions retaining a glassy appearance, PLATE 23e. Many of the fragments also contained large numbers of small voids strung out along the boundaries between adjacent tephroite laths, PLATES 23b and c.

In order to obtain further plasticity measurements from this cast, SECTION 3.2.5 (ii), one bar was hot rolled, to the same sequence of reductions, at $1350^{\circ}C$. Optical examination revealed the inclusions to have behaved in a plastic (fluid) manner at all strains, the inclusions being progressively deformed throughout the rolling sequence. Examination by S. E. M. and H. V. E. M. revealed a rippled or 'pinch and swell' structure in the elongated silicate ribbons produced, PLATES 24a and b, and also revealed the presence of many small holes

in the ribbons produced at high strains, PLATE 24b. Some degree of spherodisation was also apparent around the edges of these holes, and around the periphery of the elongated ribbons.

(iv)   Cast 8 (Aluminium-Silicon Deoxidised)

Deformation at both 925 and 1000°C produced little deformation of the inclusions, most of which crystallised during heating to the rolling temperature, PLATES 25a and b. A few inclusions did exhibit some evidence of deformation, particularly at 925°C, but these had usually been partially fragmented, PLATES 25c and d. S.E.M. revealed many of the undeformed inclusions to be cracked, and in some cases the surface of the inclusion appeared to have been depressed into the interior, PLATES 25e and f.

Deformation at 1150, 1275 and 1350°C produced highly elongated inclusions which were apparently fluid at these temperatures, PLATES 26a, b and c. As in the case of the samples from cast 6B, hot rolled at 1350°C, these inclusions exhibited a boudinage, (pinch and swell) morphology, PLATE 26c and d, and contained many holes at the higher strains. Again, the periphery of the inclusions, and the edges of any holes, appeared to be thicker than other regions, indicating some degree of spherodisation. The boudinage morphology was readily apparent when the specimens were examined optically in the rolling plane section, PLATE 26f.

In order to determine the effect of rolling reduction on the behaviour of the inclusions, two bars were rolled at 1000°C and 1150°C using a true strain per pass of 0.6 (i.e. twice the previous strain). At 1000°C the inclusions again became crystalline but in this case most of the inclusions suffered some degree of fragmentation and dissemination, PLATES 27a and b. At 1150°C the inclusions behaved plastically and deformed into long stringers. However, in this case many instances of joining of adjacent inclusions were observed, PLATE 27c.

One sample from this cast was hot rolled to a strain of $\mathcal{E}$ = 1.2 at 1150°C and then cooled to room temperature. The sample was then reheated to 925°C and further reduced to a true strain of 1.8.

After deformation all the elongated inclusions exhibited brittle transverse fractures, particularly at the ends of the ribbons, PLATE 27d. S.E.M. revealed the extent of this fracturing and also showed that the larger blocks tended to become rotated in the direction of elongation, PLATE 27e.

(v)　　　Cast 11 (Calsibar (Ca-Si) Deoxidised)

In the samples hot rolled at 925°C the inclusions exhibited very little evidence of deformation, the few which did deform being duplex, containing precipitated silica rosettes, and frequently showing extensive cracking and conical void formation, PLATE 28a. The majority of inclusions were single phase, glassy and often exhibited the formation of conical voids at low strains, PLATES 29a and b. A few inclusions had a marked duplex structure, having a silica shell around the periphery together with globular silica precipitates, in a duplex eutectic matrix, PLATE 28b.

At 1000°C the inclusions exhibited variable plasticity, some deforming to a large extent whilst others showed no deformation, PLATE 28c. Analysis of the elongated inclusions showed them to be slightly less siliceous than the average ($\sim$ 70% SiO_2 compared to 75% average) and to have a slightly higher CaO level, ($\sim$ 15 - 20% compared to 15% average). Again conical voids were formed at low strains ($\leqslant$ 1.2), in the case of the non-deformable inclusions.

At 1150° and 1275°C the inclusions exhibited considerable elongation, PLATE 28d, and showed the rippling or boudinage effect seen in the case of the other fluid silicates. The duplex silicates having a silica rim generally resisted deformation at temperatures below 1275°C, although some did become fragmented. However, at 1275°C the eutectic matrix was apparently liquid, as evidenced by its glassy nature on cooling back to room temperature, and those inclusions having only a thin silica envelope were deformed, due to fracturing of this envelope, and were disseminated into long stringers, PLATES 28e and f. Those inclusions with thicker silica envelopes were able to resist deformation to a later stage in the deformation,

but in these too the silica sheath ultimately fractured, allowing the fluid core to deform.

(vi) <u>Casts 4B (Si Deoxidised) and 12 (Superseed, Sr-Si, Deoxidised)</u>

Both these casts contained clear, glassy, single phased, binary $FeO-SiO_2$ inclusions containing over 70% SiO_2. These inclusions remained undeformed at all the rolling temperatures and exhibited the formation of conical voids at low strains. These voids were largest at the lowest strains and at the lowest working temperatures, extending into the matrix by up to one half of the inclusion diameter on each side, PLATE 29a. They were somewhat smaller at higher working temperatures usually disappearing altogether at strains greater than $\mathcal{E} = 1.2$, PLATE 29b.

(vii) <u>Casts 7B (Al Deoxidised)and 10 (Hypercal, Ca-Al, Deoxidised)</u>

Both casts 7B and 10 contained refractory aluminous cluster type inclusions which exhibited similar behaviour at all rolling temperatures.

The alumina aggregates in cast 7B, described in SECTION 3.2.2. became progressively more fragmented and strung out as the reduction increased, PLATE 30a. Examination by S.E.M. showed that low reductions had resulted in fracturing of the sinter necks between attached particles, particularly those between connecting dendrite arms, PLATES 11f and 30 b to d. These low reductions also tended to crack and fracture a few of the sintered globular types of particles, PLATES 30f and g, and also produce conical voids, PLATE 30e. At higher reductions the sintered aggregates became progressively more fragmented, forming elongated fragmentary stringers of grain shaped particles, produced by successive fracturing of the sintered agglomerates, PLATES 30h and i. At the highest reductions these strings became well disseminated producing the familiar alumina stringers often observed in wrought aluminium killed steels, PLATES 30a and j.

The clusters in cast 10 also produced fragmentary stringers having a similar appearance to the inclusions in cast 7B, PLATE 31. Since this cast was not examined by S.E.M. it is not possible to

report on the exact mechanism of the fragmentation, although it is likely to be the same as was found in the case of cast 7B.

3.2.5. Plasticity Determinations

Relative plasticity values were determined only from casts 4, 5, 6B, 8 and 11. Relative plasticities were not determined from cast 1B due to the variability in the deformation of the Fe0 inclusions. Cast 6 contained inclusions which were brittle at all temperatures, whilst those in casts 4B and 12 were glassy and behaved rigidly at all temperatures. The cluster like inclusions present in casts 7B and 10 were not amenable to plasticity measurements.

(i)   Casts 4 and 5 (Silicon Deoxidised)

Low temperature (925 and 1000°C) behaviour was brittle and a relative plasticity value of zero was recorded for all reductions. The inclusion true strain ($\mathcal{E}_i$) and inclusion relative plasticities obtained by measurement of the aspect ratios of the deformed inclusions in the samples deformed at 1150 and 1275°C are given in TABLE 10a and b and plots of inclusion strain, ($\mathcal{E}_i$), versus matrix strain, ($\mathcal{E}_m$) are shown in FIGS. 48, 49, 52, 53. The true and apparent relative plasticity values obtained from these are shown in FIGS. 50, 51, 54, 55.

(ii)   Cast 6B (Silicon-Manganese Deoxidised)

At temperatures below 1275°C the inclusions behaved in either a brittle or rigid manner, and a relative plasticity of zero was recorded.

At 1275°C the inclusions initially behaved plastically but became brittle as crystallization took place. Aspect ratios of the plastic inclusions were determined at each reduction, but at high reductions (1.5 and 1.8), the numbers of plastic inclusions were restricted and even by examining a number of sections it was only possible to obtain 10 individual measurements at a strain of 1.5, and 8 at a strain of 1.8. Accordingly these values must be treated cautiously, although the values obtained seem to fit in well with values obtained

at lower reductions. At $1350^{\circ}C$ the inclusions all behaved plastically and relative plasticity values were obtained without difficulty, TABLE 10C. As with the other casts the inclusion true strain was plotted vs matrix true strain, FIGS. 56 and 57, and values of true and apparent relative plasticity were obtained from these, FIGS. 58 and 59.

(iii)   Cast 8 (Aluminium-Silicon Deoxidised)

At $925^{\circ}C$ and $1000^{\circ}C$ the inclusions behaved in either a brittle or a rigid manner during hot rolling, and values of relative plasticity were recorded as zero. Results obtained from the plastic inclusions in samples deformed at 1150, 1275 and $1350^{\circ}C$ are recorded in TABLE 10d; again inclusion true strain was plotted vs matrix true strain, FIGS. 60, 61 and 62, and the true and apparent relative plasticities derived are plotted in FIGS. 63 and 64. TABLE 10d also shows the values of inclusion true strain and relative plasticities obtained from the inclusions in the sample deformed at a true strain per pass of 0.6, at $1150^{\circ}C$. FIGURES 65 and 66 show plots of inclusion true strain vs matrix true strain, and true relative plasticity vs matrix true strain, at $1150^{\circ}C$, for samples deformed at both 0.3 strain per pass and 0.6 strain per pass.

(iv)   Cast 11 (Calsibar (Ca-Si) Deoxidised)

At $925^{\circ}C$ the inclusions had remained undeformed and a relative plasticity of zero was recorded. At $1000^{\circ}C$ the deformation of the inclusions was very variable, some having been elongated by a large amount, others remaining apparently undeformed. A maximum value of relative plasticity was obtained by measuring the aspect ratios of the most elongated inclusions and the relative plasticity was recorded as zero up to this maximum value, TABLE 10e. At 1150 and $1275^{\circ}C$, the elongation of the inclusions appeared to be fairly uniform, the range of relative plasticities determined being quite narrow. The inclusion true strains and relative plasticities determined are shown in TABLE 10e. Inclusion true strain is plotted against matrix true strain in FIGS. 67, 68 and 69, and the relative plasticities

obtained are plotted in FIGS. 70 and 71. Since a range of true strains
were obtained from the samples deformed at 1000°C, the non-plastic/
plastic transition exhibited by these inclusions must have occurred
over an extended range of temperature. The upper and lower limits
of this temperature range are represented by the dotted and full lines
in FIGS. 70 and 71.

(v)   Some General Observations

In every case the behaviour of the silicate inclusions changed
from either rigid or brittle behaviour to fluid or plastic behaviour over
quite a narrow temperature range, the initial value of relative
plasticity increasing from zero to a value in the range 2.0 to 3.0.
This is in agreement with previous results from the literature, (92,
114, 141, 142). At temperatures in excess of the non-plastic/plastic
transition, the relative plasticity was observed to decrease as the
temperature of deformation was increased; this was a general feature
of the behaviour of all the silicates examined.

Both true and apparent relative plasticities decreased, from
a maximum initial relative plasticity at zero matrix strain, as the
matrix strain increased. The magnitude of this initial relative
plasticity varied from cast to cast, the maximum value obtained being
3.0 in the case of cast 8.

The measured aspect ratios were taken from the larger more
easily measured inclusions and thus represent the maximum relative
plasticities exhibited by the inclusions, smaller inclusions exhibiting
significantly lower relative plasticities. Consequently the results
obtained had very small standard deviations, TABLE 10, but these
do not reflect the general range of deformation exhibited by the whole
of the inclusion population.

(vi)   Relative Plasticity Assessment by Quantitative Television
         Microscopy (Q.T.M.).

Hot rolled samples from casts 8 and 11 were examined by
Q.T.M. in order to determine the projected lengths of the deformed
inclusions. Unfortunately these projected lengths, even when corrected

for variations in the inclusion area fraction, gave quite erratic results, indicating that the inclusion size distribution varied from specimen to specimen, (see APPENDIX 2). Consequently relative plasticity determinations using this technique were abandoned.

SECTION 4

DISCUSSION OF RESULTS

4.   DISCUSSION OF RESULTS

4.1   The Inclusions present in the As-Cast Materials

Generally the inclusions present in the as-cast materials
were of the types expected, and in the few cases which gave unexpected
results, the absence of the intended species or the appearance of
additional species was usually readily explained.

Oxygen analyses of the cast materials showed clearly the
effects of the different deoxidation practices. The undeoxidised melt,
cast 1B, retained all the dissolved oxygen into the ingot stage, giving
rise to an interdendritic distribution of wustite globules on solidification,
PLATE 1. The oxygen content of 0.18%, TABLE 9, was somewhat
higher than had been expected, (113) but was not far from the predicted
value of 0.16%.

Small additions of silicon ($\sim$ 0.1%) to casts 4 and 5, reduced
the total oxygen level only slightly, TABLE 9, most of the primary
products of deoxidation persisting into the solid ingot. These primary
deoxidation products were binary iron silicates having silica contents
in the region of 15 - 20%, FIG. 44, TABLE 8, PLATES 2 and 3, and
were associated with an interdendritic distribution of secondary
wustite globules which had precipitated on solidification. The large
numbers of primary silicates persisting into the solid ingot is
indicated by the difference in the soluble and total silicon levels
obtained on chemical analysis, TABLE 9.

The simultaneous addition of aluminium and silicon to cast
8, further reduced the total oxygen content, with the levels of
deoxidant added, but a large number of the primary inclusions still
persisted into the ingot. Again the large numbers of siliceous
inclusions present in the ingot, PLATE 7a, is reflected in the difference
between the total and soluble silicon levels. An interesting feature
of this cast was the wide composition range of the inclusions, FIG. 46,

and the presence of large numbers of small alumina dendrites distributed between the siliceous globular inclusions, PLATE 7d. Pickering (85) has stated that the practice of making simultaneous additions of silicon and aluminium can lead to the formation of local regions of widely differing deoxidant concentration, during the deoxidation process. This can lead to the formation of complex non-equilibrium inclusions of markedly differing compositions, as they are transferred from one region to another by melt turbulence. In the case of this particular cast the observation of dendritic phases within some of the glassy inclusions, PLATE 7b, suggests that these silicates had nucleated heterogeniously on the dendritic products of deoxidation formed in regions having a high aluminium concentration. Subsequent transport of these solid precipitates to regions of higher silicon concentration then resulted in the heterogenious precipitation of a liquid siliceous deoxidation product around the solid nuclei. Although a few of these internal dendritic phases were found to have non-stoichiometric compositions, containing both wustite and silica, these were probably spurious analyses arising from the exitation of the glassy matrix by the electron beam. The dendrites were most probably pure alumina, as was in fact found to be the case in one particular instance. This hypothesis seems to be supported by the presence of large numbers of small alumina dendrites distributed throughout the ingot, which were presumably precipitated within the aluminium rich regions formed on first adding the deoxidants. However, in view of the method of making this cast (SECTION 3.1.2) it could also be argued that these small dendrites were the remnant products of a previous deoxidation treatment involving an addition of 0.36% Aluminium, (SECTION 3.1.2). Although the melt was subsequently reoxidised, some alumina may have remained in the melt. However, this would seem improbable in view of the rapid rate of removal of alumina from melts deoxidised by aluminium alone (SECTION 3.2.2.). Alternatively, the dendrites may have been produced on atmospheric re-oxidation during teeming through air, the level of dissolved silicon,

found by chemical analysis to be 0.003%, TABLE 9, being insufficient
to produce any silicate inclusions. The angular precipitates present
in a few of the glassy inclusions, PLATE 7c, were found to be hercynite
of almost stoichiometric composition, but although a number of
inclusions were observed containing a phase having a rosette morphology,
during examination by S.E.M., PLATES 7c and e, no such inclusions
could be found on optical examination. The matrix cracks apparently
associated with this 'phase', PLATE 7e, are characteristic of
crystallisation cracking. In fact the rosette morphology is quite
characteristic of precipitated silica, although there is currently some
dispute as to whether this precipitate is, in fact, crystalline cristobalite
or a vitreous form of silica precipitated within an extended miscibility
gap in the supercooled liquid state (80). However, the majority of the
inclusions contained no precipitates, even though they exhibited rather
variable compositions, TABLE 8.

The simultaneous addition of 1% manganese with the silicon
(0.075% and 0.3%), casts 6 and 6B, reduced the oxygen content still
further, TABLE 9, the rather high oxygen content of cast 8 (Al-Si)
undoubtedly being due to the low residual aluminium and silicon
levels, which allowed rapid reoxidation to occur. The ternary iron-
manganese silicates produced in casts 6 and 6B were duplex crystalline
types, in the case of cast 6, PLATE 5, but were glassy more siliceous
types in the case of the higher silicon addition, cast 6B, PLATE 6,
FIG.45. Although the composition range of the inclusions present
in cast 6 was quite narrow, FIG.45, it fell in the region of the
tephroite composition and extended across the tephroite-mangano-
wustite eutectic valley into the primary (Fe,Mn)O phase field.
Consequently inclusions exhibiting several different constitutions were
observed:-

(i)   Inclusions containing primary manganowustite in a tephroite-
        manganowustite matrix, PLATE 5a, were present in slight
        excess of inclusions containing tephroite as the primary
        phase. Large numbers of inclusions also had compositions
        in the region of the tephroite-manganosite eutectic, PLATE 5b.

(ii)   A number of inclusions having an internal lath like constitution were found to be of the tephroite composition, PLATE 5c. However inclusions containing a tephroite-rhodonite eutectic matrix were not observed.

(iii)   A number of small background globular inclusions had a glassy appearance but were of a similar composition to the larger inclusions containing tephroite laths, PLATE 5c.

(iv)   The secondary population of manganowustite inclusions, PLATE 5d, was to be expected in view of the high residual manganese content of the melt, TABLE 9.

The higher silicon addition and lower manganese recovery in cast 6B gave rise to a population of small secondary glassy silicates precipitated during solidication and cooling; these can be seen in the background of PLATE 22a.

The more complete deoxidation produced by the addition of 1% silicon to cast 4B, resulted in the production of highly siliceous glassy inclusions, PLATE 4. These had relatively high melting points, did not coalesce so easily to produce the larger, more easily removed types and in consequence many were retained into the solid ingot.

Cast 12 contained inclusions of very similar size and composition to those observed in cast 4B, PLATE 10, FIG. 44, though of slightly lower silica content. This is not surprising since the deoxidant employed contained $\sim$ 70% silicon, TABLE 5, and its addition at a level of 1% would be equivalent to an addition of 0.7% silicon metal; its chief advantage over the more usual silicon deoxidants being its greater density. Many of the silicates presented in this cast could also have been carried over from the predeoxidation stage which employed an addition of 0.8% silicon metal (SECTION 3.1.2).

Deoxidation by the addition of 1% Calsibar, cast 11, resulted mainly in the production of single phased glassy silicates, PLATE 9. A few duplex types were observed, PLATE 28b, as was a calcium enrichment in the periphery of several of the glassy inclusions, PLATES 9b and c. The predeoxidation treatment, employing a 0.8% silicon addition, would have produced a distribution of siliceous, single phased, glassy inclusions, not all of which would have been

removed before the Calsibar addition was made. Those remaining
after the Calsibar addition would have then reacted with the calcium
added giving rise to a progressive surface enrichment. The duplex
inclusions observed were probably less siliceous and developed their
two phased structure in the miscibility gap of the $CaO-FeO-SiO_2$
system, FIG. 47. The presence of CaO in these inclusions would have
the effect of lowering their viscosity, by reducing the silica network
structure, allowing greater ionic mobility and resulting in a more
equilibrium constitution. The effect of CaO on the network structure
has an important effect on the plastic behaviour of the inclusions and
is discussed in more detail later in connection with their behaviour
during hot working. The oxygen content of this cast was quite low,
(0.018%), TABLE 9, and indicates the effect of calcium in rendering
the inclusions less viscous, promoting easier coalescence and hence
easier removal from the melt.

Cast 10 was deoxidized with a 1% addition of Hypercal in
which the deoxidizing species were calcium and aluminium, the
silicon content being as high as 40%, TABLE 5, but having little
effect in this case because of the predeoxidation treatment employing
a 0.8% silicon addition. This treatment resulted in the production
of small clusters of aluminous inclusions consisting mainly of
numerous small particles of corundum, PLATE 8a, but also
containing occasional particles of calcium hexaluminate. The small
inclusions observed containing corundum laths and calcium hex-
aluminate blocks in a silicate matrix, PLATE 8b, were probably the
remnant silicate population, resulting from the predeoxidation
treatment with silicon, which had reacted with the calcium and
aluminium, producing these more complex forms. The oxygen content
of this cast was very low, TABLE 9, and reflected both the efficiency
of deoxidation by calcium and aluminium and the rapidity with which
the deoxidation products were removed from the small experimental
melts. This rapid rate of removal is a consequence of the high
surface energy of these inclusions, resulting in the formation of large

inclusion clusters which are readily absorbed onto the furnace lining and into the covering slag. Only cast 7B, which was deoxidized with a heavy addition of aluminium, had a lower final oxygen content. The deoxidation of cast 7B with aluminium is discussed more fully in SECTION 4.5.1.

4.2 The Effects of Heat Treatment on the Inclusions Present in Casts 6, 6B and 8

4.2.1. Cast 6 (Si-Mn)

The temperatures employed in the heat treatment programme were all below $1317^{o}C$, which is the temperature of the manganosite-tephroite eutectic in the $MnO-SiO_2$ system, FIG.45. Consequently the phase assemblages in the inclusions all remained substantially unchanged throughout the treatment programme. Most temperatures served only to spherodise and coarsen the eutectic matrices, producing the granular structures seen in PLATES 14a and b.

The metallic iron globules were precipitated most intensely at the lower two treatment temperatures, PLATES 14b and c, and were probably formed by the oxidation of iron from the ferrous to ferric state, within the inclusion, resulting in the precipitation of the excess metal.

$$3Fe^{2+} \longrightarrow 2Fe^{3+} + Fe$$
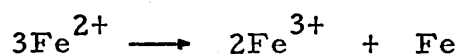
This may also offer some explanation for the apparent partial glassification of the matrix on treatment at temperatures as low as $1000^{o}C$, PLATE 14c.

Although manganese sulphide was not observed as a constituent phase in the inclusions in the as-cast state, it is unlikely that this phase would be precipitated during heat treatment. The sulphur content of this cast, 0.0056%, was not appreciably higher than that of the other casts, and the few inclusions observed, which contained MnS, were probably isolated examples.

4.2.2 Cast 6B (Si-Mn)

At 925 and 1000°C the glassy inclusions precipitated silica, PLATES 15a and b, possibly as a result of the liquid miscibility gap in the $MnO-SiO_2$ system being extended below the equilibrium solidus temperature into the supercooled liquid state. Treatments in excess of 5 hours resulted in the complete devitrification of the remaining glassy phase producing a matrix having a granular appearance, PLATE 15b. The precipitation of metallic iron globules probably evidenced once again, a partial oxidation from the ferrous to ferric state.

At these temperatures the inclusion compositions lay within the silica + rhodonite or rhodonite + tephroite regions of the phase diagram, FIG. 45, and also lay well below the minimum solidus temperature; which in this case was the rhodonite-tephroite eutectic temperature at 1251°C. However, this would be depressed slightly due to the presence of a small amount of FeO in these inclusions. Although rhodonite was the equilibrium phase, its nucleation had apparently been inhibited, and although the analysis of the inclusion matrix came near to the rhodonite composition, 54% SiO_2, 30% MnO, 14% FeO, (Rhodonite 46% SiO_2, 54% MnO), its granular constitution indicated a mixture of phases. These were possibly silica and tephroite.

The structures observed in the samples heat treated for 5 hours at 1150°C, PLATES 15c, d and e, probably represented the early stages in the decomposition of the glassy inclusions and were at a non-equilibrium transition stage. Again, there were many globular silica precipitates, most probably of a vitreous type, sometimes observed in a glassy matrix, PLATE 15c, but more usually in a granular matrix, PLATES 15d and e. The lighter areas having a composition close to that of the rhodonite-tephroite eutectic, PLATES 15d and e, possibly represented either a non-crystalline stage before devitrification was complete or alternatively an unresolvable eutectic structure.

Longer treatments at 1150°C resulted in all the inclusions developing a granular type of matrix with an overall composition lying within the rhodonite + (rhodonite-tephroite) eutectic phase field, PLATE 15f.

After heat treatment at 1275°C the silica had precipitated in the form of both large and small rosettes, PLATES 15g and h, whilst the matrix had developed a lath like or feathery appearance. It is probable that this matrix was liquid at the treatment temperature, which was somewhat above that of the rhodonite-tephroite eutectic at 1251°C. After the initial precipitation of silica, at 1275°C, the liquid matrix should have precipitated rhodonite on cooling through a peritectic reaction with the precipitated silica, FIG. 45. However, on air cooling this reaction was effectively suppressed and resulted in the crystallisation of the matrix as a micro-crystalline mixture of rhodonite and tephroite, PLATES 15g and h.

4.2.3 Cast 8 (Al-Si)

Treatments at 925°C produced inclusions which exhibited complex non-equilibrium structures, containing a number of non-stoichiometric phases, PLATES 16a to d. These resulted from the rather variable compositions of the as cast inclusions, and represent the initial stages of precipitation reactions. The formation of small metallic globular precipitates was again observed and once more indicates the partial oxidation from the ferrous to ferric state, PLATES 16b and c. The cordierite phase, $(2FeO.2Al_2O_3.5SiO_2)$, was apparently very slow to form at this temperature and was not observed in any of the structures examined.

The rim-core inclusions observed in the samples treated for 5 and 50 hours, PLATE 16c, could have been produced in either of two ways. They may have developed through a reaction between the aluminium dissolved in the metal matrix around the inclusion, and the less stable oxides in the inclusion, particularly the FeO, resulting in the gradual development of a crystalline rim. Alternatively they may have been produced by the preferential nucleation of specific crystalline phases at the inclusion/matrix interface.

Evidence in support of the former hypothesis was obtained from the analysis of the inclusion. This showed that the rim regions were richer in alumina than the core, which contained an excess of FeO, PLATE 16c. However this would seem to be contradicted by the chemical analysis of the bulk sample, which showed that the metal matrix only contained 0.008% of dissolved aluminium, which is probably too low to support such an extensive reaction. It is conceivable that both mechanisms played a role in the development of these structures.

Non-equilibrium structures were again produced on heat treatment at 1000°C. After 5 hours the inclusions contained as many as four separate phases, PLATE 16e, these being the equilibrium hercynite and fayalite phases and transition metastable phases of non-stoichiometric and alamandine compositions. In addition many regions had a lamellar or eutectic structure, the ternary cordierite phase again being conspicuous by its absence. After 50 and 100 hours at temperature the pseudo-equilibrium three phased structures were developed, consisting of hercynite, fayalite and silica, present in various proportions, PLATES 16g and h. These structures probably developed through the initial precipitation of hercynite, followed by, or simultaneously with, that of fayalite. The residual highly siliceous glass could then have crystallised in the remaining spaces resulting in the skeletal morphology of the silica phase. As was the case with the rhodonite phase in cast 6B, the cordierite phase, though present in the equilibrium diagram, was not formed during any of the heat treatments given.

At 1150°C, hercynite was again the primary precipitate, PLATE 16i. After extended treatments, of 100 hours, silica was precipitated and exhibited a characteristic block like morphology, which frequently contained numerous crystallisation cracks. Although tridymite is the equilibrium modification of silica at this temperature, FIG. 45, it more usually has a lath like morphology, (65). The

fayalite phase is apparently not precipitated at this temperature, the composition of the inclusions possibly lying within a metastable silica-hercynite-liquid region of the phase diagram. The presence of a liquid phase of lower viscosity is evidenced by the formation of equilibrium dihedral angles at the inclusion-matrix grain boundary intersections.

At 1275°C the inclusions were mostly liquid, although a few did contain one or two small hercynite precipitates.

4.3 The Effect of Hot Rolling on the Morphology of the Inclusions

4.3.1 Cast 1B (Undeoxidised)

The marked variability of deformation, exhibited by the wustite inclusions present in this cast was unexpected, PLATE 17, other workers having previously obtained satisfactory results using similar techniques, (9, 112). This variability could have been due to a sulphur-segregation effect, much of the sulphur being segregated into the larger primary wustite particles. Although no quantitative analyses were obtained, the second phase deposit frequently observed on the surface of these particles was identified qualitatively, by Energy Dispersive X-ray Analysis, (E.D.A.X), as FeS, PLATES 17c and d. This deposit may have originated from a pseudo-binary eutectic precipitation between the metallic iron matrix and FeS at the inclusion surface during solidification. However, these deposits were observed on both highly elongated and only slightly elongated inclusions and hence can offer only a partial explanation for the observed variation in behaviour. A marked difference in behaviour between the large primary and smaller secondary inclusions can clearly be seen in PLATES 17b, c and d, the small secondary inclusions exhibiting practically no deformation.

From the structures observed during scanning electron microscopy it would appear that there is a minimum inclusion size below which the inclusions will not deform. Although a variation in inclusion composition with size can be invoked to explain this observation in the present case, it is unlikely that this explanation

is applicable to similar observations made in the case of the other casts containing deformed inclusions. The effect of inclusion size on the relative plasticity of the inclusions is discussed in more detail in SECTION 4.4.3

4.3.2   Casts 4, 5 and 6 (Si and Si-Mn Deoxidised)

The brittle behaviour of the inclusions contained in casts 4 and 5, on deformation at 925 and 1000°C, and of those in cast 6 at temperatures up to 1275°C, was typical of the low temperature behaviour of the larger duplex crystalline silicates. The larger inclusions, (> 70μm diameter), which usually contained a finer distribution of primary phase than the smaller inclusions, were generally fractured at lower strains, PLATES 18c and d, often producing long fragmentary stringers at high strains. These inclusions were initially fractured into a few large fragments, which became quite widely disseminated, before being fractured further at higher matrix strains. At these higher strains the stresses generated within the steel matrix increase markedly, and this undoubtedly accounts for the fracturing of the smaller inclusions which had resisted fragmentation at the lower strains. The magnitude of the hydrostatic stress, developed during deformation, can be judged from the depth to which the plastic metal matrix has been intruded into the cracks produced on the initial fracturing of the inclusions, PLATES 18c and d. In contrast to the behaviour of the large inclusions, the smaller ones became disseminated through the decohesion of the interfaces between the primary phase particles and the silicate matrix, resulting in a finer scale fragmentation. At high strains this mechanism could lead to the formation of extremely long thin fragmentary stringers, particularly if the rolling temperature were lower, as in cold rolling, where the forces produced are greater and matrix welding is less likely to occur.

The transition from brittle to fluid (plastic) behaviour, in the case of casts 4 and 5, occurred in the region of 1150°C, FIGS. 48 - 55. In fact, allowing for heat losses during the transfer of the

test bar from the furnace to the rolling mill, and due to the roll chilling effect, this temperature may have been even lower. This temperature lies somewhat below the accepted value of 1178°C for the wustite-fayalite eutectic in the $FeO-SiO_2$ system, which is the solidus temperature of these inclusions and is the temperature at which the brittle-plastic transition would logically have been expected to occur. However the difference between the measured transition temperature and the solidus temperature can probably be explained by the adiabatic heating effect occurring in the roll throat during deformation. It is also well known that high hydrostatic pressures can render normally brittle substances quite ductile, (147), and it is possible that some similar mechanism might apply here. However, this mechanism would be expected to lower the non-plastic/ plastic transition temperature to a greater extent at the higher strains, where the hydrostatic stresses generated are highest. In fact such an effect was not observed, although the experimental method may not have been sensitive enough to detect such changes.

The stripping of the liquid silicate matrix from the primary FeO particles, on deformation at 1150°C, is directly attributable to their low relative plasticity, PLATE 19. At 1275°C the primary FeO was largely dissolved in the liquid silicate matrix and consequently very little stripping could take place during deformation, PLATE 20.

The background population of secondary FeO inclusions were again deformed by varying amounts, as was the case in cast 1B, the deformation being more apparent at 925 and 1000°C, PLATE 18, than at 1150 and 1275°C, PLATES 19 and 20. This was presumably due to the more rapid softening of the iron matrix, compared with that of the wustite inclusions, on increasing the temperature of deformation. The rigidity of the smaller inclusions was again apparent from examination of the extracted inclusions by S.E.M., PLATE 19g.

In cast 6, the addition of 1% manganese with the silicon deoxidant produced a primary inclusion population of ternary iron-

manganese silicates of a similar constitution to the inclusions present in casts 4 and 5 (compare PLATES 2, 3 and 5), but which were predominantly manganese rich, the FeO content being less than 15%. The solidus temperature of this type of inclusion is much higher than that in the corresponding binary iron-silicate system, approximately $1300^{\circ}C$ as compared with $1178^{\circ}C$, FIG. 45; consequently these inclusions did not exhibit the transition from brittle to plastic behaviour within the deformation temperature range employed.

4.3.3   Cast 6B (Si-Mn Deoxidised)

At deformation temperatures of 925, 1000 and $1150^{\circ}C$ the glassy iron-manganese silicate inclusions behaved in a rigid manner, giving rise to the usual conical voids, at low matrix strains, and retaining their glassy appearance throughout the deformation sequence, PLATE 21a. Some inclusions did, however, take on an opaline appearance after deformation at $1150^{\circ}C$, indicating the initiation of devitrification. These observations agree quite well with the observations made on the heat treated samples, which developed only small globular silica precipitates within periods at temperature of less than 5 hours.

The rapid transition from rigid to plastic, or fluid, behaviour on increasing the deformation temperature from $1150^{\circ}C$ to $1275^{\circ}C$, FIGS 56 - 59, is characteristic of the behaviour of all glassy silicates, and has been extensively reported in the literature, (92, 93, 101, 113, 114, 141, 142). The transition temperature of 1150 - $1200^{\circ}C$ observed in the present case lies more than $100^{\circ}C$ below the corresponding solidus temperature of the equilibrium crystalline form, FIG. 45, and although the effects of adiabatic heating and hydrostatic pressure may be sufficient to explain the small difference between the transition temperature and the solidus temperature observed in casts 4 and 5, it is improbable that these effects can account for the much greater difference observed in the present case. It is unlikely that the solidus temperature in the equilibrium situation

has any great bearing on the behaviour of glassy, non-crystalline, non-equilibrium inclusions, and the controlling influence is more likely to be the viscosity-temperature relationship of the glassy phase. A possible relationship between the relative plasticity exhibited by this type of inclusion and its viscosity at the deformation temperature is described in more detail in SECTION 4.4.1

The change in the behaviour observed during deformation at 1275°C was quite striking, and occurred upon the crystallisation of the glassy inclusions. This observation confirms that the solidus temperature of the crystalline silicate is not the factor controlling the behaviour of the glassy silicate, and is further supported by Shiraiwa's report of a marked difference in the softening temperature, as measured by hardness testing, between the crystalline and non-crystalline forms of synthetic silicate slags, (81), FIG. 37. The more rapid precipitation of silica occurring during heating to the working temperature and during subsequent deformation and reheating treatments, compared with that observed during static heat treatment, PLATES 21b and c, suggests that the extra energy supplied by the deformation process may have accelerated this precipitation. However, in contrast to the inclusions heat treated at 1275°C, which were composed of silica rosettes in a feathery rhodonite-tephroite matrix, PLATES 15g and h, the inclusions present in the samples hot rolled at this temperature, ultimately developed a more equilibrium structure, containing many rhodonite crystallites, PLATES 21e and 22a, b, and d - g. Such structures probably developed through a reaction between the glassy matrix and the silica precipitates formed earlier in the deformation sequence, FIG. 45. This difference between the structures developed during heat treatment and on hot rolling, may again lie in the additional energy supplied to the viscous inclusions as they deformed. This could have helped in the nucleation of the complex rhodonite lattice and would certainly have aided the reaction between the primary silica precipitates and the glassy matrix, through the redistribution of silica tetrahedra and iron and manganese ions.

The mechanisms by which the various inclusion morphologies were produced, upon deformation at $1275^{\circ}C$, PLATES 21b to n, can be explained by consideration of the devitrification reactions taking place. Provided that deformation occurred whilst the inclusions were in a non-crystalline, glassy state, they behaved in a plastic manner, producing the elongate morphologies shown in PLATES 21b and c. In fact all the inclusions behaved in this way during the first hot rolling pass. At this stage, a few of the inclusions began to precipitate rhodonite crystallites, by the reaction of the glassy matrix with the precipitated silica, this being induced by the preceding deformation. This reaction probably occurred initially in the less silicous inclusions in which the silica precipitation was almost complete, the more siliceous inclusions retaining enough silica in solution to maintain their glassy nature. These latter types again behaved plastically during the succeeding rolling pass. However, this pass took place before the reaction between the glassy matrix and the silica precipitates, in the less siliceous inclusions, was complete and the rhodonite crystallites already formed were pulled apart and the remaining glassy matrix stretched out between the separating crystalline fragments, PLATES 22a, b and d. This structure was, however, only observed on examination by S.E.M., the amount of remaining glassy matrix usually being so small that on optical examination the inclusions appeared to be fragmented by what was originally believed to be a brittle fracture mechanism, PLATES 21d to g. Subsequent crystallisation of this matrix material, on cooling, initially precipitated more rhodonite, ultimately leaving a small quantity of liquid which solidified as a binary rhodonite-tephroite eutectic, at temperatures slightly below $1250^{\circ}C$, FIG. 45. The rhodonite precipitated by this mechanism was continuous with the primary rhodonite crystallites but formed a network structure in which globular volumes of the eutectic were contained, PLATE 22c. Those inclusions which were more siliceous, had to precipitate a greater quantity of silica before the silica-matrix reaction could

take place. This resulted in the plastic glassy state being retained to a later stage in the rolling schedule, successive passes enabling more silica to precipitate. Ultimately the driving force was sufficient for the deformation introduced to initiate the silica-matrix reaction, which occurred rapidly due to the greater quantity and finer distribution of the precipitated silica. The resultant crystalline inclusions were composed of numerous small rhodonite crystallites containing little or no plastic silicate matrix, PLATES 21h, i, k and 22f. At higher strains the inclusions which had crystallised early in the deformation sequence became widely disseminated and the remaining film of plastic inclusion matrix, still adhering to the rhodonite crystallites, was gradually stripped away. This gave the crystallites the appearance of fragments deforming by a surface flow mechanism, PLATES 21m, n and 22e.

The smaller secondary inclusions present in this cast were also plastically deformed on rolling at $1275^{o}C$, though the extent of their deformation was somewhat less than that exhibited by the larger primary inclusions. These inclusions were probably less siliceous than the primary inclusions, since they were found to contain numerous tephroite laths, PLATE 22h. Examination by High Voltage Electron Microscopy, of the inclusion fragments extracted from the sample deformed to a true strain of 1.8 at $1275^{o}C$, showed lath like structures similar to those observed in the secondary inclusions, PLATES 23a, b and c, and it is most likely that these fragments originated from the secondary inclusion population, the fragments originating from the primary types of inclusion being too thick for the electron beam to penetrate. The diffraction patterns obtained from these structures were indexed as tephroite, PLATE 23c, and although a number of patterns contained two sets of diffraction spots, one indicating the presence of another phase having a much larger 'd' spacing, these were usually complicated by double diffraction effects, making indexing difficult. Although the presence of rhodonite was not confirmed by this technique, this does

not preclude its existence in these structures. The large numbers of small voids observed along the lath boundaries in these fragments, PLATES 23b and c, have the appearance of creep cavities and indicate that some of the deformation occurred by shearing along these boundaries. However, the deformation temperature employed, $1275^{\circ}C$, lies well above the rhodonite-tephroite eutectic temperature, $1251^{\circ}C$, and it is difficult to see how these inclusions could have been crystalline during the deformation; although the heat loss due to roll chilling may have been sufficient to cause the inclusions to crystallise during the pass. The small voids observed in the longitudinal sections of some of the deformed primary inclusions, PLATE 22g, may also have been formed by this cavitation mechanism.

At $1350^{\circ}C$ the compositions of the inclusions lay within the liquid + silica region of the phase diagram, FIG. 45, and consequently the inclusions behaved plastically upon deformation. Although the silica precipitates were again expected to form at this temperature, very few were actually observed, indicating either that the inclusions still retained a non-equilibrium structure, or that their compositions were actually less siliceous than the analyses obtained from the inclusions in the as-cast samples had indicated. A reduction in the silica content of only 5%, from the 51% obtained on analysis of the cast specimens, would render the inclusions completely liquid at this temperature, FIG. 45. Deformation during the first and second passes, produced flat, oblate, plate-like inclusions, which exhibited a slight rippling effect on their surface, PLATE 24a. At higher strains the inclusions were deformed into long thin ribbons, having a relatively uniform width but exhibiting a marked pinch and swell (Boudinage) structure; as was revealed by transmission electron microscopy, PLATE 24b. Numerous holes were observed in these ribbons and the increased thickness around the peripheries of these holes, and around the edges of the inclusion, was probably due to a surface energy effect. The boudinage structure of these inclusions

was observed in every sample, from several different casts, which contained highly elongated liquid silicates. Although this effect is not easily explained, it is discussed in more detail in SECTION 4.1.4(ii): As was the case with the plastic inclusions in casts 4 and 5, the relative plasticity exhibited by the inclusions began to decrease as the deformation temperature was increased above the non-plastic/plastic transition. This once more indicated an increase in the strength of the inclusions, relative to the metal matrix, at these temperatures.

4.3.4   Cast 8 (Al-Si Deoxidised)

Because of the wide composition range exhibited by the inclusions present in this cast, it was expected that they would exhibit a range of temperatures over which the non-plastic/plastic transition would occur. This was in fact observed, though to a limited extent, and a few inclusions exhibited plastic behaviour at temperatures as low as $925^{\circ}C$. However, these apparently devitrified during the early stages of deformation, or during the first interpass reheating, and in most cases became fragmented during subsequent passes, PLATES 25c and d. It would seem logical to assume that the inclusions which behaved plastically at these lower working temperatures, were the less siliceous types, these being more likely to have a lower non-plastic/plastic transition temperature. However, an alternative explanation can be offered for the opposite case, i.e. inclusions with a higher silica content. Here the more siliceous inclusions would have been more resistant to crystallisation than the less siliceous types, and in consequence could have retained their glassy state into the first, or even second, pass sequence. Provided that the non-plastic/plastic transition temperature of these glassy forms was below $925^{\circ}C$, plastic behaviour would have occurred on deformation. The less siliceous inclusions, though initially less viscous, would have crystallised more rapidly, probably on heating to the working temperature, and would have been converted to the non-plastic crystalline form before deformation took place. It was interesting to note that although the majority of the inclusions which became crystalline whilst retaining their spheroidal morphology were highly

resistant to fracturing, PLATES 25a and b, those inclusions which became elongated by even the smallest amount before crystallisation took place, invariably became fractured during subsequent passes, PLATES 25c and d.

At rolling temperatures of $1150^{\circ}C$ and above, all the inclusions showed plastic or fluid behaviour, producing elongated morphologies of the type seen in cast 6B, PLATE 26. At low matrix strains the inclusions were deformed into ellipsoids, PLATES 26a and b, but at high strains the boudinage structures were again developed, PLATES 26c, d and f, often containing holes in the elongated ribbons. Spherodisation around the edges of these ribbons and the peripheries of the holes produced was again apparent.

Although a few of the deformed inclusions contained angular precipitates, PLATE 26e, these were uncommon, the vast majority being single phased glasses. This is in contrast to the structures produced during heat treatment, which contained numerous hercynite and silica precipitates, particularly after treatments at $1150^{\circ}C$, PLATE 16i and j. However, since the minimum time employed for the heat treatments was 5 hours, the much shorter periods at temperature during hot rolling may have been insufficient to produce these precipitates. At temperatures of $1275^{\circ}C$ and above the inclusions were in the liquid state and fluid behaviour was to be expected. An interesting observation, made during the S.E.M. examination of these inclusions, was the extent of the matrix welding, occurring through the holes formed in the fluid ribbons, and between the separating inclusion fragments produced at lower temperatures. In every case, where the matrix metal had been able to make contact, complete welding had occurred, eliminating the matrix discontinuities. The reduction in relative plasticity at temperatures in excess of the non-plastic/plastic transition temperature, observed in casts 4, 5 and 6B, was again observed, FIGS. 63 and 64, TABLE 10, once more indicating an increase in the relative strength of the inclusions at these temperatures.

The effect of increasing the reduction per pass from 0.3 to 0.6, at 1000°C was to make the crystalline inclusions more brittle, nearly all the inclusions being fractured under the increased rolling loads. This led to the formation of long fragmentary stringers at the higher strains, PLATES 27a and b. At 1150°C the increased strain rate had only a marginal effect on the relative plasticity of the inclusions, FIGS. 65 and 66, and lies within the limits of experimental error. However, although this result suggests that the strain rate has little effect on the relative plasticity of liquid silicate inclusions, its effect on the behaviour of crystalline plastic types, such as the manganese sulphides, may be quite different.

The elongated fluid inclusions produced on deformation at 1150°C exhibited brittle transverse fracturing on further deformation at 925°C, PLATES 27d and e. These structures suggest the operation of shearing forces of unequal magnitude acting along the opposite faces of the inclusion. This mechanism also explains the generation of the couple necessary to cause the observed rotation of the larger inclusion fragments once fracture had occurred, PLATES 27d and e.

The mechanics of the deformation mechanism are discussed more fully in SECTION 4.4.2

4.3.5 Cast 11 (Calsibar (Ca-Si) Deoxidised)

On deformation at 925°C only the less siliceous inclusions, which had developed a duplex glassy structure, exhibited any degree of deformation. These inclusions were initially less viscous than inclusions of higher silica content, and were able to develop a coarse duplex structure within the miscibility gap of the FeO-CaO-SiO_2 system, FIG.47. The removal of silica from solution in these inclusions, lowered the viscosity of the inclusion matrix sufficiently for the inclusions to behave plastically upon deformation. However, this silica depletion also made the glassy matrix unstable, which then crystallised during continued deformation and rendered the inclusion brittle, PLATE 28a. In some cases the silica second phase

was precipitated at the inclusion-metal interface as a continuous film, forming a highly rigid envelope which prevented the inclusion from deforming, PLATE 28b. This mechanism also prevented these inclusions from deforming at the higher temperatures, a number of non-plastic inclusions of this type being observed in the specimens deformed at $1275^{\circ}C$. However, the silica envelopes often became fractured under the action of the higher stresses developed at high strains, and the inclusions then deformed into long stringers, PLATES 28e and f.

The extended range of temperatures over which the non-plastic/plastic transition occurred in this cast, can be attributed to the variation in the CaO content of the inclusions. Those inclusions having higher CaO contents had a lower viscosity, at the rolling temperature, than inclusions with lower CaO contents; due to the effect of the Ca^{++} ions in breaking down the silica network structures. Consequently the more calcareous types of inclusions exhibited lower transition temperatures, and plastic behaviour of some inclusions was observed at temperatures as low as $1000^{\circ}C$, PLATE 28c. However, the majority of the inclusions exhibited a transition in the region of $1100^{\circ}C$, FIGS. 70 and 71. Those inclusions which had calcium enriched rims, PLATES 9b and c, often exhibited tail like extensions, on deformation at $1000^{\circ}C$, where the less viscous calcareous rim was stripped away from the more viscous core.

At high strains the plastic inclusions again developed a boudinage morphology, and contained numerous holes.

4.3.6   Casts 4B and 12 (Si and Superseed Deoxidised)

The rigid behaviour of the stable glassy silicates present in these casts indicated that the non-plastic/plastic transition temperature of these highly siliceous inclusions was above $1275^{\circ}C$.

The voids produced at low matrix strains were formed on deformation at all four working temperatures, PLATE 29, similar types of voids being produced at each temperature. At matrix strains greater than 1.2 the voids had mostly been closed up. Those

voids present at the 1.2 strain were small and occurred only at the larger types of inclusion, PLATE 29b. The maximum extent of the voids was observed in the samples deformed to a true strain of 0.3, subsequent passes apparently reducing their extent. These observations can be fully explained by the action of the hydrostatic stress developed during rolling. This stress increases as the reduction increases, due to the increased rolling load and reduced arc of contact between the work rolls and the strip. This results in the gradual closing up of the voids produced at lower strains.

The mechanisms of formation of these voids and the factors influencing their formation are quite well understood and the literature on this subject has been reviewed in SECTION 2.2.3.

4.4 Some General Observations on the Factors affecting the Behaviour of Non-Metallic Inclusions during Hot Working

4.4.1 The Effects of Inclusion Composition and Constitution

The rigid or brittle behaviour exhibited by the inclusions, observed on deformation at the lower working temperatures, was found to depend primarily on the constitution of the inclusions and also on the magnitude of the stresses developed during the deformation of the steel matrix. Generally the glassy inclusions were found to be the most resistant to fracture, and fracturing of this type of inclusion was not observed under any of the hot rolling conditions employed. However, this is not to say that they would not become fractured under more severe conditions of deformation. The coarse duplex types of silicate, of lower silica content, were found to be the least resistant to fracturing and became fragmented, through cracking along the interphase boundaries, at even the lowest reductions. The more siliceous microcrystalline types of inclusion were more resistant to fracturing than the coarser duplex types, but were less resistant than the glassy types; for although they resisted fracturing on deformation at intermediate strain rates, (0.3/pass), they

became fractured under the action of the higher stresses generated during deformation at higher strain rates, (0.6/pass).

The temperature at which the transition from rigid or brittle behaviour to plastic behaviour took place was found to vary from one type of inclusion to another. In the case of the crystalline inclusions it was found that the transition temperature was roughly equal to the solidus temperature of the oxide system involved, the small discrepancies observed usually being attributable to the effects of adiabatic heating and hydrostatic pressure. However, in the case of the glassy types of inclusions, this transition temperature was found to occur at temperatures much lower than the equilibrium solidus temperature. This gave a ready explanation for the transition from viscous to brittle behaviour observed on the crystallisation of the less stable glassy silicates. Since the non-plastic/plastic transition temperature is directly related to the equilibrium solidus temperature, in the case of the crystalline types of inclusions, it should be possible to predict the effect of various elements on this transition temperature from a knowledge of the relevant oxide equilibrium diagrams. Thus, the replacement of iron by manganese in duplex crystalline silicates containing primary manganowustite, raises the temperature of the eutectic matrix from $1178^{\circ}C$ to $1317^{\circ}C$, FIG. 45. The effect this has on the transition temperature has been seen in casts 4, 5 and 6, TABLE 12. However, in the case of glassy inclusions the effects of the same elements may be quite different, and would depend on their effect on the viscosity-temperature relationship of the vitreous phase involved. Malkiewicz and Rudnik (93), found that glassy silicates of higher manganese content exhibited plastic behaviour at lower temperatures than iron rich silicates. The effect of manganese in this case is opposite to its effect on the crystalline inclusions reported in this investigation.

Because of its relevance to the behaviour of vitreous inclusions during hot working, it will be useful to discuss briefly the viscosity-temperature relationship of a typical vitreous phase. In the manufacture of glass the melt is kept at a temperature at which the viscosity is in the region of 10 N.s.m^{-2}, (10^2 poise). This temperature is usually slightly in excess of the liquidus temperature, which usually corresponds to a viscosity in the region of 10^2 N.s.m^{-2} (10^3 poise). The most dangerous temperature range for crystallisation is stated to be the range in which the viscosity is 10^3 N.s.m^{-2} (10^4 poise). At the glass transition temperature, Tg, the viscosity is 10^{12} N.s.m^{-2}, (10^{13} poise); although the viscosity changes rapidly in this region between 10^8 and 10^{16} N.s.m^{-2}, (10^9 to 10^{17} poise), this change sometimes occurring within a temperature range as small as 25 - 50°C. The normal working temperature range, during glass manufacture, corresponds to a viscosity range of 10^5 to 10^7 N.s.m^{-2}, (10^6 - 10^8 poise). By definition any liquid, or super-cooled liquid, whose viscosity exceeds 10^{13} poise is called a glass, and this is the viscosity chosen to define the boundary between the liquid and glassy states. At room temperature a normal glass will have a viscosity at least as high as 10^{19} N.s.m^{-2}, (10^{20} poise), and will behave as an ideal elastic solid. These relationships are summarised in FIG. 72, which shows schematically the variation in viscosity with temperature for a typical silicate glass. The effects that various elements have on the transition from rigid to plastic behaviour, shown by glassy non-metallic inclusions in steel, will depend on how they affect the viscosity-temperature relationships just outlined. Many metal oxides produce cations within the glassy phase which help to break down the silica networks and hence reduce the viscosity. This pushes the glass transition to lower temperatures. However, although it would seem logical to assume that higher valency cations would be more effective in this respect, this is often complicated by the tendency of these elements to form oxy-anions which

help maintain or even increase the network structures. The lower valency elements, such as Na, Ca, Fe and Mn, usually act as glass modifiers and break-up the network structures, whilst the higher valency elements such as Cr and Al, can behave as glass modifiers at low concentrations and as glass formers at higher concentrations. The probable effects of Fe, Mn and Ca, on the non-plastic/plastic transition of glassy inclusions, is to reduce the transition temperature, whilst the effects of Al and Cr are likely to be more complex and may be variable. This hypothesis disagrees to some extent with that of Kiessling (113), who suggested that although the effect of manganese was to reduce the transition temperature, the effects of iron and calcium were to increase it, FIG. 36. However, this work was based on relative plasticity determinations taken from various sources, and it is not known whether all the inclusions were of the glassy type. The effect that different species of cation have on the viscosity of glassy inclusions is readily apparent from a comparison of the behaviour of the inclusions in casts 11 and 12. The inclusions in these casts both had compositions in the range 70 - 80% SiO_2. Both contained FeO, the inclusions in cast 12 having an average of 25% FeO, those in cast 11 being rather more variable but in the range 10 - 20% FeO. The casts differed mainly in the CaO content of the inclusions, those in cast 12 containing none, whilst those in cast 11 contained 10 - 20% CaO. The transition from non-plastic to plastic behaviour occurred at temperatures between $1000^{\circ}C$ and $\sim 1070^{\circ}C$ in the case of cast 11, FIGS. 70 and 71, the lower temperature corresponding to the more calcareous inclusions, whilst the inclusions in cast 12 remained non-plastic at all temperatures up to and including $1275^{\circ}C$. The effect of Ca^{2+} ions in lowering the temperature of the non-plastic/ plastic transition is already used to advantage in the area of free machining steels.

At the temperature of transition from non-plastic to plastic behaviour the initial relative plasticity exhibited by the inclusions

is about unity, FIGS. 48 - 71.

Therefore at Tc

$$\mathcal{V}_i \longrightarrow 1.0$$

where

$\quad$ Tc $\;=\;$ The transition Temperature

$\quad$ $\mathcal{V}_i$ $\;=\;$ The Initial Relative Plasticity

Ashok, (107), has shown that the Relative Strength of unbonded second phases, which exhibit initial relative plasticities of unity, are in the region of 0.5, FIG. 24.

Hence at Tc

$$\mathcal{V}_i \longrightarrow 1.0 \quad \text{and} \quad \beta \longrightarrow 0.5$$

where

$\quad$ β $\;=\;$ The Inclusion Relative Strength

$\quad$ Now by definition

$$\beta = \frac{\mathcal{T}_i}{\mathcal{T}_m}$$

where

$\quad$ $\mathcal{T}_i$ $\;=\;$ The Inclusion Shear Strength

and $\quad$ $\mathcal{T}_m$ $\;=\;$ The matrix Shear Strength

Hence at Tc

$$\beta = \frac{\mathcal{T}_i}{\mathcal{T}_m} = 0.5$$

$\quad$ The shear strength of a viscous fluid is a function of the strain rate at which deformation occurs, or more simply the velocity gradient under which the fluid is deformed,

i.e.

$$\mathcal{T}_i = \mu \, \frac{dV}{dx}$$

where

$\quad$ μ $\;=\;$ The coefficient of viscosity

and $\quad$ $\dfrac{dV}{dx}$ $\;=\;$ The velocity gradient acting across the inclusion.

Hence at Tc :-

$$\frac{\mu \ ^{dV}/dx}{\tau_m} = 0.5 \tag{1}$$

It can be shown that the amount of simple shear is related to the true strain by :

$$\gamma = 2 \ \text{Sinh} \ \varepsilon \tag{2}$$

where γ is the unit of simple shear. This is related to the velocity gradient by :-

$$\frac{dV}{dx} = \frac{d\gamma}{dt} = \dot{\gamma} \tag{3}$$

where t is time.

But since $\gamma = 2 \ \text{Sinh} \ \varepsilon$

differentiating (2) w.r.t. time

$$\dot{\gamma} = \frac{d\gamma}{dt} = 2 \ \dot{\varepsilon} \ \text{Cosh} \ \varepsilon \tag{4}$$

where $\dot{\varepsilon}$ = Strain Rate = $\frac{d\varepsilon}{dt}$

Substituting (3) in (1) :-

$$\frac{\mu \dot{\gamma}}{\tau_m} = 0.5$$

and by (4) :-

$$\frac{2 \mu \dot{\varepsilon}_i \ \text{Cosh} \ \varepsilon_i}{\tau_m} = 0.5 \tag{5}$$

where

$$\varepsilon_i = \text{The Inclusion True Strain}$$

At $\varepsilon_i = 0.0$:-

$$V_T = \frac{\dot{\varepsilon}_i}{\dot{\varepsilon}_m} = V_i$$

where

$$V_T = \text{True Relative Plasticity}$$
$$V_i = \text{Initial Relative Plasticity}$$

$\dot{\mathcal{E}}_m$ = Matrix Strain Rate

Thus :-

$$\left| \overset{\circ}{\mathcal{E}}_i \right|_{\mathcal{E}_i = 0} = V_i \, \dot{\mathcal{E}}_m$$

and hence, from (5) :-

$$\frac{2 \mu \, V_i \, \dot{\mathcal{E}}_m \, \text{Cosh} \, \mathcal{E}_i}{\mathcal{T}_m} = 0.5$$

Since Cosh $\mathcal{E}_i$ = 1.0, at $\mathcal{E}_i = 0$:-

$$\frac{2 \mu \, V_i \, \dot{\mathcal{E}}_m}{\mathcal{T}_m} = 0.5 \qquad (6)$$

At Tc, V_i = 1.0, thus :

$$\frac{2 \, \mu_c \, \dot{\mathcal{E}}_m}{\mathcal{T}_m} = 0.5 \qquad (7)$$

where
μ_c = The critical viscosity at Tc.

Hence :-

$$\mu_c = \frac{\mathcal{T}_m}{4 \, \dot{\mathcal{E}}_m} \qquad (8)$$

Thus, for glassy inclusions in steel, the transition from rigid to fluid behaviour will occur at a temperature where the viscosity of the inclusion falls to a value equal to one quarter of the shear yield strength of the steel, divided by the strain rate at which the deformation occurs.

Data presented by Cook (115) on the yield strength of mild steel, at strain rates between 1 and 100 per second, during deformation at temperatures between 900 and 1200°C, gives a critical viscosity range of :-

$$\underline{0.11 \text{ to } 11.67 \text{ MN.s.m}^{-2}}$$

or $\quad \underline{10^{6.0} \text{ to } 10^{8.1} \text{ Poise}}$

TABLE 11.

From the values presented in TABLE 11, it can be seen that the temperature of deformation has only a marginal effect on the critical viscosity, this being in the range 0.19 to 11.67 MN.s.m^{-2}, ($10^{6.3}$ to $10^{8.1}$ poise), at 900°C and in the range 0.11 to 4.17 MN.s.m^{-2}, ($10^{6.0}$ to $10^{7.6}$ poise), at 1275°C. However, the effect of strain rate can be seen to be substantial, an increase in strain rate of one order of magnitude producing an equivalent reduction in the critical viscosity. For example, at 1000°C, increasing the strain rate from 8 to 100 s^{-1} decreases the value of critical viscosity, at low strains, from 1.56 to 0.16 MN.s.m^{-2} ($10^{7.2}$ to $10^{6.2}$ poise). This result is interesting since it predicts that the temperature at which the transition from non-plastic to plastic behaviour occurs, is increased by increasing the rate at which the steel is deformed. This may have an important effect on the behaviour of glassy silicate inclusions during operations which involve very high rates of strain; e.g. machining operations. Although Ekerot, (141), states a value of $10^{7.5}$ poise, (3.2 Mn.s.m^{-2}), as the value of the critical viscosity, it has already been shown that the equation used in the calculation was invalid, and that this value could not have neen obtained using the strain rate and flow stress data given, SECTION 2.2.4 (iii).

It can be seen that the values of critical viscosity obtained from equation (8), correspond to the normal working temperature range used in glass manufacture 0.1 to 10 MN.s.m^{-2}, (10^{6} to 10^{8} poise), FIG. 72.

At temperatures in excess of the non-plastic/plastic transition temperature the silicate inclusions all exhibit a reduction

in the measured relative plasticities, FIGS. 48 - 71. Similar observations have previously been reported by Ekerot,(141, 142), but no explanation for this behaviour has so far been proposed. Such behaviour can only be due to an increase in the strength of the inclusions relative to that of the matrix, and a ready explanation for this is apparent from the viscosity-temperature relationships already discussed, FIG. 72. Since the silicate inclusions do not begin to deform until a viscosity well within the working range is reached, i. e. at the upper end of the glass transformation temperature range, further increases in temperature have a substantially reduced effect in lowering the viscosity. Since the yield strength of the steel matrix continues to decrease rapidly, with increasing temperature in this range, the net result is a gradual reduction in the true relative plasticity exhibited by the inclusions.

If the behaviour of the silicate inclusions reported in the present work is compared with the behaviour of manganese sulphide inclusions, reported by Baker and Charles, (95), it will be seen that the two types of inclusions behave in completely different ways; with respect to both temperature and degree of deformation. The sudden increase in relative plasticity exhibited by the silicate inclusions, on reaching some critical temperature, is not exhibited by the manganese sulphides, which instead show a continuous decrease in relative plasticity as the working temperature is increased. Similarly, the initial relative plasticity exhibited by the sulphide is much lower than that of the silicate, FIG. 73, but with increasing matrix strain the true relative plasticity exhibited by the silicate decreases rapidly, whilst that of the sulphide can remain almost constant, particularly during deformation at lower temperatures, FIG. 74. This results in the sulphide producing the more elongated inclusions at high matrix strains, even though the silicate is initially much more deformable. The data presented in FIGS. 73 and

74 are for type I manganese sulphides which inherently have lower relative plasticities than type III manganese sulphides. The effects just described are even more pronounced when the behaviour of this latter type of sulphide is considered. From the foregoing discussion, it can be appreciated that the quotation of a single value for the relative plasticity of a second phase, either true or apparent, at the temperature of deformation, is of little significance in giving information on the ability of the inclusions to produce long planar defects in wrought products. It can be seen that the behaviour of the inclusions, with respect to both the temperature and degree of deformation, must be fully understood before any predictions can be made concerning the ultimate morphologies developed by the inclusions.

The difference in behaviour between liquid silicates and manganese sulphides on increasing the matrix strain, possibly lies in the nature of the interface via which the deforming stresses are transferred to the inclusions. Since the sulphide is crystalline, it is likely to be more strongly bonded to the matrix than the liquid silicates, and consequently the deformation stresses are transferred more effectively, thus allowing the deformation of the second phase to continue to higher matrix strains. In fact the continued deformation of manganese sulphides at high matrix strains, could be considered as evidence of some degree of bonding, even if slight, between the sulphide and the metal matrix, at normal hot working temperatures. There is, however, a fundamental difference in structure between the second phases themselves which may also account for their difference in behaviour. In the case of the manganese sulphide, the crystalline nature ensures that the shear stresses are transferred throughout the bulk of the inclusion, producing shear deformation. In the case of the liquid silicates, the much weaker intermolecular bonding, may allow internal fluid flow mechanisms to operate without appreciable elongation of the inclusion occurring.

4.4.2 Relative Plasticity Determinations and the Mechanisms of Inclusion Deformation

The maximum values of initial relative plasticity obtained in the present investigation, occurred at temperatures slightly above the actual transition temperature, which is in fact the median temperature of the transition range. These values were all in the range 2.5 to 3.0, FIGS. 48 - 71, and were somewhat in excess of the values predicted by theoretical and model studies, SECTION 2.2.2 (i), which give a maximum value in the region of 2.0 - 2.5 for inclusions of zero relative strength. However, the values obtained do agree very closely with those reported by Ekerot, (141, 142), who obtained values as high as 2.0 for the apparent relative plasticities of silicate inclusions at matrix true strains of 0.7 (50% reduction). The initial relative plasticities, corresponding to these apparent relative plasticity values, must have been in the region of 3.0, although they were not actually determined. Although this discrepancy would seem to point to a fundamental difference between the various theories and the practical results obtained, the difference could possibly lie in the experimental methods used in making the relative plasticity measurements.

The equations used to define the relative plasticity of an inclusion, APPENDIX I, are based on the supposition that the inclusion deforms from a sphere into a prolate ellipsoid, of constant aspect ratio in the longitudinal section. Although it has been found that such a geometry is approximated to in the early stages of deformation, e.g. PLATES 21b and c and 24a, at high strains the morphologies of the inclusions become irregular, PLATES 19f, 24b and 26c and d, and the relationship between the measured aspect ratio and the true strain no longer holds. Thus relative plasticities determined from inclusions deformed by more than a small amount, say 0.6 to 0.9 true strain, must be regarded with caution. The relative plasticity obtained by extrapolation to zero strain, the initial relative plasticity (ν_i) should be regarded as the only

satisfactory means of assessing the relative plasticity of the inclusions.

Before it is possible to describe the mechanisms by which an inclusion is deformed, it is necessary to discuss briefly the processes occurring during the deformation of the matrix which contains the inclusions. When such a matrix undergoes plastic deformation it does so predominantly by a mechanism of slip, the yield criterion being the maximum shear stress resolved into the plane and direction of slip. There thus exists within the deforming plastic matrix, regions of shear inclined at 45° to the directions of principal stress. Across these regions of shear there exists a velocity gradient, or strain rate gradient, analagous to the velocity gradient across the boundary layers of a fluid as it flows through a narrow pipe. It is within these zones of shear that the inclusions are deformed.

These conditions give rise to a couple acting on any non-metallic inclusions present in the regions of shear, and the inclusions may deform under the action of the applied stresses. When deformation takes place, it occurs by a shear mechanism, the inclusion being deformed into an ellipsoidal volume whose longitudinal axis lies at an angle to the direction of shear, which is determined by the amount of shear taking place, FIG.75. However, the couple acting on the deforming inclusion will also tend to rotate it into the direction of shear and the resulting streamlined profile will reduce the size of the couple generated. This may account for the reduction in relative plasticity observed on increasing the matrix strain. If, however, the inclusions do not deform they are likely to be rotated under the action of the applied couple. Although this process is not normally apparent in the case of spherical as-cast inclusions, the effect can frequently be seen during the dissemination of the larger fractured inclusion fragments. For example the fragments seen in PLATE 18d show some degree of rotation as do the fragments in PLATES 25c and 27e.

In order to study further the behaviour of fluid particles deforming under the action of a velocity gradient, in a matrix undergoing deformation by shear, a model system was constructed which consisted of two concentric cylinders, the outer of which was static whilst the inner one was able to rotate freely about the vertical axis. The gap between the inner and outer cylinders was filled with a viscous liquid, usually glycerol or an aqueous solution of sodium silicate, into which small globules of another liquid, which was immiscible with and whose density had been matched to the first liquid, were introduced via a hyperdermic syringe. Rotation of the inner cylinder then caused a velocity gradient to be set up in the carrier (matrix) liquid which, in turn, caused the globular inclusions to deform, FIG. 76. Although it had been hoped to obtain quantitative data on the deformation of inclusions of differing relative viscosities and differing sizes, by this means, this was not accomplished; largely due to a lack of time but also due to experimental difficulties in measuring the state of strain of both inclusions and matrix. Qualitative data was, however, obtained.

Initially all the inclusions deformed by simple shear, as shown in FIG. 76, but as deformation increased these elongated forms also rotated into the direction of shear. At this stage the smaller inclusions appeared to cease elongating, remaining unchanged during further deformation. The larger inclusions continued to deform and produced extremely long stringers. These long strings ultimately became unstable and broke up into numerous smaller globules which behaved in the manner described above, showing no further deformation with increasing matrix strain.

The behaviour exhibited by inclusions of different sizes is discussed in more detail in the following section, but the break-up of the more elongated types will be considered here. The deformation of long inter-bedded layers of viscous fluid materials has been considered in some detail by Smith (108) who has shown that the laminar deformation of such layered structures is unstable, and boudinage (Pinch and Swell) or fold type structures must develop.

Although the equations derived, which describe this type of behaviour, were concerned with the development of fold, boudinage and mullion structures in the layered sedimentary deposits of rock strata, deformed over periods on a geological time-scale, the resulting equations were time independant and hence can apply to the behaviour of elongated forms of non-metallic inclusions. The formation of boudinage structures during the deformation of elongated inclusion ribbons has already been presented, for the cases of the fluid deformation of the inclusions present in casts 6B, 8 and 11, PLATES 24b, 26c, d and f, and 28d. The break-up of the elongated forms of inclusion seen in the model system probably occurred for similar reasons.

4.4.3 Surface Energy and the Effect of Inclusion Size

The reports in the literature of a reduced relative plasticity exhibited by the smaller inclusions (60, 93, 112), have been confirmed in this investigation. Not only were the smaller inclusions present in the experimental casts found to deform to a lesser extent, but the smaller globules introduced into the model system were also observed to exhibit a reduced deformability.

In the case of the wustite inclusions present in cast 1B it was observed that the smallest inclusions exhibited no discernable deformation (PLATE 17b) and that only those inclusions greater than a minimum critical size were deformed by any large, though variable amount. In the case of the model system, however, it was observed that although the smallest globules remained largely undeformed, the deformation increased rapidly as the size of the globules increased. However, the behaviour of the larger globules became very similar and indicated that the effect of inclusion size, on the deformation exhibited, decreased as their size increased.

Baker and Charles (95) have postulated that the energy required to create new interface, as an inclusion deforms, may be·

responsible for the observed reduction in relative plasticity with increasing strain. Although this argument has been questioned in this context, it may offer an explanation for the observed reluctance of small inclusions to deform.

If we consider an initially cubic inclusion of side 'a' which deforms by plane strain into a rectangular volume of dimensions 'a', 'l', and 'b',

where

        a = inclusion width

        l = inclusion length

        b = inclusion thickness

then assuming constancy of volume:-

$$\text{Volume} = a^3 = a.l.b. = \text{const.}$$

$$\text{Therefore } a^2 = lb \text{ and } b = a^2/l \qquad (1)$$

Since

$$\varepsilon_i = \log_e l/a$$

$$l = ae^{\varepsilon i} \qquad (2)$$

The surface area of the deformed inclusion is :-

$$A = 2 (la + ba + lb)$$

Substituting for b and l from (1) and (2)

$$A = 2a^2 (e^{\varepsilon i} + e^{-\varepsilon i} + 1) \qquad (3)$$

Differentiating to get the rate of change in area with time

$$\frac{dA}{dt} = \overset{\circ}{A} = \frac{dA}{d\varepsilon_i} \cdot \frac{d\varepsilon_i}{dt} = \overset{\circ}{\varepsilon}_i \frac{dA}{d\varepsilon_i}$$

Thus from (3)

$$\overset{\circ}{A} = 2a^2 \overset{\circ}{\varepsilon}_i (e^{\varepsilon i} - e^{-\varepsilon i})$$

Hence $\quad \overset{\circ}{A} = \underline{4a^2 \overset{\circ}{\varepsilon}_i \text{ Sinh } \varepsilon_i} \qquad (4)$

Dividing by a^3 to obtain the rate of change of surface area per unit volume,

$$\frac{\overset{\circ}{A}}{V} = \frac{4\overset{\circ}{\varepsilon}_i}{a} \text{ Sinh } \varepsilon_i$$

and the rate of change of surface energy per unit volume is,

$$\frac{\dot{E}}{V} = \frac{4\dot{\gamma}}{a} \; \dot{\mathcal{E}}_i \; \text{Sinh} \; \mathcal{E}_i \qquad\qquad (5)$$

where

$\dot{E}$ = The rate of change of surface energy

$\dot{\gamma}$ = The interfacial energy per unit area

If we now consider this inclusion to be a manganese sulphide exhibiting a relative plasticity of 0.8, which shows little or no change in value over the initial stages of deformation, FIG. 74; then assuming a typical matrix strain rate of 50 sec^{-1}, the rate of strain exhibited by the inclusion will be 40 sec^{-1}. Taking the surface energy to be 1.5 joules per square metre, then the rate of energy absorption, per unit volume, required for the creation of new interface is,

$$\frac{\dot{E}}{V} = \frac{240}{a} \; \text{Sinh} \; \mathcal{E}_i$$

The change in the rate at which energy is absorbed, by the creation of new interface, as the inclusion deforms, is shown in FIG. 77, for inclusions of various initial diameters. A typical value for a 1 μ m diameter inclusion, at a true strain of 1.0 and deforming at a rate of 40 per second, is approximately 280 $\text{MJ.m}^{-3}\text{s}^{-1}$.

The rate at which energy (per unit volume) is expended in deforming the steel matrix, assuming the shear yield strength to be in the range 40 to 100 MNm^{-2} at normal hot rolling temperatures, TABLE 11, (115), is given by :-

$$\frac{\dot{E}}{V} = 2 \; \mathcal{T}_m \; \dot{\mathcal{E}}_m$$

This equation gives values in the range :-

$$\underline{4000 \text{ to } 10,000 \text{ MJ.m}^{-3}\text{s}^{-1}}$$

If the rates of energy absorption per unit volume for the creation of new interface, for inclusions of different initial sizes, are compared with the rate at which energy per unit volume is expended in deforming the steel matrix, it can be seen that although surface energy considerations are likely to be significant in the behaviour of inclusions of less than 1 μ m diameter, FIG. 77, its effect on the

behaviour of the larger inclusions, ($> 5\mu$ m), is probably minimal. Although surface energy effects can be seen to offer a partial explanation for the restricted deformability of the smaller inclusions, it does not offer a complete explanation. This effect predicts a reduced relative plasticity for the smaller inclusions, but these are actually observed to remain almost completely undeformed during hot working.

4.4.4. The Effect of Hydrostatic Pressure

The magnitude of the hydrostatic pressure generated during deformation in the experimental casts examined, is readily apparent from the depth to which the matrix has been forced into the fissures produced by the fracture of brittle inclusions, PLATES 18c and d, 21f, h and k, 25c and 27a. Since it is known that the magnitude of the hydrostatic stress generated during rolling, is equal to the rolling load divided by the area of contact between the roll and the work-piece (148), hydrostatic stresses in the region of 50 - 100 MN/m^2 should not be uncommon in commercial rolling practices.

Bridgeman (147) has shown that hydrostatic pressure can increase the ductility of many materials and can even render normally brittle substances ductile; and the magnitude of the hydrostatic pressure developed during rolling undoubtedly accounts for the extreme plasticity exhibited by manganese sulphide inclusions during hot working. Since the hydrostatic pressure is the main reason for the plastic behaviour of manganese sulphide inclusions it would not be unreasonable to assume that the relative plasticity exhibited is dependent on the magnitude of the hydrostatic pressure generated in the surrounding matrix. Thus the relative plasticity exhibited under deformation conditions where significantly higher stress levels are developed as, for example, within the shear and flow zones of the metal chips produced during machining operations, will probably be quite different from that exhibited under more normal deformation conditions.

The effects of hydrostatic pressure on the behaviour of oxide inclusions are likely to be even more complex, since the phase equilibria and transformation temperatures of the constituent phases may be modified. In these cases larger hydrostatic pressures may have an effect on the non-plastic/plastic transition temperature and this could have important consequences on the behaviour of these types of inclusions during machining operations.

4.5   The Mechanisms of Formation of the Aluminous Inclusions
        Produced during Deoxidation by Aluminium and their
        Subsequent Behaviour during Hot Working

4.5.1   The Mechanisms of Formation of Aluminous Inclusions

The number of particle morphologies present in the inclusion clusters observed in cast 7B, PLATE 11, gives some indication of the complexity of the mechanisms by which these clusters are produced. The literature on this subject, though voluminous, is inconclusive concerning the mechanisms of formation of such clusters, (42 - 58), SECTION 2.1.2 (i). In summary, it is suggested that alumina itself is reluctant to precipitate directly as a deoxidation product, except at high degrees of supersaturation, due to the high activation energy for formation of the alumina molecule (42, 51). At high degrees of supersaturation the alumina probably precipitates in a dendritic morphology by a diffusion controlled mechanism (51); though Ooi's work (58) shows that stirring of the melt tends to destroy the dendritic character of the inclusions and that there is a fundamental difference in morphology between the inclusions produced in stirred and unstirred melts. Plockinger's work (42 - 45) indicates that liquid mixed oxides are often formed as an intermediate stage in the formation of more aluminous inclusions. However, this hypothesis must be regarded with some caution in view of the sampling techniques employed. Examination of the morphology of alumina inclusions by S.E.M., most notably by Japanese workers, (55 - 58), has revealed the variability of the morphologies produced, but has done little to elucidate the mechanisms through which they arise.

The alumina clusters present in cast 7B, PLATE 11,
consisted of a mixture of small dendrites, and small irregular
and large globular particles, which contained enclosed metal,
PLATES 11c and d. The latter were often perfectly spherical in
shape and were quite distinct from the smaller irregular particles,
in which the metal was in the form of small globules separating
the core of the inclusion from its rim, PLATE 11d. The various
particles were interwoven into large inclusion clusters by the sintering
of adjacent particles. Consequently the morphologies of the individual
particles were best observed when the sintered structure was partially
broken down after a light deformation treatment, PLATES 11f and 30b -
d. The large spherical globules containing enclosed metal were well
sintered structures, being composed of many individual particles.
The surface of one such particle is shown in PLATE 11g, and the
'grains' which compose it can clearly be seen. The enclosed metal,
often seen in the polished section, PLATE 11c, is contained in the
sinter porosity within the particle which is clearly revealed by
deep etching, PLATE 11h. Although many dendritic particles were
observed, these were usually quite small, had few sidearms, and
were often partially spherodized, sometimes giving the dendrite the
appearance of a string of connected globules, PLATES 11f and 30b and
c. The absence of large sintered globular particles from the ingot
which had been deoxidized with aluminium added to the mould,
confirms that this particular morphology is not produced initially
but forms at some later stage. In fact the absence of all but the
smallest inclusion clusters from this ingot indicates that cluster
formation takes considerably longer than the formation of the initial
products of deoxidation.

The most significant feature observed in the mould deoxidized
ingot, were the bands of alumina dendrites, which separated deoxidized
and undeoxidized regions, PLATE 12a. The configuration of these
bands is essentially the same as that reported by Bogdandy, (51),
where the aluminium deoxidant had been allowed to diffuse uni-

directionally into an oxygen rich iron melt. The banded structure
consisted of an undeoxidized region containing wustite inclusions,
a region of low oxygen activity which contained few inclusions and
finally a band containing large alumina dendrites in the region nearest
to the source of the deoxidant, FIG. 78a. The amount of aluminium
dissolved in the matrix, in the case of the band shown in PLATE 12a,
decreased from 0.8% in the region behind the dendrite band, to 0.2%
in the centre of the band, to an undetectable level in the undeoxidized
region. A possible distribution of the dissolved aluminium and
oxygen levels present in the melt during reaction at this interface
is shown schematically in FIG. 78b. Consider two liquids, one
oxygen rich and the other aluminium rich, brought into contact. At
the interface an extremely high supersaturation of both aluminium
and oxygen would exist momentarily and alumina would be precipitated,
possibly in a dendritic form. Aluminium would then begin to diffuse
from the aluminium rich region, down the concentration gradient
produced by the removal of aluminium from solution, and a corresp-
onding diffusion of oxygen would take place on the opposite side of the
interface. The concentration gradients produced must be extremely
steep in order to create a region of low oxygen activity in front
of the dendritic band, as shown by the absence of inclusions in this
region. A steady state situation is eventually reached when the
diffusion of oxygen into the dendritic band is just sufficient to react
with the aluminium diffusing in the opposite direction. A curious
feature of the interface shown in PLATE 12a was the presence of a
number of duplex hercynite-wustite inclusions in the undeoxidized
region adjacent to the dendritic band. These particles have a
characteristic morphology consisting of angular crystals of hercynite
bound together in a wustite matrix, PLATE 12d. Closer inspection
of the small wustite globules in the undeoxidized region closest to
the inclusion free zone, revealed that nearly all of these globules
had nucleated a number of small alumina dendrites, which were
growing out from their surfaces, PLATE 12e. The majority of

these particles also showed some evidence of a surface reaction with the dissolved aluminium, PLATE 12f. These observations suggest that aluminium had diffused into the oxygen rich liquid ahead of the interface without the homogenious nucleation of aluminous deoxidation products. The greater diffusivity of the aluminium, compared with that of oxygen, is to be expected in view of the difference in size between the aluminium ion and the oxygen ion, and the high activation energy for the formation of the alumina molecule, readily explains the absence of homogenious nucleation.

Regions where turbulent mixing, between highly oxidised liquid and liquid rich in aluminium, had occurred could be seen at the extremities of the dendritic bands, PLATE 12j. In these regions the sudden supersaturation caused by the mixing resulted in the precipitation of many types of inclusion. Where the aluminium level was insufficient to precipitate alumina, mixed oxides of the hercynite + wustite type were initially precipitated. Subsequent transport of these inclusions into regions of higher aluminium concentration, or alternatively an increase in the aluminium content of their immediate environment through diffusion, resulted in a rapid reaction between the liquid wustite and the dissolved aluminium, producing hercynite-alumina type inclusions, PLATES 12l, m and n. In these, the hercynite was prevented from more complete reaction by the sheath of alumina produced. The reduction of the Fe0 in the outer layers of the hercynite resulted in the precipitation of small globules of metallic iron along the interface separating the hercynite core from the alumina rim. A number of inclusion clusters containing both reacted and unreacted particles can be seen in PLATE 12j; the cluster indicated is shown at a higher magnification in PLATE 12k. The particles in the lower left of this plate have been partially reacted with aluminium which was diffusing into the region of the melt containing the cluster. The direction of diffusion of the aluminium is shown by the aluminium concentration in the matrix obtained at the positions indicated in PLATE 12j. The increased level of aluminium

also led to further deoxidation of the melt and more alumina was precipitated heterogeneously onto the surface of these reacted particles, sometimes growing in a dendritic fashion, PLATE 12l. In many cases the rate of mixing of aluminium rich and oxygen rich liquids was so rapid that high levels of supersaturation were reached very quickly. Alumina was then precipitated directly from the melt, often onto nuclei produced at lower degrees of supersaturation but which had had insufficient time to grow. The precipitates produced in this way often consisted of extensive arrays of alumina dendrites, PLATE 12g, although very many had a less marked dendritic structure and often had a partially spherodized appearance, PLATE 12h. In a few extreme cases the precipitates were composed entirely of a partially sintered mass of small spherical globules of alumina, PLATE 12i and p. The ingot section examined contained extensive regions containing numerous but well separated dendritic masses of alumina, together with isolated partially reacted particles, indicating that the major part of the deoxidation had occurred by rapid mixing.

Although in this case the oxidized metal was added to the deoxidant contained in a small metal mould, it is probable that very similar conditions are initially set up in the immediate vicinity of dissolving lumps of deoxidant during commercial deoxidation practices. It is possible to envisage a situation where small undefined volumes within the melt, which contain a high concentration of the deoxidant, are carried around in the general turbulence, possibly creating interfaces of the type seen in PLATE 12a, as the deoxidant diffuses into the surrounding oxygen rich melt. Where mixing is more violent, large numbers of alumina dendrites may be produced, and the less aluminous duplex mixed oxides produced in regions of lower aluminium content, may ultimately become reacted as the aluminium distribution becomes more homogeneous. It is quite likely that under these conditions many regions of a low aluminium concentration would initially be formed, resulting in the precipitation of large quantities of mixed hercynite + wustite, or

even liquid mixed oxide types of precipitate. This would explain Plockinger's observation of these precipitates on first adding the aluminium deoxidant (42). It is not the inhibition of nucleation of the alumina which gives rise to the less aluminous inclusions, but the fact that the aluminium concentration has not reached a level sufficient to cause alumina precipitation.

The change in morphology of the alumina dendrites from the spikey dendritic growths shown in PLATE 12g to the clusters of fully spheroidal particles shown in PLATE 12i, is not easily explained. However, the change in morphology may be due to the changing oxygen concentration of the liquid from which the particles were precipitated. Initially this liquid would be quite rich in dissolved oxygen and, according to Kozakevitch and Olette (54), the surface energy of the alumina-melt interface is quite low at these oxygen levels, TABLE 1. Under such conditions there is little opposition to the dendritic growth of the deoxidation products and extensive arrays of large, branched, alumina dendrites are able to form, PLATE 12g. However, as the oxygen content is reduced, the surface energy of the alumina-melt interface increases markedly, that of the alumina-pure iron interface being more than three times as high as the interface with a melt containing 0.07% dissolved oxygen, TABLE 1. Consequently dendrites precipitated at these low levels of dissolved oxygen have a strong tendency to spherodise, and dendrites of the type shown in PLATE 12h are produced. At the very lowest levels of dissolved oxygen the surface energy is such that, in order to minimise the surface energy, a fully spheroidal morphology results, PLATE 12p, and clusters of small spherical alumina particles are produced, PLATE 12i. This reduction in the level of dissolved oxygen not only effects the growth morphology of the alumina but also causes adjacent particles to cluster. Knuppel, Brotzman and Forster, (145), first showed that adjacent particles of alumina would be brought into contact due to the retraction of the liquid metal from the space between them, FIG. 79. The compressive forces generated in this way increase with increasing surface energy, and thus at low residual

oxygen levels there is a marked tendency for the particles to sinter into large clusters. However, in regions where the residual oxygen level is high, the tendency to cluster and sinter is less pronounced.

Direct evidence for the operation of the mechanism postulated by Knuppel et al. was obtained from the suction sample taken from the melt fully deoxidised by a 1.2% aluminium addition. This sample, taken approximately 30 seconds after the deoxidizing addition was made, contained many very large alumina clusters which themselves contained many particles having a configuration of the type shown in FIG. 79b. A central void had been produced between the adjacent particles due to retraction of the matrix metal. This mechanism would also operate in the liquid metal separating adjacent arms in the arrays of alumina dendrites produced on initial deoxidation. On reaching the final homogeneous low level of dissolved oxygen, there would be a strong tendency for these dendrites to reduce their interfacial area of spheroidizing, or by the sintering together of adjacent dendrite arms. As these arms spherodised and sintering of the closest elements took place, the matrix metal would tend to retract more and more from the ever-decreasing interdendritic spaces, and the whole dendritic array would ultimately collapse into an irregular sintered mass of alumina. This sequence of events is clearly shown in PLATES 13c, d and e. Ultimately, as sintering became more complete the mass would take on a spheroidal morphology of the type shown in PLATES 11b, c and f and 13f and g. Any process which results in a greater degree of turbulence would enhance both the formation of sintered clusters and the spherodization and collapse of the dendrites. This must be borne in mind when the results of experiments using techniques such as suction sampling are considered. The alumina clusters present in the suction sample obtained in the present case were mainly of the form shown in PLATE 13b, and can be seen to be composed mostly of irregular sintered masses of alumina. A few regions contained particles which had

escaped such a high degree of spheroidisation and sintering, PLATES 13a, c, d and e. The almost perfectly spherical sintered globules seen in PLATES 13b, f and g were probably produced in the melt prior to sampling by the collapse and almost complete sintering of all the inclusion material contained in small isolated inclusion clusters. The isolated globules produced then became entrapped in the larger more loosely bound irregular clusters, produced by the turbulence induced during suction sampling. Similar turbulence effects during teeming, could have led to the formation of the clusters observed in cast 7B, which also contained particles having this globular morphology. The central cavity and exterior opening, observed in nearly all of these sintered globular forms, may be explained by the need for an orifice through which the matrix metal could escape during the initial collapse of the inclusion clusters. The effects of turbulence on the spherodization and sintering processes just discussed also explain Ooi's observation of the difference in the morphology of alumina produced in stirred and unstirred melts (58).

The extreme rapidity with which the alumina deoxidation products are removed from the melt is indicated by the lack of inclusion material in the suction sample taken after 90 seconds. A similar loss of alumina from the melt into which alumina powder was added, was probably due to the stirring effect of the H.F. current. Linder (146) has recently shown that the interaction of the coil current with the current induced in the melt, sets up a pressure gradient in the region of the furnace walls which, in the case of H.F. furnaces, can create a force on the inclusions as great as the gravitational force. This causes the inclusions in the vicinity of the furnace walls to be accelerated outwards and thus explains the extremely rapid transfer of alumina from the melt to the furnace walls, in the present case. Ooi, Sekine and Kasai (58) have suggested that most of the primary inclusions produced on deoxidation by aluminium are eliminated before teeming takes place. The aluminous inclusions

found in the ingot stage it is suggested, result from stream reoxidation during teeming. The results obtained in this investigation would seem to support this view.

4.5.2   The Behaviour of Alumina Inclusions during Hot-Working

The alumina clusters observed in the samples from cast 7B, hot rolled at all four working temperatures, were all very similar, indicating that the rolling temperature had little effect on the behaviour of the inclusion clusters. At all four rolling temperatures the sintered clusters were progressively broken up as the matrix strain increased, the alumina particles themselves being completely non-plastic at all the temperatures employed.

At low matrix strains the loosely sintered aggregates were only partially fragmented, the more highly sintered particles being able to withstand the forces imposed on them. At these strains many of the arms were broken off the parent dendrites and numerous sinter necks were fractured, PLATES 30b, c and d. Conical voids were produced at many of the larger inclusion particles, PLATE 30e, but at higher strains these particles themselves were fractured under the increased rolling pressure, PLATES 30f and g. Ultimately even the highly sintered globular forms became fragmented, resulting in the formation of long stringers of angular or grain shaped fragments which once constituted the sintered mass, PLATES 30h and i.

During the fragmentation and dissemination of the inclusion fragments, voids would be continually formed, as the particles fractured and the fragments separated, and would be closed up again, under the action of the hydrostatic pressure, as the fragments were pulled further apart.

These types of inclusions are particularly deleterious to the fatigue   properties and to the surface finish of polished components. Their effects could be minimised by either eliminating the inclusions altogether, by rendering the particles softer, or by ensuring that they were present in the form of small well dispersed particles instead of the discontinuous stringers normally produced. The first

of these alternatives would obviously be preferred and could largely be accomplised by correct stream protection during teeming, this being the most probable source of this type of inclusion. The second alternative is already used commercially by treating the steel s concerned with calcium, in various ways, producing larger but fewer and softer calcium rich calcium aluminate inclusions. Although this usually intensifies the effect on fatigue, (149), it also has the benefits of sulphide modification. The latter alternative could be promoted by employing a very heavy reduction sequence during hot working, in order to begin the fragmentation of the more highly sintered alumina particles at an early a stage as is possible; this could be followed by a sequence of heavy reductions during cold rolling ensuring that the inclusion fragments were as well dispersed as possible; the increased hydrostatic pressure ensuring that the voids produced were kept to a minimum. However, such a procedure is obviously not applicable commercially and calcium treatment, with stream protection during teeming, seems to be the main practical solution.

If commercial working treatments allow some of the sintered alumina particles to remain intact and undispersed, then these are likely to become fractured and disseminated by the higher stresses generated during subsequent cold deformation treatments. In this case the inter-particle voids produced would be more reluctant to close up and matrix welding, at the discontinuities produced, would be less likely to occur. Under these circumstances the defects produced are likely to be more detrimental to the mechanical properties than those produced during hot working.

4.6   Implications to Commercial Practices

Machinability

The beneficial effect of manganese sulphide inclusions on the machinability of steel is well known, and it has been shown that silicate inclusions, having low softening temperatures, can also be

beneficial, (150 - 152). At the higher cutting temperatures developed during machining with carbide tools, these silicates behave similarly to manganese sulphides, becoming elongated in the shear and flow zones of the chip. They also form protective coatings on the rake faces of carbide cutting tools, which prevent or minimise cratering; thus increasing tool life. The silicates which enhance machinability in this way, have specific compositions in the $MnO-CaO-Al_2O_3-SiO_2$ system, and usually lie close to one of the eutectic troughs in the region of the Anorthite, $(CaO.Al_2O_3.2SiO_2)$, or Gehlenite, $(2CaO.Al_2O_3.SiO_2)$, compositions, FIG. 13. These silicates are glassy and consequently have non-plastic/plastic transition temperatures well below the equilibrium crystalline solidus temperature. The efficacy of CaO in reducing the temperature of this transition has been demonstrated in the present investigation and it is to be expected that other alkalii and alkaline earth oxides will have a similar or even greater effect. If it were possible to introduce a small amount of Na_2O or Li_2O into the silicates, the reduced softening temperatures would enable protective deposits to be produced at even lower temperatures, and hence at reduced cutting speeds. Although such deposits have not been observed during machining with high speed steel tools, the lower softening temperatures may be beneficial in producing chip embrittlement.

The drastic reduction in machinability arising from the use of aluminium, in the production of fine grained steels, is usually thought to be due to the formation of alumina deoxidation products. Even in the presence of silicon it is possible to produce small abrasive alumina particles, as was seen in cast 8, (Al-Si deoxidised); which are not normally observed on optical examination. However, this is not the only mechanism by which the loss of machinability may arise. It was shown in cast 8 that spinel phases can be precipitated in the more aluminous glassy silicates. During hot working the plastic silicate can be stripped away from these non-plastic precipitates which are left as isolated particles within

the metal matrix. These would be particularly detrimental to the machinability. It has been postulated that the higher valency elements chromium and aluminium may form oxy-anions, in glassy silicate inclusions, and although this would tend to make the glassy phase more stable, it would also increase the viscosity, and hence the non-plastic/plastic transition temperature. This may render the more aluminous calcium-silicates non-plastic at the temperatures developed at normal cutting speeds. Hence the benefits of chip embrittlement and layer formation will only be conferred at higher cutting speeds. Crystallisation of the glassy silicates would also render the inclusions non-plastic to higher temperatures and would thus impair the machinability.

The very high hydrostatic pressures generated during machining will undoubtedly have an effect on the behaviour of the inclusions, although this is at present unresearched. It has been shown that the non-plastic/plastic transition temperature of glassy silicate inclusions is actually increased by increasing the strain rate, although this effect may be offset to some extent by the effect of the hydrostatic pressure. The more refractory sulphides produced in steels treated with alloys containing the elements, Ca, Ti, Zr or the rare earths, are thought to be non-plastic during hot working. They may, however, be rendered plastic during machining operations, by the high pressures and strain rates developed. The possibilities of improved machinability through the use of sulphide modifiers, will undoubtedly be the subject of continued research.

Polishability

The polishability of bright rolled strip products is greatly impaired by the presence of abrasive inclusion stringers, produced by alumina and the more aluminium rich calcium aluminates during working. These inclusions are pulled out of the strip surface during the polishing operation, producing surface drags and scratches.

These effects can be eliminated by employing a deoxidation practice which gives rise to highly siliceous small glassy silicates, which will remain undeformed during working. However, it must be borne in mind that the presence of crystalline silicate inclusions will give rise to long fragmentary stringers, during deformation, which are likely to be very detrimental to the polishability. Similarly silicates which are plastic during hot rolling will produce long fragmentary stringers on working at temperatures below the non-plastic/plastic transition temperature. These will also impair the polishability.

Controlled Rolling

Modern controlled rolling practices are designed to produce fine grained steels with increased strength and toughness. However, the higher deformation stresses and low finishing temperatures involved can produce very long inclusion ribbons which can offset the improvement in the mechanical properties, and lead to marked mechanical anisotropy. Manganese sulphide inclusions produce longer ribbons during controlled rolling than during conventional hot rolling, due to their higher relative plasticities at the lower deformation temperatures involved. This effect increases the succeptability of controlled rolled steels to lamellar tearing in welded structures and the problem is so severe in the production of steel pipelines that sulphide modification treatments are commonly employed. However, such treatments can also affect the oxide inclusions. For example, calcium treatments may render silicate inclusions plastic at lower working temperatures and thus produce long silicate ribbons. It has been shown however, that silicate inclusions will not form ribbons as elongated as those produced by manganese sulphides. Siliceous inclusions which are plastic on the commencement of the deformation will usually be non-plastic well before the deformation is complete, and will produce long fragmentary stringers. Similarly the higher deformation stresses involved will be able to fracture initially crystalline inclusions at an earlier stage in the deformation,

giving rise to similar long fragmentary inclusion stringers.

Rod and Wire Production

Alumina clusters present in wire steels lead to excessive die wear and to wire breaks during the drawing operation. Consequently steels used in the production of wire are rarely, if ever, deoxidised with deoxidants containing aluminium. Small rigid glassy silicates are probably the most innocuous inclusions in steel for this application and deoxidation practices should be designed to ensure that such inclusions are the only types produced. The fragmentary silicate stringers arising from initially crystalline inclusions, and from inclusions initially plastic but which become fragmented at lower working temperatures, will be more detrimental to the drawing operation than small non-deformable glassy silicates. However, most large tonnage commercial steels also contain many large primary deoxidation products which persist into the cast ingots. If these inclusions behave rigidly during hot working, and maintain their spherical morphology, then the inclusions can have a very detrimental affect during the subsequent production of fine gauge wire, e.g. tyre wire. In such cases the diameter of the inclusions can constitute an appreciable fraction of the final wire diameter and may lead to frequent wire breaks during the final drawing operation. In these cases it would be preferable for the inclusions to have a very low softening temperature so that they become elongated into very fine rotary ellipsoids during the early stages of rod production. In these circumstances the effect of CaO in reducing the non-plastic/plastic transition temperature may become increasingly important. As yet commercial practices seldom use calcium bearing deoxidants specifically for this purpose in the production of wire steels.

SECTION 5

CONCLUSIONS AND SUGGESTIONS FOR FURTHER WORK

5.   CONCLUSIONS

Steel ingots containing predetermined types of oxide inclusions have been prepared by deoxidising pure iron melts with various combinations of the elements silicon, manganese, aluminium and calcium.   The types of inclusions produced were explained in terms of the reaction kinetics and phase equilibria involved.

5.1.1   The Effects of Heat Treatment

(i)   The effects of soaking treatments, lasting up to 100 hours at temperatures in the range $925 - 1275^{\circ}C$, on the constitutions of the inclusions, has been investigated and it has been shown that glassy iron-manganese and iron-alumino silicate inclusions, having silica contents in the region of 50%, can devitrify during such treatments.

(ii)   It has been shown that complex transition structures containing both equilibrium and non-equilibrium phases can be produced during the initial stages of devitrification, and evidence of a ferrous/ferric reduction reaction has been presented.

(iii)   The more siliceous inclusions, having silica contents in excess of 70% were shown to be highly resistant to devitrification.

5.1.2   The Assessment of Inclusion Deformation

(i)   The term 'Relative Plasticity' as assessed by conventional techniques is misleading and would be more correctly termed the 'Apparent Relative Plasticity' or 'Relative Deformation' of the inclusions.

(ii)   The 'True Relative Plasticity' of the inclusions can only be obtained from a more complete description of the behaviour as the inclusions deform over a range of matrix strains.

(iii) The most convenient parameter by which to assess the inclusion deformability is the 'Initial Relative Plasticity', obtained by extrapolating the apparent relative plasticity to the state of zero matrix strain.

5.1.3   The Effects of Deformation on the Inclusions

(i) The effects of both the temperature of deformation and the degree of matrix strain, on the values of relative plasticity exhibited by plastic silicate inclusions, has been investigated in the range 925 to $1275^{\circ}C$.

(ii)   All the silicate inclusions displayed a rapid transition from non-plastic to plastic behaviour, on reaching some narrow critical deformation temperature range.

(iii) The initial relative plasticity exhibited by the inclusions increased from a value of zero, at temperatures below the transition temperature, to a maximum value of 2.0 to 3.0 at a temperature slightly above the transition temperature.

(iv) The relative plasticity of the inclusions decreased as the deformation temperature was increased above the transformation temperature range.

(v) The transition temperature exhibited by crystalline silicate inclusions is equivalent to the equilibrium solidus temperature and thus corresponds to the appearance of a liquid phase.

(vi) The transition temperature exhibited by glassy silicate inclusions occurs on reaching a temperature where the viscosity of the glassy phase falls below a critical value, in the range 0.1 to 10.0 MN.s.m^{-2} (10^6 to 10^8 poise) and corresponds to the working temperature range used in glass manufacture. This often occurs at temperatures substantially below the equilibrium solidus temperature.

(vii) An equation has been derived which relates the critical viscosity to the shear yield strength of the matrix metal and the strain rate at which deformation takes place,

$$\mu_c = \frac{\gamma_m}{4 \dot{\varepsilon}_m}$$

where μ_c = The critical viscosity

$\dot{\varepsilon}_m$ = The matrix strain rate

γ_m = The shear yield strength of the metal matrix

(viii) The effect of other oxides on the non-plastic/plastic transition temperature is dependent on the nature of the inclusions. In the crystalline form the effects of the various oxides can be predicted from their effect on the solidus temperature in the relevant equilibrium system, but in the case of the glassy silicates their effect will depend on their behaviour as glass modifies, intermediates or as glass formers. Iron, manganese and calcium are likely to lower the transition temperature whilst the effects of aluminium and chromium are likely to be more complex and may be variable.

(ix) The effect of calcium in reducing the transition temperature of glassy silicate inclusions, and the effect of manganese in increasing the transition temperature in crystalline iron manganese silicates, has been demonstrated. The effect of silica in increasing the transition temperature has also been confirmed.

(x) At low deformation temperatures silicate inclusions behave in either a brittle or rigid manner, depending on their constitution and morphology, and on the magnitude of the matrix stresses developed during deformation.

(xi) In general single phase glassy inclusions are the most resistant to fracturing, whilst the coarser duplex crystalline forms are particularly prone to fragmentation.

(xii) Although some inclusions may resist fragmentation when present in a spherical morphology, if these become elongated during working at higher temperatures, subsequent deformation at lower temperatures almost invariably leads to fragmentation.

(xiii) The increased stresses developed during deformation at higher strain rates increases the tendency of the inclusions to become fragmented.

(xiv) The formation of conical voids in association with the inclusion-metal interfaces, in the case of the more rigid inclusions, has been confirmed and the gradual elimination of these voids at higher strains has been demonstrated.

(xv) Wustite inclusions behaved plastically at all temperatures in the range 925 to $1275^{\circ}C$, but exhibited relative plasticities very much lower than those exhibited by silicate inclusions.

(xvi) The deformability of wustite inclusions decreases with increasing working temperature.

5.1.4 <u>General Features of Inclusion Deformation and Factors affecting their Behaviour during Working</u>

(i) All inclusions become less plastic as the matrix strain increases and may be due, in part, to the increasing rate at which new interface is created.

(ii) The rate at which the deformability of the inclusions decreases, with increasing matrix strain, varies from one type of inclusion to another, and is possibly controlled by the work of adhesion at the inclusion-matrix interface: inclusions more strongly bound to the matrix exhibiting less dependency of deformability on the matrix strain.

(iii) The true relative plasticities exhibited by silicate inclusions decrease much more rapidly, with increasing matrix strain, than those exhibited by manganese sulphide

inclusions. Consequently the defects produced by manganese sulphide inclusions, at high matrix strains, can be much longer than those produced by equivalent silicate inclusions, even though the deformability of the silicate is initially much greater than that of the sulphide.

(iv) The deformabilities of non-metallic inclusions decreases as their size decreases, and under any given set of conditions there may be a limiting critical size, below which deformation does not occur. A critical size in the region of 2 to 3 μ m was found in the present investigation.

(v) The effects of interfacial energy on the behaviour of inclusions during working has been shown by calculation to be minimal, for inclusions of greater than 5 μ m diameter. The interfacial energy can have an affect on the behaviour of inclusions of less than 1 μ m diameter although this is probably not the only factor governing their behaviour.

(vi) The effect of strain rate on the behaviour of the inclusions was found to be marginal, although the strain rates investigated were not widely different.

(vii) The effects of both strain rate and hydrostatic pressure are likely to be of greater significance under more severe conditions of deformation and in particular their effects on the inclusions during metal cutting operations are likely to be of prime importance.

5.1.5   The Formation of Alumina Inclusions

(i) Several different inclusion morphologies can be produced during deoxidation by aluminium, the morphology depending largely on the aluminium and oxygen concentrations in the local regions where precipitation occurs.

(ii) Mixed oxide inclusion clusters can be formed in regions of the melt containing low aluminium concentrations, and these may subsequently react with more aluminium, diffusing from regions of higher concentration, producing irregular rim-core particles. The central core of these particles is prevented from further reaction by the outer rim of alumina.

(iii) In regions of high supersaturation, alumina may be precipitated directly and, depending on the local oxygen concentration, may have a fully dendritic, partially spherodised or fully spheroidal morphology.

(iv) In quieter regions of the melt, diffusion interfaces may be set up between liquid rich in aluminium and liquid rich in oxygen. Bands of alumina dendrites are produced along these interfaces. However, such interfaces are probably short lived and are soon destroyed in the general melt turbulence. They may, however, provide numerous nucleii for subsequent deoxidation reactions.

(iv) At low residual oxygen levels, alumina particles in close proximity are brought into contact by the retraction of the liquid metal from the spaces separating them. This results from the high energy of the alumina melt interface, and leads to the formation of large loosely sintered alumina clusters.

(v) Spherodization and sintering effects destroy much of the dendritic character of the alumina precipitated during the early stages of deformation, and can ultimately produce spherical sintered globules from small isolated inclusion clusters.

(vi) The high energy of the melt-alumina interface results in the rapid absorbtion of the inclusions onto the furnace and ladle linings and into the covering slag.

5.1.6 The Effects of Working on Alumina Clusters

(i)   Individual alumina particles are non-plastic at all temperatures up to $1275^{\circ}C$.

(ii) Sintered clusters of alumina particles behave similarly at all working temperatures up to $1275^{\circ}C$ and produce long disseminated fragmentary stringers at high strains.

(iii) At low and intermediate strains, $(\varepsilon < 1.2)$, many of the dendrite arms and sinter necks become fractured and voids are produced at the larger particles.

(iv) At higher strains the more highly sintered globular particles begin to fracture, and the fragmentation and dissemination of the inclusion clusters gives rise to the strings of angular grain shaped fragments, which are often observed in commercial products.

(v) The more aluminous forms of calcium aluminate produce clusters similar to those produced by alumina and these behave in a similar manner, to alumina clusters, during hot working.

1.   Ashok's observations on the effect of interfacial strength on
the behaviour of second phases of various relative strengths,
during deformation, should be confirmed by model work.
Plasticine models could be constructed containing globular
second phase particles, in the form of dispersion strengthened
plasticine balls.   These could be either bonded to the matrix
using carbon tetrachloride as a solvent, or prevented from
bonding using vaseline.

2.   The effect of inclusion size on the Relative Plasticity exhibited
during working, is not well understood and needs to be
investigated further.   Such an investigation could be approached
in a number of ways:-

(a)   The effect of inclusion size could be determined optically
by measuring the lengths and thicknesses of individual
inclusions and computing the parameters λ ($^{\text{length}}/\text{thickness}$)
and $\sqrt{ab}$ ($\sqrt{\text{length x thickness}}$).   The parameter $\sqrt{ab}$ is
a measure of inclusion size and λ a measure of inclusion
deformation.   A plot of λ vs $\sqrt{ab}$ would then show the
effect of inclusion size on deformability.

(b)   An automatic imaging and computing machine, such as
the Quantimet 720B, could be used to determine the same
parameters from a much larger number of inclusions.
The data could then be presented in the form of average
aspect ratios, for inclusions having values of the
parameter $\sqrt{ab}$ in different ranges.
Both these methods suffer the disadvantage that measure-
ments must be restricted to low strains, since the
inclusion thickness becomes variable at higher strains
and the inclusions no longer conform to an ellipsoidal
morphology.

(c) The problem would be more ideally approached by the measurement of the true length and width parameters of the deformed inclusions, which could be determined by the examination of deeply etched specimens by Scaning Electron Microscopy. This technique would also have the advantage that any systematic variation in inclusion composition could be detected, provided the instrument used had analysis facilities.

3. The effect of composition on the deformability of manganowustite inclusions has not been investigated in detail, and such an investigation could be coupled with that outlined in (2) above.

4. The effects of strain rate and hydrostatic pressure on the behaviour of non-metallic inclusions has not been reported in the literature. Since these parameters are likely to have a significant effect on the behaviour of inclusions during machining operations, the behaviour of various types of inclusions should be investigated at high rates of strain. In particular the behaviour of manganese sulphides and selenides and the low melting point glassy silicates should be investigated. The effects of iron, manganese, magnesium and calcium, and aluminium and chromium, on the non-plastic/plastic transition temperature of glassy silicates should also be determined. Such an investigation would probably involve deformation by Camm Plastometry.

5. The deformabilities of several types of inclusion have still not been assessed and the behaviour of the more calcareous calcium aluminates and the modified sulphide inclusions during hot working, remain to be investigated.

6.   Investigations into the behaviour of inclusions during working
      have, until now, concentrated on this behaviour during hot
      working, none of the investigations reported being solely
      concerned with their behaviour during deformation at low
      temperatures. Although it is likely that many types of
      silicate inclusion will behave in a brittle manner during
      cold working, the behaviour of manganese sulphide and
      mangano-wustite inclusions is unresearched. An investigation
      of this type could also investigate the behaviour of the cluster
      type inclusions produced on aluminium deoxidation. Since
      void healing, through pressure welding, is less likely to
      occur at these lower temperatures, the defects produced
      will be more severe than those produced at higher temperatures,
      and it would be interesting to compare the effects of high and
      low temperature deformation on the mechanical properties;
      particularly with regard to the ductility in the short trans-
      verse direction.

7.   The process of deoxidation by aluminium should be investigated
      further, in particular the formation of aluminous inclusions
      during stream reoxidation on teeming, at both high and low
      residual aluminium concentrations. The formation of
      alumina precipitates at both high and very low oxygen
      concentrations should also be investigated in order to confirm,
      or disprove, the suggested effect of oxygen concentration on
      growth morphology.

APPENDIX I

The Determination of Inclusion Relative Plasticity by the Measurement of Inclusion Aspect Ratios

Two conditions of deformation will be considered.

1. Deformation by Uniaxial Compression

The volume of a spherical inclusion of diameter 'a' is $\frac{4}{24}\pi a^3$ and under uniaxial compression is deformed into a prolate ellipsoid of volume $\frac{4}{24}\pi b^2 t$ where 'b' is the diameter and 't' is the thickness.

$$\text{Vol} = \text{const.} = \frac{4}{24}\pi a^3 = \frac{4}{24}\pi b^2 t$$

Thus

$$\left(\frac{a}{t}\right)^3 = \left(\frac{b}{t}\right)^2 = \lambda^2 \qquad \text{where} \quad \lambda = \left(\frac{b}{t}\right)$$

and

$$\mathcal{E} = \log_e\left(\frac{a}{t}\right) = \log_e\left(\lambda\right)^{2/3}$$

$$\mathcal{E} = \frac{2}{3}\log_e \lambda$$

Thus the Relative Plasticity ν becomes

$$\nu = \frac{\mathcal{E}_i}{\mathcal{E}_m} = \frac{2}{3}\frac{\log_e \lambda}{\mathcal{E}_m}$$

2. Deformation by Plane Strain

In this case the width of the inclusion ideally remains unchanged and the spherical volume is deformed into a volume

$$\text{Vol} = \frac{4}{24}\pi a^3 = \frac{4}{24}\pi \, a l t$$

where   a = the width of the inclusion

         l = the length

         t = the thickness

Thus $\left(\frac{a}{t}\right)^2 = \frac{l}{t} = \lambda \qquad \text{where} \quad \lambda = \frac{l}{t}$

Hence $\quad \mathcal{E}_i = \log_e \frac{a}{t} = \log_e (\lambda)^{\frac{1}{2}}$

and

$$V = \tfrac{1}{2} \ \frac{\log_e \lambda}{\mathcal{E}_m}$$

where $\quad V$ = Relative Plasticity

$\mathcal{E}_i$ = Inclusion True Strain

$\mathcal{E}_m$ = Matrix True Strain

λ = Aspect Ratio of the Deformed Inclusion

APPENDIX 2

The Determination of Inclusion Relative Plasticity by the Measurement of Inclusion Projected Length

By definition the true strain of an inclusion is given by

$$\mathcal{E}_i = \log_e \frac{a}{t}$$

where

a = The initial inclusion diameter

t = Inclusion thickness after deformation.

Now for the case of spherical inclusions deformed by plane strain:

$$\text{Volume} = \frac{4}{24} \pi a^3 = \frac{4}{24} \pi \, lat$$

where   l = Inclusion length after deformation.

Dividing by $a^2 t$

$$\frac{a}{t} = \frac{l}{a}$$

and thus

$$\mathcal{E}_i = \log_e \frac{l}{a}$$

Now the average true strain for the whole inclusion population is:

$$\overline{\mathcal{E}_i} = \frac{\sum_i^N \log_e \frac{l}{a}}{N} = \overline{\log_e \, {}^{l}/a} \qquad (1)$$

However for the case of a random distribution of <u>uniformly sized</u> spheres*

$$\overline{\log_e \frac{l}{a}} \longrightarrow \log_e \overline{\left(\frac{l}{a}\right)} \longrightarrow \log_e \frac{\overline{l}}{\overline{a}} \qquad (2)$$

*N.B.   Although these relationships hold for a unique distribution of uniform spheres, they are not true for a distribution of sizes; the error in the relationships increasing with increasing spread of diameters about the mean.

Considering unit volume of the specimen, the total inclusion length of the inclusions is

$$P_R = N_V \times \overline{l} \qquad (3)$$

where

P_R = The total inclusion length in the rolling plane

N_V = The number of inclusions per unit volume

$\bar{l}$ = The true mean inclusion length

Now considering a longitudinal cross section, the projected length per unit area actually measured in the section is

$$P_m = N_A \times \bar{l'} \tag{4}$$

where

P_m = The measured projected length in the longitudinal section

N_A = The number of inclusions per unit area in the longitudinal section

$\bar{l'}$ = The measured mean inclusion length

The number of inclusions per unit cross sectional area in the longitudinal plane is related to the number per unit volume by

$$N_A = N_V \times \bar{c}$$

where

$\bar{c}$ = The inclusion width

and for the case of plane strain:

$$\bar{c} = \bar{a}$$

thus,

$$N_A = N_V \times \bar{a} \tag{5}$$

The measured inclusion lengths in the longitudinal section are related to their true lengths by,

$$\bar{l'} = \sqrt{\frac{\pi}{4}}\, \bar{l} \tag{6}$$

Substituting (5) and (6) in (4)

$$P_m = N_V \cdot \bar{a} \cdot \sqrt{\frac{\pi}{4}}\, \bar{l} \tag{7}$$

but $\quad P_R = N_V \cdot \bar{l}$

Thus $\quad P_m = \bar{a}\, P_R \sqrt{\frac{\pi}{4}} \tag{8}$

From (3)

$$\bar{I} = \frac{P_R}{N_V} \tag{9}$$

Hence

$$\bar{a} = \frac{P_{R_o}}{N_{V_o}} \quad \text{for an undeformed sample}$$

Substituting in (2)

$$\mathcal{E}_i = \log_e \frac{P_R/N_V}{P_{R_o}/N_{V_o}} \tag{10}$$

And where N_V is constant this becomes

$$\mathcal{E}_i = \log_e \frac{P_R}{P_{R_o}}$$

From (8)

$$\mathcal{E}_i = \log_e \frac{P_m}{P_{m_o}} \tag{11}$$

This equation relates the true strain of an initially random distribution of uniformly sized spheres, deformed under conditions of plane strain, to their measured projected lengths in the longitudinal section after deformation.

However, real distributions of inclusions are never uniformly sized and the applicability of the equation depends on the extent of their deviation from this condition.

The analysis also requires the determination of projected lengths before and after deformation and consequently requires a comparison between two specimens. The relationship is only true for specimens with the same sizes and distributions of inclusions. However, it is possible to apply a correction for specimens having different volume fractions of inclusions, PROVIDED THAT THE SIZES OF THE INCLUSIONS IN THE TWO SPECIMENS ARE THE SAME.

For specimens A and B

$$\frac{(N_V)_A}{(N_V)_B} = \frac{(A_i)_A}{(A_i)_B}$$

where

A_i = The area fractions of the inclusions.

Thus from (10)

$$\mathcal{E}_i = \log_e \frac{P_R \, (N_V)_o}{P_{R_o} \, (N_V)}$$

and hence

$$\mathcal{E}_i = \log_e \frac{P_m \, (A_i)_o}{P_{m_o} \, (A_i)} \tag{12}$$

However, in the case of samples which not only contain different fractions of inclusions but also have different size distributions, applying this correction is likely to increase the error rather than to eliminate it.

COMPUTER PROGRAME TO CALCULATE THE LATTICE SPACINGS OF ANY
CRYSTAL LATTICE (EXCEPT HEXAGONAL)
TO USE THE PROGRAMME TYPE INTO THE COMPUTER :-

```
/INPUT
/INCLUDE LATT
(LATTICE NUMBER)
(MINIMUM D SPACING REQUIRED)
(LATTICE PARAMETERS)
```

THE LATTICE TYPES ARE:-

TRICLINIC	TYPE 1
MONOCLINIC	TYPE 2
ORTHORHOMBIC	TYPE 3
TETRAGONAL	TYPE 4
CUBIC	TYPE 5
HEXAGONAL	TYPE 6
RHOMBIC	TYPE 7

```
*END

*GO
```

***LATT-MAIN PROGRAMME

```
0001 /SYS TIME=MAX
0002 C   PROGRAMME TO CALCULATE THE INTERPLANAR SPACINGS OF A CRYSTAL
0003 C                              LATTICE
0004       READ(5,10)NLAT
0005    10 FORMAT(I1)
0006       READ(5,11)DMIN
0007    11 FORMAT(F10.7)
0008 C                                                        (TRICLINIC)
0009       IF(NLAT.NE.1)GOTO 2
0010     1 CONTINUE
0011       IIS=1
0012       IIF=15
0013       READ(5,20)A,B,C,Z1,Z2,Z3
0014    20 FORMAT(3F10.2,3F10.7)
0015       WRITE(6,15)A,B,C,Z1,Z2,Z3
0016    15 FORMAT(/////'CALCULATION OF THE LATTICE SPACINGS OF A '
0017      C,'TRICLINIC LATTICE WITH LATTICE PARAMETERS '
0018      C/10X,'A=',F10.7/10X,'B=',F10.7/10X,'C=',F10.7/
0019      C10X,'Z1=',F10.7/10X,'Z2=',F10.7/10X,'Z3=',F10.7)
0020       DIMENSION S(3,3)
0021       S(1,1)=(B**2)*(C**2)*(SIN(Z1))**2
0022       S(2,2)=(A**2)*(C**2)*(SIN(Z2))**2
0023       S(3,3)=(A**2)*(B**2)*(SIN(Z3))**2
0024       S(1,2)=A*B*(C**2)*(COS(Z1)*COS(Z2)-COS(Z3))
0025       S(2,3)=(A**2)*B*C*(COS(Z2)*COS(Z3)-COS(Z1))
0026       S(1,3)=A*(B**2)*C*(COS(Z3)*COS(Z1)-COS(Z2))
0027       V=A*B*C*(SQRT(1-(COS(Z1))**2-(COS(Z2))**2-(COS(Z3))**2
0028      C+(2*COS(Z1)*COS(Z2)*COS(Z3))))
0029       GOTO 100
0030 C                                                        (MONOCLINIC)
0031     2 CONTINUE
0032       IIS=1
0033       IIF=15
0034       IF(NLAT.NE.2)GOTO 3
0035       READ(5,30)A,B,C,Z
0036    30 FORMAT(3F10.2,F10.7)
0037       WRITE(6,25)A,B,C,Z
0038    25 FORMAT(/////'CALCULATION OF THE LATTICE SPACINGS OF A '
0039      C,'MONOCLINIC LATTICE WITH LATTICE PARAMETERS '/
0040      C10X,'A=',F10.7/10X,'B=',F10.7/10X,'C=',F10.7/
0041      C10X,'Z=',F10.7)
0042       GOTO 100
0043 C                                                        (ORTHORHOMBIC)
0044     3 CONTINUE
0045       IIS=1
0046       IIF=15
0047       IF(NLAT.NE.3)GOTO 4
0048       READ(5,40)A,B,C
0049    40 FORMAT(3F10.2)
0050       WRITE(6,35)A,B,C
0051    35 FORMAT(/////'CALCULATION OF THE LATTICE SPACINGS OF AN '
0052      C,'ORTHORHOMBIC LATTICE WITH LATTICE PARAMETERS '/
0053      C10X,'A=',F10.7/10X,'B=',F10.7/10X,'C=',F10.7)
0054       GOTO 100
0055 C                                                        (TETRAGONAL)
0056     4 CONTINUE
0057       IIS=1
0058       IIF=15
0059       IF(N.NE.4)GOTO 5
0060       READ(5,50)A,C
0061    50 FORMAT(2F10.2)
0062       WRITE(6,45)A,C
0063    45 FORMAT(/////'CALCULATION OF THE LATTICE SPACINGS OF A '
0064      C,'TETRAGONAL LATTICE WITH LATTICE PARAMETERS'/
```

```
0064          C,'TETRAGONAL LATTICE WITH LATTICE PARAMETERS'/
0065          C10X,'A-',F10.7/10X,'C-',F10.7)
0066             GOTO 100
0067 C                                                             (CUBIC)
0068       5 CONTINUE
0069          IIS-8
0070          IIF-15
0071          IF(NLAT.NE.5)GOTO 6
0072          READ(5,60)A
0073      60 FORMAT(F10.2)
0074          WRITE(6,55)A
0075      55 FORMAT(////'CALCULATION OF THE LATTICE SPACINGS OF A '
0076          C,'CUBIC LATTICE WITH LATTICE PARAMETERS '/
0077          C10X,'A-',F10.7)
0078             GOTO 100
0079 C                                                             (HEXAGONAL)
0080       6 CONTINUE
0081          IF(NLAT.NE.6)GOTO 7
0082          READ(5,70)A,C
0083      70 FORMAT(2F10.2)
0084          WRITE(6,65)A,C
0085      65 FORMAT(////'CALCULATION OF THE LATTICE SPACINGS OF A '
0086          C,'HEXAGONAL LATTICE WITH LATTICE PARAMETERS '/
0087          C10X,'A-',F10.7/10X,'C-',F10.7)
0088             GOTO 500
0089       7 CONTINUE
0090          IIS-1
0091          IIF-15
0092 C                                                             (RHOMBOHEDRAL)
0093          READ(5,80)A,Z
0094      80 FORMAT(F10.2,F10.7)
0095          WRITE(6,75)A,Z
0096      75 FORMAT(////'CALCULATION OF THE LATTICE SPACINGS OF A '
0097          C,'RHOMBOHEDRAL LATTICE WITH LATTICE PARAMETERS '/
0098          C10X,'A-',F10.7/10X,'Z-',F10.7)
0099             GOTO 100
0100     100 CONTINUE
0101          DIMENSION D(1500),D1(1500),L1(1500),M1(1500),N1(1500),
0102          CD2(1500),L2(1500),M2(1500),N2(1500)
0103          N-0
0104          DO 200 II-IIS,IIF
0105          H-II-8
0106          DO 200 JJ-IIS,IIF
0107          K-JJ-8
0108          DO 200 KK-IIS,IIF
0109          L-KK-8
0110          N-N+1
0111          GOTO(125,225,325,425,525,625,725),NLAT
0112     125 EQ-(1/V**2)*((S(1,1)*(H**2))+(S(2,2)*(K**2))+(S(3,3)*(L**2
0113          C))+(2*S(1,2)*H*K)+(2*S(2,3)*K*L)+(2*S(1,3)*H*L))
0114             GOTO 99
0115     225 EQ-H**2/A**2*((SIN(Z)))**2+K**2/B**2+L**2/C**2*SIN(Z)
0116          C**2-(2*H*L*COS(Z))/(A*C*(SIN(Z))**2)
0117             GOTO 99
0118     325 EQ-(H/A)**2+(K/B)**2+(L/C)**2
0119             GOTO 99
0120     425 EQ-(H**2+K**2)/A**2+L**2/C**2
0121             GOTO 99
0122     525 EQ-(H**2+K**2+L**2)/A**2
0123             GOTO 99
0124     625 EQ-4/3*(H**2+H*K+K**2)/A**2+L**2/C**2
0125             GOTO 99
```

```
                GOTO 99
0126    725 EQ=((H**2+K**2+L**2)*(SIN(Z))**2+2*(H*K+K*L+H*L)*
0127        C((COS(Z))**2-COS(Z)))/Z**2*(1-3*(COS(Z))**2+2*(COS(Z))**3)
0128     99 IF(EQ.LE.0.0)GOTO 150
0129        SP=SQRT(1/EQ)
0130        IF(SP.LT.DMIN)GOTO 150
0131        D(N)=SP
0132        D1(N)=SP
0133        L1(N)=H
0134        M1(N)=K
0135        N1(N)=L
0136        GOTO 200
0137    150 CONTINUE
0138        N=N-1
0139        GOTO 200
0140    200 CONTINUE
0141        NMAX=N
0142        N=0
0143        DO 400 M=1,NMAX
0144        B=1000.
0145        DO 300 N=1,NMAX
0146        IF(B.LT.D(N))GOTO 300
0147        B=D(N)
0148        H=L1(N)
0149        K=M1(N)
0150        L=N1(N)
0151        NN=N
0152    300 CONTINUE
0153        D2(M)=B
0154        L2(M)=H
0155        M2(M)=K
0156        N2(M)=L
0157        D(NN)=1000.
0158    400 CONTINUE
0159        WRITE(6,21)NMAX
0160     21 FORMAT(/'THE NUMBER OF LATTICE SPACINGS CALCULATED IS',I4
0161        C//4X,'( H K L)',5X,'      D   ',6X,'*',5X,'( H K L)',5X,'   D   '
)
0162        DMEM=0.0
0163        DO 500 M=1,NMAX
0164        N=M
0165        IF(D2(M).EQ.DMEM)GOTO 111
0166        DMEM=D2(M)
0167        WRITE(6,90)L1(N),M1(N),N1(N),D1(N),L2(M),M2(M),N2(M),D2(M)
0168     90 FORMAT(5X,I2,I2,I2,5X,F10.7,10X,I2,I2,I2,5X,F10.7)
0169        GOTO 500
0170    111 WRITE(6,91)L1(N),M1(N),N1(N),D1(N),L2(M),M2(M),N2(M)
0171     91 FORMAT(5X,I2,I2,I2,5X,F10.7,10X,I2,I2,I2)
0172        DMEM=D2(M)
0173    500 CONTINUE
0174        CALL EXIT
0175        END
0176 /DATA
=END

*GO
```

<u>PRINTOUT FOR THE TEPHROITE LATTICE</u>

/INPUT
/INCLUDE LATT
3
3.6
4.862   10.62   6.221
/ENDRUN
*IN PROGRESS

MAIN   - OOEA24
012100 BYTES USED
EXECUTION BEGINS   16.0S

CALCULATION OF THE LATTICE SPACINGS OF AN ORTHORHOMBIC LATTICE WITH LAT
TICE PARAMETERS
          A= 4.8620005
          B=10.6199999
          C= 6.2209997

THE NUMBER OF LATTICE SPACINGS CALCULATED IS   32

(H K L)	D	*	(H K L)	D
-1-1-1	3.6035500		1 1 1	3.6035500
-1-1 0	4.4207411		1 1-1	
-1-1 1	3.6035500		1-1 1	
-1 0-1	3.8308258		1-1-1	
-1 0 0	4.8620014		-1 1 1	
-1 0 1	3.8308258		-1 1-1	
-1 1-1	3.6035500		-1-1 1	
-1 1 0	4.4207411		-1-1-1	
-1 1 1	3.6035500		1 0 1	3.8308258
0-2-1	4.0387926		1 0-1	
0-2 0	5.3099995		-1 0 1	
0-2 1	4.0387926		-1 0-1	
0-1-1	5.3678398		0 2 1	4.0387926
0-1 0	10.6200037		0 2-1	
0-1 1	5.3678398		0-2 1	
0 0-1	6.2209997		0-2-1	
0 0 1	6.2209997		1 1 0	4.4207411
0 1-1	5.3678398		1-1 0	
0 1 0	10.6200037		-1 1 0	
0 1 1	5.3678398		-1-1 0	
0 2-1	4.0387926		1 0 0	4.8620014
0 2 0	5.3099995		-1 0 0	
0 2 1	4.0387926		0 2 0	5.3099995
1-1-1	3.6035500		0-2 0	
1-1 0	4.4207411		0 1 1	5.3678398
1-1 1	3.6035500		0 1-1	
1 0-1	3.8308258		0-1 1	
1 0 0	4.8620014		0-1-1	
1 0 1	3.8308258		0 0 1	6.2209997
1 1-1	3.6035500		0 0-1	
1 1 0	4.4207411		0 1 0	10.6200037
1 1 1	3.6035500		0-1 0	

*END

*GO

REFERENCES

1. Widdowson, R. 'Inclusion origins in steelmaking'.
    'Inclusions and their effects on steel properties'.
    B.S.C. (PMC) Conference Bodington Hall, Leeds Univ.
    Sept. 1974.

2. Simms, C.E. & Dahle, F.B. 'Trans A.F.A.' 46 1938 p.65-132

3. Baker, T.J. & Charles, J.A. 'JISI' Sept. 1972 p.702-706

4. Dahl, W. et al 'Stahl.u.eisen' 86 1966 p.796

5. Fredriksson, H. & Hillert, M. 'Scand.Jnl.Met' 2 1972 p.125-145

6. Duckworth, W.E. & Inneson, E. 'The Effects of Externally
    Introduced Alumina particles on the Fatigue Life of
    EN24 Steel'
    'Clean Steel' ISI special report 77

7. Pickering, F.B. 'The constitution of non-metallic inclusions
    in steel'
    Source as ref.1.

8. Simms, C.E., Sellar, H.A. & Boulger, F.W. 'Trans A.F.A'
    57 1949 p.233-247

9. Salmon-Cox, P.H. & Charles, J.A. 'JISI' May 1965 p.493-499

10. Kiessling, R. & Westerman, C. 'JISI'   April 1966 p.377-379

11. Kiessling, R. 'Non-metallic inclusions in steel' Pt.2 ISI
    Pub.100

12. Pickering, F.B. 'Inclusion shape control'
    Seminar presented at Sheffield Polytechnic, Jan. 1975.

13. Hilty, D.C. & Farrell, J.W. 'Modification of inclusions by
    calcium'. Source as ref.1.

14. Wilson, W.G. 'Optimum R.E. additions for improved mechanical
    properties'. Source as ref.1.

15. Arrowsmith, J.M. 'Sulphide modification in steel'.
    Source as ref.1.

16. Salter, W.J.M. & Pickering, F.B. 'JISI' July 1969 p.992

17.   Payet, R. & Levegue, R. 'Rev. de. met.' July/Aug. 1967

18.   Banks, T. M. & Gladman, T. 'Metals Soc. Meeting - The
         Directionality of Properties in Wrought Products'
         Nov. 1974 London.

19.   Buzek, Z. et al 'Slevarenstvi' 17 1969 (10) P. 398-404

20.   Kucharski, E. A. & Mickelson, C. G. 'Proc. Elec. F. Conf'
         25 1967 p. 34-38

21.   Hilty, D. C., Crafts, W. & Soloman, S. 'U. S. Patent No.
         3275433' Sept. 1966.

22.   Hilty, D. C. & Crafts, W. 'Trans AIMME' 188 1950 p. 425-436

23.   Hilty, D. C. & Popp. V. T. 'Elec. Furn. Proceedings' 1969
         p. 52 - 66.

24.   Saxena, S. K. Engh, T. & Penekar, S. 'Scand. J. Met.' 4 1975
         p. 42-48

25.   Sponseller, D. L. & Flinn, R. A. 'Trans AIMME' 230 1964
         p. 876-888.

26.   Miyashita, Y., Nishikawa, K. 'Tetsu to Hagane' 57 1971 (13)
         p. 1969-1975.

27.   Kiessling, R. & Westerman, C. 'JISI' July 1970 p. 699

28.   Kor, G. J. W. & Richardson, F. D. 'JISI' July 1968 p. 700-704

29.   Lu, W. K. & McLean, A. 'Ironmaking and Steelmaking Quarterly'
         4 1974 p. 228-233.

30.   Wilson, W. G., Kay, D. A. R. & Vahed, A. 'Jnl. of Metals'
         May 1974 p. 14-23.

31.   Wilson, W. G. & Wells, R. 'Metal Progress' Dec. 1973,
         p. 75-77.

32.   Luyckx, L. et al. 'Met. trans' 1 1970 p. 3341-3350.

33.   Schlindlerova, V. & Buzek, Z. 'Slevarentve' 12 1972 p. 492-494

34.   Davies, I. G., Randle, M. & Widdowson, R. 'Metals Technology'
         May 1974 p. 241-248.

35.   Rowntree, G., Weiner, R. J. & Micklethwaite, B. 'JISI'
         Jan. 1973 p. 83-84.

36.   Bingel, C. J. & Scott, L. V. 'Elec. Furn. Proc. (Cincinatti)'
         31 1973 p. 171-174.

37. Bennett, H.W. & Sandell, L.P. 'ibid' 31 1973 p.167-170.

38. Little, J.H. & Henderson, W.L.M. 'The effects of second
     phase particles on the mechanical properties of steel'.
     151 1971 p.183.

39. Pollard, B. 'Metals technology' July 1974 p.343-347.

40. Mihelich, J.L. et al. 'JISI' June 1971 p.469-476.

41. Jellinck, F. 'Archiv.Kemi' 20 1963 p.447

42. Straube, H., Kuhnelt, G. & Plockinger, E. 'Arch.Eisenh'
     July 1969 p.509-518.

43. Plockinger, E. 'Stahl u.Eisen' 76 1956 p.810-824.

44. Plockinger, E. & Rosegger, R. 'ibid' 77 1957 p.701-704.

45. Plockinger, E. & Wahlster, M. 'ibid' 80 1960 p.656-699.

46. Sloman, H.A. & Evans, E.L. 'JISI' May 1950 p.81-90.

47. Hilty, D.C. & Crafts, W. 'Jnl of Metals' Feb.1950
     'Trans AIMME' 188 p.414-425.

48. Waudby, P.E., British Steel Corporation - Swinden Laboratories.
     Private communication.

49. Discussion of ref.42 p.607-615.

50. Frohberg, M.G. & Potschke, J. 'Feiberger Forschung'
     B144 1969 p.31-51 (R.D. Trans. 11974).

51. Bogdandy, L.von., Meyer M. & Stanski, I.N. 'Arch Eisenh'
     34 1963 p.235-241.

52. Waudby, P.E. & Salter, W.J.M. 'JISI' July 1971 p.518-522.

53. Choudhury, A. & Wahlster, M. 'Rheinstahl-technik' 4 1966
     p.111-121

54. Kozakevitch, P. & Olette, M. 'The Production and Application
     of clean steels' Proc.Int.Conf. Blantonfured, Hungary
     June 1970 ISI Pub. p.42-49.

55. Rege, R.A., Szekeres, E.S. & Forgeng, W.D. 'Met.trans.
     AIMME' 1 1970 p.2652

56. Asano, K. & Nakano, T. 'Tetsu.to.Hagane' 57 1971 p.1951.

57.   Okohira, K., Sato, N. & Mori, H. 'Trans ISIJ' <u>14</u> 1974
        p. 102-109.

58.   Ooi, H., Sekine, T. & Kasai, G. 'Ibid' <u>15</u> 1975 p. 371-379.

59.   Waudby, P.E., Salter, W.J.M. & Pickering, F.B. 'JISI'
        July 1973 p. 486-492.

60.   Pickering, F.B. 'Jerkontorets Annaler' <u>148</u> 1964 p. 845-872.

61.   Van Vlack, L.H. & Flinn, R.A. & Colligan, G.A., 'Trans A.F.A.'
        <u>68</u> 1960 p. 132-135.

62.   Plockinger, E., Holzgruber, W. & Kuhnelt, G., 'Radex Rundsch'
        <u>2</u> 1969 p. 508-517.

63.   Wahlster, M., Choudhury, A., Knahl, H. & Freismuth, A.,
        'ibid' p. 478-494.

64.   Saxena, S.K., Engh. T. & Pednekar, S. 'Scand. Jnl. Met'.
        <u>4</u> 1975 p. 42-48

65.   Kiessling, R. & Lange, N. 'Non metallic inclusions in steel'
        Pt. I 151 5P. Rep 90.

66.   Pickering, F.B., 'Iron & Steel' Jan. 1957 (2).

67.   Fischer, W.A. & Fleischer, H.J. 'Arch Eisenh' <u>32</u> 1961
        p. 305-313.

68.   Yavoiskii, V.I. & Haase, R. 'Steel in the U.S.S.R' March 1974
        p. 195-197.

69.   Sloman, H.A. & Evans, E.L. 'JISI' Oct. 1951 p. 145-152.

70.   White, J. 'JISI' <u>148</u> 1943 p. 586.

71.   Sloman, H.A. & Evans, E.L. 'JISI' Nov. 1952 p. 296-300.

72.   Sims, C.E. 'Trans AIMME' <u>215</u> 1959 p. 367-393.

73.   Sano. N., Shiomi, S. & Matsushita, Y. 'Tetsu to Hagane' <u>51</u>
        1965 p. 19-38.

74.   Hilty, D.C. & Crafts, W. 'Trans AIMME' <u>188</u> 1950 p. 425-436.

75.   Gokcen, N.A. & Chipman, J. 'ibid' <u>194</u> 1952 p. 171-181.

76.   Zapffe, C.A. & Sims, C.E. 'ibid' <u>154</u> 1943 p. 192-227.

77. Toge, T. & Wantabe, T. 'Trans ISIJ' 15 1975 p.581-588.

78. Torsell, K. 'Jerkon.Annaler' 151 1967 p.890-949.

79. Turpin, M.L. & Elliott, J.F. 'JISI' 204 1966 p.217

80. Hillert, L. & Hillert, M. 'Jnl.mat.Sci' 5 1970 p.610-612.

81. Shiraiwa, T., Fujino, N. & Matsuno, F. 'The Sumitomo Search' 11 1974 p.85-100.

82. Briggs, G. 'Sheffield Polytechnic' Private communication.

83. Morgan, E.L. et.al. 'JISI' Oct.1968 p.987.

84. Bowen, N.L. & Schairer, J.F. 'Am.Jnl.Sci' 29 1935 p.151-217.

85. Pickering, F.B. 'The effect of processing parameters on the origins of non metallic inclusions'.
'The production and application of clean steel' ISI LOND.

86. Unkle, H. 'J.I.M' 61 (2) 1937 p.171-196.

87. Siebel, E. 'Die Formgebung im bildsamen Zutland' Dusseldorf 1932.

88. Benedicks, C. & Lofquist, H. 'Non-metallic inclusions in iron & steel' Lond.1930.

89. Schiel, E. & Schnell, R. 'Mitt Forschungsinst Verein. Stahlwerk Dortmund' 4 1934 (9) p.235.

90. Schiel, E. 'Z.Metallkunde' 27 1935 p.199.

91. Schiel, E. & Schnell, R. 'Stahl u.Eisen' 72 1952 p.683-687

92. Pickering, F.B. 'JISI' June 1958 p148-159.

93. Malkiewicz, T. & Rudnik, S. 'JISI' Jan.1963 p.33-38

94. Wardle, G. Aston Univ. Private Communication.

95. Baker, T.J.& Charles, J.A. 'JISI' Sept.1972 p.680-689.

96. Barnard, G.'IRSID Paris' Private communication.

97. Gladman, T. 'Inclusion requirements and assessments' Source as ref.1.

98. Zeisloft, R.H. & Hosford, W.F. 'Trans A.S.M.' 62 1969 p.297-300.

99.   Sundstrom, B. 'Jnl. composite. mats' 5 1971 p. 277-278.

100.   McClintock 'Jnl. applied Mech.' 35 1968 p. 363.

101   Klevebring, B. I. 'Scand. Jnl. met' 3 1974 p. 102-104.

102.   Mann, G. S. & Van Vlack, L. H. 'Met. trans' 3 1972 p. 2005-2006.

103.   Gove, K. B. & Charles, J. A. 'Met. tech.' Sept. 1974 p. 425-431.

104.   Warrick, R. J. & Van Vlack, L. H. 'Trans A. S. M.' 57 1964
        p. 672-689

105.   Baker, T. J. & Charles, J. A. & Gove, K. B. 'Met. Soc. Preprints'.
        'Directionality of properties in wrought products'
        Meeting 27 - 28th Nov. 1974 75/716 PT. I.

106.   Gay, N. C. 'Techtonophysics' 5 (3) 1968 p. 211-234.

107.   Ashok, S. K. Ph. D Thesis Cambridge University 1976.

108.   Smith, R. B. 'Geological Soc. Am. Bul.' 86 1975 p. 1601-1609.

109.   Banks, T., British Steel Corporation - Swinden Laboratories
        Private Communication.

110.   Bonizewski, T. & Baker, R. G. 'Acta met' 11 (8) 1963 p. 990.

111.   Moore, C. 'M. Met. thesis' Univ. of Sheffield 1968.

112.   Uchiyama, I. & Sumita, M. 'Trans. Nat. Res. Inst. Met. (Jap.)'
        7 1965 p. 233-241

113.   Kiessling, R. 'Non-metallic inclusions in steel'. PT. II ISI
        Pub. 115

114.   Maunder, P. J. H. & Charles, J. A. 'JISI' July 1968 p. 705-715.

115.   Cook, P. M. 'Conf. on the properties of materials at high
        rates of strain'. INST. MECH. ENG. Session 3 Paper 2
        April-May 1957 Westminster

116.   Rudnik, S. 'JISI' April 1966 p. 374-376

117.   Brown, L. M. & Embury, J. D. 'Proc. Inst. Metals' 1 1973
        p. 164-169.

118.   Fishmeister, H. F., Navara, E. & Easterling, K. E.
        'Met. Sci. Jnl' 6 1972 p. 211-215

119. Easterling, K. E., Fishmeister, H. F. & Navara, E.
'Powder Met.' 16 1973 31 p. 128-145.

120. Navara, E. & Easterling, K. E. 'Jerkon ann.' 155 1971
p. 437-441.

121. Sundstrom, B. 'Eng. Fract. Mech' 6 1974 p. 483-492.

122. Klevebring, B. I. 'Met. trans.' 6A 1975 p. 319-327.

123. Klevebring, B. I. To be published.
'Determination of the critical inclusion size with respect
to void formation during hot working'.

124. Austen, A. R. & Avitzur, B. 'Trans. Am. Jnl. Eng. for Ind.'
Nov. 1974 p. 1192-1196.

125. Thomason, P. F. 'J. I. M.' 96 1968 p. 360-365.

126. Humphreys, F. J. & Martin, J. W. 'Phil. Mag' 16 1967 p. 927

127. Humphreys, F. J. & Hirsch, P. B. 'Proc. Roy. Soc.' A318
1970 73

128. Chapman, P. F. & Stobbs, W. M. 'Phil. Mag.' 19 1969 p. 1015.

129. Brown, L. M. & Stobbs, W. M. 'Phil. Mag.' 23 1971 p. 1201.

130. Ashby, M. F. 'Phil. Mag.' 14 1966 p. 1157.

131. Klevebring, B. I. & Marhs, R. 'Scand. Jnl. Met. 2 1973 p. 310-312.

132. Humphreys, F. J. & Stewart, A. T. 'Surf. Sci.' 31 1972 p. 389-421.

133. Chao, H. C., Van Vlack, L. H., Oberin, F., Thomassen, L.
'Trans ASM' 57 1964 p. 885-891.

134. Chao, H. C., Thomassen, L. & Van Vlack, L. H. 'Trans ASM'
57 1964 p. 386-398

135. Chao, H. C. & Van Vlack, L. H. 'Trans ASM' 58 1965 p. 335-340.

136. Baker, T. J. & Charles, J. A. 'JISI' March 1973 p. 187-192.

137. Gnanamuthu, D., Kat amis, T. Z., Flemmings, M. C.,
Mehrabain, R. 'Met. trans.' 5 1974 p. 2557-2567.

138. Wilson, P. C., Murty, Y. V., Kattamis, T. Z. & Mehrabain, R.
'Met. Tech.' June 1975 p. 241-244

139.   Murty, Y. V., Marral, J. E., Kattamis, T. Z. & Mehrabain, R.
       'Met. trans.' 6A 1975 p. 2031-2035.

140.   Medircio, D. 'Sheffield Polytechnic'. Private communication.

141.   Ekerot, S. 'Scand. Jnl. Met.' 3 1974 p. 21-27.

142.   Ekerot, S. 'Scand. Jnl. Met.' 3 1974 p. 151-152.

143.   Lewis, M. H. 'Anisotropy in single crystal refractory
       compounds'. Int. Symposium Dayton, Ohio, June 1967.

144.   Salter, W. J. M. 'A manual of quantitative electron probe
       microanalysis'. Structural Publications Ltd., London 1970.

145.   Knuppel, H., Brotzmann, K. and Forster, N. W. 'Stahl. u. Eisen'
       1965 85 p. 675-688.

146.   Linder, S. 'Scand. Jnl. of Metallurgy' 3 1974 p. 137-150

147.   Bridgeman, P. W. 'Studies in Large Plastic Flow and
       Fracture'. McGraw-Hill New York 1952.

148.   Dieter, G. E. 'Mechanical Metallurgy'. McGraw-Hill
       Tokyo 1961.

149.   Andrews, K. W. 'Stress fields around inclusions and their
       effects on fatigue'. Source as ref. 1.

150.   Opitz, H. & Konig, W. ISI Spec. Rep. 94 1967 London p. 35-41.

151.   Wicher, A. & Pape, R. 'Stahl. u. Eisen' 1967 87 p. 1169-1168.

152.   Wicher, A. & Pape, R. 'ibid' 1967 87 p. 1262-1269.

TABLE I THE EFFECT OF ABSORBED SPECIES ON INTERFACIAL ENERGY (After Kozakevitch and Olette ref. 54)

ALUMINA:MELT COMPOSITION	CONTACT ANGLE ($^{\circ}$)	INTERFACIAL ENERGY (J/m^2)
Al_2O_3 : Pure Fe	140	2.279
Al_2O_3 : Fe + 4%C	133	2.080
Al_2O_3:Fe + 0.07%O	80	0.709
Al_2O_3:Fe + 0.02%S	140	1.965

TABLE 2 STOICHIOMETRIC COMPOSITIONS OF PHASES IN THE $FeO-MnO-Al_2O_3-SiO_2$ SYSTEM

PHASE	FORMULA	COMPOSITION			
		FeO	MnO	SiO_2	Al_2O_3
Corundum	Al_2O_3	-	-	-	100
Silica	SiO_2	-	-	100	-
Manganowustite	$(Fe,Mn)O$	0 to 100	0 to 100	-	-
Mullite	$3Al_2O_3.2SiO_2$	-	-	28	72
Tephroite	$2MnO.SiO_2$	-	71	29	-
Rhodonite	$MnO.SiO_2$	-	54	46	-
Galaxite	$MnO.Al_2O_3$	-	41	-	59
Mn-Cordierite	$2MnO.2Al_2O_3.5SiO_2$	-	22	46	32
Spessartite	$3MnO.Al_2O_3.3SiO_2$	-	43	37	20
Fe-Cordierite	$2FeO.2Al_2O_3.5SiO_2$	22	-	46	32
Fayalite	$2FeO.SiO_2$	71	-	29	-
Hercynite	$FeO.Al_2O_3$	41	-	-	59
Alamandine	$3FeO.Al_2O_3.3SiO_2$	43	-	37	20

TABLE 3 MEASURED SOFTENING TEMPERATURES AND RIGID-PLASTIC TRANSFORMATION TEMPERATURES OF SOME GLASSY IRON-MANGANESE ALUMINO SILICATES (ref. 81 and 141)

SiO_2	Al_2O_3	(FeMn)O	CRITICAL TEMP. Tc ref. 141 °C	SOFTENING TEMP. Ts ref. 81 °C	DIFFER-ENCE °C
47	8	45	760		80
41	10	48		680	
35	35	30	900		
26	34	40	875		300
32	30	38		600	275
58	15	27	900		200
57	10	33		700	
49	26	23	850		130
50	20	30		720	
46	28	23	900		200
44	30	26		700	
45	15	40	790		90
43	18	37		700	

TABLE 4   PHYSICAL PROPERTIES OF THE CALCIUM ALUMINATES
(from ref. 11)

PHASE	MELTING POINT	MICROHARDNESS KP/mm^2
C_3A	1535	-
$C_{12}A_7$	1455	-
CA	1605	930
CA_2	~ 1750	1100
CA_6	~ 1850	2200

TABLE 5   COMPOSITIONS OF THE THREE COMMERCIAL
DEOXIDANTS USED IN THE INVESTIGATION (Mass %)

CAST	DEOXIDANT	%Ba	%Sr	%Ca	%Si	%Al	%Fe
10	Hypercal	10	-	10	40	20	20
11	Calsibar	17	-	15	65	1	2
12	Superseed	-	1.0	-	76	0.5	23

TABLE 6   INCLUSION SPECIES PRESENT IN EACH CAST

CAST	OXIDES	INCLUSION SPECIES
1B	FeO	Wustite inclusions
4	$FeO-SiO_2$	Low silica
5	"	Medium silica
4B	"	High silica
6	$FeO-MnO-SiO_2$	Low silica
6B	"	Medium silica
8	$Al_2O_3-SiO_2$	Low alumina
8B	"	High alumina
10	$CaO-Al_2O_3$	Hypercal ⎫
11	$CaO-SiO_2$	Calsibar ⎬ Commercial deoxidants
12	$SrO-SiO_2$	Superseed ⎭
7	Al_2O_3	Alumina clusters
7B	Al_2O_3	Alumina clusters

TABLE 7   THE ROLLING SCHEDULE USED IN THIS INVESTIGATION

PASS	THICKNESS (ins)		%REDUCTION		TRUE STRAIN
	ENTRY	EXIT	THIS PASS	TOTAL	
1	0.625	0.465	25.6	25.6	0.3
2	0.465	0.344	19.4	45.0	0.6
3	0.344	0.253	14.6	59.6	0.9
6	0.253	0.190	10.4	70.0	1.2
5	0.190	0.138	8.5	78.5	1.5
6	0.138	0.104	5.5	84.0	1.8

TABLE 8   RESULTS OF ELECTRON PROBE MICROANALYSIS

CAST	DEOXIDANT	INCLUSION TYPES	PHASE	% FeO	% MnO	% SiO$_2$	% Al$_2$O$_3$	% CaO	% BaO	% SrO
1B	Undeoxidised	Single	Phase	100	-	-	-	-	-	-
4	Si	Duplex Silicates	Primary	100	-	-	-	-	-	-
			Matrix	73	-	27	-	-	-	-
			Average	86	-	14	-	-	-	-
			Secondary	100	-	-	-	-	-	-
5	Si	Duplex Silicates	Primary	100	-	-	-	-	-	-
			Matrix	74	-	26	-	-	-	-
			Average	80	-	20	-	-	-	-
			Secondary	100	-	-	-	-	-	-
4B	Si	Glassy Single Phase		12	-	88	-	-	-	-
6	Si-Mn	Duplex Silicates	Primary	19	72	-	-	-	-	-
			Matrix	9	58	32	-	-	-	-
			Average	13	64	19	-	-	-	-
		'Eutectic'	Average	14	58	27	-	-	-	-
		'Lath'	Average	10	56	34	-	-	-	-
		'Dendritic'	Secondary	30	66	-	-	-	-	-
		'Globular'	Secondary	11	56	36	-	-	-	-
6B	Si-Mn	Glassy Single Phased		12	33	51	-	-	-	-
7B	Al	Clusters		-	-	-	100	-	-	-

TABLE 8   /Cont'd....

CAST	DEOXIDANT	INCLUSION TYPES	PHASE	% FeO	% MnO	% SiO₂	% Al₂O₃	% CaO	% BaO	% SrO
8	Al-Si	Glassy Single Phased	Matrix	14/27	-	45/61	19/21	-	-	-
		Glassy +	-	35	-	43	20	-	-	-
		Dendrites	Dendrites	-/25	-	100/74	-	-	-	-
		Glassy +	Matrix	20	-	55	23	-	-	-
		Cuboids	Cuboids	41	-	-	60	-	-	-
10	Hypercal	Cluster Types	Mostly	-	-	-	100	100	ND	-
			Few	-	-	-	91	10	ND	-
			Light Laths	-	-	-	100	-	ND	-
			Dark Blocks	-	-	-	91	9	ND	-
		Multiphase	Matrix	Si DETECTED NO ANALYSIS						
11	Calsibar	Glassy Single Phased (Variable Analysis)		10/20	-	70/80	-	10/20	ND	-
12	Superseed	Glassy Single Phased		25	-	78	-	-	-	ND

* ND = NOT DETECTED

ANALYSES ARE GIVEN TO THE NEAREST 1% (by mass) AND ARE AVERAGE VALUES OBTAINED FROM A MINIMUM OF FOUR INDIVIDUAL INCLUSIONS

TABLE 9   RESULTS OF CHEMICAL ANALYSIS

TOTAL analyses by U. VAC. given in parenthesis ( )

SOLUBLE analyses by chemical methods --

      SILICON   -   Ferrous sulphate reduction
      MANGANESE -   Periodate Colourimetric
      ALUMINIUM -   Atomic absorption

OXYGEN analyses by Coulometric carrier gas fusion

Calcium, Barium and Strontium analyses for casts 10, 11 and 12 are all below the detection limits of the analytical technique employed (atomic absorption) and are not quoted.

ALL ANALYSES ARE GIVEN IN MASS PERCENT

(a)   Analysis of the base material

	C	Mn	Si	S	P
Min	0.004	Trace	0.001	0.004	0.001
Max	0.014		0.010	0.006	0.002

(b)　　　Analyses of the experimental casts

CAST	DEOXIDATION	O	Mn	Si	Al
1B	Undeoxidized	0.180	(Tr) ND	(0.001) 0.000	(0.001) ND
4	0.06%Si Metal	0.154	(0.005) 0.002	(0.010) 0.003	(ND) ND
5	+0.10%Si Metal	0.164	(0.007) 0.003	(0.010) 0.020	(ND) ND
4B	1.0%Si Metal	0.023	(0.021) 0.016	(0.380) 0.350	(ND) ND
6	1.0%Mn + 0.075% Si Metals	0.029	(0.660) 0.560	(0.005) 0.020	(ND) ND
6B	1.0%Mn + 0.3% Si Metals	0.030	(0.240) 0.210	(0.035) 0.014	(ND) ND
7B	1.3% Al Metal	0.007	(ND) ND	(ND) ND	(0.26) 0.24
8	0.13%Si + 0.3%Al Metals	0.094	(ND) ND	(0.06) 0.003	(0.009) 0.008
10	1% Hypercal	0.010	(ND) ND	(0.330) 0.330	(0.081) 0.042
11	1% Calsibar	0.018	(ND) ND	(0.580) 0.470	(0.003) ND
12	1% Superseed	0.030	(ND) ND	(0.670) (0.630)	(0.001) ND

TABLE 10   RESULTS OF PLASTICITY MEASUREMENTS

$\mathcal{E}_m$ = Matrix true strain

$\log_e \lambda$ = Mean measured logrithm of the aspect ratio of the deformed inclusions, a minimum of 25 values.

$\sigma(\log_e \lambda)$ = Standard deviation of $\log_e \lambda$ (60% Confidence Limits).

$\mathcal{E}_i$ = Inclusion true strain (Measured) = $\frac{1}{2} \log_e \lambda$

ν_A = Apparent relative plasticity = $\left| \dfrac{\mathcal{E}_i}{\mathcal{E}_M} \right| \mathcal{E}_M$ (Measured)

ν_A^* = Apparent relative plasticity interpolated from a plot of $\mathcal{E}_i$ vs $\mathcal{E}_M$.

ν_T = True relative plasticity obtained from a plot of $\mathcal{E}_i$ vs $\mathcal{E}_M$

$$= \left| \frac{d\mathcal{E}_i}{d\mathcal{E}_M} \right| \mathcal{E}_M$$

(a)   Cast 4

$\mathcal{E}_M$	$\log_e \lambda$	$\sigma(\log_e \lambda)$	$\mathcal{E}_i$	ν_A	ν_A^*	ν_T
1150°C						
0.0	-	-	-	-	-	1.00
0.3	0.5892	.05	0.295	0.982	1.03	1.00
0.6	1.2476	.06	0.624	1.040	1.03	1.00
0.9	1.8927	.07	0.946	1.051	1.03	1.00
1.2	2.1779	.06	1.089	0.907	1.00	0.69
1.5	2.7102	.05	1.355	0.903	0.90	0.35
1.8	2.8272	.04	1.414	0.785	0.78	0.07
1275°C						
0.0	-	-	-	-	-	2.35
0.3	1.1007	.09	0.550	1.831	1.83	1.34
0.6	1.6927	.07	0.846	1.411	1.40	0.71
0.9	1.9820	.05	0.991	1.101	1.11	0.38
1.2	2.1861	.05	1.093	1.091	0.91	0.31
1.5	2.3742	.04	1.187	0.791	0.79	0.30
1.8	2.6670	.03	1.334	0.741	0.71	0.30

TABLE 10 /Cont'd....

(b) Cast 5

$\mathcal{E}_M$	$\log_e \lambda$	$\sigma(\log_e \lambda)$	$\mathcal{E}_i$	$\mathcal{V}_A$	$\mathcal{V}_A *$	$\mathcal{V}_T$
1150°C						
0.0	-	-	-	-	-	0.74
0.3	0.4879	.06	0.244	0.815	0.82	0.93
0.6	1.2789	.03	0.640	1.070	1.06	2.15
0.9	2.1906	.03	1.095	1.200	1.21	0.73
1.2	2.3686	.02	1.184	0.991	1.01	0.33
1.5	2.5404	.02	1.270	0.853	0.85	0.13
1.8	2.6153	.02	1.308	0.730	0.73	0.12
1275°C						
0.0	-	-	-	-	-	2.25
0.3	1.2206	.06	0.610	2.030	1.95	1.64
0.6	1.9767	.03	0.988	1.651	1.68	1.22
0.9	2.6875	.02	1.344	1.460	1.47	0.84
1.2	3.0773	.02	1.539	1.282	1.28	0.58
1.5	3.1975	.02	1.600	1.071	1.12	0.41
1.8	3.6113	.02	1.806	1.005	0.99	0.30

(c) Cast 6B

$\mathcal{E}_M$	$\log_e \lambda$	$\sigma(\log_e \lambda)$	$\mathcal{E}_i$	$\mathcal{V}_A$	$\mathcal{V}_A *$	$\mathcal{V}_T$
1275°C						
0.0	-	-	-	-	-	2.20
0.3	1.2000	.05	0.600	2.000	1.85	1.58
0.6	1.9177	.04	0.961	1.601	1.61	1.22
0.9	2.5394	.04	1.273	1.415	1.44	0.95
1.2	3.0826	.04	1.510	1.280	1.28	0.73
1.5	3.4196	.02	1.718	1.157	1.15	0.53
1.8	3.6791	.02	1.841	1.021	1.02	0.34
1350°C						
0.0	-	-	-	-	-	1.90
0.3	0.9601	.06	0.481	1.600	1.62	1.30
0.6	1.5386	.04	0.773	1.298	1.36	0.95
0.9	2.1413	.03	1.071	1.189	1.17	0.69
1.2	2.3971	.03	1.200	1.001	1.00	0.46
1.5	2.5623	.02	1.281	0.851	0.86	0.25
1.8	2.5649	.01	1.285	0.200	0.72	0.05

TABLE 10   /Cont'd.....

(d)   Cast 8

$\mathcal{E}_M$	$\log_e \lambda$	$\sigma(\log_e \lambda)$	$\mathcal{E}_i$	V_A	V_A^*	V_T
1150°C						
0.0	-	-	-	-	-	2.38
0.3	1.3482	.04	0.673	2.241	1.87	1.60
0.6	1.7844	.03	0.892	1.490	1.58	1.17
0.9	2.3962	.03	1.198	1.329	1.40	1.01
1.2	3.0630	.03	1.531	1.281	1.29	0.90
1.5	3.4633	.02	1.732	1.149	1.19	0.77
1.8	4.0668	.02	2.033	1.130	1.11	0.63
1275°C						
0.0	-	-	-	-	-	3.00
0.3	1.2360	.04	0.618	2.061	2.10	1.62
0.6	1.9850	.03	0.993	1.648	1.68	1.16
0.9	2.6425	.03	1.321	1.470	1.47	0.98
1.2	3.1628	.02	1.581	1.310	1.33	0.89
1.5	3.6630	.02	1.832	1.219	1.23	0.77
1.8	4.0472	.02	2.023	1.121	1.14	0.65
1350°C						
0.0	-	-	-	-	-	2.38
0.3	1.0990	.03	0.550	1.831	1.83	1.34
0.6	1.7352	.03	0.868	1.449	1.43	0.97
0.9	1.2282	.03	1.105	1.230	1.23	0.75
1.2	2.6402	.02	1.320	1.098	1.11	0.60
1.5	3.0102	.02	1.505	1.001	1.01	0.50
1.8	3.4920	.01	1.746	0.975	0.93	0.43
1150°C Hot Rolled at a true strain per pass of 0.6						
0.0	-	-	-	-	-	2.52
0.6	2.1242	.04	1.062	1.771	1.80	1.20
1.2	3.6243	.03	1.812	1.509	1.45	0.90
1.8	4.2121	.01	2.106	1.172	1.18	0.58

TABLE 10 /Cont'd.....

(e)   Cast 11

ε_M	$\log_e \lambda$	$\sigma(\log_e \lambda)$	ε_i	ν_A	$\nu_A{}^*$	ν_T

$1000^{\circ}C^*$ (MAXIMUM VALUES)

ε_M	$\log_e \lambda$	$\sigma(\log_e \lambda)$	ε_i	ν_A	$\nu_A{}^*$	ν_T
0.0	-	-	-	-	-	0.67
0.3	0.3790	.07	0.190	0.631	0.67	0.67
0.6	0.8710	.09	0.436	0.730	0.67	0.67
0.9	1.1726	.05	0.586	0.649	0.67	0.67
1.2	1.6432	.09	0.822	0.682	0.66	0.67
1.5	1.9020	.06	0.951	0.630	0.64	0.50
1.8	2.2020	.06	1.101	0.609	0.61	0.41

$1150^{\circ}C$

ε_M	$\log_e \lambda$	$\sigma(\log_e \lambda)$	ε_i	ν_A	$\nu_A{}^*$	ν_T
0.0	-	-	-	-	-	2.76
0.3	1.4168	.09	0.708	2.361	2.17	1.65
0.6	1.9001	.07	0.950	1.580	1.77	1.17
0.9	2.7778	.02	1.389	1.539	1.54	1.00
1.2	3.5849	.02	1.793	1.492	1.39	0.87
1.5	3.5967	.04	1.798	1.200	1.27	0.78
1.8	4.3231	.04	2.162	1.201	1.19	0.71

$1275^{\circ}C$

ε_M	$\log_e \lambda$	$\sigma(\log_e \lambda)$	ε_i	ν_A	$\nu_A{}^*$	ν_T
0.0	-	-	-	-	-	1.95
0.3	1.3805	.12	0.690	2.301	1.70	1.58
0.6	1.6172	.09	0.809	1.348	1.58	1.33
0.9	2.6102	.04	1.305	1.450	1.46	1.13
1.2	3.2815	.03	1.641	1.369	1.37	0.96
1.5	3.8323	.02	1.916	1.281	1.26	0.79
1.8	4.2706	.01	2.135	1.190	1.18	0.70

* At this temperature the inclusion plasticity was variable, some
  inclusions remaining non-plastic whilst others deformed slightly.
  Plasticity values were determined from the most highly deformed
  inclusions and the values recorded should read from zero to this
  maximum value.

TABLE 11   CRITICAL VISCOSITIES

Derivation of the Critical Viscosity for the Non-Plastic/Plastic Transition of Glassy Silicate Inclusions in Steel; According to the Relationship:-

$$\mu_c = \frac{\tau_m}{4\,\dot{\varepsilon}_m}$$

where

μ_c = The critical viscosity

τ_m = The matrix shear yield strength

$\dot{\varepsilon}_m$ = The matrix strain rate

Using data given by Cook, (115), for the values of yield strength of mild steel, the critical viscosities are :-

$T\,^{\circ}C$	$\dot{\varepsilon}_m$	τ_m at $\dot{\varepsilon}_m$ = 0.05	τ_m at $\dot{\varepsilon}_m$ = 0.70	$\mu_c(0.05)$	$\mu_c(0.70)$
	(Sec^{-1})	$(MN.m^{-2})$	$MN.m^{-2})$	$(MNs.m^{-2})$	$(MNs.m^{-2})$
900	1.8	45	84	6.25	11.67
	8.0	53	101	1.66	3.16
	40.0	66	115	0.42	0.72
	100.0	76	125	0.19	0.31
1000	1.8	39	57	5.42	7.92
	8.0	50	81	1.56	2.53
	40.0	57	95	0.36	0.59
	100.0	64	105	0.16	0.26
1100	1.8	32	43	4.44	5.97
	8.0	35	61	1.09	1.91
	40.0	47	77	0.29	0.48
	100.0	52	85	0.13	0.21
1200	1.8	23	30	3.19	4.17
	8.0	30	45	0.94	1.41
	40.0	40	60	0.25	0.38
	100.0	44	66	0.11	0.17

NB: The value of the matrix yield strength is reported to increase as the matrix strain increases, only reaching a plateau at strains greater than 0.2 to 0.3. Accordingly values of critical viscosity have been determined using shear yield strengths corresponding to both low, (ε = 0.05), and high, (ε = 0.70), matrix strains.

TABLE 11   /Cont'd.....

$$\tau_m = \frac{\sigma_m}{2}$$

where σ_m = The matrix yield strength

τ_m = The matrix shear yield strength

The critical viscosity range for silicate inclusion in mild steel, under normal hot rolling conditions, for low matrix strains is :-

0.11 to 6.25 MNsm^{-2}, (or $10^{6.0}$ to $10^{7.8}$ poise)

and at higher matrix strains is :-

0.17 to 11.67 MNsm^{-2}, (or $10^{6.2}$ to $10^{8.1}$ poise)

TABLE 12   COMPARISON OF THE EQUILIBRIUM CRYSTALLINE
SOLIDUS TEMPERATURES WITH THE MEASURED NON-
PLASTIC/PLASTIC TRANSITION TEMPERATURES FOR
THE VARIOUS TYPES OF INCLUSIONS INVESTIGATED

CAST	OXIDE SYSTEM	DESCRIPTION	SOLIDUS TEMP.	TRANS-ITION TEMP.
4 5	$FeO-SiO_2$	Duplex crystalline silicates comprising primary wustite particles in a wustite-fayalite eutectic matrix.	1178^oC	1150^oC
6	$(Fe, Mn)O-SiO_2$	Duplex crystalline silicates comprising primary mangano-wustite particles in a manganowustite-tephroite eutectic matrix	$\sim 1300^oC$	1275^oC
6B	$(Fe, Mn)O-SiO_2$	Initially glassy single phased silicates	$\sim 1400^oC$	1170^oC
8	$FeO-Al_2O_3-SiO_2$	Initially glassy single phased silicates	$\sim 1200^oC$	1100^oC
11	$FeO-CaO-SiO_2$	Glassy single phased silicates	$\sim 1700^oC$	1000 to 1050^oC

FIG. I

THE Fe-S BINARY PHASE DIAGRAM

FIG. 2

THE Fe-MnO-MnS PSEUDO-TERNARY PHASE DIAGRAM

FIG. 3

THE Fe-MnS PSEUDO-BINARY PHASE DIAGRAM
(After Baker & Charles ref. 3).

SULPHUR, at.-%

10 20 30 40 50 60 70 80 90 100

TEMPERATURE °C

1365°

989°

Fe (α·δ)   913°
769° Magn. trans.

298° Magn. trans.

138°   FeS (α)

1190°

p_{S_2} = 1 atm.

1 atm

FeS+α (β)

FeS₂

p_S = 1 atm

?   ?   ?

Fe   20   40   60   80   S

SULPHUR wt -%

TEMPERATURE, °C

1400 1500 1400 1200

Fe-MnO

MnO

MnO-MnS

1100

20

30

40

1785

50

60

70

1500

1600

Fe   MnS

1200
1300
1400
1500
1600

Fe - MnS

pure Fe—MnS system
Fe—MnS and alloy additions
initial steel compositions

L₁   L₂

L₁ L₂

X₂ X

T

To

L₁ + MnS

Fe + MnS

Fe   MnS

FIG. 4

THE FeS-MnS PSEUDO-BINARY PHASE DIAGRAM

FIG. 5

THE FeO-Al$_2$O$_3$ BINARY PHASE DIAGRAM

FIG. 6

THE FeO-MnO-Al$_2$O$_3$ TERNARY PHASE DIAGRAM

Al−Fe−O
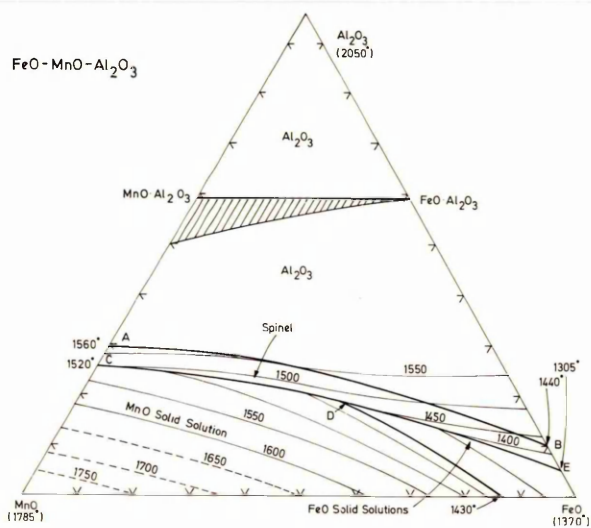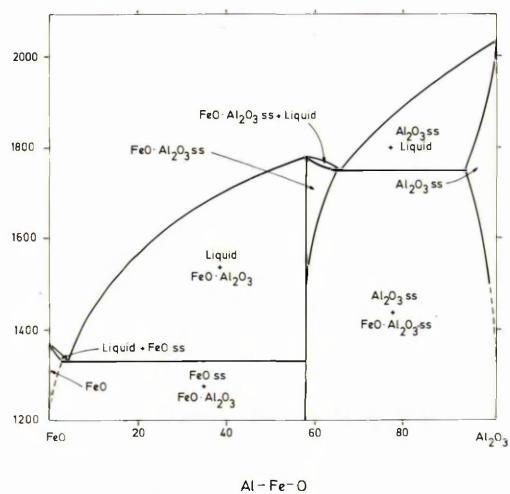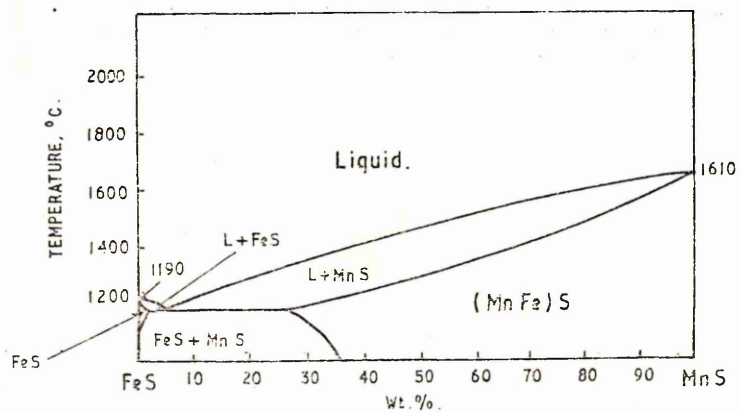
FeO−MnO−Al$_2$O$_3$

FIG. 7

THE CaO-Al$_2$O$_3$ BINARY PHASE DIAGRAM

FIG. 8

THE Fe-O BINARY PHASE DIAGRAM

SYSTEM CaO -Al₂O₃
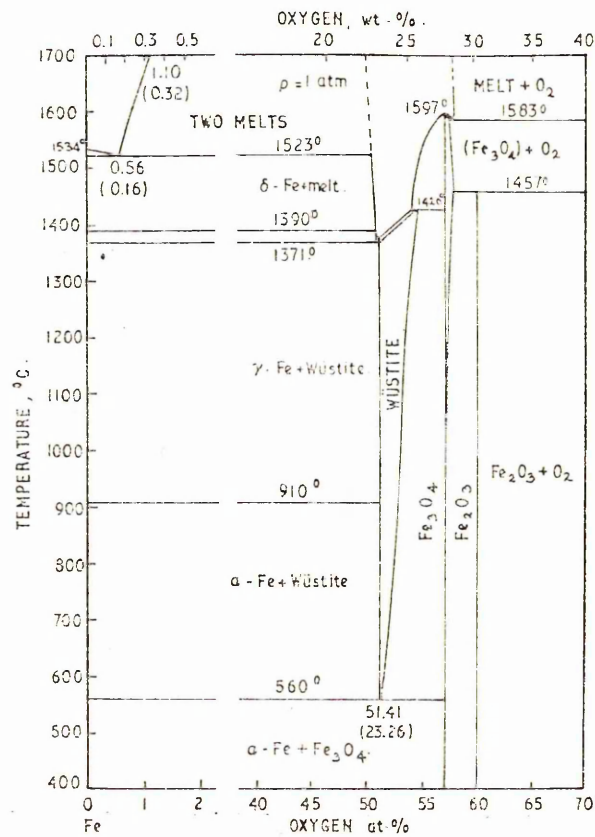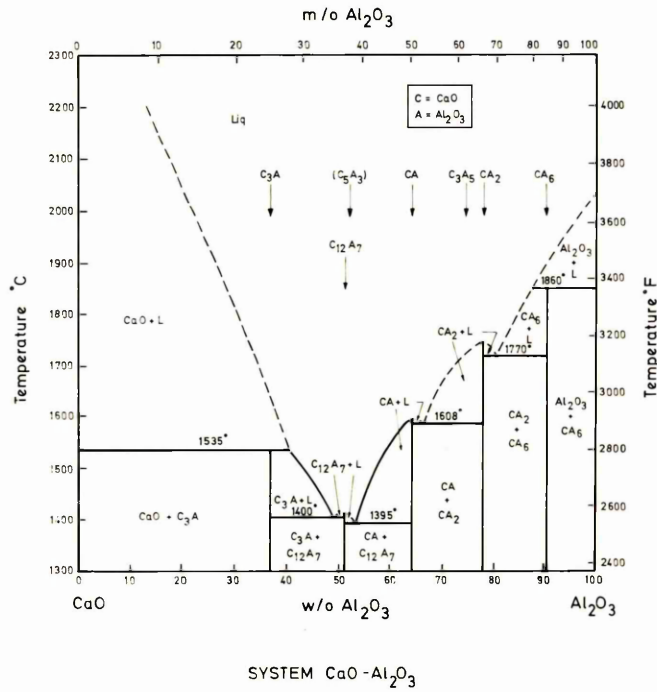
PLOT OF Fe0-Mn0 COMPOSITION OF MANGANO-WUSTITE
INCLUSIONS IN RIMMING STEEL ON REHEATING TO 1000°C
(After Yavoiskii & Haase ref. 68)

FIG. 10

THE Fe0-Mn0-SiO$_2$ PSEUDO-TERNARY PHASE DIAGRAM

FIG. 11

THE Fe0-Al$_2$O$_3$-SiO$_2$ PSEUDO-TERNARY PHASE DIAGRAM

FeO/MnO IN INCLUSION

HOLDING TIME (HRS)

MnO

FeO

1723

SiO₂

Two L

1698 Two L

Cr + L

Tr + L

F + Tr

L + Cr

R + Tr

1705

1470

1291

Cr
Cristobalite

L

1474

1178

Cr

1600

Tr   Tridymite

Rhodonite R

R + L

R + Te

L + Te

MnO + L

L

F + L

1200

Olivine

1300

1317

W + L

1200

Manganowüstite

1600

1800

MnO + Te

1369   W + F

1300

1850

FeO

MnO

(FeMn)O

1369

L

(FeMn)O + L

1850

SiO₂
1723°

1698°

~1590°

Two
Liquids

Cristobalite

1698°   1600

1470°

Mullite

Tridymite

1400

1210°   1205°

2FeO·2Al₂O₃·5SiO₂

1470°   1200   1083°
1178°   1063°   1300

Fayalite   Iron Cordierite   1380°

2FeO·SiO₂
1205°

1200

1177°   1150°   1300

3Al₂O₃·2SiO₂
~1850°

~1840°

1148°   Hercynite   1500

Corundum

Wüstite

1700

~1900

FeO
1365   1329°

FeO·Al₂O₃
~1780°   ~1750°

Al₂O₃
~2020°

SYSTEM "FeO"- Al₂O₃- SiO₂

FIG. 12

THE MnO-Al_2O_3-SiO_2 PSEUDO-TERNARY PHASE DIAGRAM

FIG. 13

THE CaO-Al_2O_3-SiO_2 PSEUDO-TERNARY PHASE DIAGRAM

Top diagram

SiO$_2$

CRISTOBALITE

MULLITE

A

TRIDYMITE

2MnO.2Al$_2$O$_3$.5SiO$_2$

MnO.SiO$_2$

RHODONITE   SPESSARTITE

TEPHROITE

2MnO.SiO$_2$

3MnO.Al$_2$O$_3$.3SiO$_2$

3Al$_2$O$_3$.2SiO$_2$

MANGANOSITE   GALAXITE

CORUNDUM

MnO   10   20   B   30   40   50   MnO.Al$_2$O$_3$ 70   80   90   Al$_2$O$_3$

WEIGHT, %.

1200 1300 1400 1500 1600 1700 1800 1900 2000

Bottom diagram

CaO– Al$_2$O$_3$– SiO$_2$

SiO$_2$

2 Liquids

Cristobalite

Tridymite

Pseudo-wollastonite   Anorthite   Mullite

CaO·SiO$_2$

CaO·Al$_2$O$_3$·2SiO$_2$

3CaO·2SiO$_2$

2CaO·SiO$_2$

3CaO·SiO$_2$ 2CaO·SiO$_2$ Gehlenite   Corundum   3Al$_2$O$_3$·2SiO$_2$

2CaO·Al$_2$O$_3$·SiO$_2$

Lime   CaO·2Al$_2$O$_3$

3CaO·Al$_2$O$_3$ CaO·Al$_2$O$_3$ CaO·6Al$_2$O$_3$

CaO   20   3CaO·Al$_2$O$_3$ 5CaO·3Al$_2$O$_3$ CaO·Al$_2$O$_3$ CaO·2Al$_2$O$_3$ CaO·6Al$_2$O$_3$ Al$_2$O$_3$

1300 1400 1500 1600 1700 1800 1900 2000 2200 2400

FIG. 14

(a) ELLINGHAM DIAGRAM FOR
    SELECTED SULPHIDES

(b) ELLINGHAM DIAGRAM FOR
    SELECTED OXIDES

FIG. 15

PLOT OF RELATIVE STRENGTH $\left(\dfrac{Ki}{Km}\right)$ VS RELATIVE

DEFORMATION $\left(\dfrac{Ri}{Rm}\right)$ (After Unkle ref. 86)

a

2H₂ + S₂ = 2H₂S

2Fe + S₂ = 2FeS

2Mn + S₂ = 2MnS

⁴⁄₃Al + S₂ = ²⁄₃Al₂S₃

4Na + S₂ = 2Na₂S

2Mg + S₂ = 2MgS₂

2Ba + S₂ = 2BaS

2Sr + S₂ = 2SrS

2Ca + S₂ = 2CaS

2Ce + S₂ = 2CeS₂

$\Delta G_0 = RT \ln P S_2$ (kilojoules)

Temperature °C x10⁻²

b

2Ni + O₂ = 2NiO

2CO + O₂ = 2CO₂

C + O₂ = CO₂

4Na + O₂ = 2Na₂O

⁴⁄₃Cr + O₂ = ²⁄₃Cr₂O₃

2Mn + O₂ = 2MnO

Si + O₂ = SiO₂

Ti + O₂ = TiO₂

⁴⁄₃Al + O₂ = ²⁄₃Al₂O₃

2Mg + O₂ = 2MgO

2Ca + O₂ = 2 CaO

$\Delta G_0 = RT \ln P O_2$ (kilojoules)

Temperature °C x10⁻²

$\frac{Ki}{Km}$

Ri / Rm
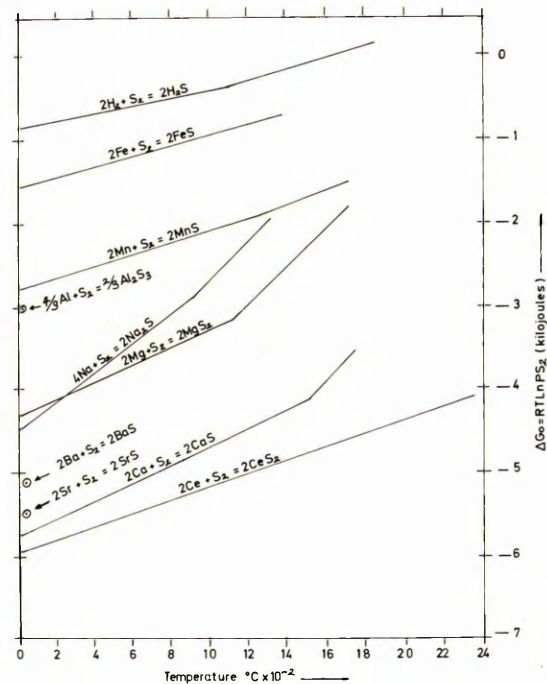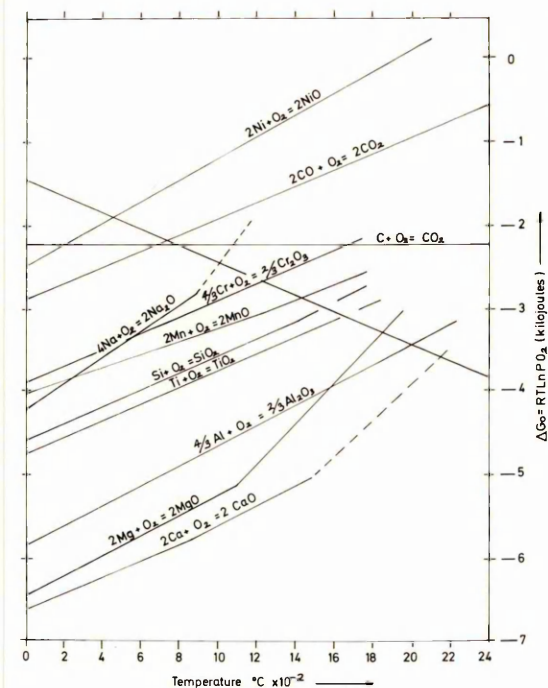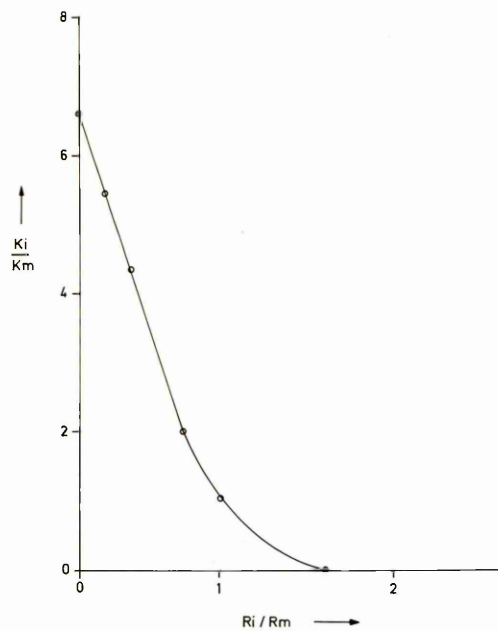
FIG. 16

PLOT OF INCLUSION TRUE
STRAIN (ε_i) VS MATRIX
TRUE STRAIN (ε_M)

(After Zeisloft & Hosford
    ref. 98)

FIG. 17

PLOT OF INCLUSION RELATIVE
PLASTICITY (ν) VS RELATIVE
STRENGTH (β)

(After Zeisloft & Hosford
    ref. 98)

FIG. 18

PLOT OF INCLUSION RELATIVE
PLASTICITY (ν) VS RELATIVE
YIELD STRENGTH (β) FOR
DIFFERENT VALUES OF THE
WORK HARDENING EXPONENT
(n)

(After Sundstrom ref. 99)

FIG. 19

COMPARISON OF THEORETICAL
AND MEASURED RELATIVE
PLASTICITY FOR MANGANESE
SULPHIDE

(After Klevebring ref. 101)

Wm/H$_2$O
Wm/Pb
Wm/Sn
Wm/Pb SPHERICAL
$\varepsilon_i = \varepsilon_m$
Pb/Sn
Pb/Wm
Wm/Pb-Sn
Wm/Pb-Sb-Sn

ε_i
1·5
1·0
0·5
0·0
0·0   ·2   ·4   ·6   ·8
ε_m

$\mathcal{V}$
3
2
1
β
1   2

$\mathcal{V} = \dfrac{2 \sinh (1-n)}{(1 + \beta k)(1-n)}$

$\mathcal{V}$
3
2
1
n=1·0
0·8
0·6
0·4
0·2
0·1
0·0
β
1   2   3   4   5   6

RELATIVE PLASTICITY ($\mathcal{V}$)
2·0
1·5
1·0
0·5
0
PEARLITE - AUSTENITE TRANSFORMATION
THEORETICAL (ref 101)
$|\mathcal{V}|$ ε =0 (ref 103)
$|\mathcal{V}|$ ε =2·1 (ref 103)
TEMPERATURE (°C)
0   200   400   600   800   1000   1200
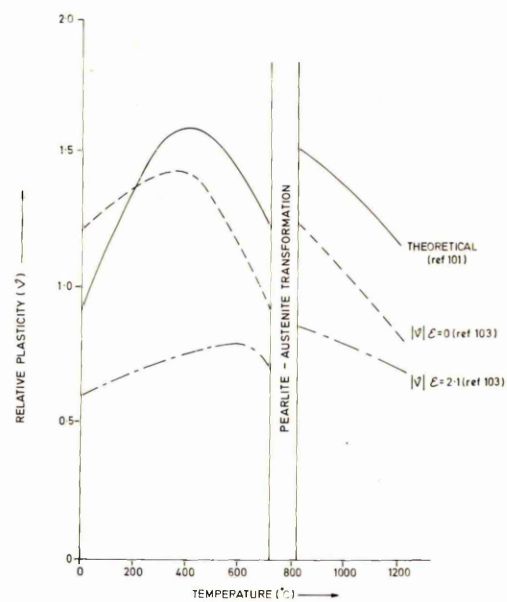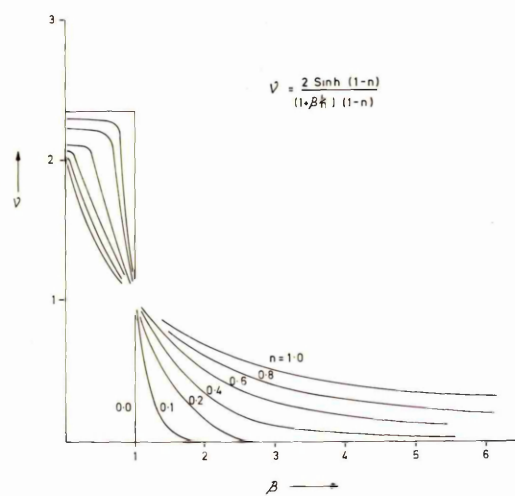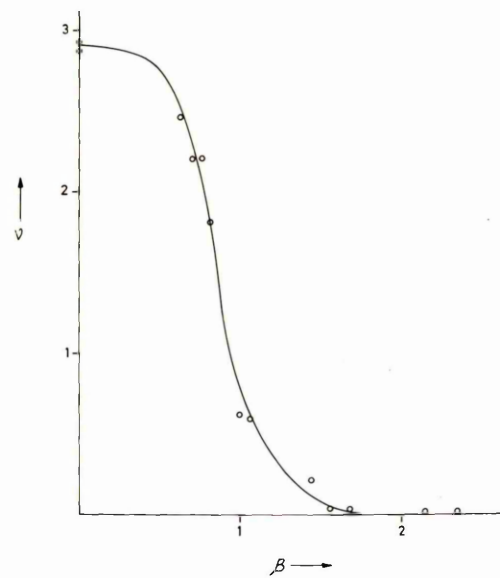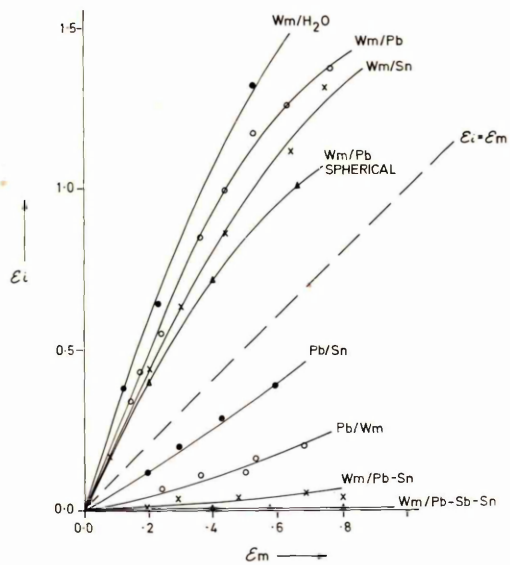
FIG. 20

PLOT OF INCLUSION DEFORMATION
(L/w) VS RELATIVE HARDNESS
$\left(\dfrac{Hm}{Hi} \right)$

(After Warrick & Van Vlack
ref. 104)

FIG. 21

PLOT OF INCLUSION RELATIVE
PLASTICITY (ν) VS RELATIVE
HARDNESS (β)

(Derived from data reported by
Warrick & Van Vlack ref. 104)

FIG. 22

PLOT OF INCLUSION RELATIVE
PLASTICITY (ν) VS RELATIVE
STRENGTH (β)

(After Gove & Charles ref. 103)

FIG. 23

PLOT OF INCLUSION RELATIVE
PLASTICITY (ν) VS RELATIVE
VISCOSITY (β)

(After Gay ref. 106)
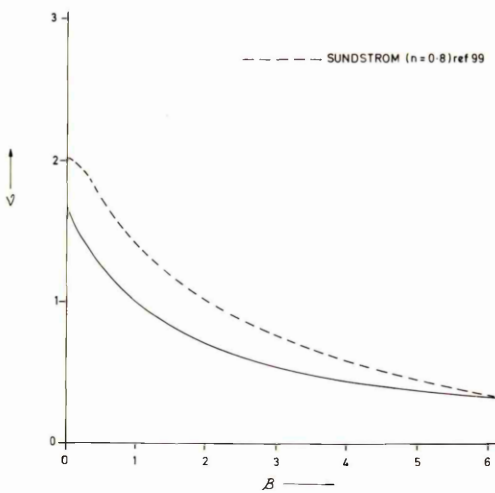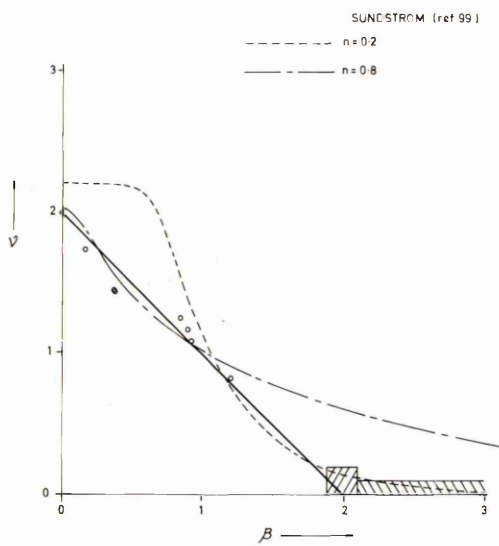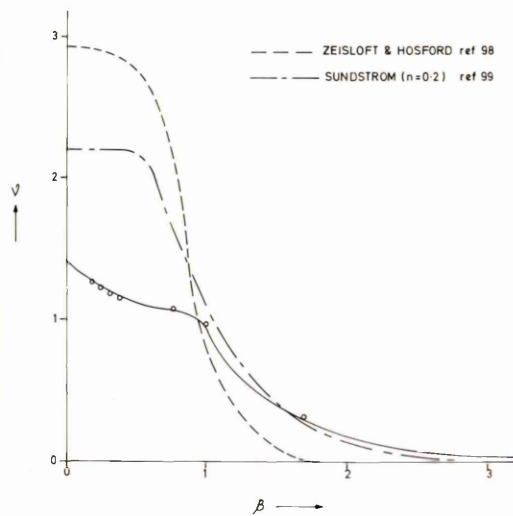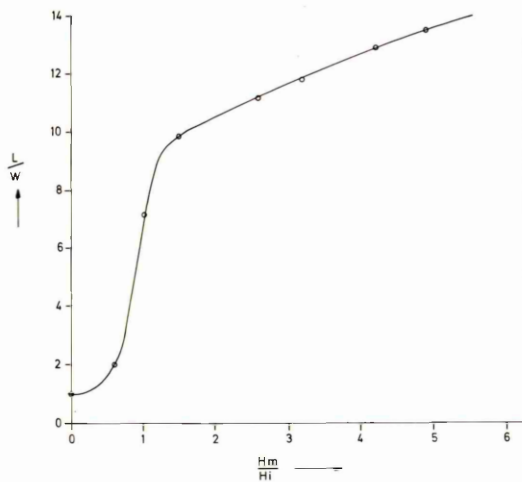
FIG. 24

PLOT OF INCLUSION RELATIVE
PLASTICITY (V) VS RELATIVE
HARDNESS (β) FOR
(a) UNBONDED AND (b) BONDED
PHASES

(After Ashok ref. 107)

FIG. 25

PLOT OF INCLUSION TRUE STRAIN
(ε_i) VS MATRIX TRUE STRAIN (ε_I

(Derived from data reported by
Unkle ref. 86)

FIG. 26

PLOT OF INCLUSION RELATIVE
PLASTICITY (V) VS RELATIVE
YIELD STRENGTH (β)

(Derived from data reported by
Unkle ref. 86)

FIG. 27

SCHEMATIC REPRESENTATION OF
INCLUSION TRUE STRAIN (ε_i) VS
MATRIX TRUE STRAIN (ε_m)^i

(After Smith ref. 108)

SUNDSTROM n = 0·8 (ref 99)

GAY (ref 106)

UNKLE (ref 86)

3

ν

2

1

(a)   (b)

0   1   2   3   4   5   6

β

ε_i

2

$\varepsilon_i = \varepsilon_m$

BRASS - Pb

1

α/β BRASS

Cu-Fe α/δ TIN BRONZE

0   1   2   3

ε_m

2·0

1·0

ν

1   2   3   4   5   6

β

ε_i

ε_m
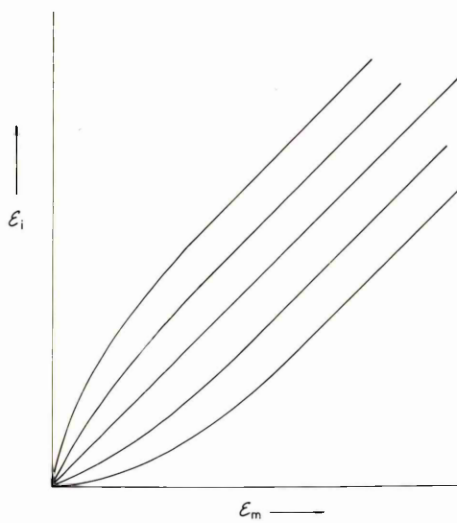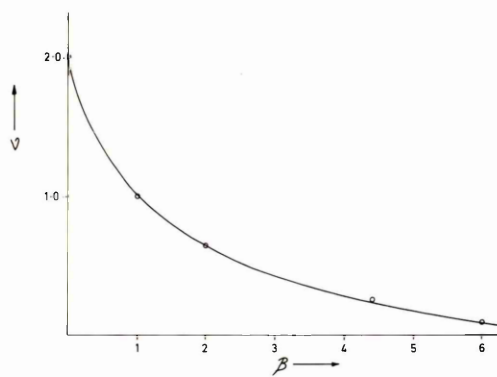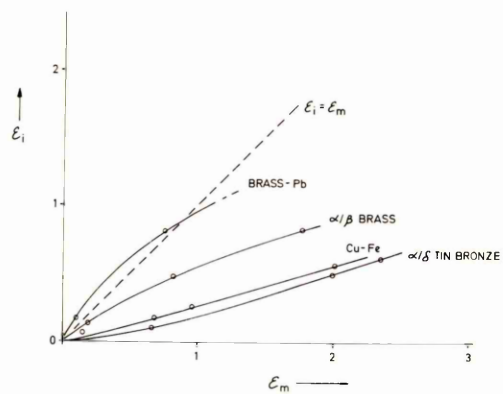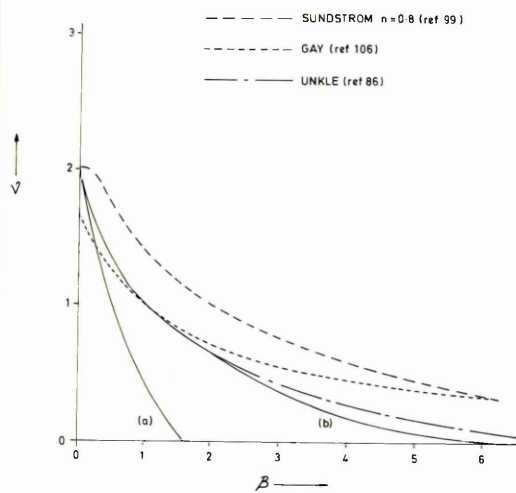
FIG. 28

PLASTICINE MODELS SHOWING THE MATRIX FLOW AROUND
ELONGATE INCLUSIONS HAVING A LOW RELATIVE PLASTICITY

(a) UNLUBRICATED STRONGLY BONDED INTERFACE

(b)   WELL LUBRICATED UNBONDED INTERFACE

FIG. 29

SCHEMATIC REPRESENTATION
OF THE FORCES OPERATING ON
AN INCLUSION OF LOW REALTIVE
PLASTICITY LEADING TO THE
FORMATION OF A CONICAL
VOID

(After Rudnik ref. 116)

FIG. 30

REPRESENTATION OF THE
CRITICAL STRESSES FOR VOID
FORMATION AS A FUNCTION OF
THE WORK OF ADHESION FOR
INCLUSION OF VARIOUS DIAMETER

(After Sundstrom ref. 112)

a

b

V_1 V_2 V_2 V_1 V_3

INCLUSION VOID

$$\sigma_c = \sigma_{c_0} \sqrt{\frac{W d_0}{W_0 d}}$$

$$\sigma_c = 606 \sqrt{\frac{W d_0}{W_0 d}} \quad MPa$$

$d_0 = 1\,\mu m$

$W_0 = 1\,J/m^2$

CRITICAL STRESS (M.Pa)

1500

1000

500

$d\,(\mu m)$

0·5

1·0

2·0

0·5   1·0   1·5   2·0   2·5

WORK OF ADHESION (J/m^2)
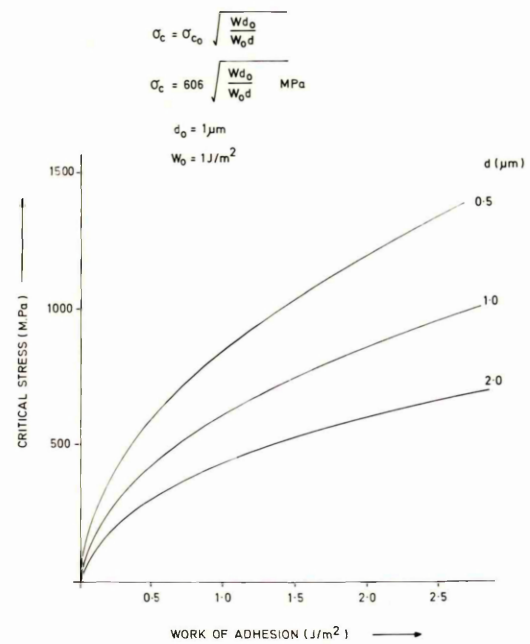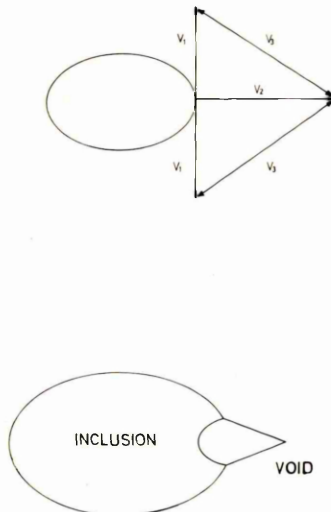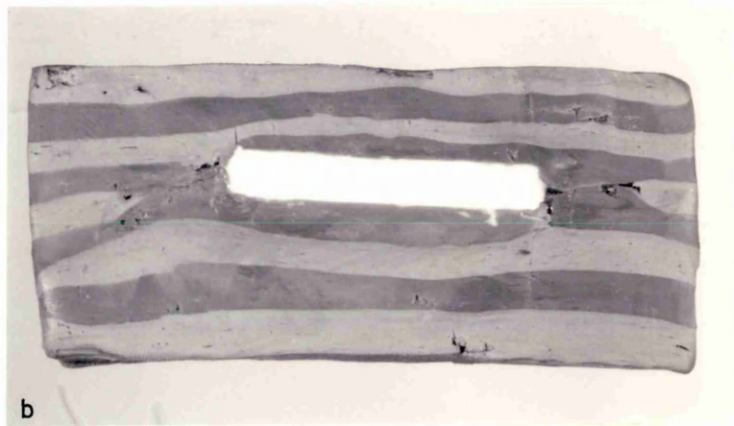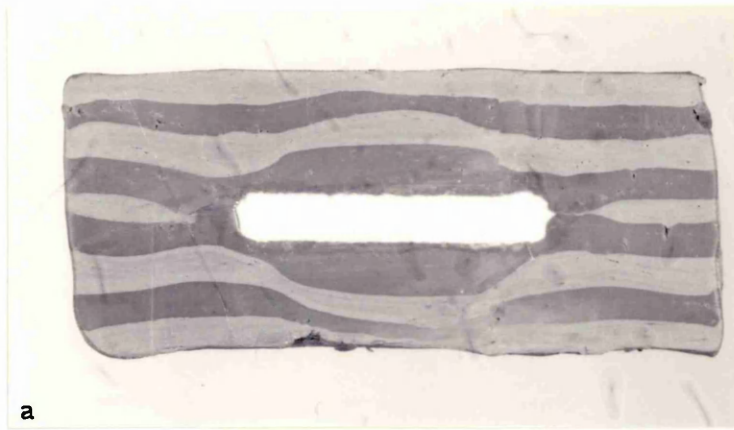
FIG. 31

DENSITY CHANGE OF A 0.2%C
STEEL WITH ROLLING
REDUCTION

(After Gove & Charles
ref. 103)

FIG. 32

PLOT OF HARDNESS VS
TEMPERATURE FOR MANGANESE
SULPHIDE

(After Chao et al ref. 133)

FIG. 33

PLOT OF HARDNESS VS
TEMPERATURE FOR VARIOUS
STEELS AND FOR SINGLE
CRYSTAL MANGANESE SULPHIDE

(After Chao ref. 133)

FIG. 34

PLOT OF RELATIVE PLASTICITY
(V) VS WORKING TEMPERATURE
FOR MANGANESE SULPHIDE
INCLUSIONS

(Various Sources)

FIG. 35
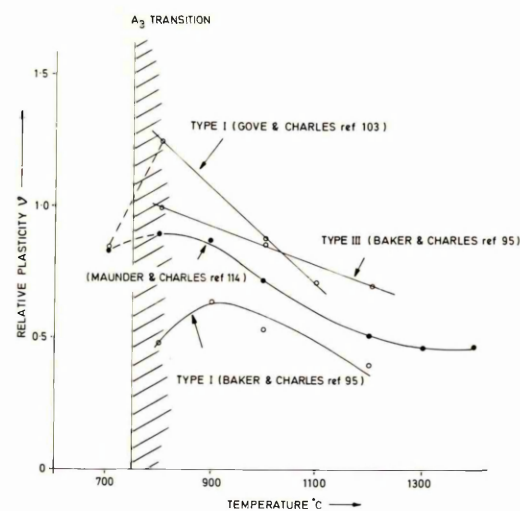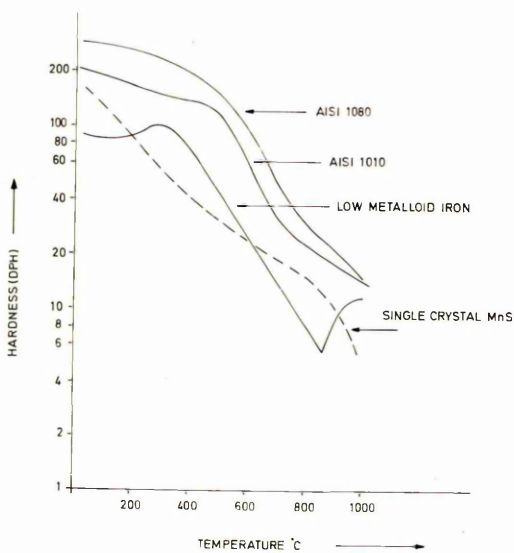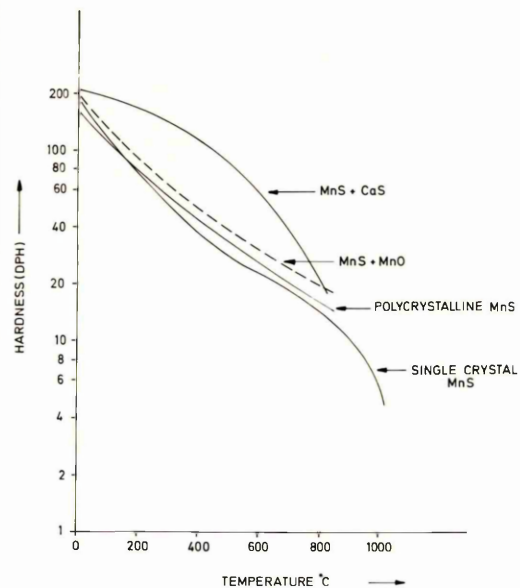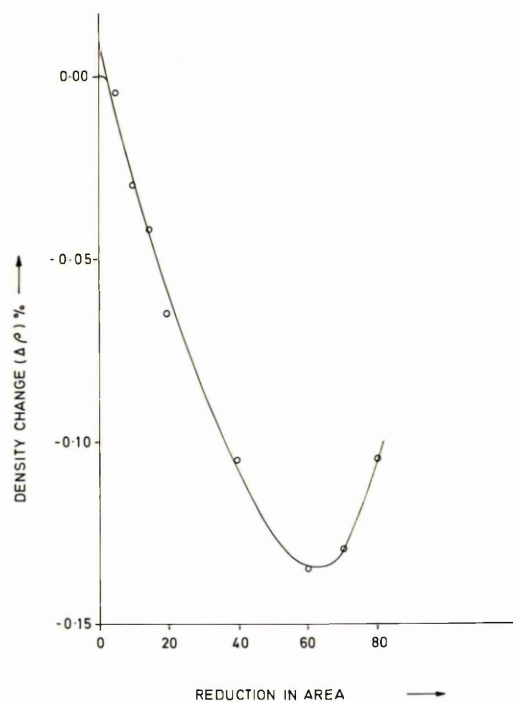
(a) SOLID SOLUBILITY LIMITS FOR THE FIRST PERIOD
    TRANSITION ELEMENTS IN MANGANESE SULPHIDE (AT %)

    (After Kiessling ref. 11)

(b) MICROHARDNESS VALUES FOR THE DIFFERENT (Mn. Me)S
    SOLID SOLUTIONS. ROOM TEMPERATURE VALUES ON
    QUENCHED SPECIMENS.

    (Kiessling ref. 11)

FIG. 36

SCHEMATIC REPRESENTATION OF THE EFFECT OF COMPOSITION
ON RELATIVE PLASTICITY OF SILICEOUS INCLUSIONS

(After Kiessling   ref. 113)
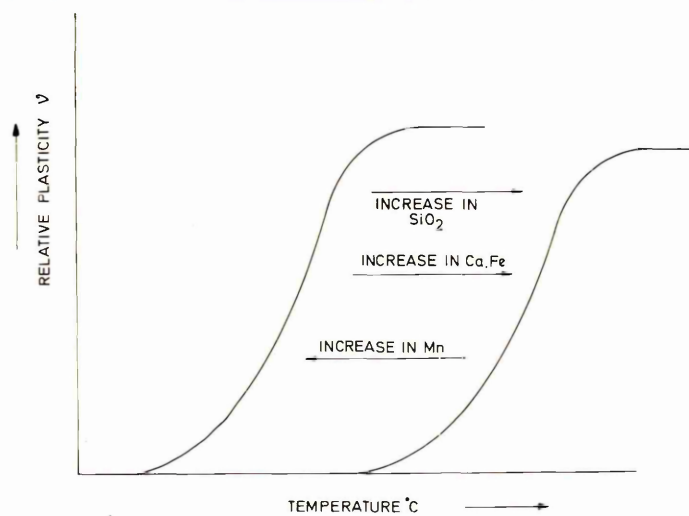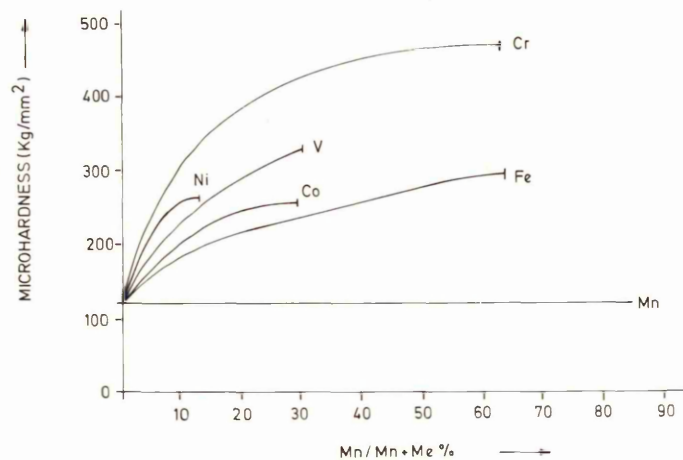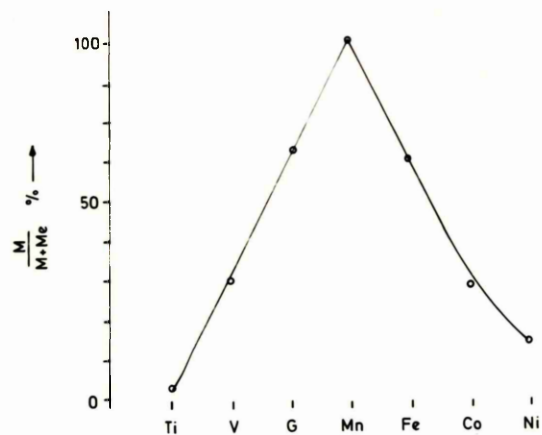
FIG. 37

VICKERS HARDNESS VALUES AT ELEVATED TEMPERATURES FOR
A SYNTHETIC SLAG COMPOSITION
49% MnO, 41% SiO$_2$, 10% Al$_2$O$_3$

(After Shiraiwa ref. 81)

FIG. 38

RELATIVE PLASTICITY VS ROLLING TEMPERATURE FOR WUSTITE
INCLUSIONS

(Values derived from data presented by Pickering ref. 92)

FIG. 39

PLOT OF INCLUSION DEFORMATION VS MANGANESE CONTENT
FOR MANGANOWUSTITE INCLUSIONS

(After Uchiyama & Sumita ref. 112)
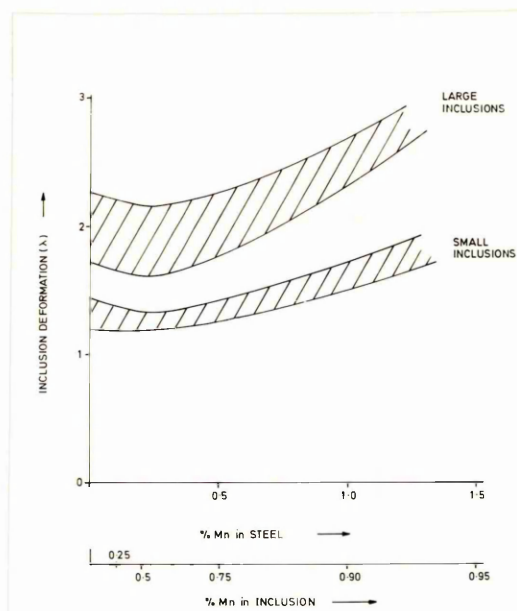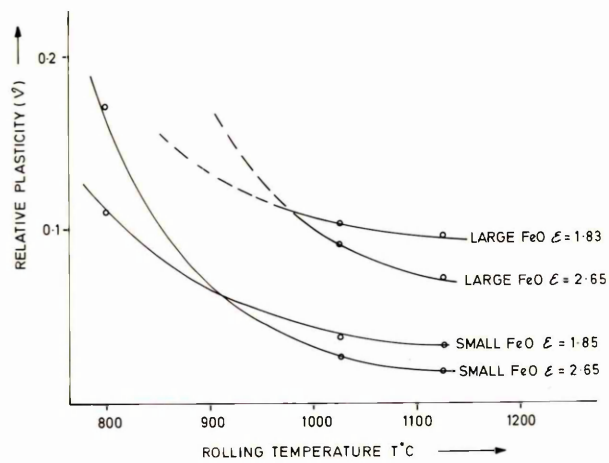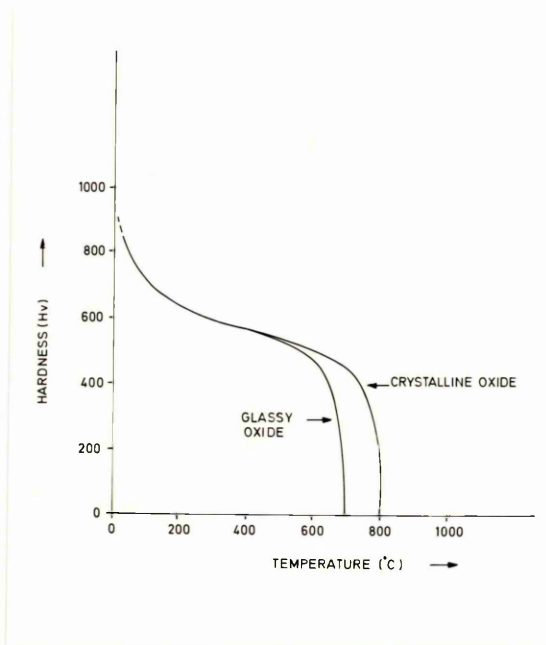
FIG. 40

INGOT SECTIONS

FIG. 41

BINARY CORRECTION DATA FOR
MICROPROBE ANALYSIS
(Al_2O_3-SiO_2 SYSTEM)

FIG. 42

KLINGER-KOCH ELECTROLYTIC
EXTRACTION CELL. USED TO
EXTRACT INCLUSION FRAGMENTS
FROM HOT ROLLED SPECIMENS

FIG. 43

TYPICAL PLOT OF INCLUSION
TRUE STRAIN VS MATRIX TRUE
STRAIN FOR PLASTIC INCLUSIONS
(SCHEMATIC ONLY)

INGOT SECTIONS
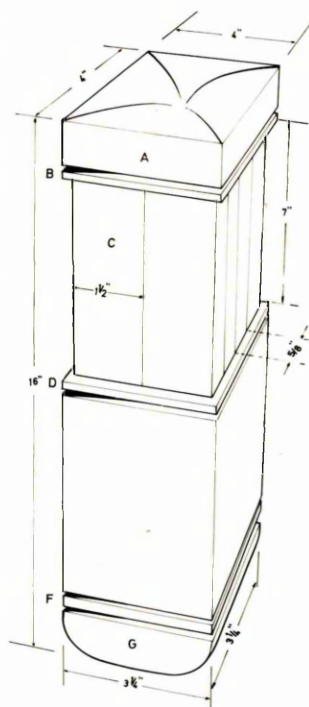
SAMPLE

A + G   FOR CHEMICAL ANALYSIS

B,D+F   FOR OPTICAL EXAMINATION

C   SAMPLES FOR HOT ROLLING

Al_2O_3— SiO_2 BINARY CORRECTION CHART

KLINGER-KOCH ELECTROLYTIC EXTRACTION CELL

GAS OUTLET   COVER PLATE   GAS INLET

ANODE CHAMBER

CATHODE DIAPHRAGM

SPECIMEN

COLLECTING FUNNEL

COLLECTING VESSEL

OUTLET
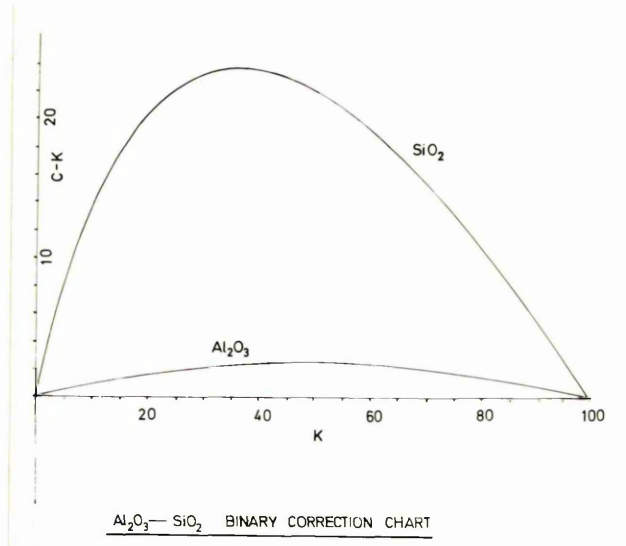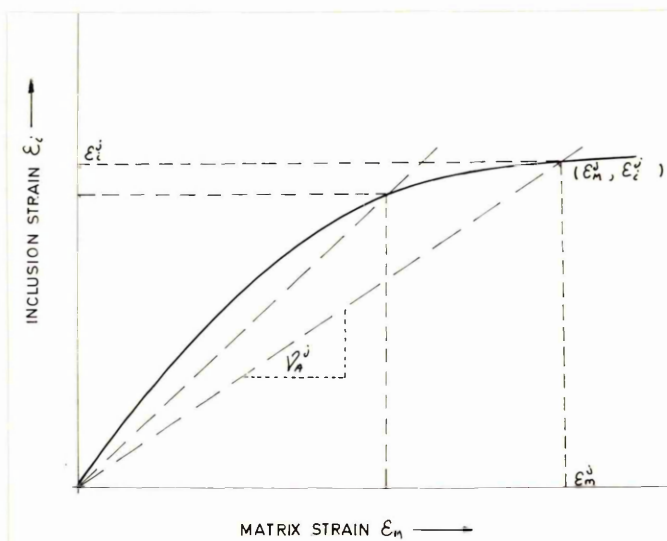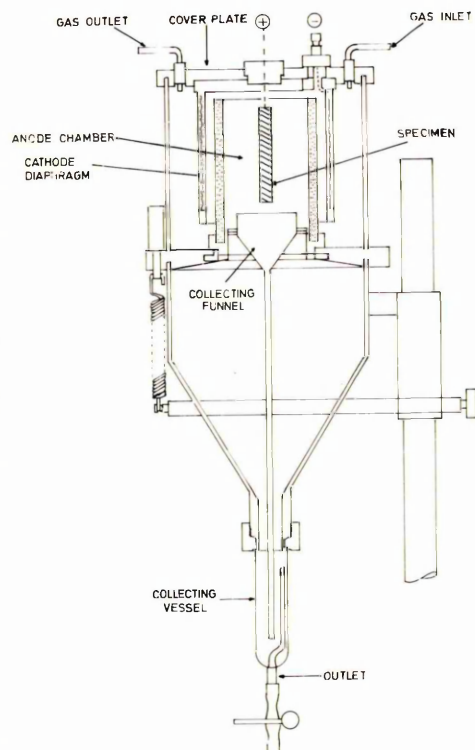
FIG. 44

COMPOSITION RANGES FOR BINARY $FeO-SiO_2$ TYPE INCLUSIONS
PRESENT IN CASTS 4, 4B, 5 AND 12.

FIG. 45

COMPOSITION RANGES FOR BINARY AND TERNARY $FeO-MnO-SiO_2$
TYPE INCLUSIONS PRESENT IN CASTS 4, 4B, 5, 6, 6B AND 12.
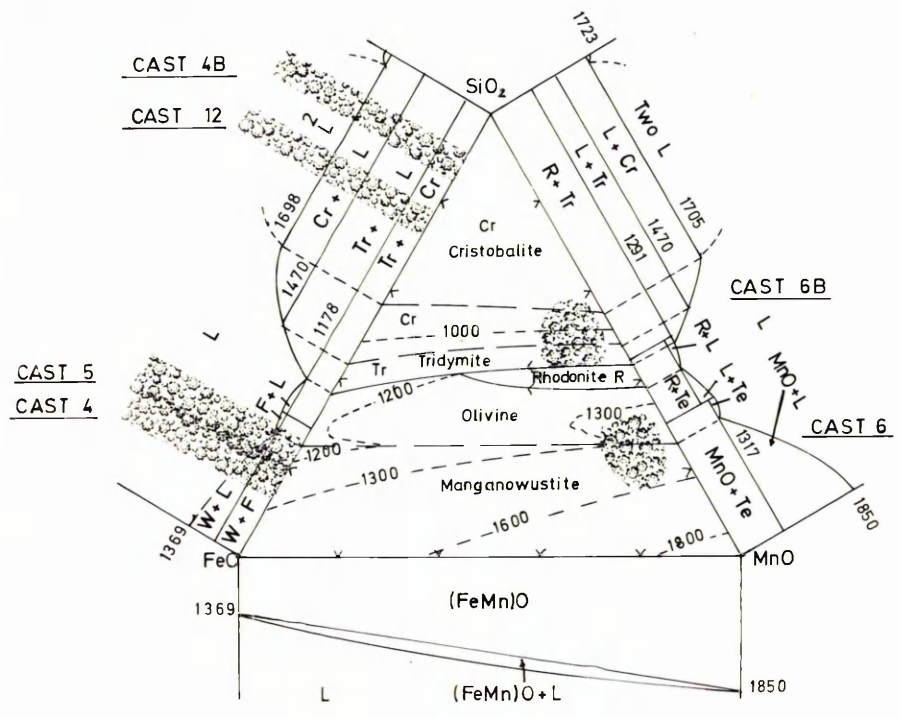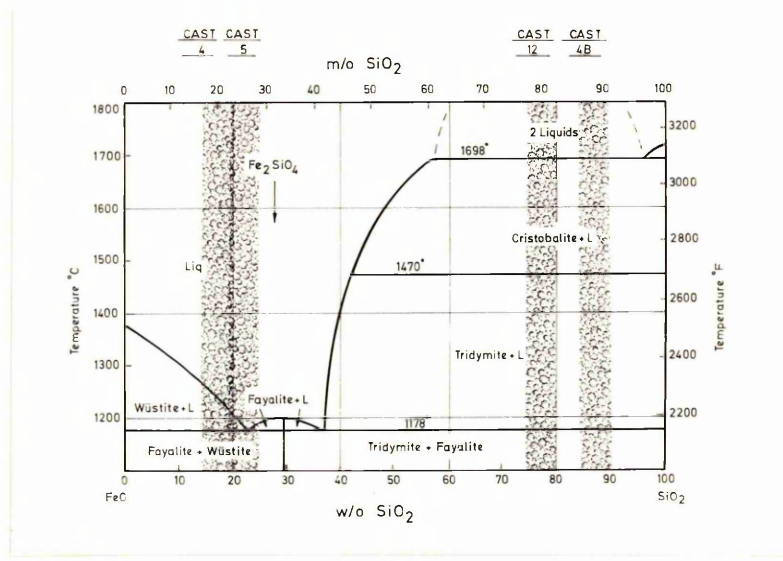
FIG. 46

COMPOSITION RANGE OF TERNARY FeO-Al$_2$O$_3$-SiO$_2$ TYPE INCLUSIONS PRESENT IN CAST 8.

FIG. 47

COMPOSITION RANGE OF TERNARY CaO-Al$_2$O$_3$-SiO$_2$ TYPE INCLUSIONS PRESENT IN CAST 11.
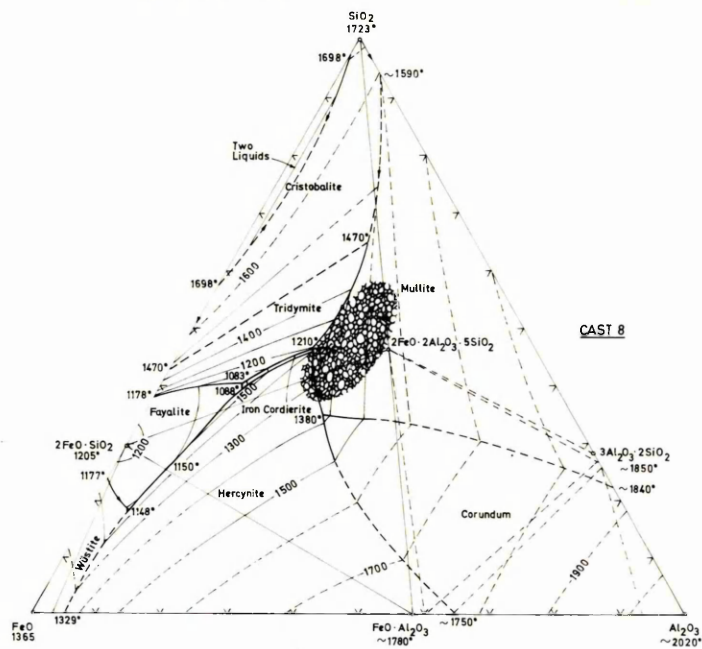
SYSTEM "FeO"- Al₂O₃ - SiO₂
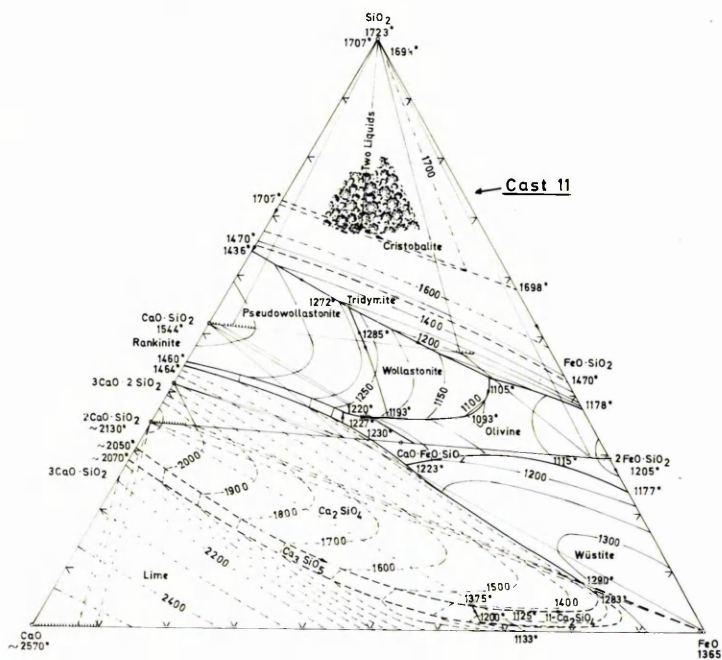
SYSTEM CaO -"FeO"- SiO₂

FIG. 48

INCLUSION TRUE STRAIN (ε_i)
VS MATRIX TRUE STRAIN (ε_M^i)
FOR CAST 4 DEFORMED AT
1150°C

FIG. 49

INCLUSION TRUE STRAIN (ε_i)
VS MATRIX TRUE STRAIN (ε_M^i)
FOR CAST 4 DEFORMED AT
1275°C

FIG. 50

INCLUSION TRUE RELATIVE
PLASTICITY (ν_T) VS MATRIX
TRUE STRAIN (ε_M^T) VS ROLLING
TEMPERATURE (T°C) FOR
CAST 4

FIG. 51

INCLUSION APPARENT RELATIVE
PLASTICITY (ν_A) VS MATRIX
TRUE STRAIN VS ROLLING
TEMPERATURE (T°C) FOR CAST
4

FIG. 52

INCLUSION TRUE STRAIN (ε_i)
VS MATRIX TRUE STRAIN (ε_M^i)
FOR CAST 5 DEFORMED AT
1150°C

FIG. 53

INCLUSION TRUE STRAIN (ε_i)
VS MATRIX TRUE STRAIN (ε_M^i)
FOR CAST 5 DEFORMED AT
1275°C

CAST 4   1150°C

CAST 4   1275°C

PLOT OF TRUE RELATIVE PLASTICITY U_T VS MATRIX TRUE STRAIN $\mathcal{E}_M$ FOR CAST 4.

PLOT OF APPARENT RELATIVE PLASTICITY U_A VS MATRIX TRUE STRAIN $\mathcal{E}_M$ FOR CAST 4.

CAST 5   1150°C

CAST 5   1275°C
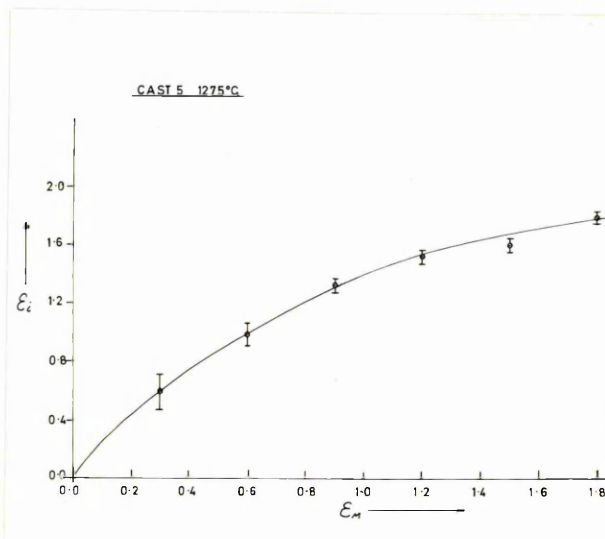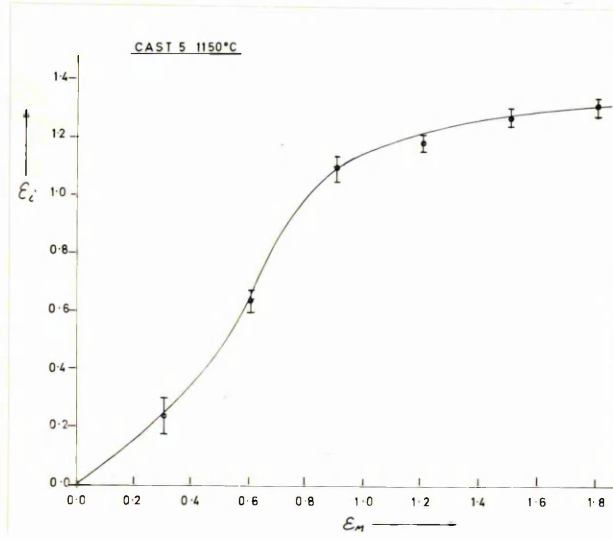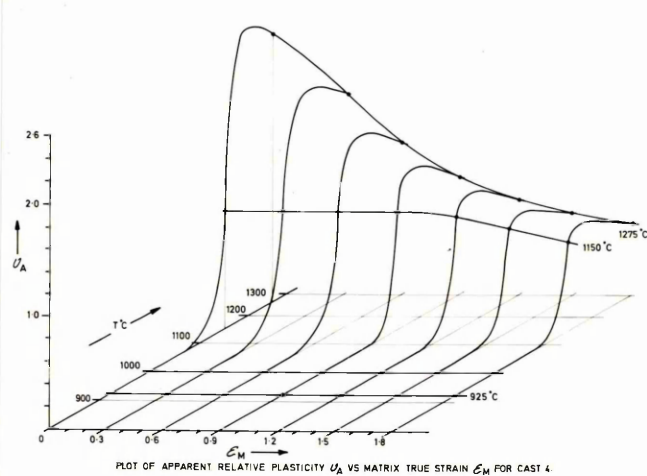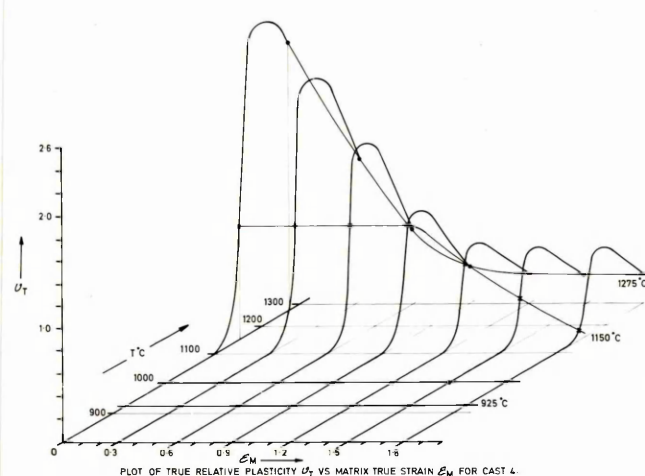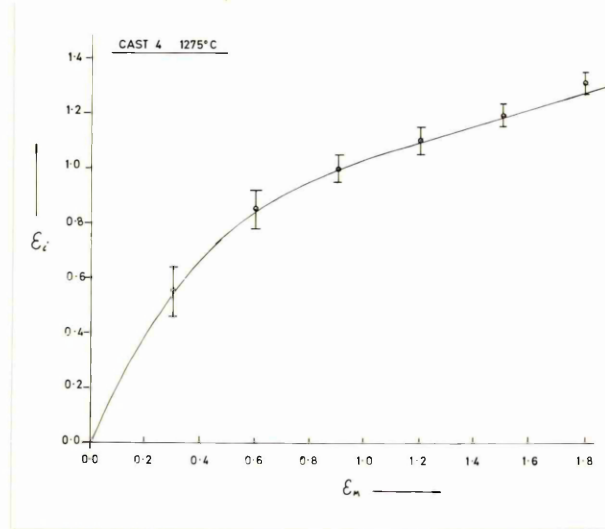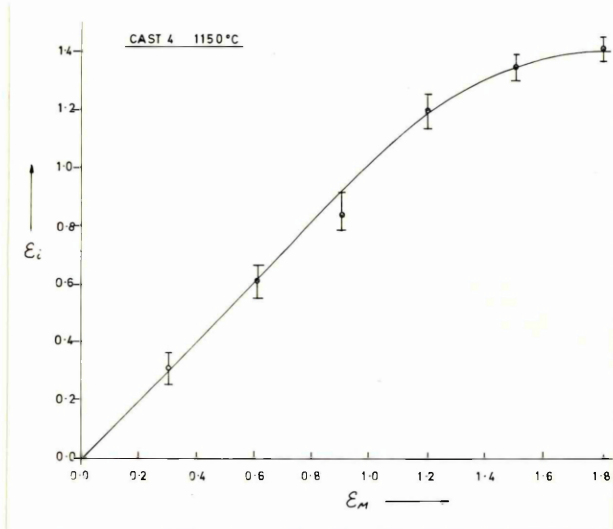
INCLUSION TRUE RELATIVE PLASTICITY (ν_T) VS MATRIX TRUE STRAIN (ε^T_M) VS ROLLING TEMPERATURE (T^{o}C) FOR CAST 5

INCLUSION APPARENT RELATIVE PLASTICITY (ν_A) VS MATRIX TRUE STRAIN (ε^A_M) VS ROLLING TEMPERATURE (T^{o}C) FOR CAST 5

FIG. 56

FIG. 57

INCLUSION TRUE STRAIN (ε_i) VS MATRIX TRUE STRAIN (ε^i_M) FOR CAST 6B DEFORMED AT 1275°C

INCLUSION TRUE STRAIN (ε_i) VS MATRIX TRUE STRAIN (ε^i_M) FOR CAST 6B DEFORMED AT 1350°C

FIG. 58

FIG. 59

INCLUSION TRUE RELATIVE PLASTICITY (ν_T) VS MATRIX TRUE STRAIN (ε^T_i) VS ROLLING TEMPERATURE (T^{o}C) FOR CAST 6B

INCLUSION APPARENT RELATIVE PLASTICITY (ν_A) VS MATRIX TRUE STRAIN (ε^A_M) VS ROLLING TEMPERATURE (T^{o}C) FOR CAST 6B

PLOT OF TRUE RELATIVE PLASTICITY υ_T VS MATRIX TRUE STRAIN ε_M FOR CAST 5.

PLOT OF APPARENT RELATIVE PLASTICITY υ_A VS MATRIX TRUE STRAIN ε_M FOR CAST 5.

CAST 6B 1275°C

CAST 6B 1350°C

PLOT OF TRUE RELATIVE PLASTICITY υ_T VS MATRIX TRUE STRAIN ε_M FOR CAST 6B.

PLOT OF APPARENT RELATIVE PLASTICITY υ_A VS MATRIX TRUE STRAIN ε_M FOR CAST 6B.
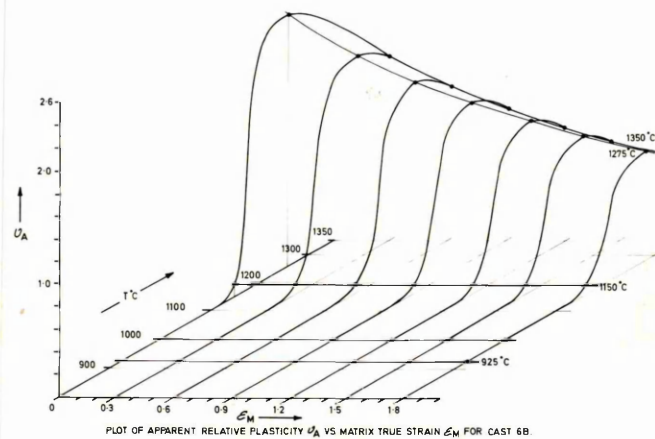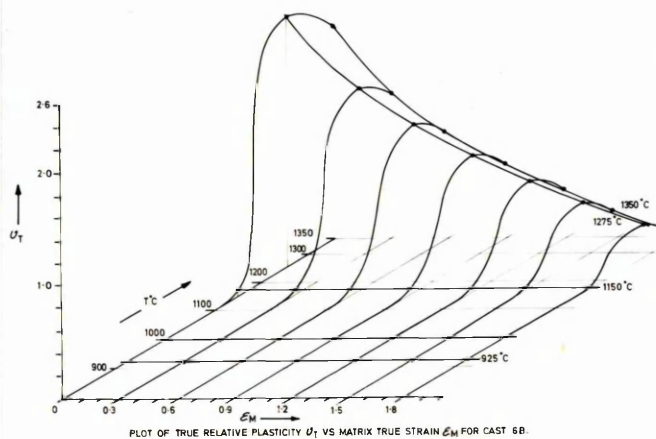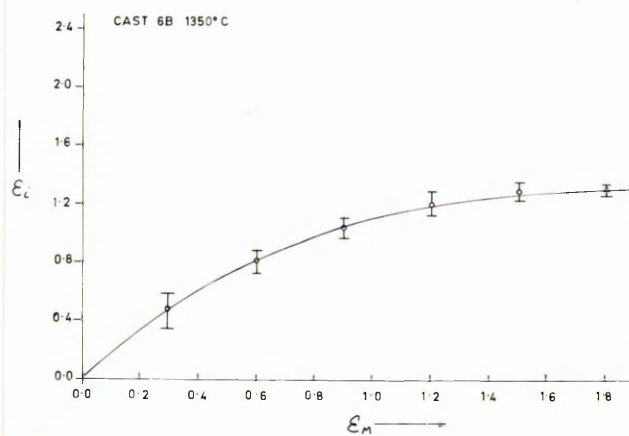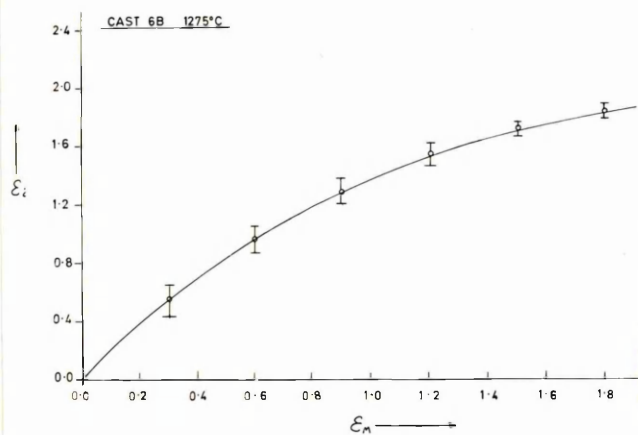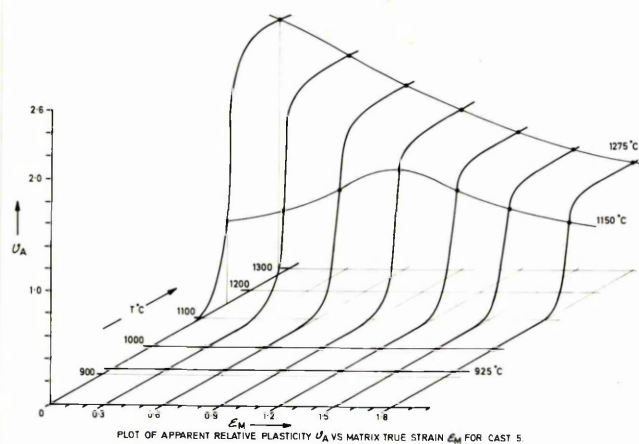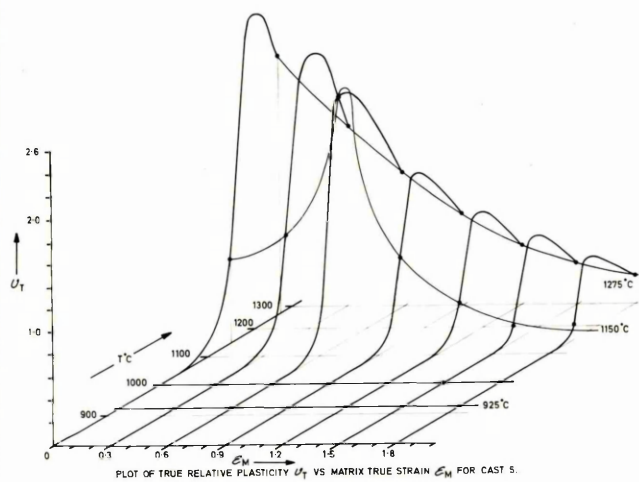
FIG. 60

INCLUSION TRUE STRAIN (ε_i)
VS MATRIX TRUE STRAIN (ε_M^i)
FOR CAST 8 DEFORMED AT
1150°C

FIG. 61

INCLUSION TRUE STRAIN (ε_i)
VS MATRIX TRUE STRAIN (ε_M^i)
FOR CAST 8 DEFORMED AT
1275°C

FIG. 62

INCLUSION TRUE STRAIN (ε_i) VS MATRIX TRUE STRAIN (ε_M)
FOR CAST 8 DEFORMED AT 1350°C

FIG. 63

INCLUSION TRUE RELATIVE PLASTICITY (V_T^2) VS MATRIX TRUE
STRAIN (ε_M) VS ROLLING TEMPERATURE (T$^{\circ}$C) FOR CAST 8

CAST 8 1150°C

CAST 8 1275°C

CAST 8 1350°C

PLOT OF TRUE RELATIVE PLASTICITY U_T VS MATRIX TRUE STRAIN $\mathcal{E}_M$ FOR CAST 8.
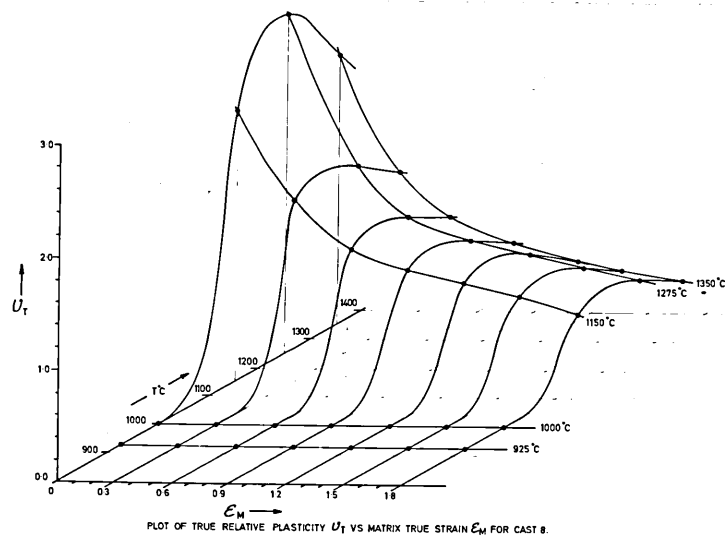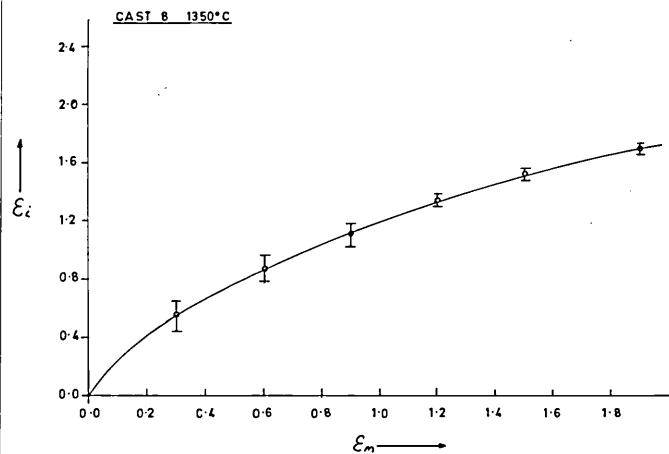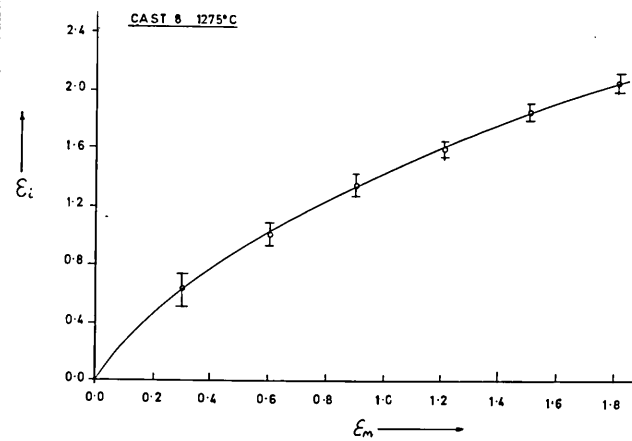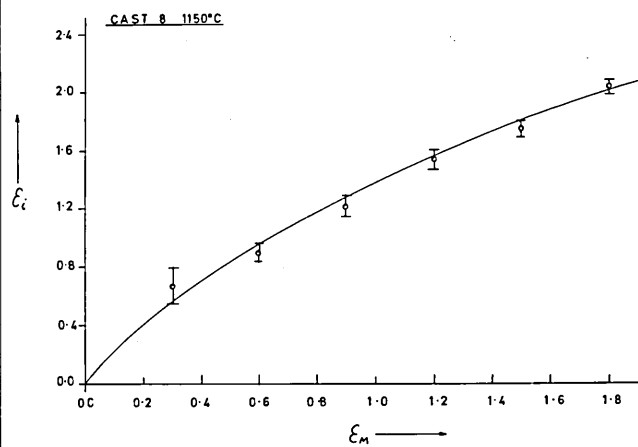
FIG. 64

INCLUSION APPARENT RELATIVE PLASTICITY (ν_A) VS MATRIX
TRUE STRAIN (ε_M) VS ROLLING TEMPERATURE (T°C) FOR
CAST 8

FIG. 65

INCLUSION TRUE STRAIN (ε_i) VS MATRIX TRUE STRAIN (ε_M)
FOR INCLUSION IN SAMPLES OF CAST 8 DEFORMED AT
RATES OF 0.3 AND 0.6 TRUE STRAIN PER PASS, AT 1150°C.

FIG. 66

INCLUSION TRUE RELATIVE PLASTICITY (ν_T) VS MATRIX TRUE
STRAIN (ε_M) FOR INCLUSIONS IN SAMPLES OF CAST 8 DEFORMED
AT RATES OF 0.3 AND 0.6 TRUE STRAIN PER PASS AT 1150°C.
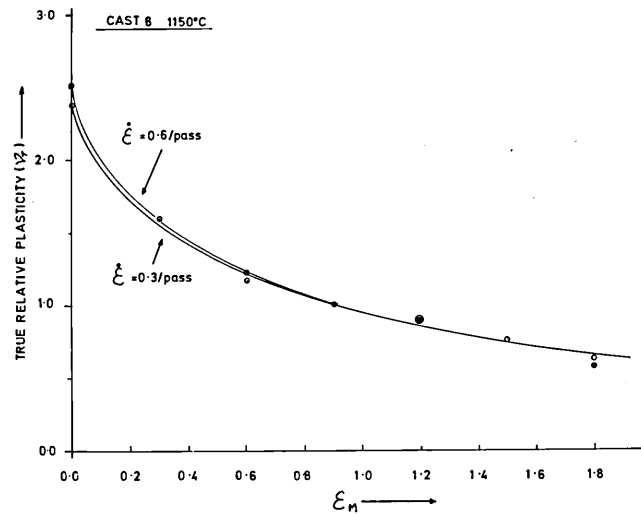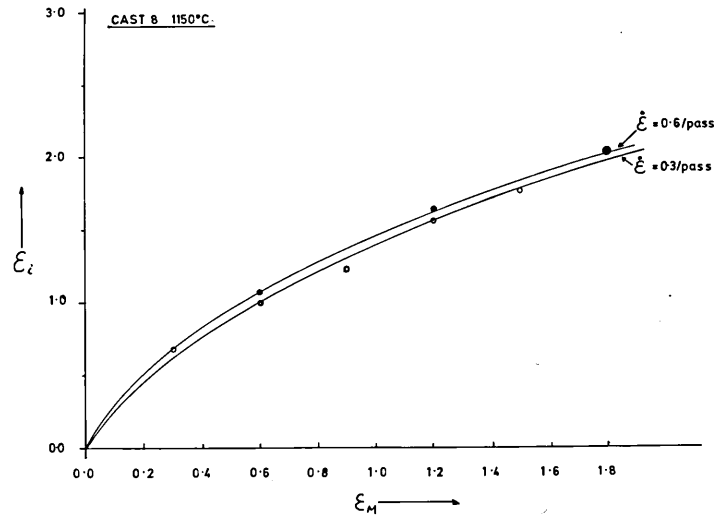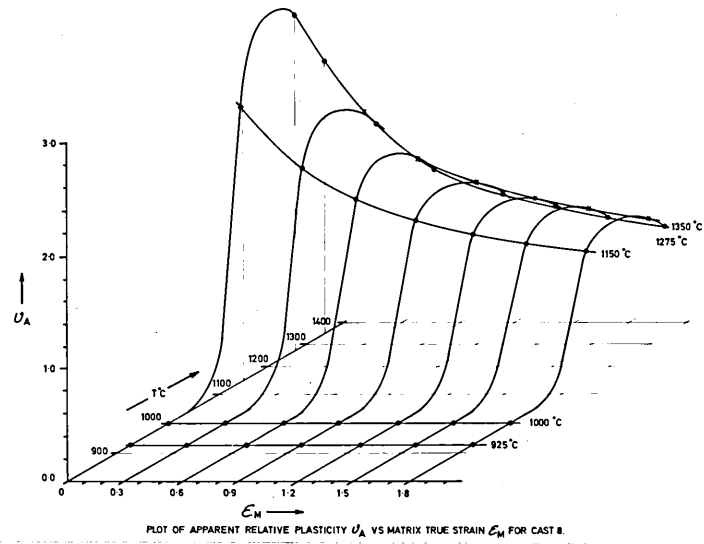
PLOT OF APPARENT RELATIVE PLASTICITY U_A VS MATRIX TRUE STRAIN $\mathcal{E}_M$ FOR CAST 8.

CAST 8 1150°C.

$\dot{\mathcal{E}} = 0.6$/pass

$\dot{\mathcal{E}} = 0.3$/pass

CAST 8 1150°C

$\dot{\mathcal{E}} = 0.6$/pass

$\dot{\mathcal{E}} = 0.3$/pass

FIG. 67   FIG. 68

INCLUSION TRUE STRAIN ($\mathcal{E}_i$)   INCLUSION TRUE STRAIN ($\mathcal{E}_i$)
VS MATRIX TRUE STRAIN ($\mathcal{E}^i_M$)   VS MATRIX TRUE STRAIN ($\mathcal{E}^i_M$)
FOR CAST 11 DEFORMED AT   FOR CAST 11 DEFORMED AT
1000°C 1150°C

FIG. 69

INCLUSION TRUE STRAIN ($\mathcal{E}_i$) VS MATRIX TRUE STRAIN ($\mathcal{E}_M$)
FOR CAST 11 DEFORMED AT 1275°C.

FIG. 70   FIG. 71

INCLUSION TRUE RELATIVE   INCLUSION APPARENT RELATIVE
PLASTICITY (ν_T) VS MATRIX   PLASTICITY (ν_A) VS MATRIX
TRUE STRAIN ($\mathcal{E}^T_M$) VS ROLLING   TRUE STRAIN ($\mathcal{E}_M$) VS ROLLING
TEMPERATURE (T$^{\circ}$C) FOR   TEMPERATURE (T$^{\circ}$C) FOR
CAST 11   CAST 11

CAST 11   1000°C

CAST 11   1150°C

CAST 11   1275°C

PLOT OF TRUE RELATIVE PLASTICITY υ_T VS MATRIX TRUE STRAIN ε_M FOR CAST 11.

PLOT OF APPARENT RELATIVE PLASTICITY υ_A VS MATRIX TRUE STRAIN ε_M FOR CAST 11.
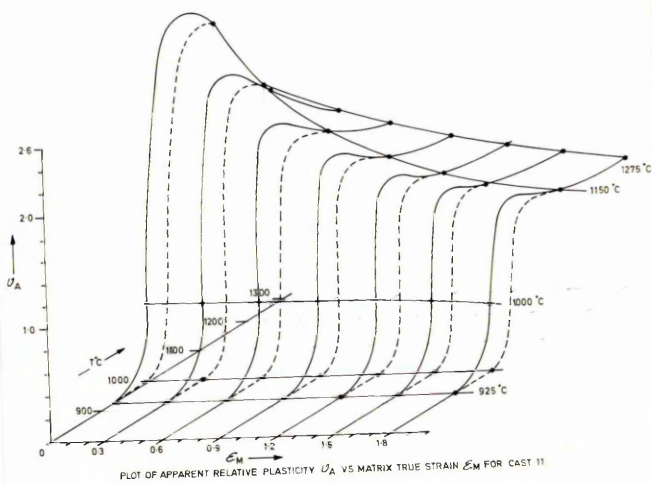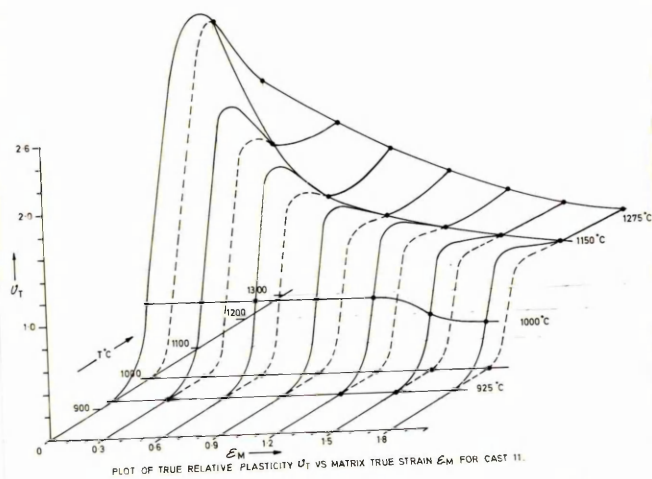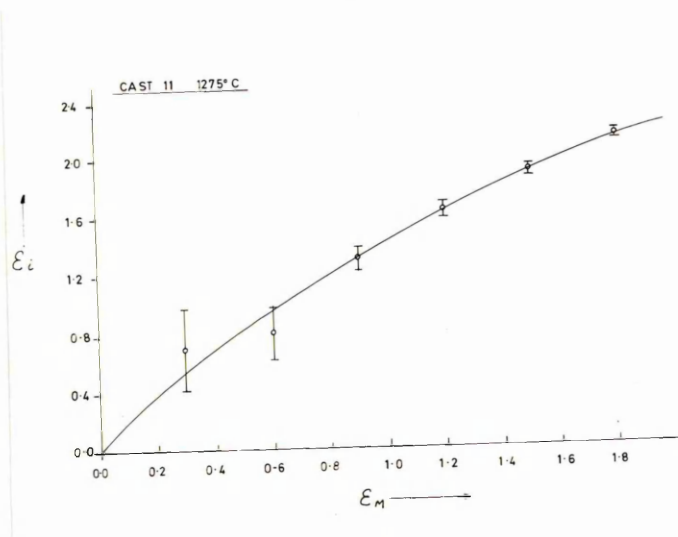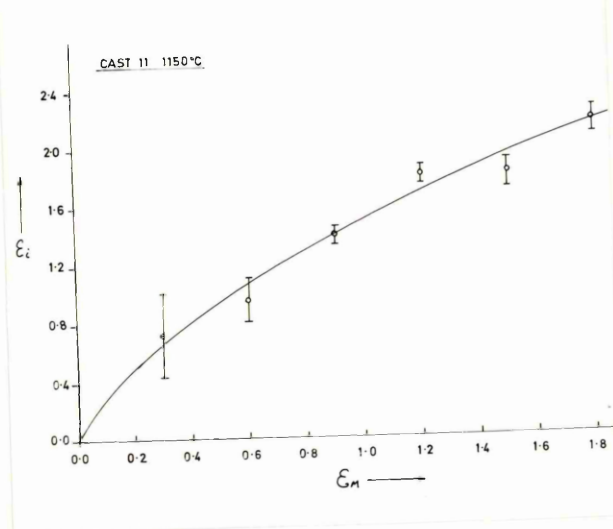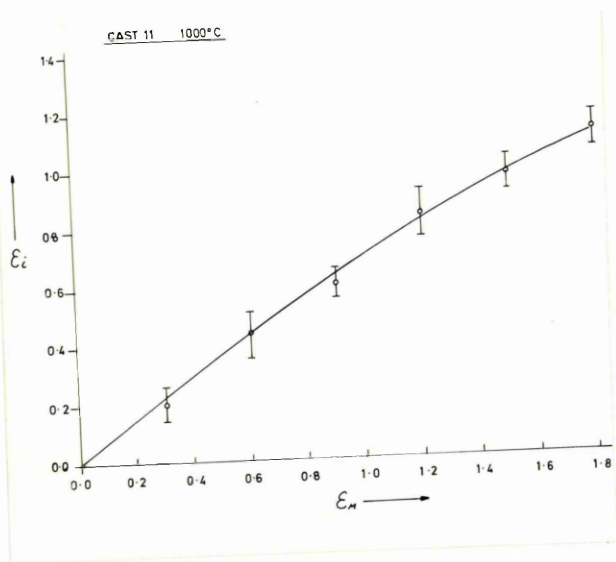
FIG. 72

SCHEMATIC REPRESENTATION OF THE VARIATION IN VISCOSITY
OF A TYPICAL SILICATE GLASS WITH TEMPERATURE

FIG. 73

COMPARISON OF THE BEHAVIOUR OF TYPICAL FLUID SILICATE
INCLUSIONS WITH THAT OF TYPE I MANGANESE SULPHIDE
INCLUSIONS, DURING HOT WORKING OF THE STEEL MATRIX.

$$\mathcal{E}_M = \text{MATRIX TRUE STRAIN}$$
$$\mathcal{E}_i = \text{INCLUSION TRUE STRAIN}$$

FIG. 74

VARIATION IN THE TRUE RELATIVE PLASTICITY EXHIBITED BY
SULPHIDE AND SILICATE INCLUSIONS AS A FUNCTION OF MATRIX
STRAIN.
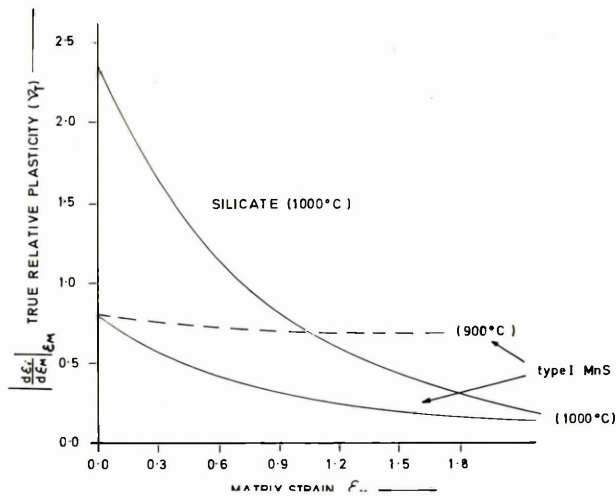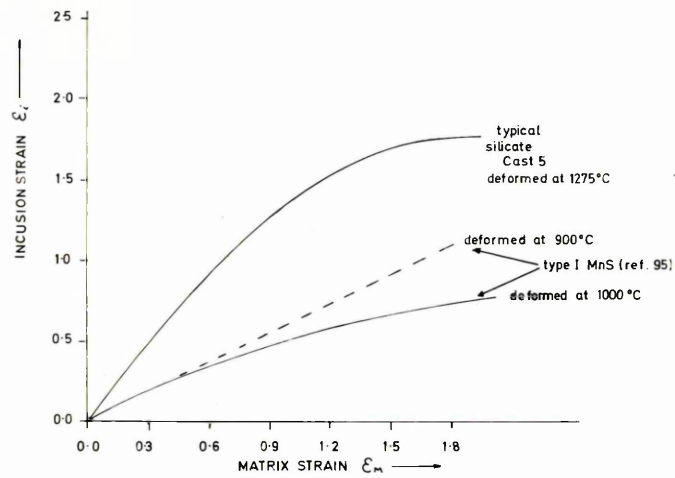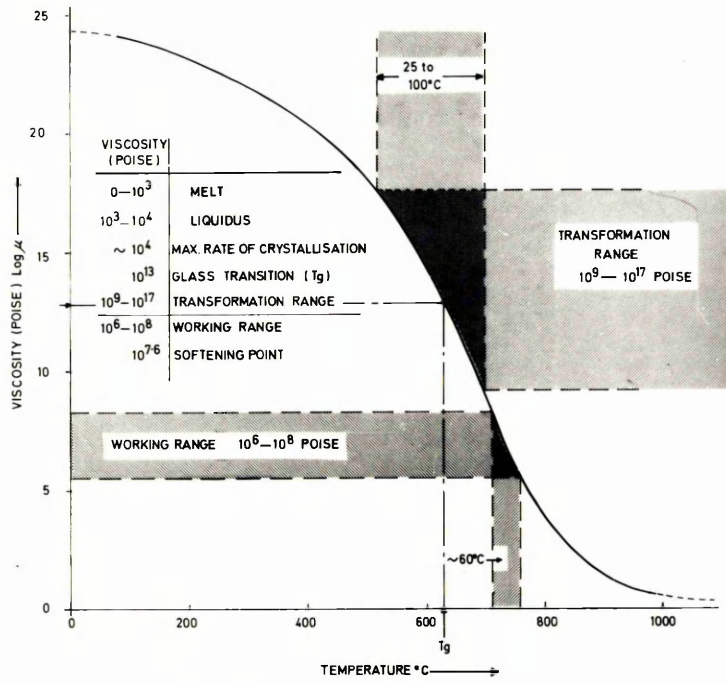
FIG. 75

DEFORMATION OF A CIRCULAR ELEMENT BY SIMPLE SHEAR

FIG. 76

MODEL SYSTEM USED FOR INVESTIGATING THE BEHAVIOUR OF
FLUID INCLUSIONS IN A VELOCITY GRADIENT

FIG. 77

GRAPH SHOWING THE RATE OF ENERGY ABSORPTION, PER
UNIT VOLUME, FOR INCLUSIONS OF VARIOUS INITIAL DIAMETERS
DEFORMING BY PLANE STRAIN AT A STRAIN RATE OF 40SEC^{-1},
ACCORDING TO THE EQUATION

$$\frac{\dot{E}}{V} = \frac{4 \gamma \dot{\mathcal{E}}_i}{a} \; \text{Sinh} \, \mathcal{E}_i$$

$\dfrac{\dot{E}}{V}$ IS PLOTTED AS MJ.m^{-2}.s^{-1}

SHEAR

SHEAR

DATUM

SODIUM SILICATE SOLUTION

INNER ROTATING CYLINDER

OUTER STATIC CYLINDER

INCLUSION

PLOT OF THE RATE OF ENERGY ABSORBTION PER UNIT VOLUME FOR
INCLUSIONS OF VARIOUS INITIAL SIZES DEFORMING BY PLANE STRAIN
AT A STRAIN RATE OF 40 sec^{-1}

$$\frac{E}{V} = \frac{4 \, \gamma \, \varepsilon_i}{a} \, \sinh \varepsilon_i$$
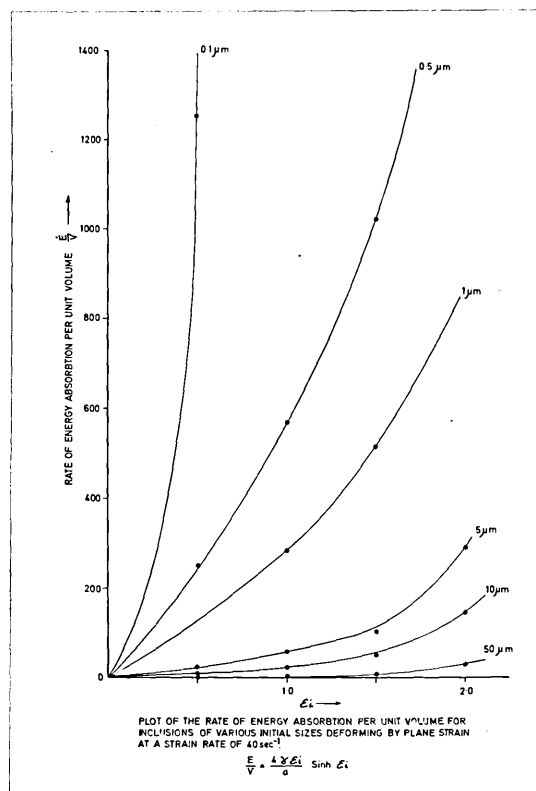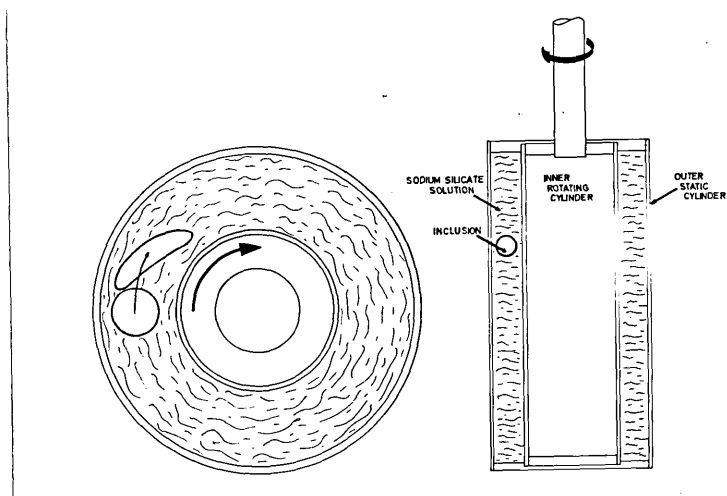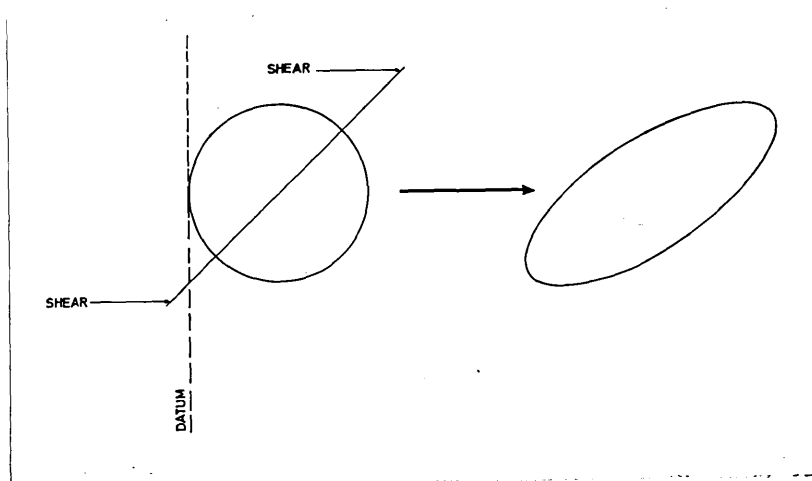
FIG. 78

(a) THE CONFIGURATION OF THE REACTION INTERFACE
PRODUCED WHEN ALUMINIUM DEOXIDANT IS FLOATED ON
THE SURFACE OF MOLTEN IRON IN A HIGHLY DEOXIDIZED
STATE

(After Bogandy   ref. 51)

(b) THE POSSIBLE DISTRIBUTION OF DISSOLVED ALUMINIUM
AND OXYGEN IN THE REGION OF THE INTERFACE

FIG. 79

(a) THE MECHANISM OF INCLUSION AGGLOMERATION AFTER
KNUPPEL, BROTZMAN & FORSTER, REF. 145

(b) PHOTOMIGROGRAPH OBTAINED FROM AN ALUMINIUM
DEOXIDIZED MELT EXHIBITING AGGLOMERATION OF THE
ALUMINA INCLUSIONS BY THE MECHANISM PROPOSED BY
KNUPPEL ET AL (REF. 145) 2000X

CONCENTRATION

DEOXIDANT (Al)

STEEL MELT

[Al]   DEOXIDANT

interface

ALUMINA
DENDRITES

INCLUSION
FREE
ZONE

UNDEOXIDISED
REGION
(containing primary wüstite
inclusions)

[O]

(a)   (b)

Metal
Bath

Metal-Void
Meniscus

Void

a   b
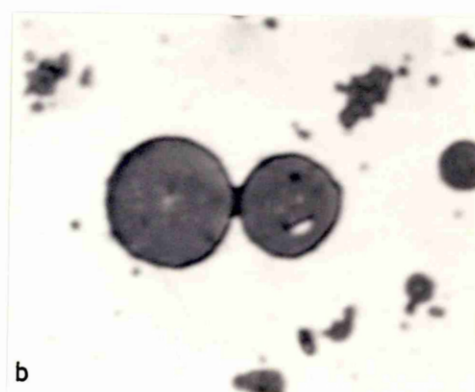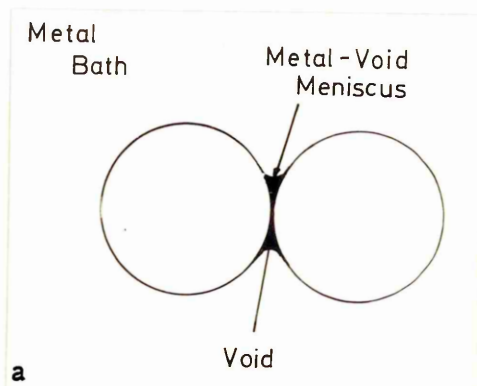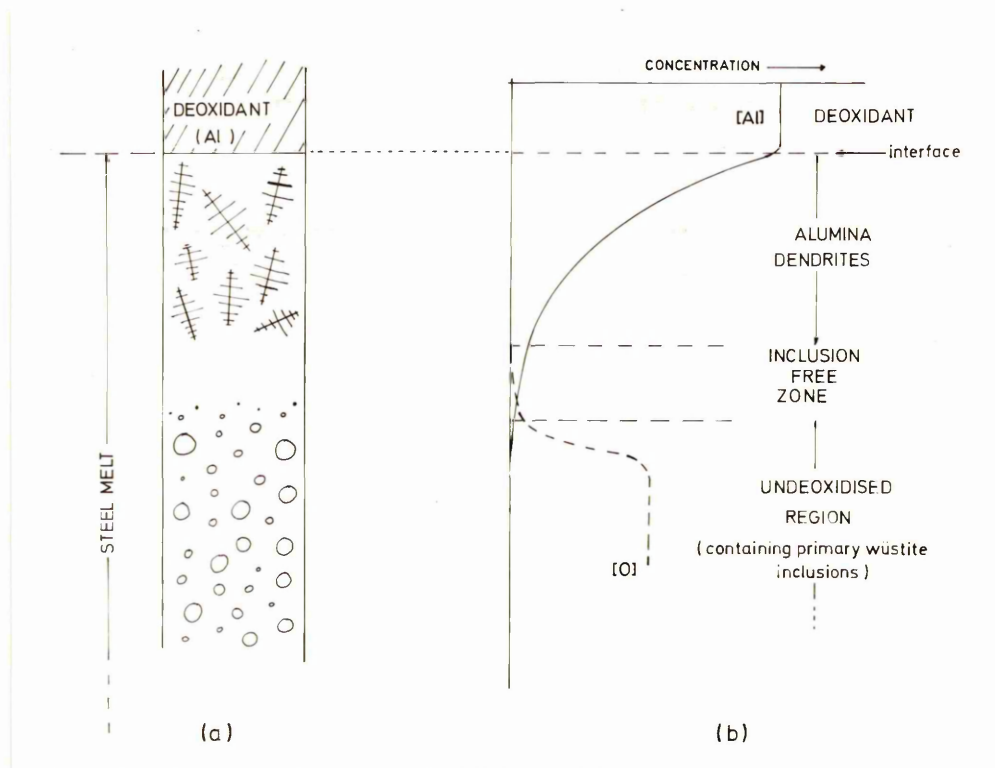
INTERDENDRITIC DISTRIBUTION OF WUSTITE

x 500

       COMPOSITION 100% Fe0

PLATE 2. CAST 4

PRIMARY BINARY IRON-SILICATE INCLUSION CONTAINING
Fe0 IN A EUTECTIC MATRIX

x 500

A	MATRIX COMPOSITION	73% Fe0, 27% SiO$_2$
B	PRIMARY PHASE	100% Fe0

       AVERAGE ANALYSIS

PLATE 3. CAST 5

(a)   LARGE AND SMALL INCLUSIONS SHOWING A FINER
           DISTRIBUTION OF WUSTITE DENDRITES IN THE LARGER
           INCLUSION

x 400

(b)   HIGHER MAGNIFICATION OF A SMALLER TYPE SHOWING
           THE DUPLEX NATURE OF THE MATRIX

x 1000

A	MATRIX COMPOSITION	72% Fe0, 29% SiO$_2$
B	PRIMARY PHASE	100% Fe0

       AVERAGE ANALYSIS
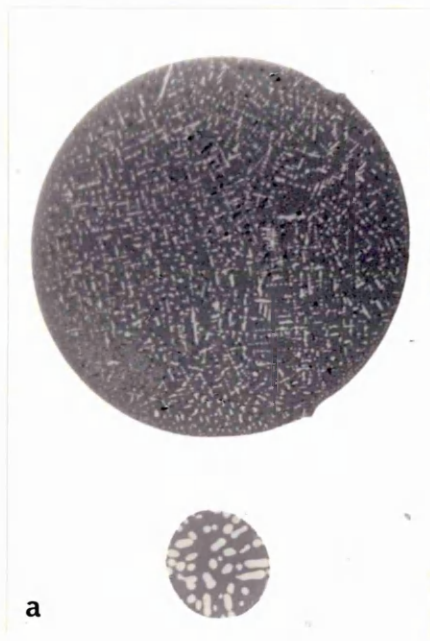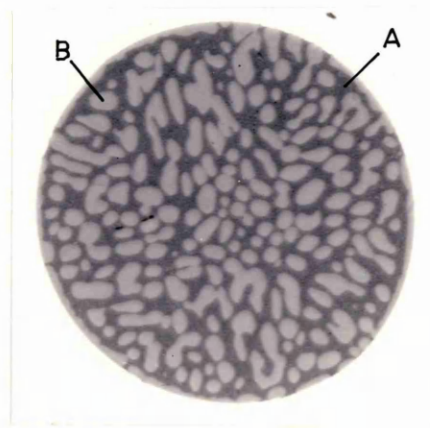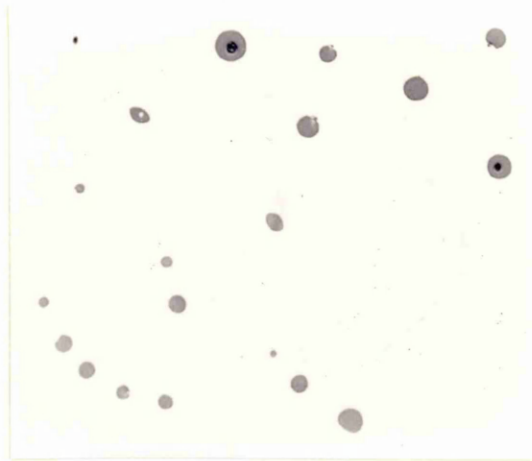
(a)   GLASSY SINGLE PHASED SILICATES SOLIDIFIED WHILST
      COALESCING
                                                  x 800

      COMPOSITION   11% FeO, 91% SiO$_2$

(b)   POLARISED LIGHT

PLATE 5. CAST 6

(a)   DUPLEX PRIMARY SILICATE CONTAINING MANGANOWUSTITE
      PRIMARY PHASE IN A EUTECTIC TYPE MATRIX
                                                  x 500

      A   MATRIX COMPOSITION   9%FeO, 58% MnO, 32% SiO$_2$
      B   PRIMARY PHASE   72% FeO, 19% SiO$_2$
          AVERAGE ANALYSIS

(b)   EUTECTIC TYPE OF INCLUSION
                                                  x 800

          AVERAGE ANALYSIS   14% FeO, 58% MnO, 27% SiO$_2$

(c)   COALESCING FORM AND BACKGROUND TYPES
                                                  x 500

      A   LATH TYPE   10% FeO, 56% MnO, 34%SiO$_2$
      B   GLASSY TYPE   11% FeO, 56% MnO, 36%SiO$_2$

(d)   SECONDARY DENDRITIC TYPE
                                                  x 800

      COMPOSITION   30% FeO, 66% MnO

a

b

a

b

c

d
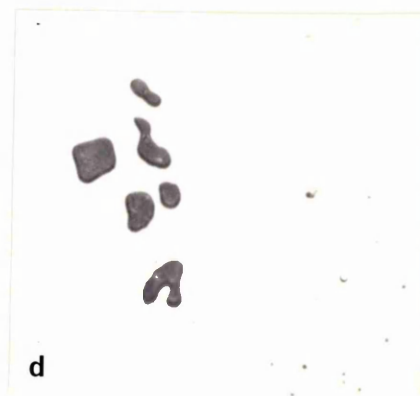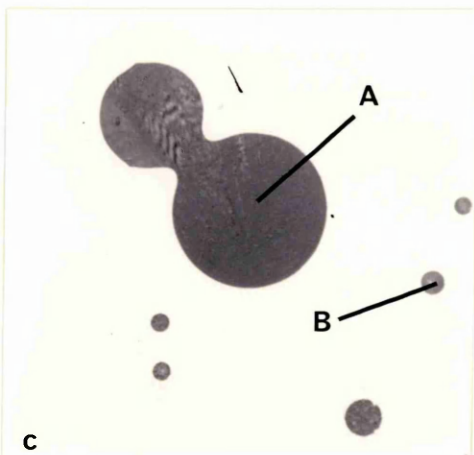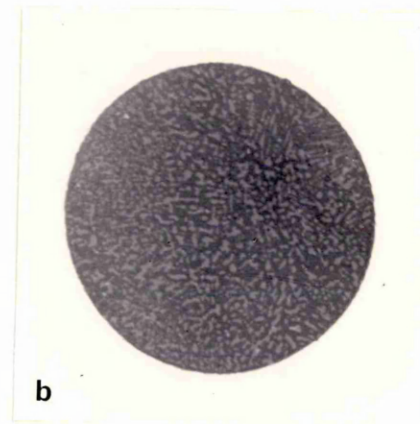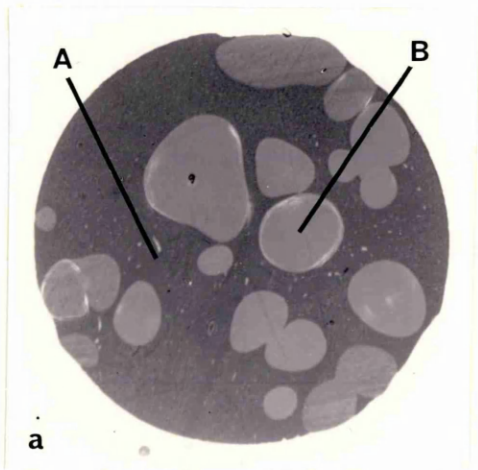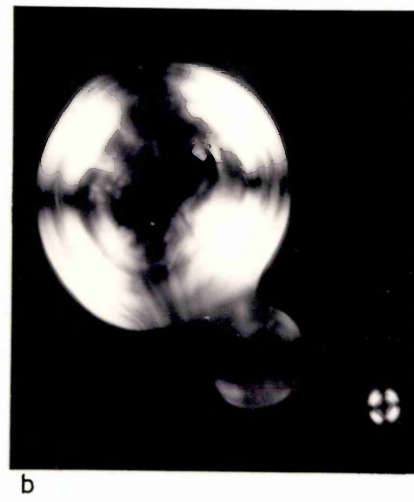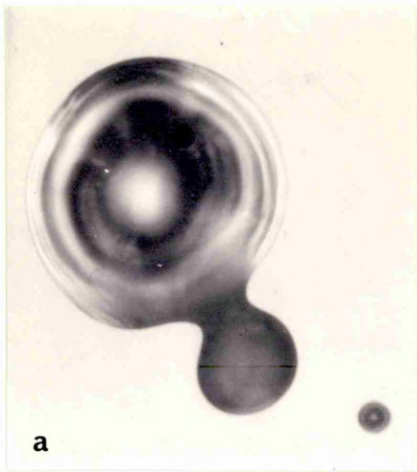
PLATE 6.   CAST 6B

(a)   COALESCING GLASSY SILICATES   x 800

            COMPOSITION   12% FeO, 36% MnO, 54% SiO$_2$

(b)   POLARISED LIGHT

PLATE 7.   CAST 8

(a)   GENERAL DISTRIBUTION OF GLASSY SILICATES
                                                            x 250

(b)   SILICATE CONTAINING AN INTERNAL DENDRITIC PHASE
                                                            x 400

      A   DENDRITE ANALYSIS   74% Al$_2$O$_3$, 25% FeO
      B   MATRIX ANALYSIS   35% FeO, 43% SiO$_2$, 20% Al$_2$O$_3$

(c)   S.E.M. IMAGE OF AN INCLUSION CONTAINING BLOCKY AND
            ROSETTE TYPE PHASES
                                                            x 650

a

b

a

A   B

b

c
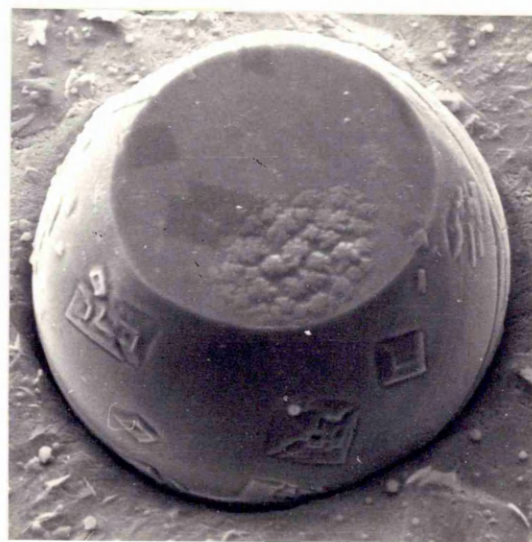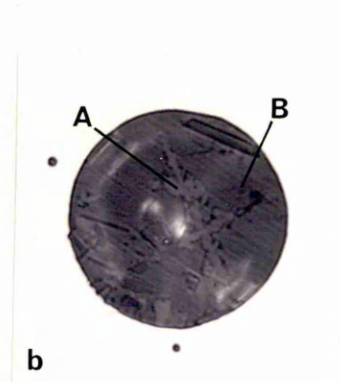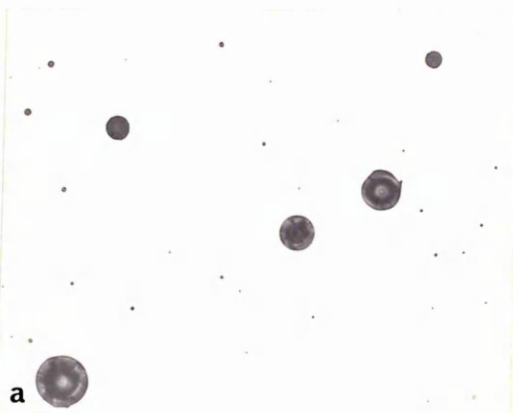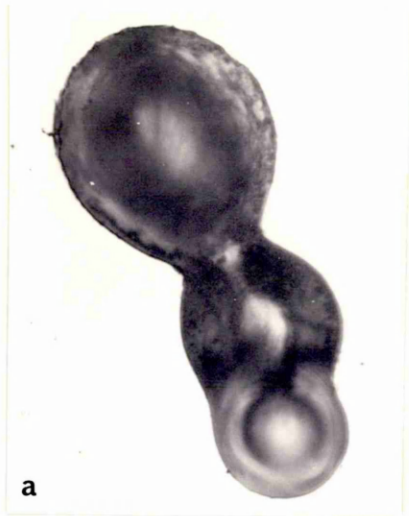
PLATE 7. CAST 8

(d)   S.E.M. IMAGE SHOWING ALUMINA DENDRITES
        DISTRIBUTED BETWEEN THE LARGER SILICATE GLOBULES.
                                                    x 770

(e)   S.E.M. IMAGE OF THE POLISHED SURFACE OF AN
        INCLUSION CONTAINING ROSETTE AND BLOCKY PHASES
        SHOWING CRACKING OF THE SILICATE MATRIX
                                                    x 1680

PLATE 8. CAST 10

(a)   IRREGULAR CLUSTER CONTAINING ALUMINA AND
        CALCIUM HEXALUMINATE PARTICLES
                                                    x 600

        A   ALUMINA   100% Al_2O_3
        B   Ca-HEXALUMINATE   92% Al_2O_3, 7% CaO

(b)   MULTIPHASE INCLUSION CONTAINING ALUMINA AND
        CALCIUM HEXALUMINATE BLOCKS AND LATHS IN A
        SILICEOUS MATRIX
                                                    x 600

        A   Ca-HEXALUMINATE   93% Al_2O_3, 8% CaO
        B   ALUMINA   100% Al_2O_3
        C   IRON GLOBULES   100% Fe
        D   SILICATE MATRIX - NO ANALYSIS Si DETECTED

d

e
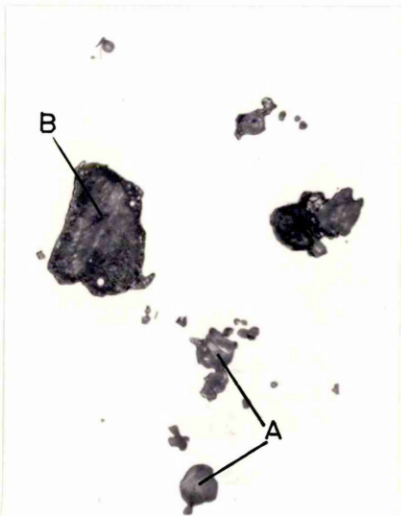
a
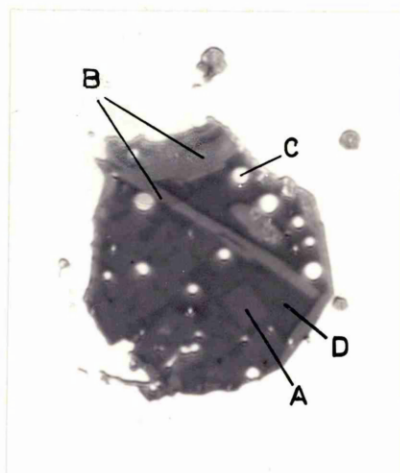
b

<u>PLATE 9. CAST 11</u>

(a)   CLUSTER OF GLASSY SILICATES

                                                                x 200

(b)   X-RAY LINE TRACES ACROSS A SILICATE INCLUSION
           SHOWING CALCIUM ENRICHMENT IN THE RIM

               FeK_α , SiK_α , CaK_α .

(c) CaK_α X-RAY IMAGE
                                                                x 2.0K

<u>PLATE 10. CAST 12</u>

(a)   GENERAL AREA SHOWING GLASSY SILICATES
                                                                x 250

(b)   GROUP OF COALESCING INCLUSIONS
                                                                x 620

a

Fe

Ca
Si
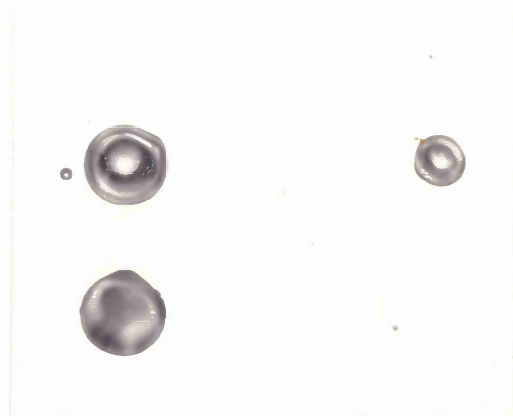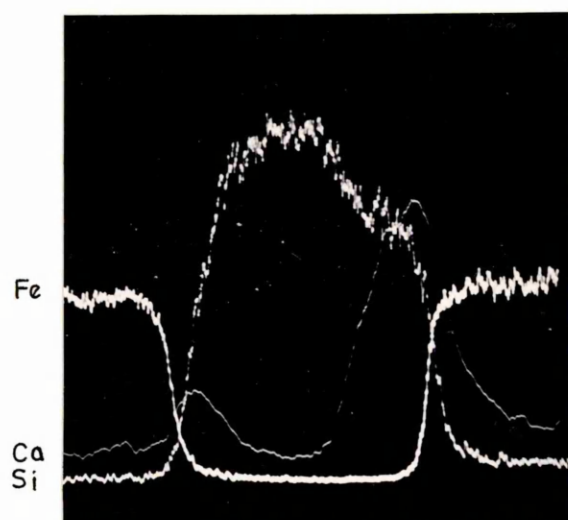
b
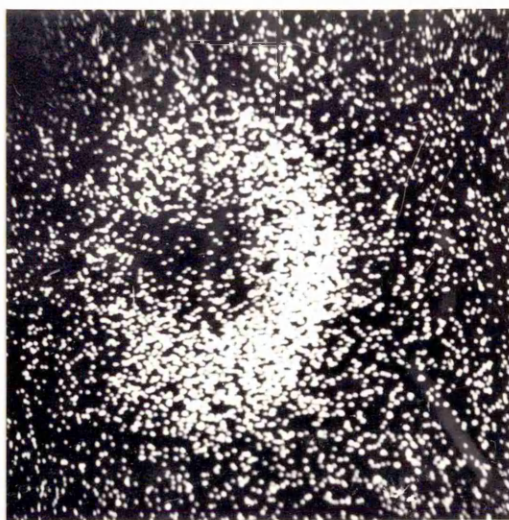
c

a
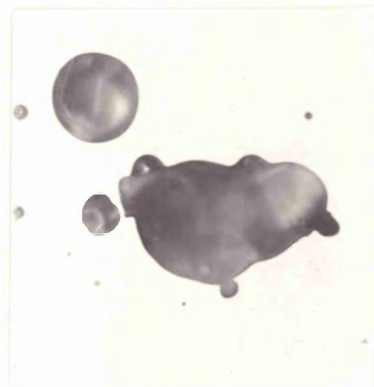
b

PLATE 11.   CAST 7B

(a)   GENERAL FORM OF A LARGE ALUMINA CLUSTER

x 88

(b)   DETAIL FROM THE CLUSTER SHOWING SEVERAL
         DIFFERENT PARTICLE MORPHOLOGIES

x 200

(c)   LARGE SPHERICAL GLOBULE OF PURE ALUMINA WITH
         ENCLOSED METAL

x 1000

    A   GLOBULE ANALYSIS   100% Al_2O_3
    B   ENCLOSED METAL   100% Fe

(d)   IRREGULAR TYPE OF PARTICLE WITH ENCLOSED METAL

x 1700

    A   CORE ANALYSIS   70% Al_2O_3, 31% FeO
    B   RIM ANALYSIS   90% Al_2O_3
    C   METAL GLOBULES   98% Fe

(e)   DUPLEX TYPE CONTAINING ALUMINA BLOCKS IN A
         HERCYNITE MATRIX

x 400

    A   ALUMINA BLOCKS   100% Al_2O_3
    B   MATRIX   71% Al_2O_3, 29% FeO

a

b
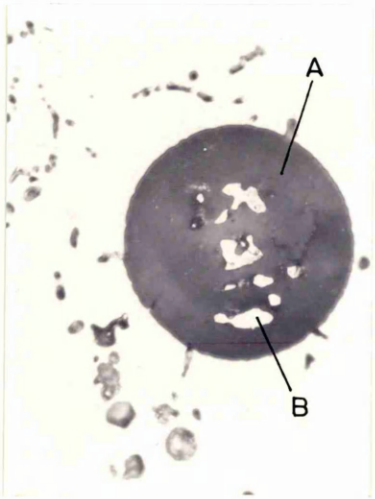
c
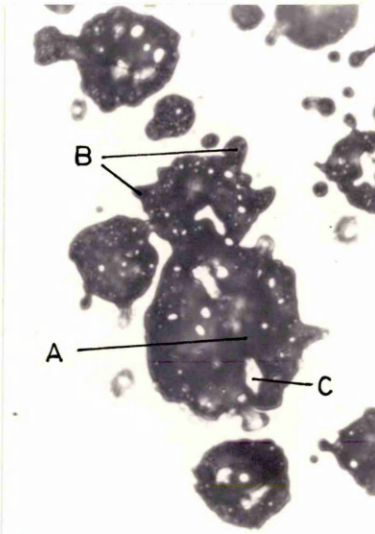
d
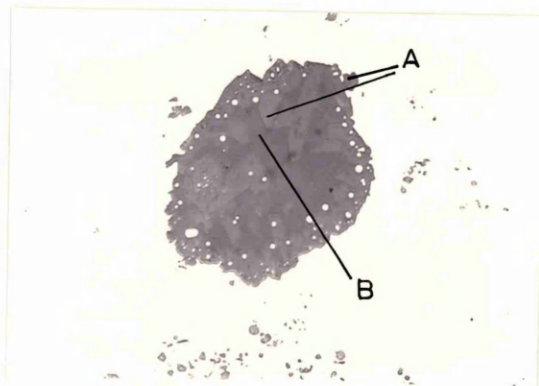
e

PLATE 11 (Cont'd....).

(f)   S.E.M. IMAGE SHOWING THE DIFFERENT PARTICLE
       MORPHOLOGIES MAKING UP AN ALUMINA CLUSTER

                                                    x 1.8K

(g)   HONEYCOMB OR GRAIN STRUCTURE ON THE SURFACE
       OF THE LARGE GLOBULAR FORMS

                                                    x 9K

(h)   SINTER POROSITY ON THE POLISHED SURFACE OF ONE
       OF THE LARGE SINTERED GLOBULES AFTER ETCHING
       IN BROMINE-METHANOL

                                                    x 9K
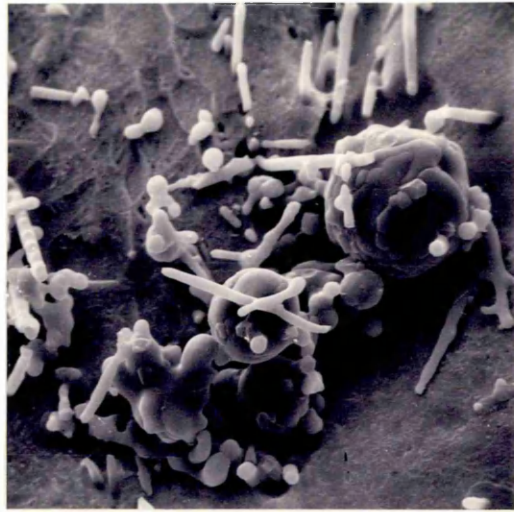
f
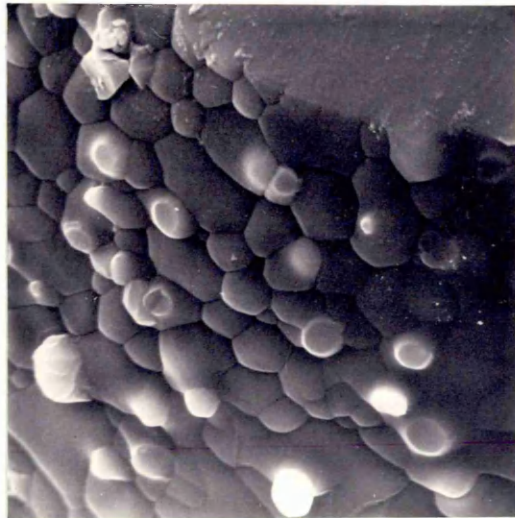
g
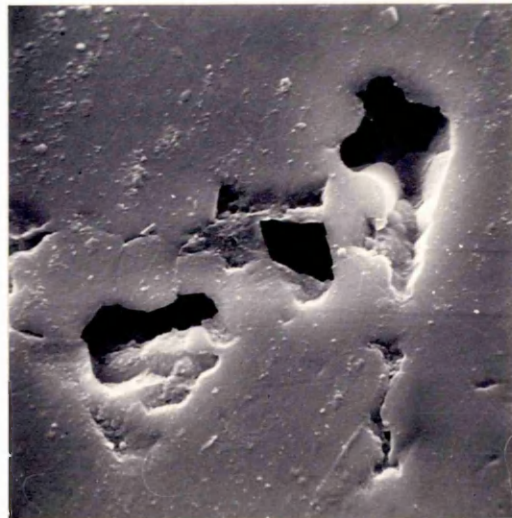
h

PLATE 12. MOULD DEOXIDISED WITH AL

(a)   DENDRITIC BAND SEPARATING AN UNDEOXIDIZED AND
        FULLY DEOXIDIZED REGION
                                                    x 40

        A = 0.8% Al   B = 0.2% Al   C = NOT DETECTED

(b)   S.E.M. IMAGE SHOWING THE DENDRITIC NATURE OF
        THE INTERFACE
                                                    x 550

(c)   DIFFERENT DENDRITE MORPHOLOGIES WITHIN THE
        INTERFACE
                                                    x 1.5K

(d)   HERCYNITE + WUSTITE PARTICLE IN THE REGION CLOSEST
        TO THE DEOXIDIZED REGION
                                                    x 1.1 K

(e)   WUSTITE GLOBULES IN THE REGION CLOSEST TO THE
        DENDRITIC BAND SHOWING EVIDENCE OF REACTION AND
        NUCLEATION OF ALUMINA DENDRITES
                                                    x 1.1 K

(f)   HIGHER MAGNIFICATION SHOWING EVIDENCE OF REACTION
        AT THE INCLUSION SURFACE
                                                    x 5 K

(g)   ALUMINA DENDRITE
                                                    x 1.1 K

(h)   PARTIALLY SPHERODIZED DENDRITE
                                                    x 5 K

(i) SPHEROIDAL AGGLOMERATE
                                                    x 2.2K
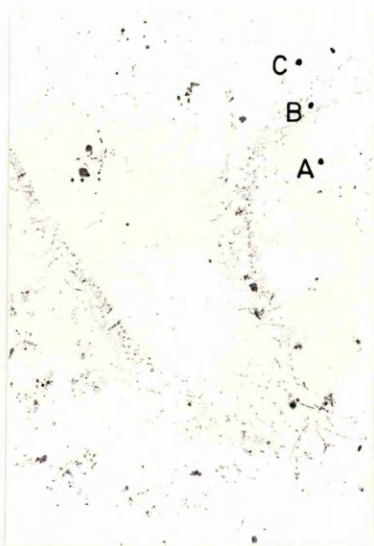
a

b
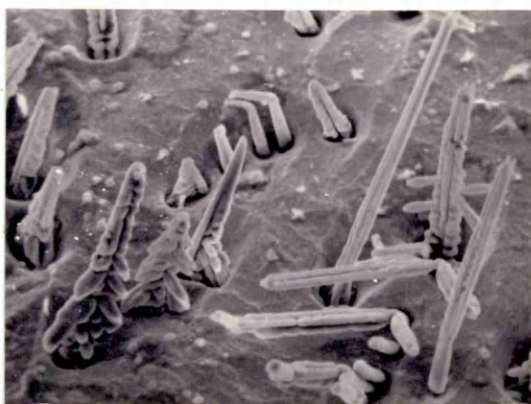
c

d
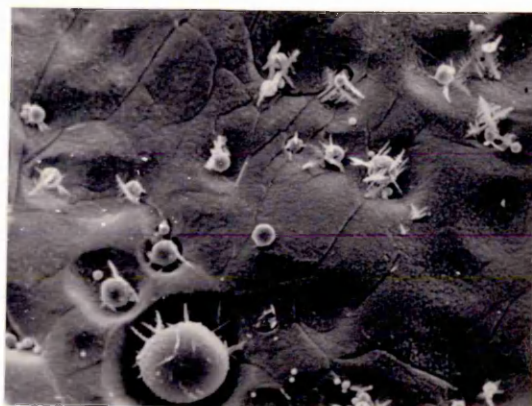
e
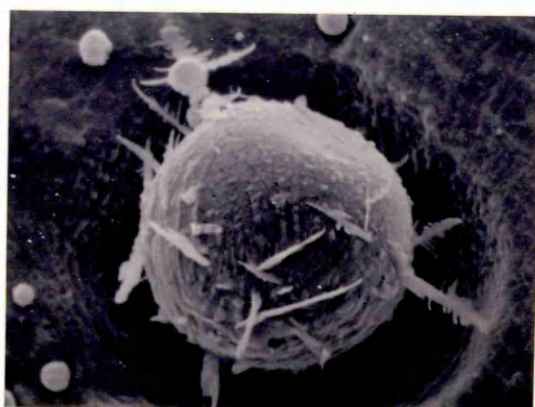
f
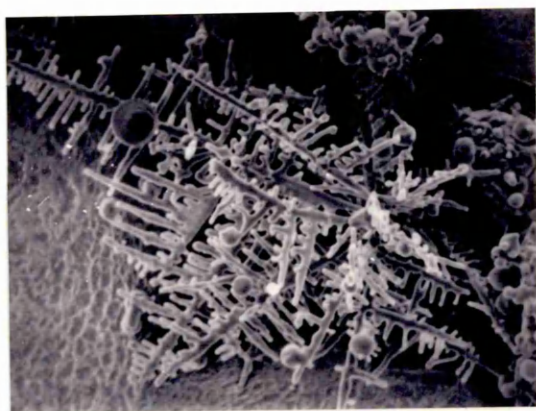
g
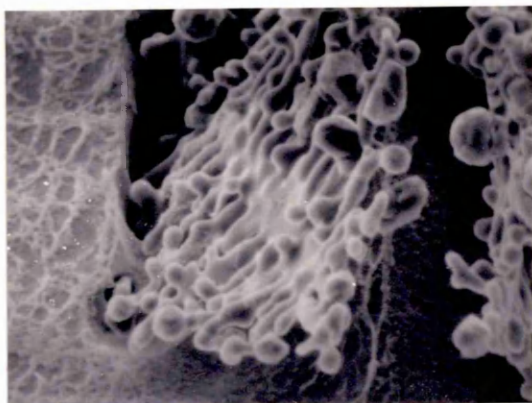
h
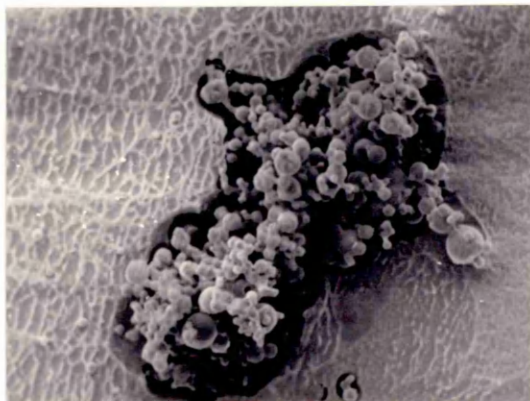
i

PLATE 12 (Cont'd....)

(j) REGION OF MIXED HERCYNITE + WUSTITE TYPES TOGETHER
WITH IRREGULAR REACTED TYPES HAVING ALUMINA
ENRICHED RIMS AND CORES WITH COMPOSITIONS CLOSE
TO THAT OF HERCYNITE

x 80

A = 0.5% Al
B = 0.6% Al
C = 0.4% Al
D = 0.1% Al

(k) HIGHER MAGNIFICATION OF ONE OF THE CLUSTERS IN
PL 12J SHOWING HERCYNITE + WUSTITE TYPES BECOMING
REACTED IN THE REGION CLOSEST TO THE DENDRITE
BAND.

x 500

(1) S.E.M. IMAGE OF A PARTIALLY REACTED TYPE SHOWING
ALUMINA SPHERES AND DENDRITES NUCLEATED AT THE
SURFACE

x 2.2 K

(m) OPTICAL IMAGE OF A PARTIALLY REACTED TYPE SHOWING
THE REACTED RIM WITH ENCLOSED METAL SURROUNDING
AN UNREACTED HERCYNITE CORE

x 1000

A CORE ANALYSIS $\quad$ 61% Al_2O_3, 40% FeO
B RIM ANALYSIS $\quad$ 95% Al_2O_3

(n) S.E.M. IMAGE OF THE SAME PARTICLE AS IN (m) SHOWING
THE 3-D MORPHOLOGY

x 1000

(p) CLUSTER OF SPHERICAL GLASSY APPEARING ALUMINA
PARTICLES

x 1000

COMPOSITION $\qquad$ A = 100% Al_2O_3
B = 100% Al_2O_3, 1% FeO
C = 100% Al_2O_3, 2% FeO
D = 98% Al_2O_3, 3% FeO
E = 98% Al_2O_3, 4% FeO
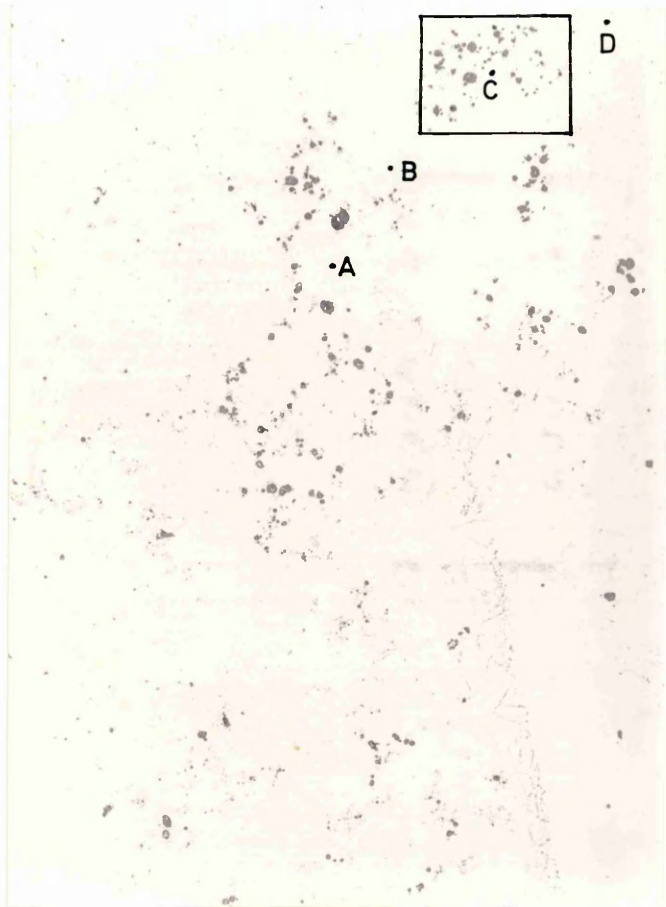
j

k
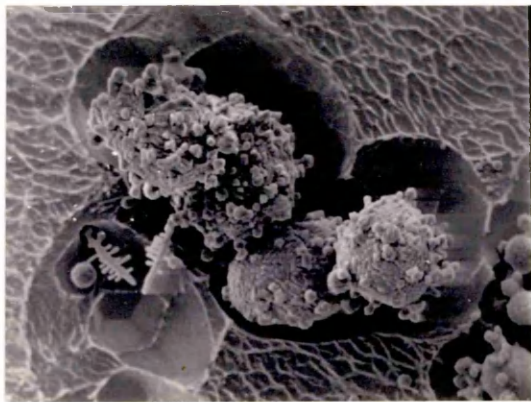
l
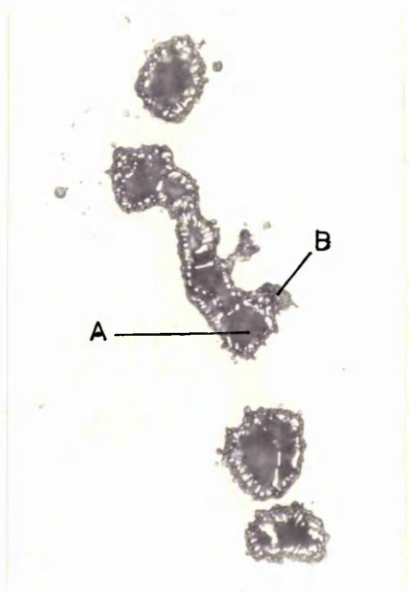
m
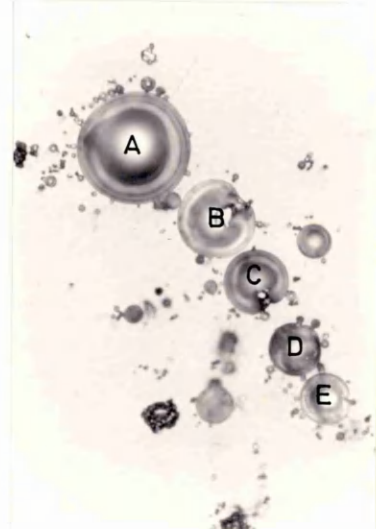
p
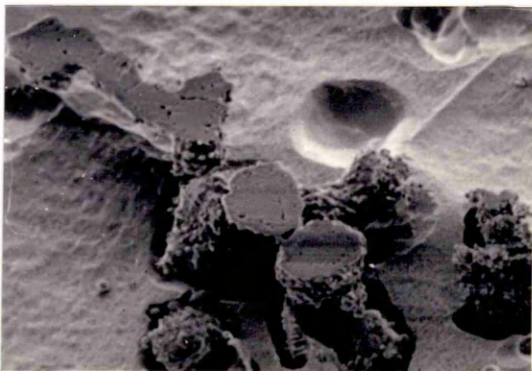
n

PLATE 13. SUCTION SAMPLE 2 AL KILLED MELT

(a)   DENDRITIC REGION

x 1.4 K

(b)   SPHERODIZED AND SINTERED REGION

x 700

(c)   SPHERODIZING DENDRITE ARMS

x 2.5K

(d)   SPHERODIZING AND COLLAPSING DENDRITE

x 2.5K

(e)   COLLAPSED AND PARTIALLY SINTERED PARTICLE

x 1.7K
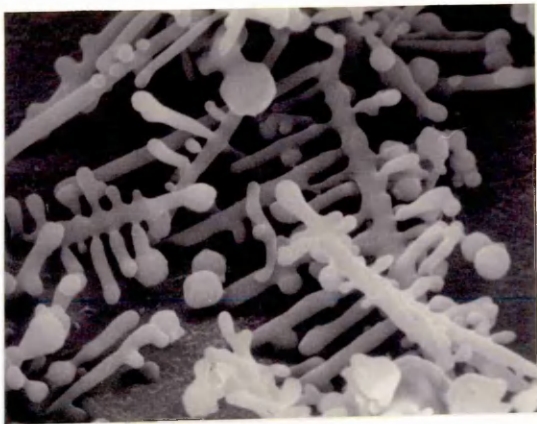
a

b
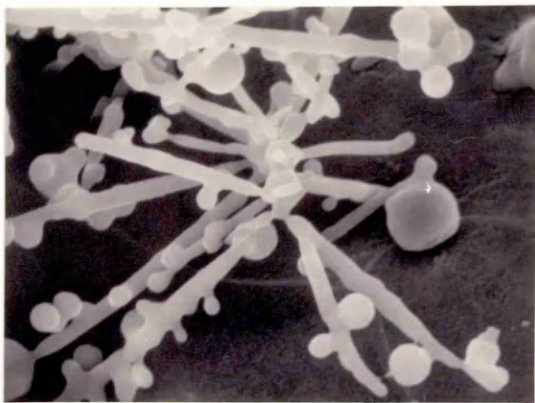
c
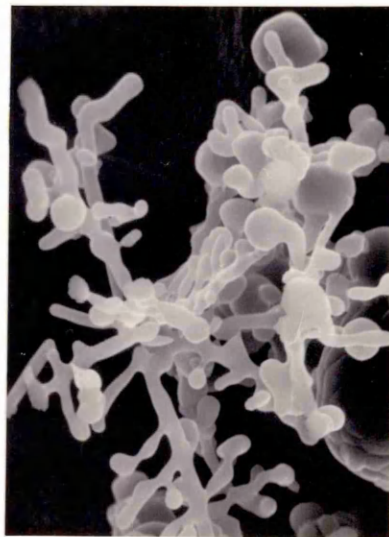
d
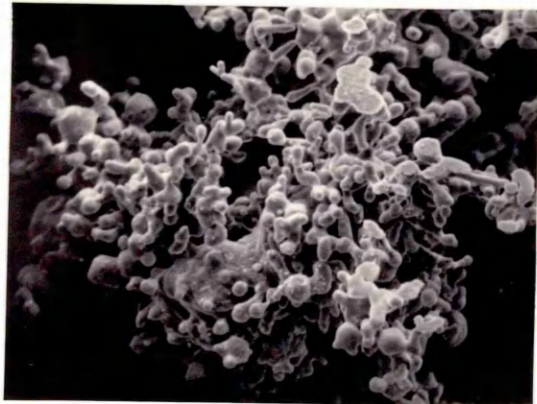
e

PLATE 13 (Cont'd....)

(f)   OPTICAL MICROGRAPH OF A LARGE SINTERED GLOBULE
      SHOWING ENTRAPPED METAL

                                                x 400

      A + B COMPOSITION   100% Al_2O_3

(g)   S. E. M. IMAGE OF A LARGE SINTERED GLOBULE SHOWING
      THE OPENING TO THE CENTRAL CAVITY OBSERVED IN
      MOST OF THESE PARTICLES

                                                x 840
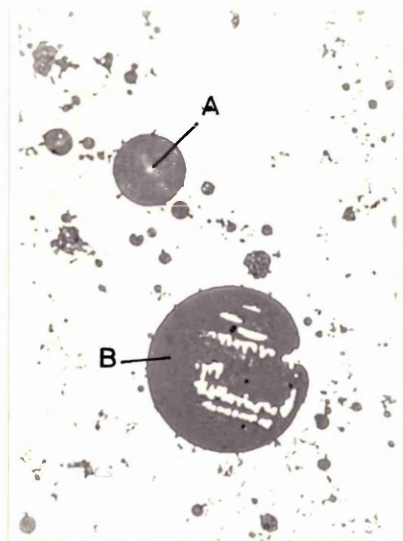
f
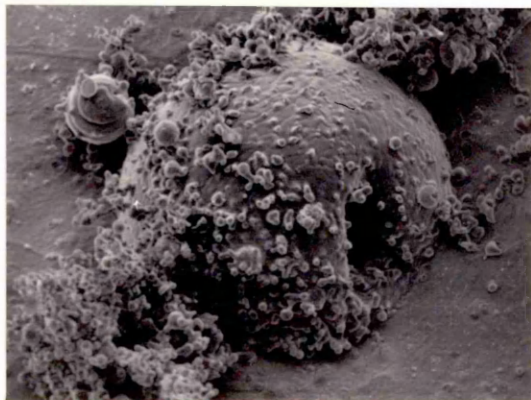
g

PLATE 14.   HEAT TREATED INCLUSIONS IN CAST 6

(a)   AFTER 100 HOURS AT 925°C SHOWING SPHERODIZATION
         OF THE EUTECTIC MATRIX

x 600

(b)   100 HOURS AT 925°C SHOWING THE PRECIPITATION OF
         NUMEROUS IRON GLOBULES WITHIN THE INCLUSION

x 1000

(c)   AFTER 5 HOURS AT 1000°C SHOWING THE FORMATION OF
         FEWER BUT MUCH LARGER IRON GLOBULES

x 1500

(d)   AFTER 100 HOURS AT 1150°C SILICATE CONTAINING
         MANGANESE SULPHIDE

x 600

         A - MnS with 6% FeS
         B - PRIMARY PHASE 5% FeO, 95% MnO
         C - MATRIX TEPHROITE 67% MnO, 2% FeO, 30% SiO_2
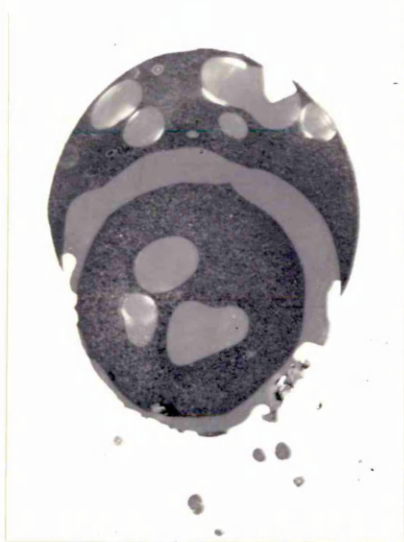
a
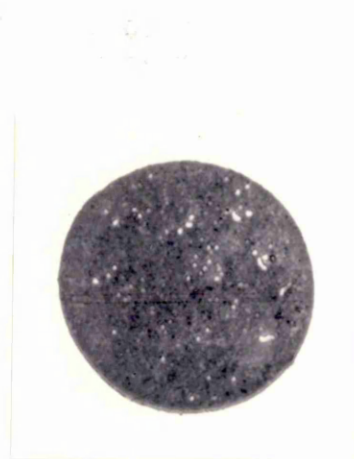
b
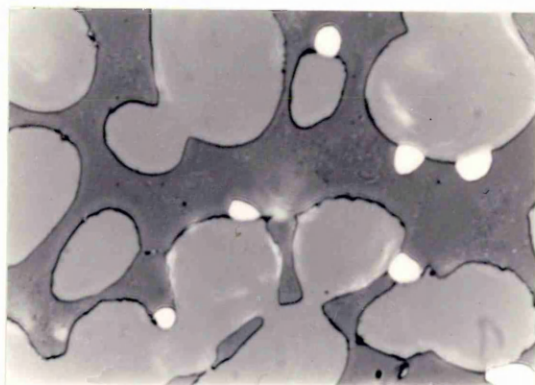
c
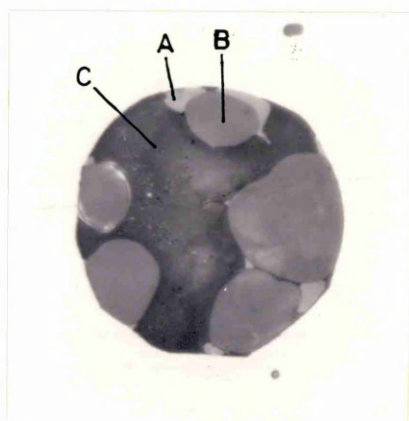
d

PLATE 15. HEAT TREATED INCLUSIONS IN CAST 6B

(a)   AFTER 5H AT 1000°C SHOWING THE FORMATION OF
         SILICEOUS PRECIPITATES
                                                                    x 400

    A   DARK PRECIPITATE   90% SiO_2
    B   GLASSY MATRIX   14% FeO, 40% MnO, 48% SiO_2

(b)   AFTER 100H AT 1000°C SHOWING THE PRECIPITATION OF
         A NUMBER OF PHASES GIVING A GRANULAR TYPE OF
         STRUCTURE. AGAIN IRON GLOBULES HAVE FORMED.
                                                                    x 1000

    A   DARK PRECIPITATE   90% SiO_2
    B   MATRIX   54% SiO_2, 30% MnO, 14% FeO
    C   METAL GLOBULES   95% Fe

(c)   AFTER 5H AT 1150°C
                                                                    x 1000

(d)   AS (c) BUT SHOWING DEVITRIFICATION OF THE MATRIX
                                                                    x 1000

    A   DARK PRECIPITATE   100% SiO_2
    B   LIGHT PHASE   61% MnO, 4% FeO, 38% SiO_2
    C   MATRIX   47% MnO, 4% FeO, 51% SiO_2

(e)   AS (d) BUT SHOWING A LARGER AMOUNT OF THE LIGHT
         PHASE.
                                                                    x 1000

(f)   AFTER 50H AT 1150°C
                                                                    x 1000

(g)   AFTER 50 HOURS AT 1275°C. SILICA PRECIPITATES IN A
         FEATHERY OR LATH-LIKE MATRIX
                                                                    x 1000

    A   DARK PRECIPITATE   100% SiO_2
    B   MATRIX   54% MnO, 3% FeO, 43% SiO_2

(h)   AS IN (g) BUT WITH A FINER DISTRIBUTION OF SILICA
         PRECIPITATES
                                                                    x 1000
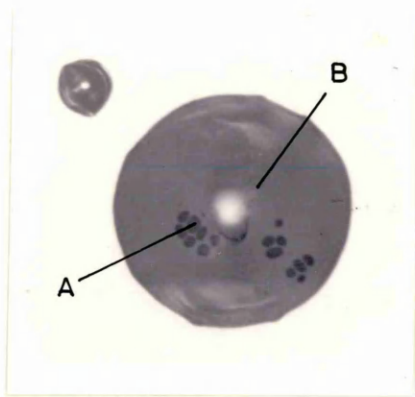
a
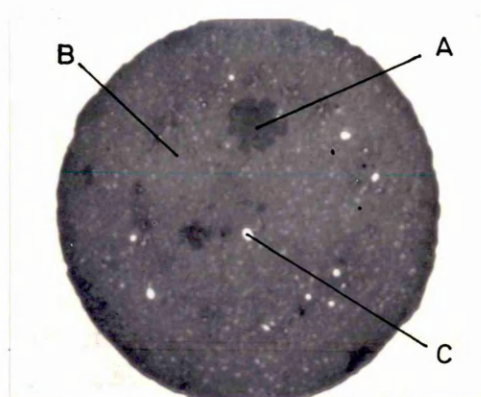
b
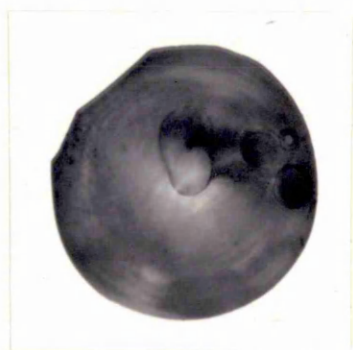
c
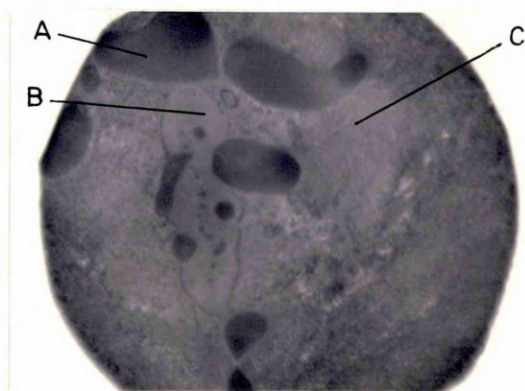
d
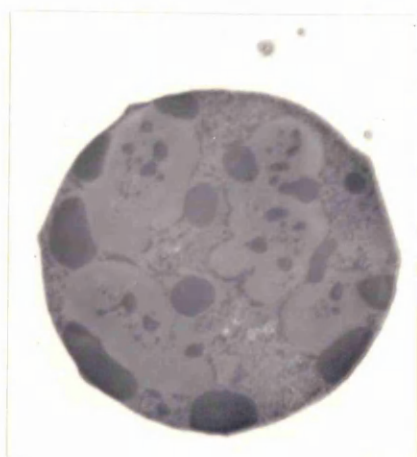
e
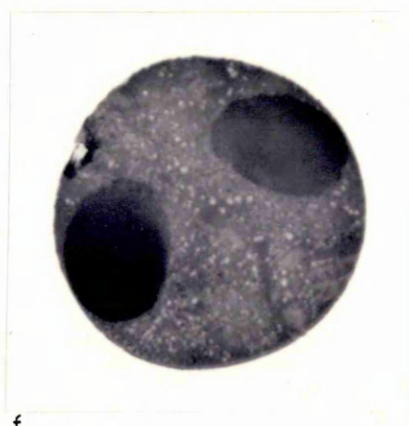
f
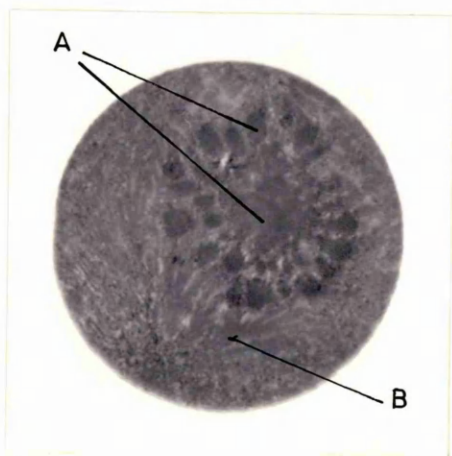
g
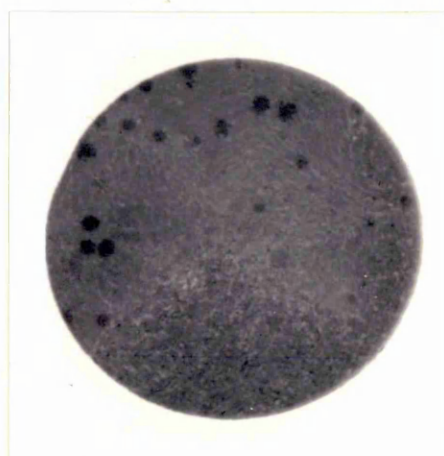
h

PLATE 16. HEAT TREATED INCLUSIONS IN CAST 8

(a)   AFTER 50 HOURS AT 925°C SHOWING A LATH LIKE STRUCTURE

x 600

(b)   AS IN (a) BUT SHOWING DARKER CRESCENT SHAPED AREAS AND EVIDENCE OF A RECTION RIM

x 1000

A	RIM REGION	20% FeO,	54% SiO_2,	27% Al_2O_3
B	GREY MATRIX	46%	48%	8%
C	LIGHT GREY PHASE	36%	35%	38%
D	DARKER CRESCENT	31%	46%	27%

(c)   AS IN (a and b) BUT SHOWING A PRONOUNCED RIM-CORE STRUCTURE

x 1000

A	RIM REGION	21% FeO,	53% SiO_2,	26% Al_2O_3
B	CORE REGION	47%	41%	10%
C	DARK BOUNDARY	28%	54%	16%
D	METAL GLOBULES	100% Fe		

(d)   AS IN (a, b and c) SHOWING THE LATH LIKE STRUCTURES SEEN IN (a)

x 1000

A	LATHS	37% FeO,	47% SiO_2,	16% Al_2O_3
B	GRANULAR MATRIX	26%	49%	24%

a

b

c

d
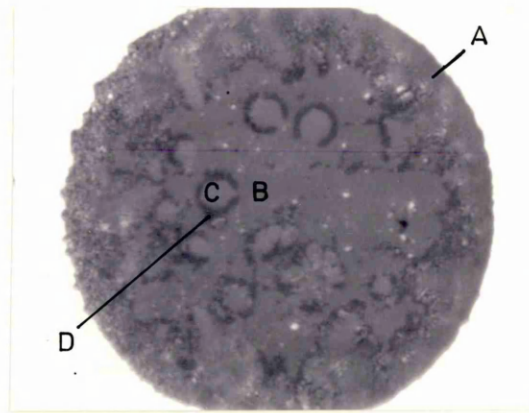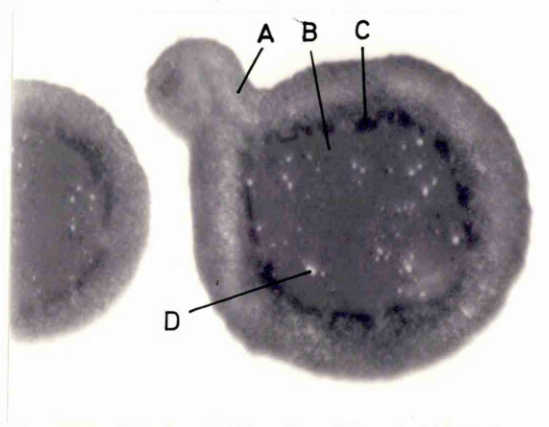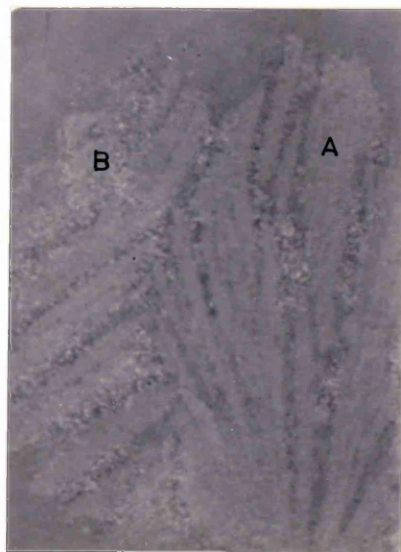
PLATE 16 (Cont'd....)

(e)   AFTER 5H AT 1000°C SHOWING A COMPLEX NON-
EQUILIBRIUM ASSEMBLAGE OF PHASES

x 400

		% FeO	%SiO_2	%Al_2O_3	
A	BLOCKY STRUCTURES	39	–	61	(HERCYNITE)
B	LIGHT AREAS	50	36	11	(ALAMANDINE)
C	DARK AREAS	28	70	2	(FAYALITE)
D	EUTECTIC AREA	16	70	20	
E	MID-GREY AREAS	15	70	15	(NON-STOICHIO-METRIC)
	AVERAGE ANALYSIS	23	35	42	

(f)   AS IN (e) BUT SHOWING HERCYNITE BLOCKS HAVING SILICA
ENRICHED ENVELOPES IN A EUTECTIC TYPE MATRIX

x 680

A   HERCYNITE (STOICHIOMETRIC)
B   EUTECTIC MATRIX

(g)   AFTER 100H AT 1000°C SHOWING A THREE PHASE
ASSEMBLAGE

x 600

A   SILICA   100% SiO_2

B   FAYALITE   70% FeO, 30% SiO_2

C   HERCYNITE   40% FeO, 60% Al_2O_3

(h)   AS IN (g) BUT TWO-PHASE ONLY - NOT ANALYSED

x 1000

(i)   AFTER 50 H AT 1150°C SHOWING HERCYNITE PRECIPITATES
IN A GLASSY MATRIX

x 1000

(j)   AFTER 100H AT 1150°C HERCYNITE AND SILICA PRECIPITATES
IN A GLASSY MATRIX

x 400

A   HERCYNITE   39% FeO, 62% Al_2O_3

B   SILICA   100% SiO_2

C   MATRIX   34% FeO, 50% SiO_2, 17% Al_2O_3

    AVERAGE   31% FeO, 39% SiO_2, 36% Al_2O_3

e
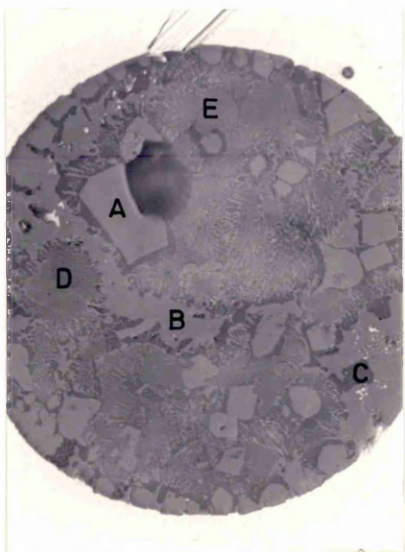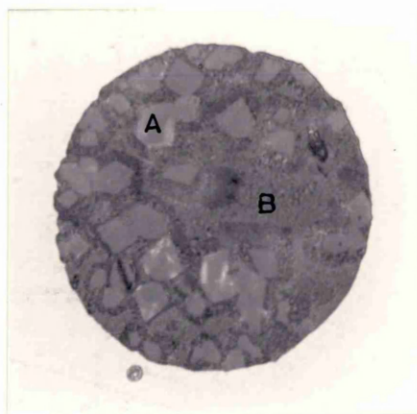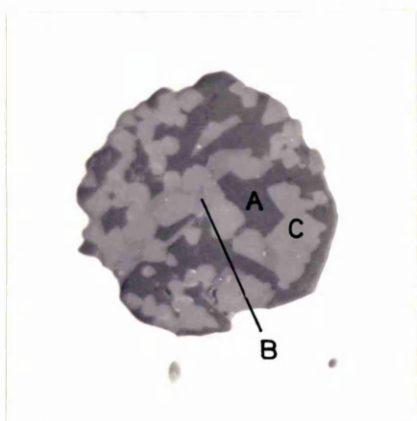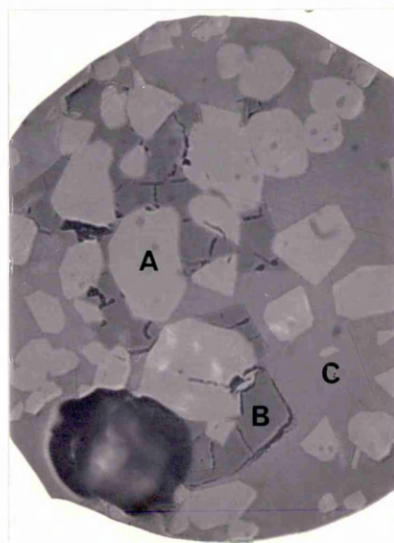
PLATE 17.   CAST 1B - HOT ROLLED

(a)   OPTICAL MICROGRAPH IN THE LONGITUDINAL SECTION
        AFTER HOT ROLLING TO A TRUE STRAIN OF 1.8 AT
        $1150^\circ C$

                                                    x 200

(b)   SCANNING ELECTRON MICROGRAPH AFTER DEEP ETCHING
        SHOWING THE VARIABILITY OF DEFORMATION OF THE
        FeO INCLUSIONS

                                                    x 1.5K

(c)   HIGHER MAGNIFICATION SHOWING A SECOND PHASE ON
        THE SURFACE OF A HIGHLY DEFORMED INCLUSION

                                                    x 3K

(d)   AS IN (c) BUT ON THE SURFACE OF A LESS HIGHLY
        DEFORMED INCLUSION

                                                    x 3K

        * A   WUSTITE   100% FeO
        * B   IRON SULPHIDE   FeS with FeO

        * QUALITATIVE EDAX ANALYSIS

a

b

c

d

PLATE 18.   CAST 5 HOT ROLLED AT 925°C
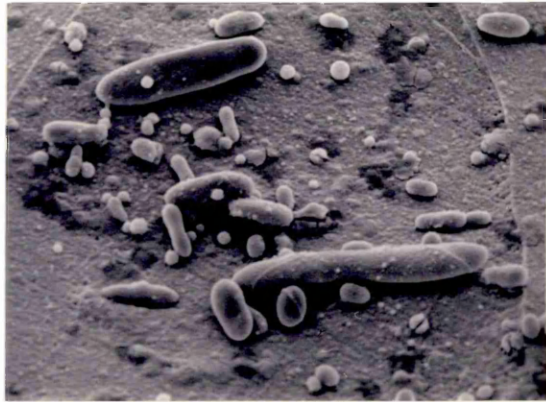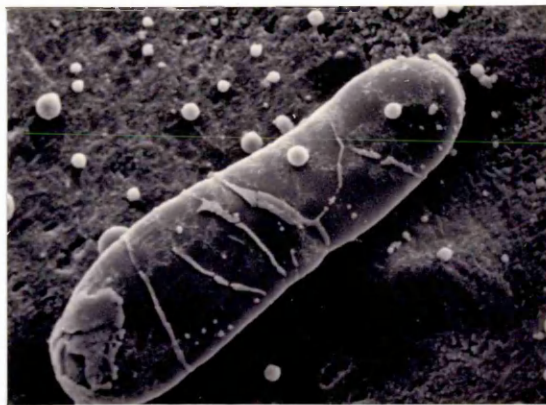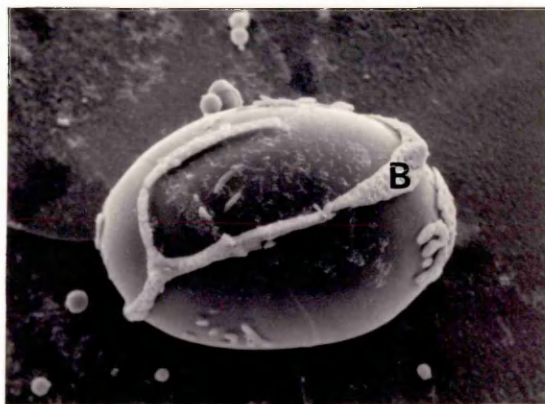
(a)   CONICAL VOID FORMATION WITH CRUSHING AND ENTRANE-
       MENT OF INCLUSION FRAGMENTS AT LOW STRAINS $\mathcal{E} = 0.6$

                                                              x 400

(b)   AS IN (a) BUT SHOWING FRACTURING OF THE INCLUSION

                                                              x 400

(c)   LARGER DUPLEX INCLUSION EXHIBITING FRACTURING
       AT HIGHER STRAINS. NOTE THE INTRUSION OF THE
       METALLIC MATRIX INTO THE CRACKS, WHICH LIE AT
       45°C TO THE ROLLING DIRECTION $\mathcal{E} = 1.5$

                                                              x 200

(d)   AS IN (c) BUT SHOWING FRAGMENTATION, ENTRANEMENT
       AND ROTATION OF THE INCLUSION FRAGMENTS $\mathcal{E} = 1.8$

                                                              x 200
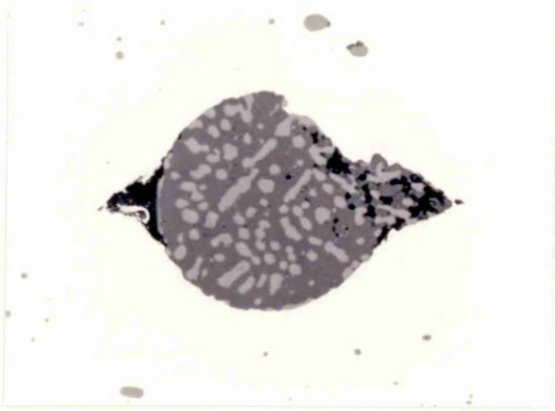
a
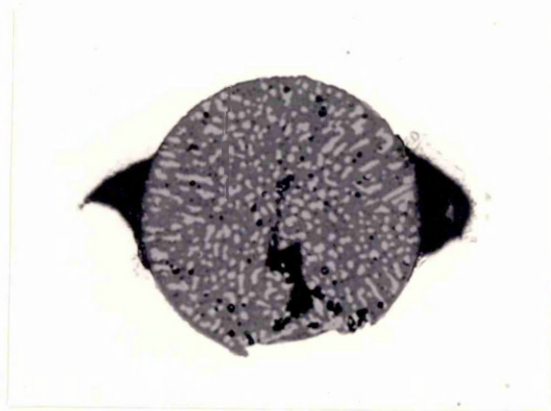
b
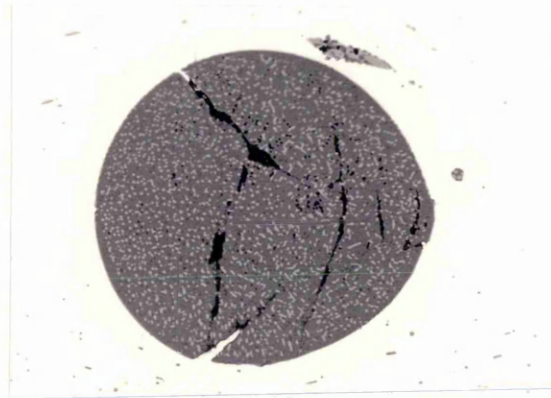
c
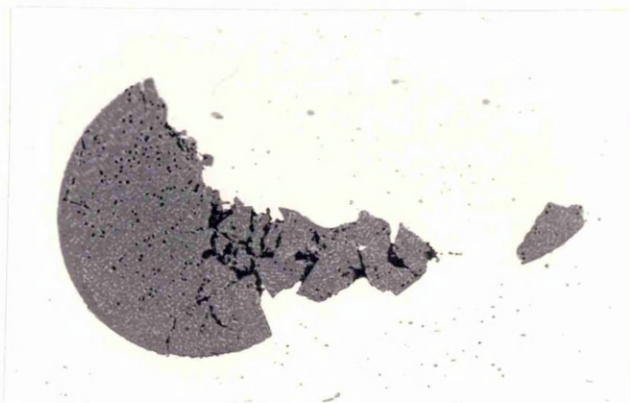
d

PLATE 19.   CAST 5 HOT ROLLED AT 1150°C

(a)   PLASTIC DEFORMATION AT A MATRIX STRAIN OF 0.6

x 400

(b)   PLASTIC DEFORMATION AT A MATRIX STRAIN OF 0.9

x 400

(c)   PLASTIC DEFORMATION AT A MATRIX STRAIN OF 1.2

x 400

(d)   PLASTIC DEFORMATION AT A MATRIX STRAIN OF 1.5

x 400

(e)   PLASTIC DEFORMATION AT A MATRIX STRAIN OF 1.8

x 400

PLATE 19.   CAST 5 HOT ROLLED AT 1150°C

a

b

c

d

e

PLATE 19 (Cont'd.....)
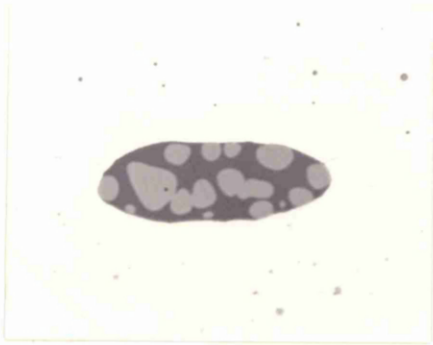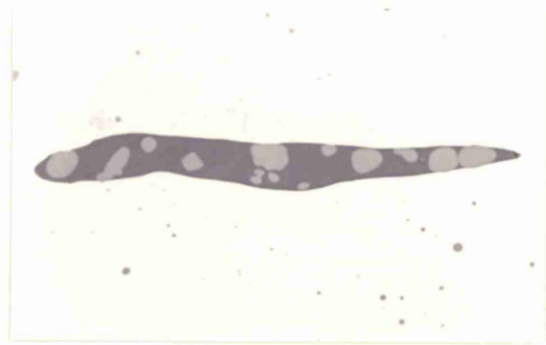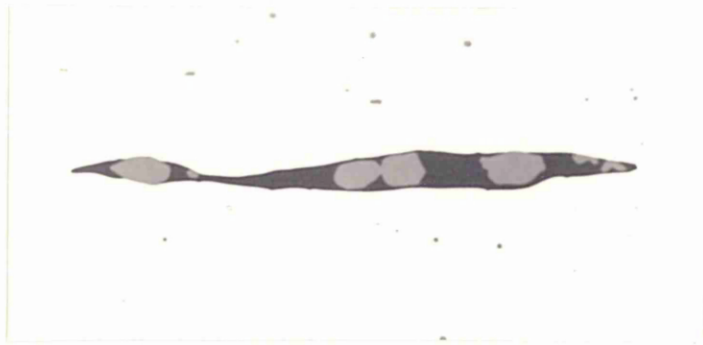
(f)   SCANNING ELECTRON MICROGRAPH OF A DUPLEX SILICATE
      SHOWING STRIPPING OF THE MATRIX FROM THE LESS PLASTIC
      PRIMARY WUSTITE $\mathcal{E}$ = 1.2

                                                    x 2K

(g)   SCANNING ELECTRON MICROGRAPH OF SECONDARY Fe0
      INCLUSIONS WHICH ARE UNDEFORMED AT THIS TEMPERATURE
      AND STRAIN

                                                    x 2K
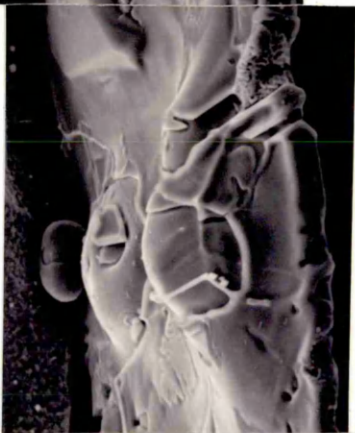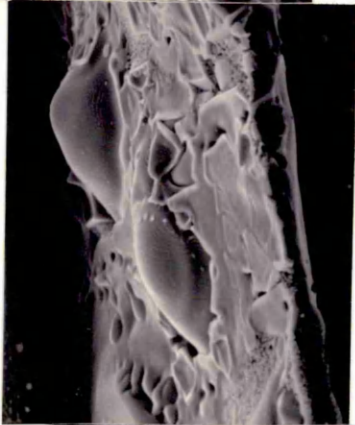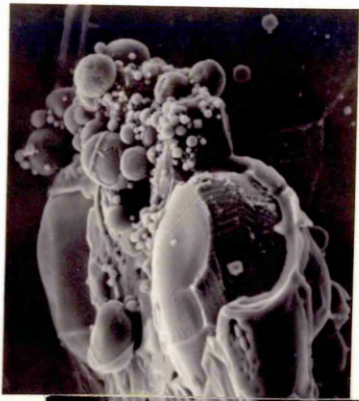
f
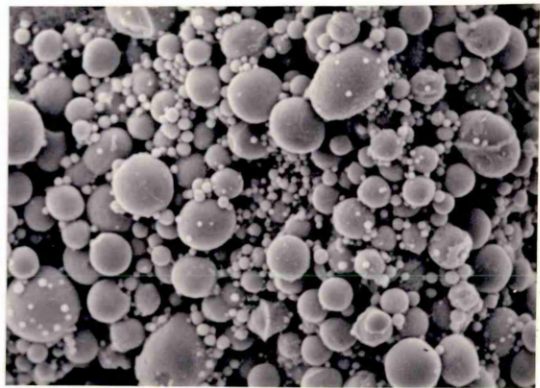
g

PLATE 20. CAST 5 HOT ROLLED AT 1275°C

(a)   PLASTIC DEFORMATION AT A MATRIX STRAIN OF 0.6

x 400

(b)   PLASTIC DEFORMATION AT A MATRIX STRAIN OF 0.9

x 400

(c)   PLASTIC DEFORMATION AT A MATRIX STRAIN OF 1.2

x 400

(d)   PLASTIC DEFORMATION AT A MATRIX STRAIN OF 1.5

x 400

(e)   PLASTIC DEFORMATION AT A MATRIX STRAIN OF 1.8

x 400

a

b

c

d

e

PLATE 21. CAST OB HOT ROLLED AT 1150 AND 1275°C
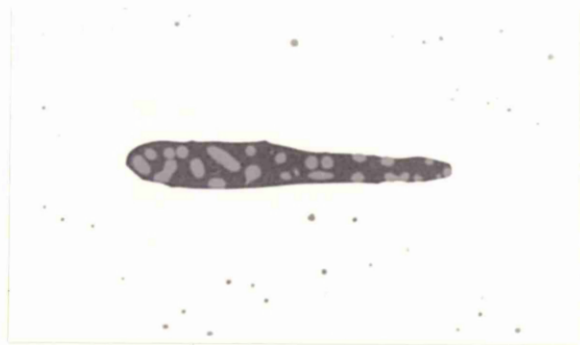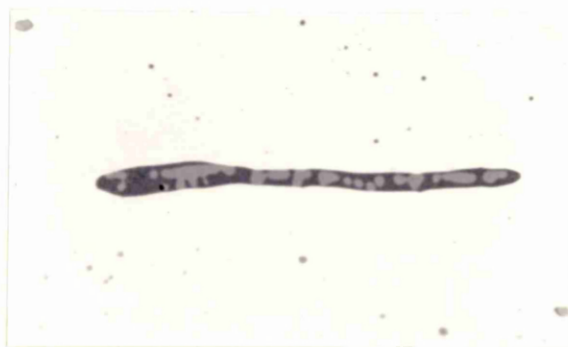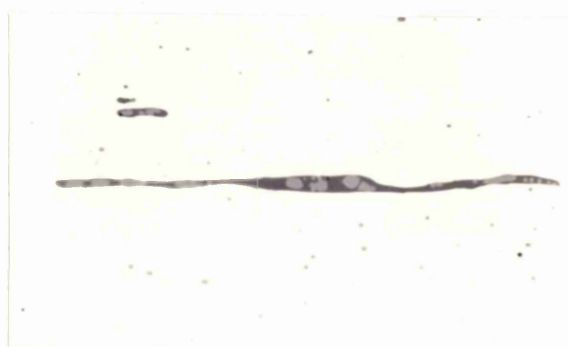
(a)   CONICAL VOID FORMATION AT A MATRIX STRAIN OF
0.3 WHEN DEFORMED AT 1150°C

x 80

(b)   PLASTIC DEFORMATION AND PRECIPITATION OF SILICA
ROSETTES AT A MATRIX STRAIN OF 0.3 ON DEFORMATION
AT 1275°C

x 400

(c)   PLASTIC DEFORMATION AT A MATRIX STRAIN OF 0.6 ON
DEFORMATION AT 1275°C

x 400

(d)   FRACTURE OF A DEVITRIFIED INCLUSION AT A MATRIX
STRAIN OF 0.6 ON DEFORMATION AT 1275°C

x 400

(e)   PLASTIC/BRITTLE BEHAVIOUR OF A CRYSTALLINE
INCLUSION SHOWING THE FORMATION OF INTERNAL
VOIDS AT A MATRIX STRAIN OF 0.9 ON DEFORMATION
AT 1275°C

x 400

a

b

c

d

e

PLATE 21 (Cont'd....)
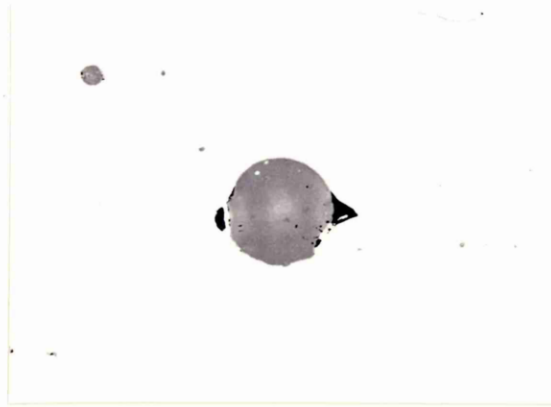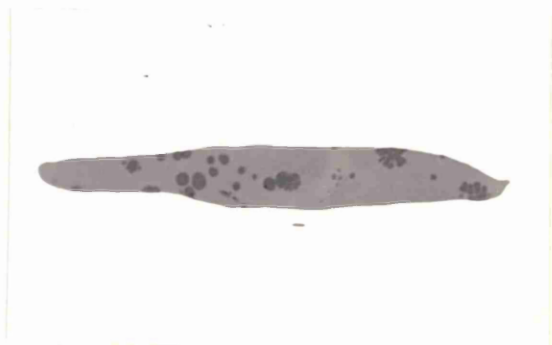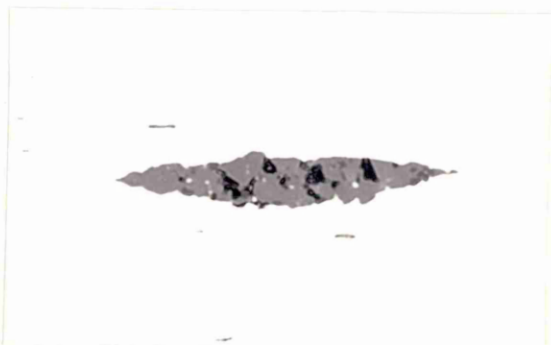
(f)   FRAGMENTATION, DISSEMINATION AND ROTATION OF
INCLUSION FRAGMENTS AT A MATRIX STRAIN OF 0.9
ON DEFORMATION AT 1275°C. NOTE THE VOIDS
PRODUCED BETWEEN ADJACENT FRAGMENTS

x 400

(g)   FRACTURING AT A MATRIX STRAIN OF 1.2 ON DEFORMATION
AT 1275°C

x 400

(h)   FRAGMENTATION AT A MATRIX STRAIN OF 1.2 ON
DEFORMATION AT 1275°C

x 400

f

g

h

PLATE 21 (Cont'd.....)
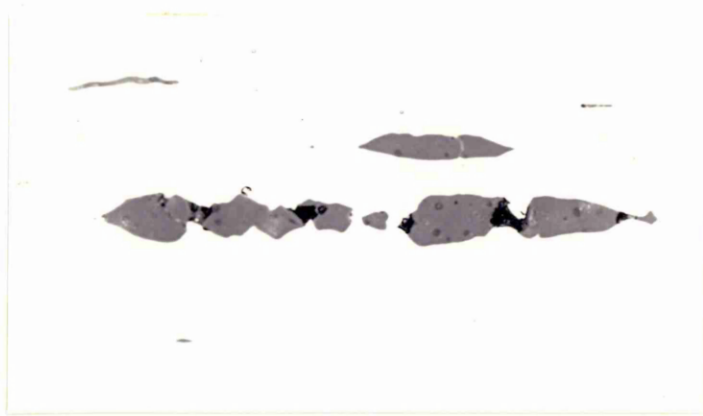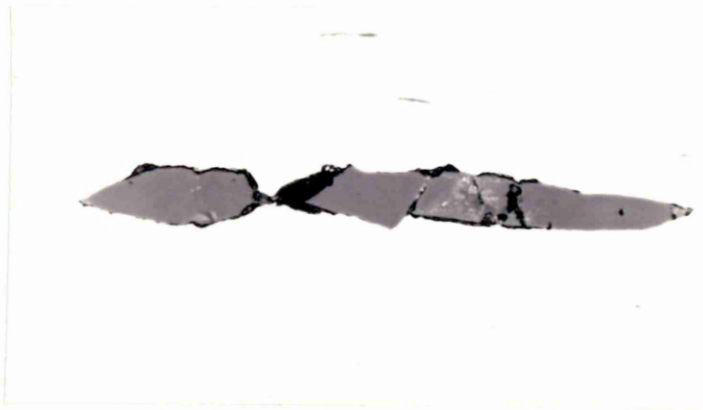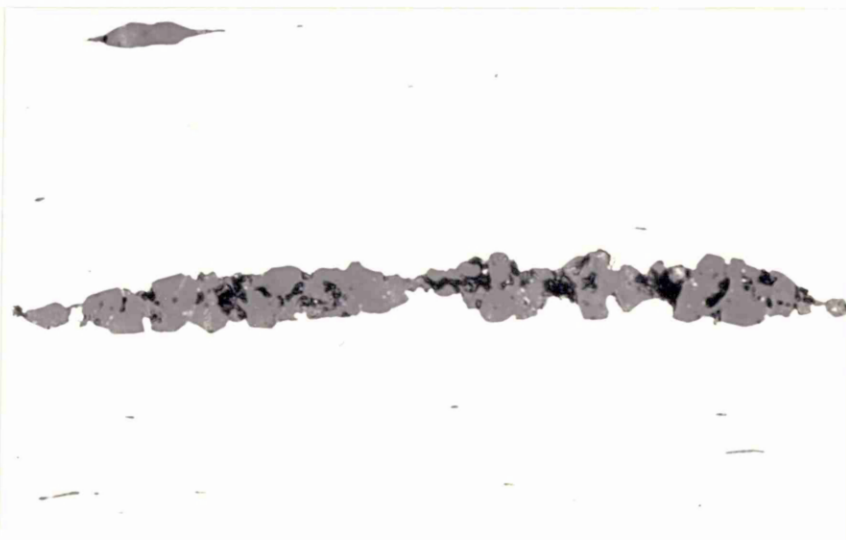
(i)   FRAGMENTATION AT A MATRIX STRAIN OF 1.8 ON
      DEFORMATION AT 1275°C

                                                    x 100

(j)   DISSEMINATED INCLUSION FRAGMENTS AT A MATRIX
      STRAIN OF 1.8 ON DEFORMATION AT 1275°C

                                                    x 200

(k)   FRAGMENTATION AND DISSEMINATION AT A MATRIX
      STRAIN OF 1.5 ON DEFORMATION AT 1275°C

                                                    x 200

(1)   DISSEMINATED INCLUSION FRAGMENTS IN THE SAMPLE
      DEFORMED TO A MATRIX STRAIN OF 1.8 AT 1275°C

                                                    x 200

(m)   DISSEMINATION, ROTATION AND SURFACE DEFORMATION
      OF INCLUSION FRAGMENTS IN THE SAMPLE HOT ROLLED
      AT 1275°C TO A MATRIX STRAIN OF 1.2

                                                    x 400

(n) · SURFACE FLOW OF AN INCLUSION FRAGMENT AT A
      MATRIX STRAIN OF 1.8 ON ROLLING AT 1275°C. THIS
      FRAGMENT WAS ORIGINALLY PART OF AN INCLUSION
      FRAGMENTED AT A LOW MATRIX STRAIN

                                                    x 1000

i

j

k

l

m

n
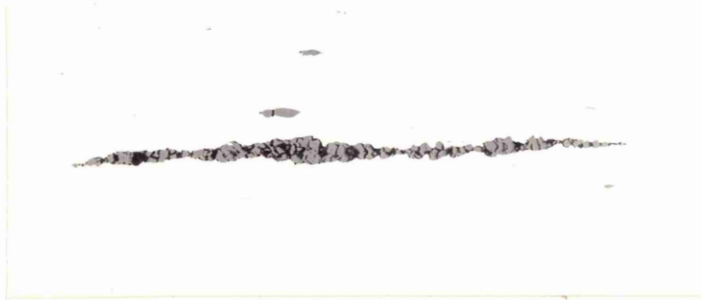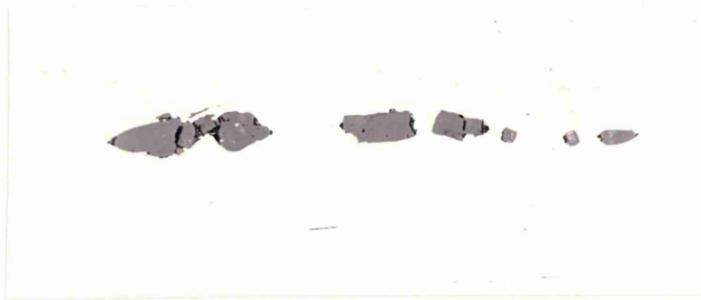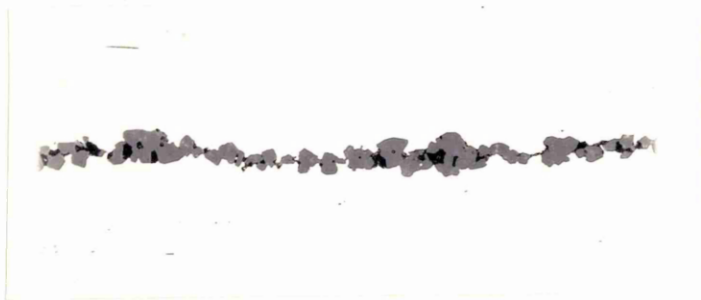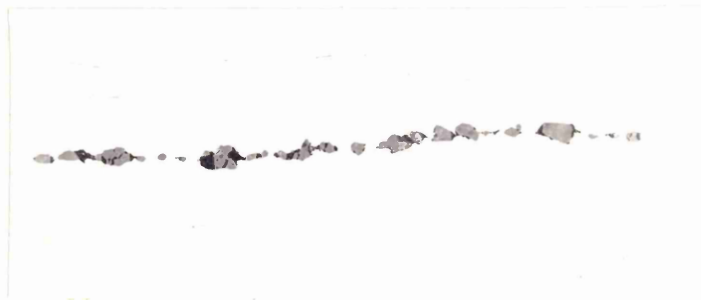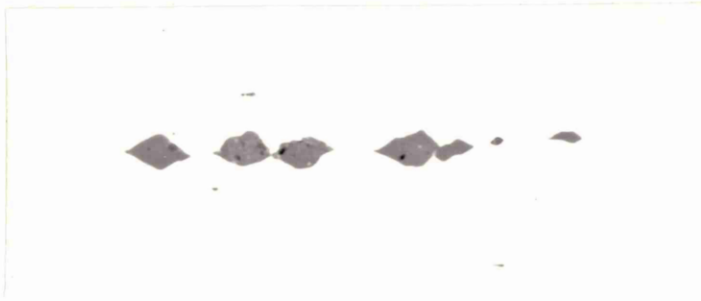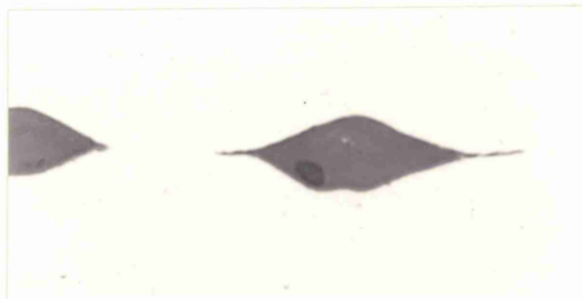
(a)   POLISHED FACE OF A FRAGMENTARY STRINGER SHOWING
        THE COMPLEX STRUCTURE OF THE CRYSTALLINE INCLUSION
        $\varepsilon = 1.2$

                                                        x 400

(b)   PARTIALLY DISSEMINATED INCLUSION SHOWING THE
        THIN FILM OF PLASTIC MATRIX CONNECTING THE
        SEPARATED PRIMARY CRYSTALLITES $\varepsilon = 1.5$

                                                        x 1.5K

(c)   HIGHER MAGNIFICATION SHOWING THE FINE STRUCTURE
        OF THE MATRIX $\varepsilon = 1.5$

                                                        x 12K

(d)   DISSEMINATED INCLUSION EXHIBITING HOT-TEARING
        OF THE PLASTIC MATRIX BETWEEN THE PRIMARY
        CRYSTALLITES $\varepsilon = 1.5$

                                                        x 1.2K

a

b

c

d
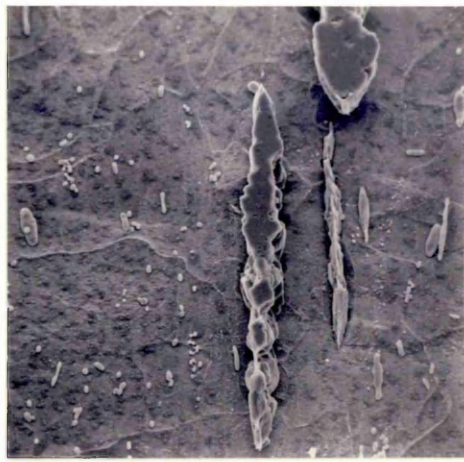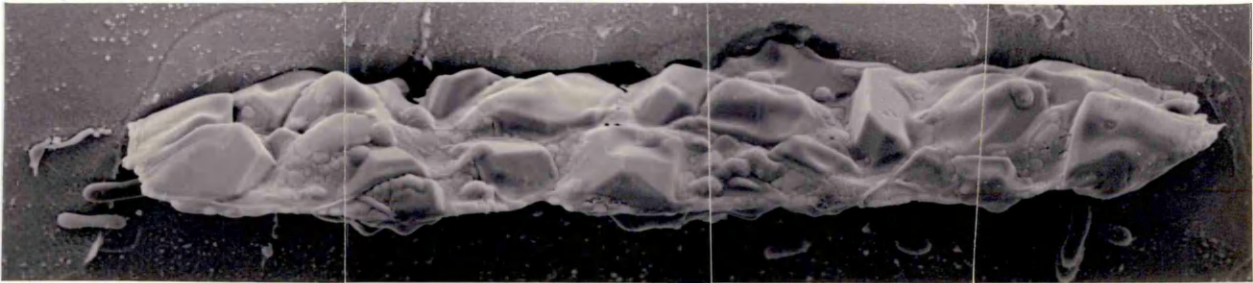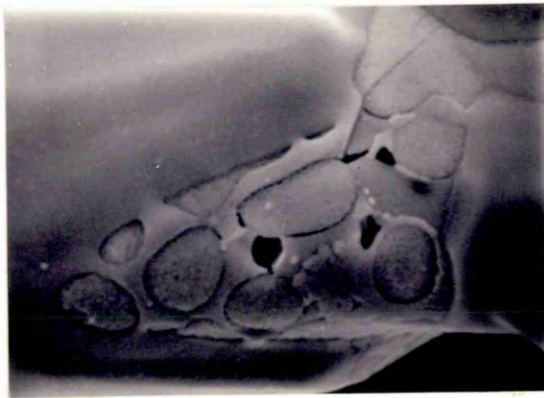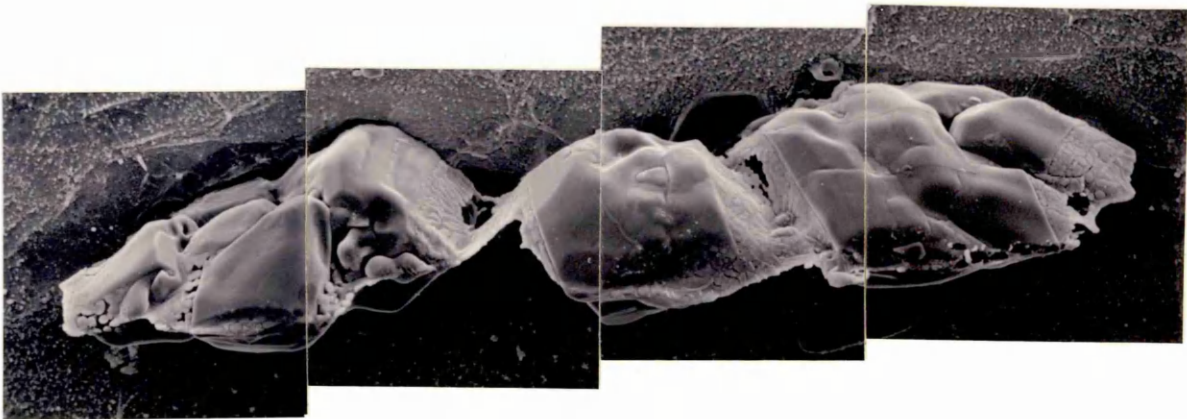
PLATE 22 (Cont'd.....)

(e)   DISSEMINATED INCLUSION FRAGMENT WITH A PLASTIC
       SURFACE FILM GIVING THE APPEARANCE OF SURFACE
       DEFORMATION $\mathcal{E} = 1.5$

                                                    x 2.5K

(f)   FRAGMENTED ELONGATED INCLUSION CONTAINING MANY
       PRIMARY CRYSTALLITES AND LITTLE EUTECTIC TYPE
       MATRIX $\mathcal{E} = 1.5$

                                                    x 500

(g)   POLISHED SURFACE OF AN INCLUSION SHOWING VOIDS
       PRODUCED WITHIN THE STRUCTURE $\mathcal{E} = 1.5$

                                                    x 1.2K

(h)   SMALL BACKGROUND INCLUSION HAVING A LATH-LIKE
       APPEARANCE $\mathcal{E} = 1.5$

                                                    x 2.7K

e

f

g

h

PLATE 23. CAST OR HOT ROLLED AT 900°C + 800°C
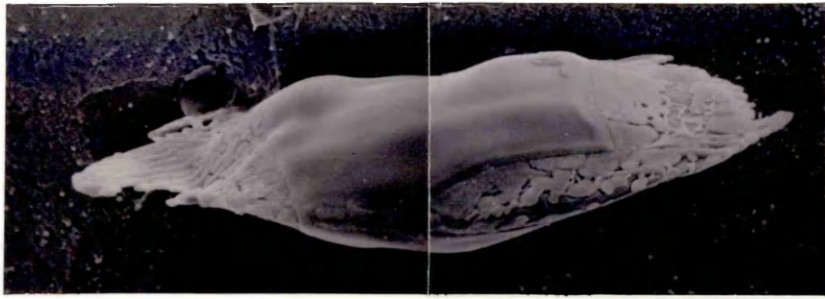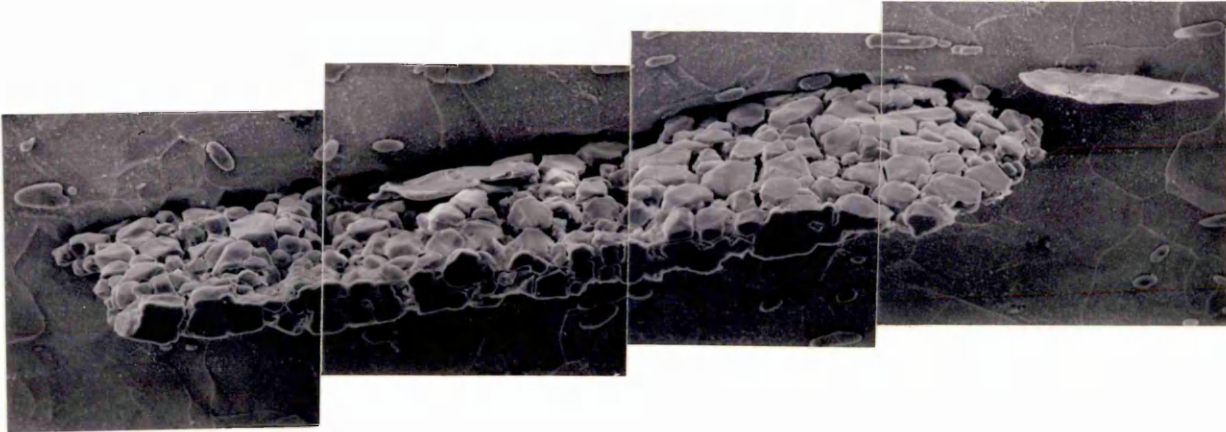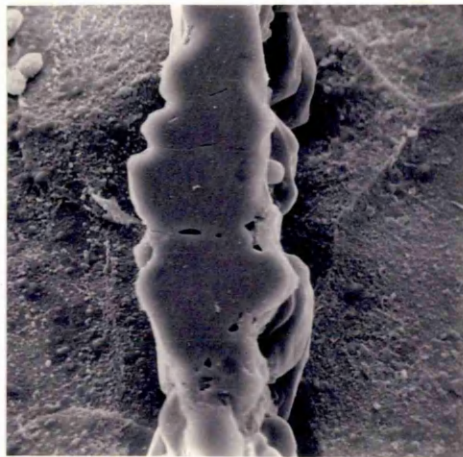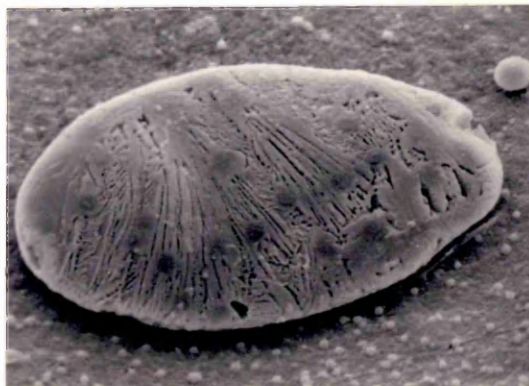
EXAMINATION BY HIGH VOLTAGE ELECTRON MICROSCOPY

(a) LOW MAGNIFICATION SHOWING THE LATH-LIKE INTERNAL
STRUCTURE OF THE FRAGMENTS

x 1.7K

(b) HIGHER MAGNIFICATION SHOWING THE LARGE NUMBER
OF MICROVOIDS PRESENT ALONG THE LATH BOUNDARIES

x 8.0K

(c) BRIGHT FIELD SHOWING A FEATHERY TYPE OF MATRIX
ASSOCIATED WITH THE LATHS

x 8.0K

S.A.D.P. INDEXED FOR THE TEPHROITE LATTICE

DARK FIELD OF (c)

a

b

(300)

(122)   (2 2̄ 2̄)

(2̄ 2̄ 2̄)   (1̄ 2̄ 2̄)

(3̄00)

c

PLATE 23 (Cont'd.....)
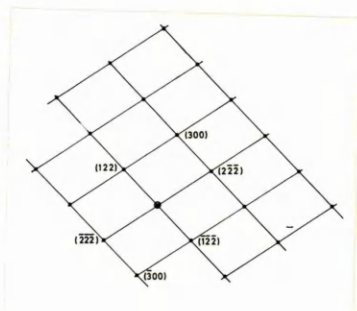
(d)   DUPLEX GLASSY OR MICROCRYSTALLINE INTERNAL
STRUCTURE

x 12.0K

(e)   PARTICLE CONTAINING BOTH LATH-LIKE AND DUPLEX
TYPE STRUCTURES

x 8.0K

PLATE 24. CAST 6B HOT ROLLED AT 1350°C

(a)   S.E.M. IMAGE OF A PLASTICALLY DEFORMED SILICATE
AFTER A MATRIX STRAIN OF 0.6. NOTE THE IMPRESSIONS
LEFT BY THE MATRIX GRAIN BOUNDARIES ON THE SURFACE
OF THE SILICATE, AND THE RIPPLED OR BOUDINAGED
APPEARANCE OF THE INCLUSION

x 1000

(b)   H.V.E. MICROGRAPH OF A PLASTIC SILICATE, EXTRACTED
BY CARBON REPLICA TECHNIQUE, AFTER DEFORMATION TO
A MATRIX STRAIN OF 3.0. NOTE THE THICKER PERIPHERY
TO THE STRINGER AND ITS BOUDINAGE MORPHOLOGY.
THE STRINGER ALSO CONTAINS A NUMBER OF SMALL HOLES.

x 2.0K

d

e

a

b

PLATE 25. CAST 8 HOT ROLLED AT 925°C
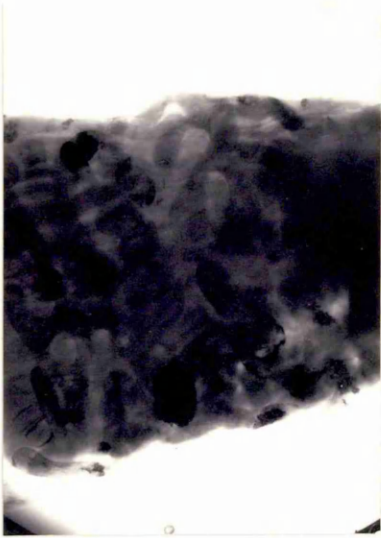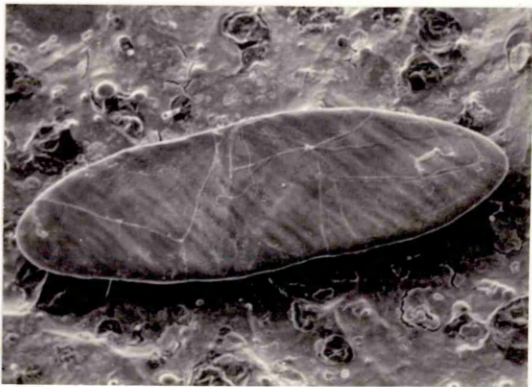
(a) DEVITRIFIED INCLUSION AFTER A MATRIX STRAIN OF
0.3

x 400

(b) DEVITRIFIED INCLUSION AFTER A MATRIX STRAIN OF
1.2

x 400

(c) PARTIALLY ELONGATED, CRACKED AND DISSEMINATED
INCLUSION AFTER A MATRIX STRAIN OF 1.5

x 400

(d) S.E.M. IMAGE OF A PARTIALLY ELONGATED AND CRACKED
TYPE $\mathcal{E} = 1.5$

x 600

(e) UNDEFORMED TYPE SHOWING SOME EVIDENCE OF
SURFACE REACTION $\mathcal{E} = 1.5$

x 2K

(f) CRUSHED AND FRACTURED TYPE OF INCLUSION $\mathcal{E} = 1.5$

x 800

a

b

c

d

e

f

PLATE 26. CAST 8 HOT ROLLED AT 1150 AND 1275 C
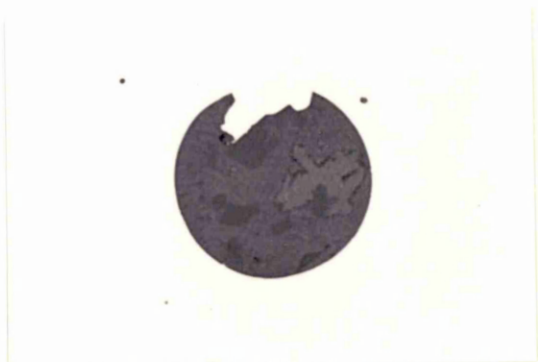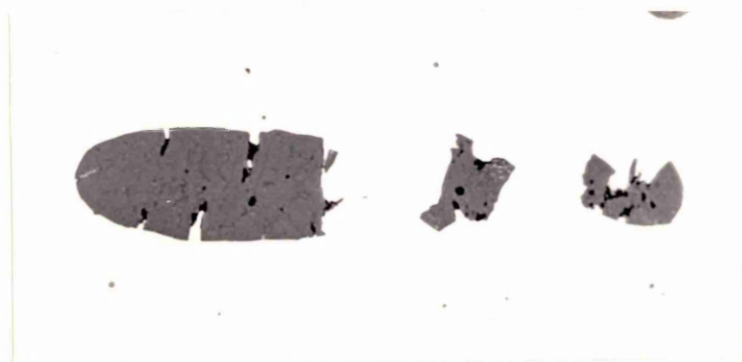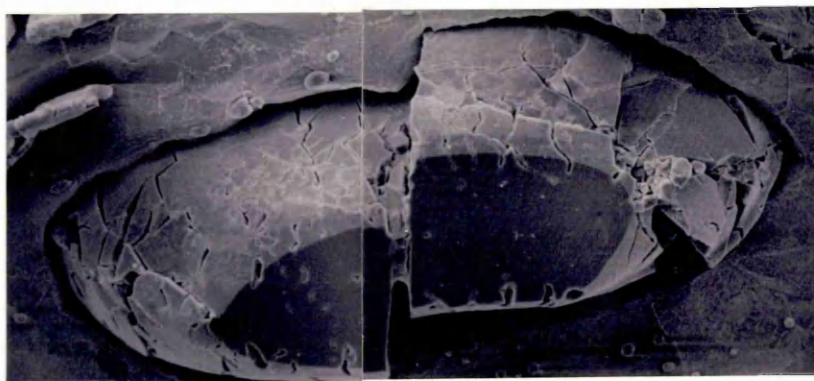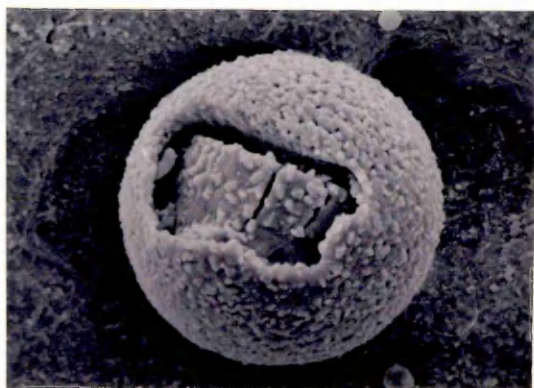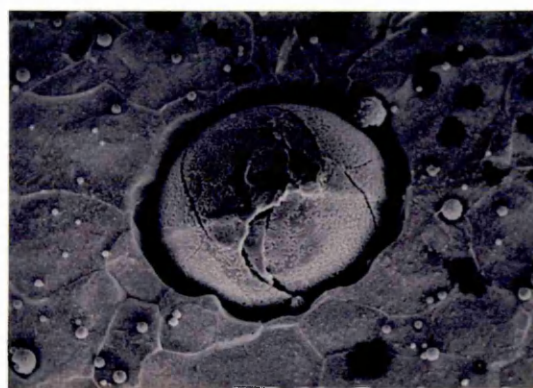
(a)   DEFORMED AT 1150°C TO A MATRIX STRAIN OF 0.3

x 250

(b)   DEFORMED AT 1150°C TO A MATRIX STRAIN OF 0.9

x 250

(c)   DEFORMED AT 1150°C TO A MATRIX STRAIN OF 1.8

x 250

(d)   S.E.M. IMAGE OF AN ELONGATED STRINGER, AT A
MATRIX STRAIN OF 1.8, AFTER DEFORMATION AT 1275°C.
NOTE THE BOUDINAGE MORPHOLOGY AND THE PRESENCE
OF HOLES IN THE RIBBONS

x 250

(e)   HIGHER MAGNIFICATION SHOWING THE PRESENCE OF
PRECIPITATES IN SOME OF THE ELONGATED RIBBONS

x 1.5K

(f.)   OPTICAL MICROGRAPH TAKEN FROM A POLISHED
SECTION LYING IN THE ROLLING PLANE SHOWING THE
BOUDINAGE MORPHOLOGY OF THE DEFORMED
INCLUSIONS

x 400

PLATE 26. CAST 8 HOT ROLLED AT 1150 AND 1275 C
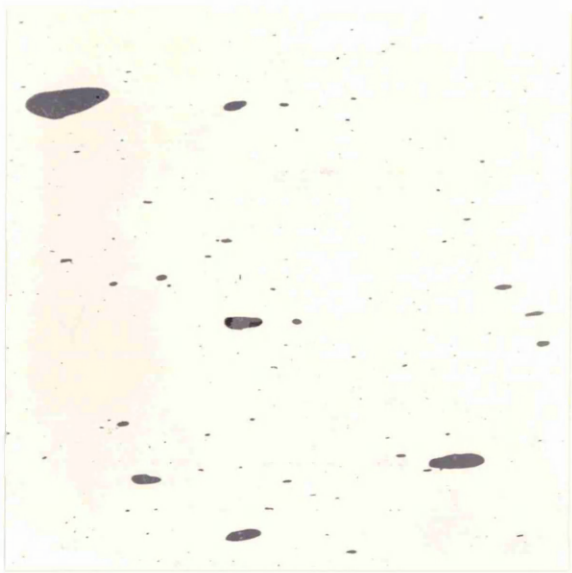
a
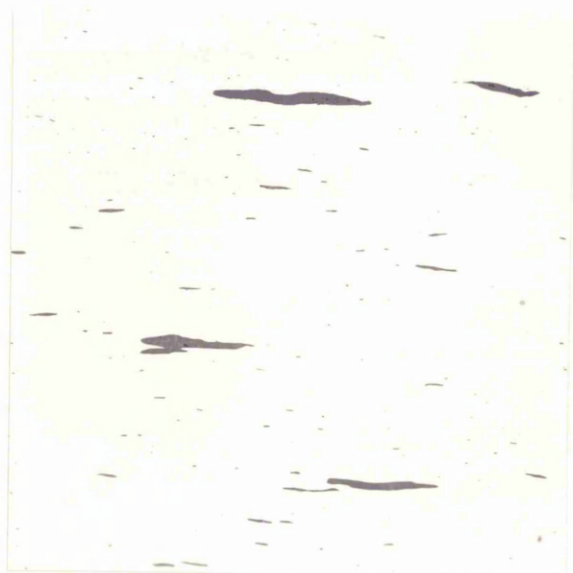
b
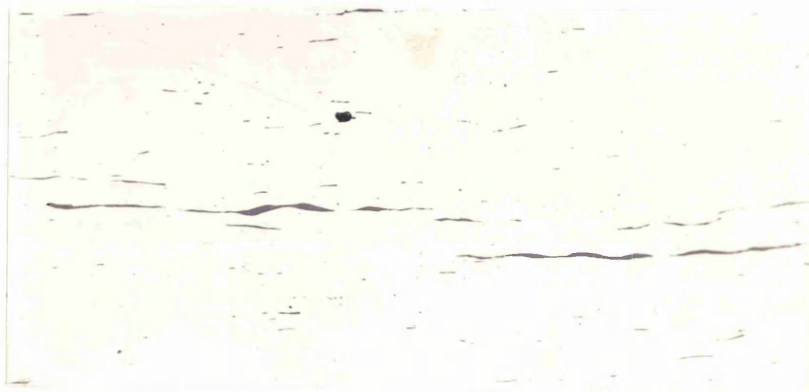
c

d
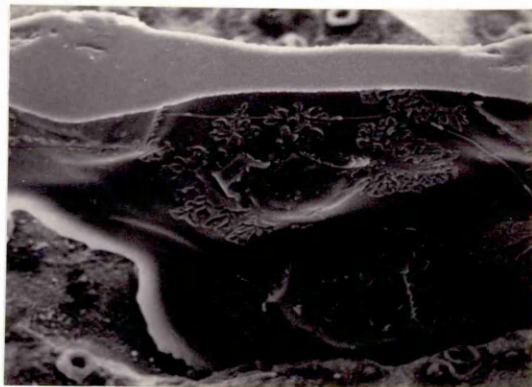
e
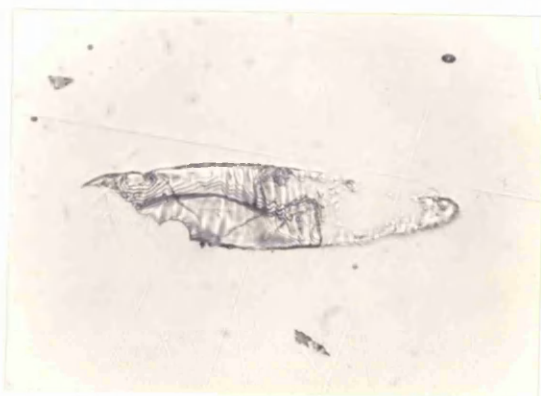
f

(a)   CRUSHED INCLUSION AFTER DEFORMING TO A MATRIX
STRAIN OF 0.6 AT 1000°C, USING A STRAIN RATE OF
0.6 PER PASS

                                                              x 650

(b)   CRUSHED INCLUSION AFTER DEFORMING TO A MATRIX
STRAIN OF 1.2

                                                              x 150

(c)   JOINING FLUID STRINGERS ON ROLLING TO A MATRIX
STRAIN OF 1.2 AT 1150°C USING A STRAIN RATE OF 0.6
PER PASS. NOTE THE CRYSTALLIZATION IN THE REGION
OF JOINING

                                                              x 250

(d)   STRINGERS EXHIBITING MULTIPLE FRACTURING ON
REDUCING THE ROLLING TEMPERATURE FROM 1150°C
TO 925°C

                                                              x 450

(e)   S.E.M. IMAGE SHOWING THE FRAGMENTATION IN (d)

                                                                x 400

PLATE 28. CAST 11 HOT ROLLED
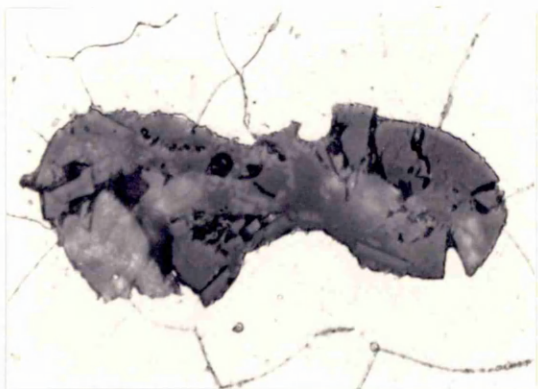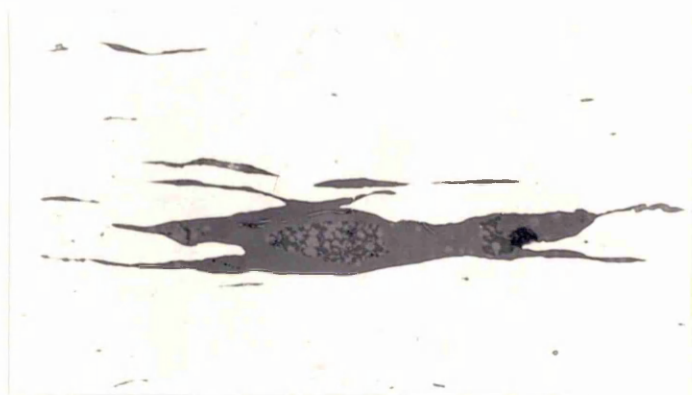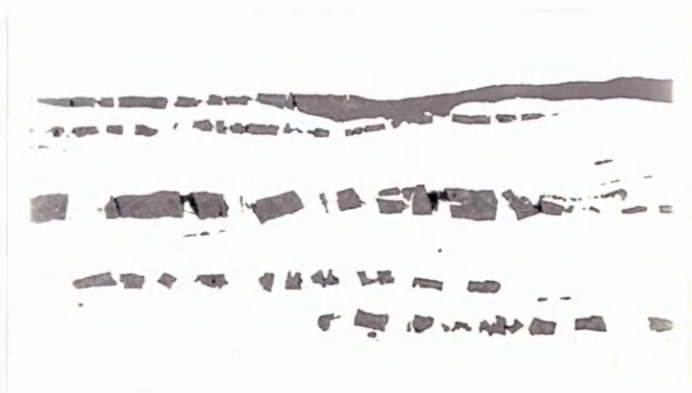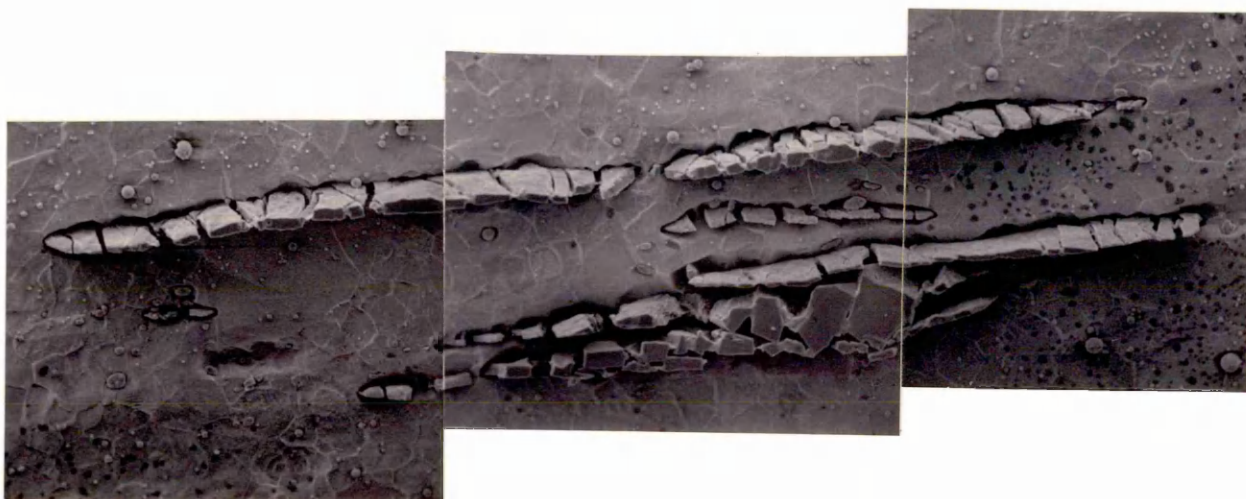
(a)   ELONGATED DUPLEX TYPE OF INCLUSION SHOWING
       CONICAL VOID FORMATION AND EXTENSIVE CRACKING,
       ON DEFORMING TO A MATRIX STRAIN OF 1.2 AT $925^{\circ}C$

                                                    x 240

(b)   DUPLEX TYPE HAVING A SILICA RICH RIM PREVENTING
       DEFORMATION. $\varepsilon = 0.9$ AT $925^{\circ}C$
                                                    x 400

              A   98% SiO_2
              B   54% SiO_2, 20% CaO, 28% FeO

(c)   PLASTIC INCLUSIONS EXHIBITING VARIABLE PLASTICITY
       ON DEFORMING TO A MATRIX STRAIN OF 1.5 AT $1000^{\circ}C$

                                                    x 100

(d)   HIGHLY ELONGATED INCLUSIONS EXHIBITING A
       BOUDINAGE MORPHOLOGY ON DEFORMING TO A MATRIX
       STRAIN OF 1.8 AT $1275^{\circ}C$

                                                    x 200

a

b

c

d
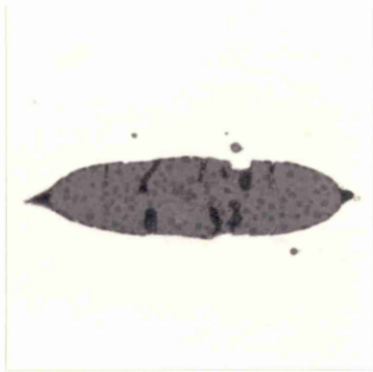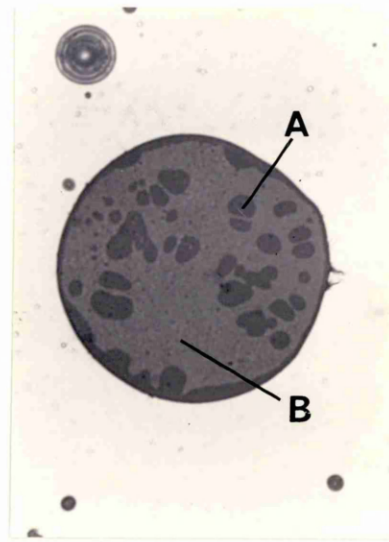
PLATE 28 (Cont'd.....)

(e)   DUPLEX TYPE OF INCLUSION, PROBABLY HAVING A
       LIQUID MATRIX AT THE DEFORMATION TEMPERATURE OF
       1275°C, EXHIBITING PLASTIC DEFORMATION AND CRACKING
       OF THE SILICA RIM AT A MATRIX STRAIN OF 0.3

                                                    x 400

(f)   DUPLEX TYPE OF INCLUSION ELONGATED AND
       DISSEMINATED AT A MATRIX STRAIN OF 1.2 AT 1275°C

                                                    x 400

PLATE 29.   CASTS 4B AND 12 HOT ROLLED

(a)   CONICAL VOID PRODUCED AT A RIGID SILICEOUS
       INCLUSION ON DEFORMING TO A MATRIX STRAIN OF 0.3
       AT 1275°C.

                                                    x 400

(b)   CLOSING OF VOIDS AT HIGHER MATRIX STRAINS ($\varepsilon = 1.2$)

                                                    x 800

e

f

a

b

PLATE 30. CAST 7B HOT ROLLED
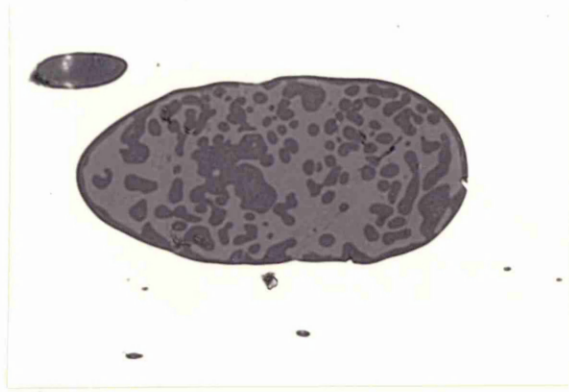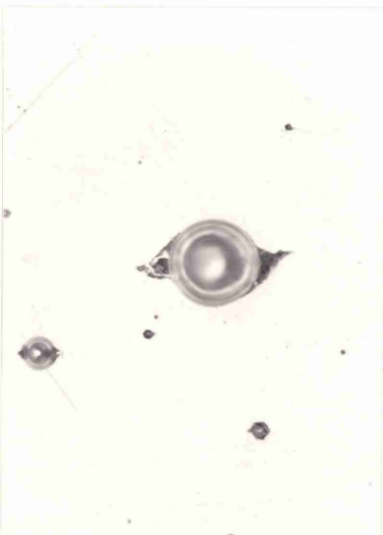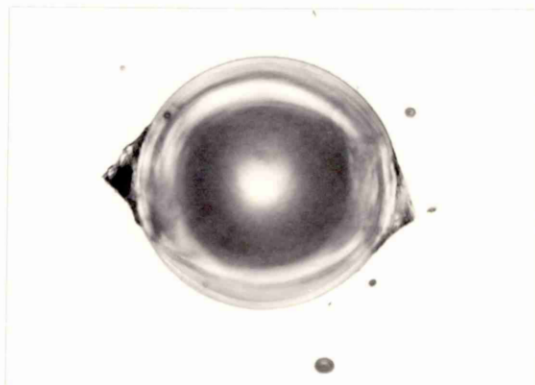
(a)   OPTICAL MICROGRAPH OF A TYPICAL ALUMINA STRINGER
       PRODUCED ON HOT ROLLING TO A MATRIX STRAIN OF
       1.8 AT 925°C

                                                        x 75

(b)   S.E.M. IMAGE SHOWING FRACTURING OF DENDRITE
       ARMS AND SINTER NECKS

                                                        x 1.5 K

(c)   S.E.M. HIGHER MAGNIFICATION SHOWING LARGE NUMBERS
       OF BROKEN DENDRITE ARMS

                                                        x 1.8K

(d)   S.E.M. IMAGE SHOWING FRACTURING OF SINTERED
       GLOBULES AND SPHERODIZED PARTICLES

                                                        x 3.9K

a

b

c

d
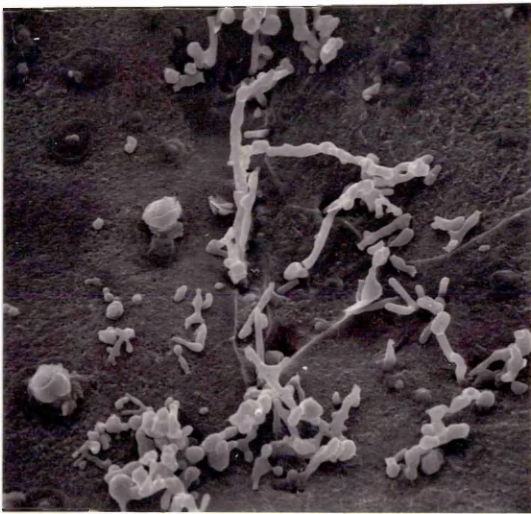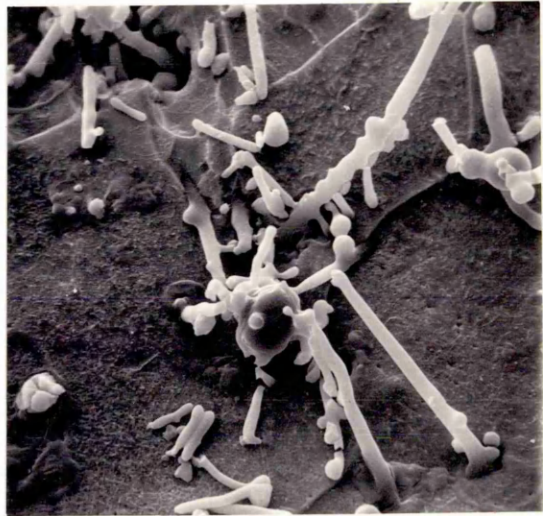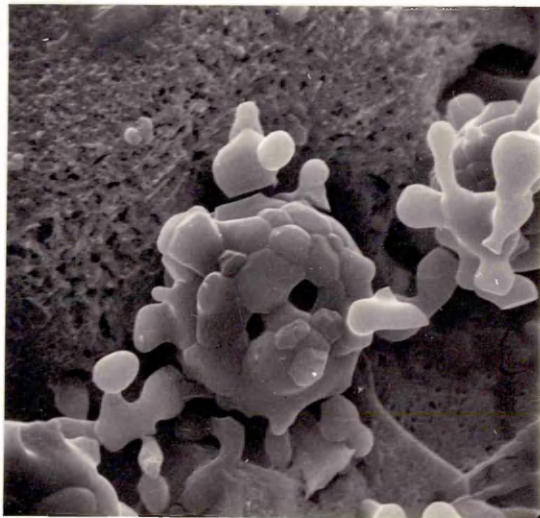
PLATE 30 (Cont'd.....)

(e)   OPTICAL MICROGRAPH SHOWING CONICAL VOID
                FORMATION OF SPHERICAL ALUMINA PARTICLES
                    $\mathcal{E} = 1.2$ $T = 1150^{\circ}C$

x 1.3K

(f)   CONICAL VOID FORMATION AND CRACKING OF SPHERICAL
                ALUMINA PARTICLES $\mathcal{E} = 1.2$ $T = 1150^{\circ}C$

x 1000

(g)   S.E.M. IMAGE OF A CRACKED SINTERED ALUMINA
                PARTICLE AFTER DEFORMING TO A MATRIX STRAIN
                OF 1.2

x 1.3K

e

f

g

PLATE 30 (Cont'd.....)
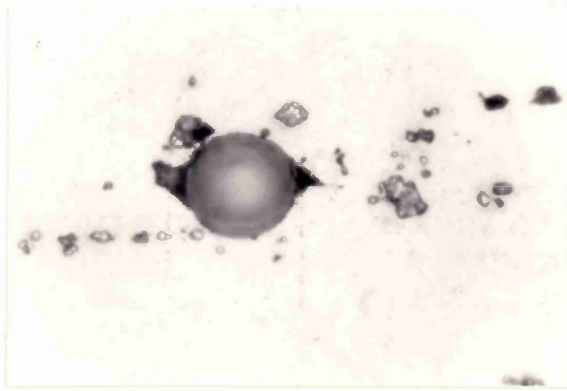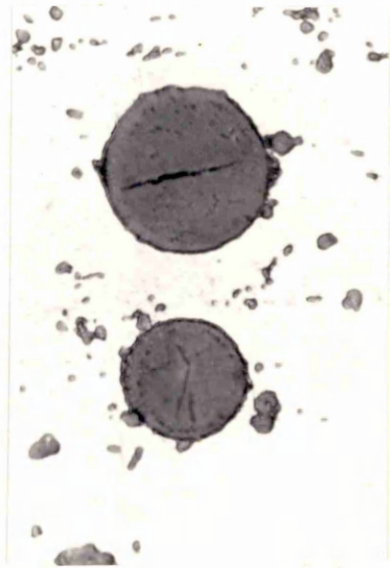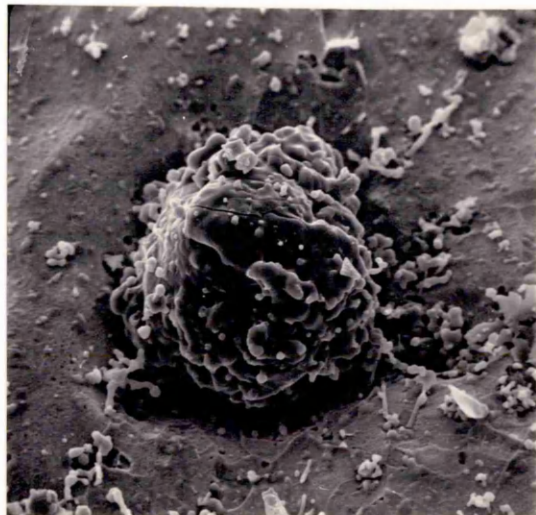
(h)   FRAGMENTARY ALUMINA STRINGER COMPOSED OF GRAIN
       SHAPED PARTICLES ON DEFORMATION TO A MATRIX
       STRAIN OF 1.8 AT 925°C

                                              x 800

(i)   FRAGMENTARY ALUMINA STRINGER COMPOSED OF
       GRAIN SHAPED PARTICLES AT HIGHER MAGNIFICATION
       SHOWING THE PARTICLE MORPHOLOGY

                                              x 4K

(j)   MONTAGE OF AN EXTENSIVE STRINGER PRODUCED ON
       DEFORMING TO A MATRIX STRAIN OF 1.8 AT 925°C

                                              x 2.5K

h

i
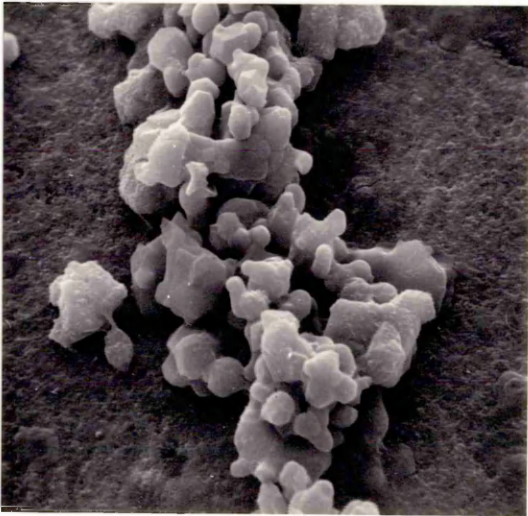
<u>PLATE 31. CAST 10 HOT ROLLED</u>

FRAGMENTARY STRINGER PRODUCED ON DEFORMATION TO
A MATRIX STRAIN OF 0.9 AT 925°C

x 500

SHEFFIELD POLYTECHNIC

LIBRARY

LOAN OF THESIS

Author... ROBINSON, S. W.

Title The Plastic Deformation of Non-Metallic

Inclusions in Steel

Thesis Number ....

I undertake that neither the whole nor any
part of the above-mentioned thesis shall
be copied, quoted or published without the
consent of the Author and of the
Sheffield Polytechnic.

Signature .F.C.B. Asante

Address .Dept. of Metallurgy and Materials

Univ. of Aston:

Gosta Green. B'Ham B4 7ES.

Date ..8/3/78.

This undertaking is to be signed by the
reader consulting the thesis and
returned to:-

The Librarian,
Sheffield Polytechnic,
Pond Street,
Sheffield S1 1WB.